Structural Dynamic Analysis and Model Updating for a Welded Structure made from Thin Steel Sheets

Thesis submitted in accordance with the requirements of the University of Liverpool for the degree of Doctor in Philosophy

by

Muhamad Norhisham Abdul Rani

February 2012

To my dear mother , father and sister

Abstract

Modern large, complex, engineering structures normally encompass a number of substructures which are assembled together by several types of joints. Despite, the highly sophisticated finite element method that is widely used to predict dynamic behaviour of assembled complete structures, the predicted results achieved, of assembled structures are often far from the experimental observation in comparison with those of substructures. The inaccuracy of prediction is believed to be largely due to invalid assumptions about the input data on the initial finite element models, particularly those on joints, boundary conditions and also loads. Therefore, model updating methods are usually used to improve the initial finite element models by using the experimentally observed results.

This thesis is concerned with the application of model updating methods to a welded structure that consists of several substructures made from thin steel sheets that are assembled together by a number of spot welds. However, the welded structure with a large surface area is susceptible to initial curvature due to its low flexible stiffness or manufacturing or assembling errors and to initial stress due to fabrication, assembly and welding process of substructures. Nevertheless, such initial stress is very difficult to estimate by theoretical analysis or to measure. This thesis puts forward the idea of including initial curvature and/or initial stress (which have a large effect on natural frequencies) as an updating parameter for improving the performance of the finite element model of a structure made from thin steel sheets.

The application of conventional iterative model updating methods which use a full finite element model has been widely practised. However when updating large, complex structures with a very large number of degrees of freedom, this application becomes impractical and computationally expensive due to the repeated solution of the eigensolution problem and repeated calculation of the sensitivity matrix. It is therefore preferable to use a substructuring scheme based model updating which is highly computationally efficient for the reconciliation of the finite element model with the test structure. However, in certain practical cases,

where the confidential and proprietary issues of modelling work are of concern between the collaborating companies, in which the finite element models of the substructures could not be revealed and only the condensed matrices of the substructures are used instead, the areas of the substructures having fewer number of interface nodes would always be the first choice as the interface nodes. For welded structures, the nodes in the vicinity of spot weld element models are few and hence are usually taken as the interface nodes for connecting substructures. However, the present MSC. NASTRAN superelement model reduction procedures are known not to allow the nodes of CWELD elements to be the interface nodes of substructure.

Prior to the present study, no work appears to have been done to use the nodes of CWELD elements as the interface nodes of substructures in the investigation of dynamic behaviour of welded structures. In this work, the application of branch elements as the interface elements of substructure are proposed and tested. Prior to the present study, it also appears that there has been no work done concerning the adjustment of the finite element model of the welded structure by including the effects of initial curvatures, initial stress and boundary conditions that are contributing to the modelling errors, via the combination between the Craig-Bampton CMS and model updating.

This thesis presents two approaches for model updating of the welded structure: the conventional methods which use full finite element model and the substructuring scheme based model updating which uses the Craig-Bampton CMS technique. The accuracy and efficiency of both approaches are thoroughly discussed and presented and are validated with the experimentally observed results.

Acknowledgements

With this opportunity, I would like to extend my gratitude and appreciation to my dearest supervisor **Prof. Huajiang Ouyang** who I knew two years before I decided to pursue my PhD. During that period I often emailed to him seeking his expertise in the issues of structural dynamics. His highly responsive attitude to every question that I emailed and his intellectual approaches to the issues I brought forward were the chief reasons that I decided on doing a PhD under his supervision. On top of that, I would like to record my sincerest thankfulness to him for his many helpful suggestions, excellent discussions, supervision and also encouragement throughout this research. I also would like to thank my second supervisor **Dr. T. Shenton** for his helpful inputs and generosity in his time.

I would like to acknowledge **Prof. John E. Mottershead** for his work on model updating, his valuable textbook and papers have become very good resources, not only for my research but for other scientific and engineering communities. I also would like to thank him for his willingness to lend me all his paper references and to take a photo with me for the sake of my Malaysian friends.

I owe a debt of gratitude to **Dr. Simon James** for his expertise and invaluable advice in ensuring my experimental work was successfully carried out. I would also like to express my appreciation to **Mr. Tommy Evans** from the Core Services Department for his readiness to fabricate the weld structure and his special attention to my project. This research would not have been completed without their great support.

Special appreciation to **Mr. Ir. John**, **Dr. Dan. Stancioiu**, **Dr. Huaxia Deng** and **Dr. Ruiqiang** for their valuable advice and great suggestions and with whom I have always been working, having coffee and generally hanging out together.

Special thanks to **Dr. H. Haddad Khodaparast**, **Dr. N. Abu Husain**, **Dr. M. Prandina** and **Dr. Mimi Liza** for their great help and support especially during the important first year of my research.

In addition, thank you to the following people: **Mr. M.S. Mohd Sani, Dr. Weizhuo Wang, Ms. N. Hassan, Mr. M. Y. Harmin, Mr. A. S. Omar** and **Mr. R. Samin** who have aided me in my research and through difficult times; and to **K. Zhang** and **Q. Ouyang** who have often spent time together with me having coffee and discussing the technical and global economic issues.

I am also grateful to my dearest sister **Ms. Norhayati** who has always cheered me up in times of trouble and to my best friends **Dr. Bob Kana, Mr. Herry Yunus, Mr. Syaiful** and **Mr David Paul Starbuck** for their kindness , great continuous support and encouragement.

Lastly, it would not have been possible for me to complete my research without the outstanding moral support from my loving parents, my dearest wife **Azurina Hj Zainal Ratin** and son, **Umar Haziq**. My future son **Mansor Haziq** and daughter **Sarah Haziq** are certainly not to be omitted from my acknowledgements.

And finally, I would like to deeply acknowledge the generous financial support provided by **Majlis Amanah Rakyat (MARA) of Malaysia.**

Table of Contents

List of Figures

Chapter 2

Chapter 3

Chapter 4

Chapter 5

Chapter 6

List of Tables

Chapter 3

Chapter 4

Chapter 5

Chapter 6

List of Symbols and Abbreviations

E	Young's modulus
G	shear modulus
ρ	mass density
ν	Poisson's ratio
ω	frequency in rad/sec
λ_i^{FE}	i^{th} numerical eigenvalue
λ_i^{EXP}	i^{th} experimental eigenvalue
$\mathbf{Z}_m$	vector of measured data involving eigenvalues or eigenvectors
$\mathbf{Z}_j$	vector of analytical response
$\boldsymbol{\theta}$	vector of structural updating parameters
$\mathbf{S}$	eigenfrequency sensitivities
$\mathbf{M}$	mass matrix
$\mathbf{C}$	damping matrix
$\mathbf{K}$	stiffness matrix
$\mathbf{f}(t)$	vector of applied forces
$\mathbf{q}$	vector of displacements
$\dot{\mathbf{q}}$	vector of velocities
$\ddot{\mathbf{q}}$	vector of accelerations
$\boldsymbol{\phi}$	vector of eigenvectors
$\mathbf{M}^S$	S^{th} substructure's mass matrix vector
$\mathbf{K}^S$	S^{th} substructure's stiffness matrix vector
$\mathbf{X}^S$	S^{th} substructure's displacement matrix vector
$\mathbf{F}^S$	S^{th} substructure's force vector
$\hat{\mathbf{M}}_{BB}^S$	reduced mass matrix
$\hat{\mathbf{K}}_{BB}^S$	reduced stiffness matrix
$\boldsymbol{\Psi}_B$	constraint modes or boundary node functions
$\boldsymbol{\Psi}_I$	fixed boundary modes or component normal modes

Ψ_F	inertia-relief modes
B	boundary degrees of freedom
I	interior degrees of freedom
r	rigid body

BC	boundary conditions
CEAF	CWELD element ALIGN format
CEEF	CWELD element ELPAT format
CMS	component mode synthesis
CWELD	weld element connection
EMA	experimental modal analysis
EXP	experimental
FE	finite element
FFEM	full finite element model
IFEM	initial finite element model
MAC	modal assurance criteria
NGV	natural gas vehicle
NoMF	number of measured frequencies
NVH	noise vibration and harshness
PELAS	scalar elastic property
RSW	resistance spot weld
S1	stopper 1
S2	stopper 2
SEMU	substructuring or superelement based model updating
SW1	side wall 1
SW2	side wall 2
UFEM	updated finite element model
UYM	updated Young's modulus
UYMP	updated Young's modulus and PELAS
VoOF	value of the objective function

Chapter 1

Introduction

1.1 Introduction

Structural dynamic analyses continue to present a major concern for a very wide range of engineering products today. This concern has constantly demanded and challenged engineers who need efficient and practical methods for accurately predicting and investigating structural dynamic problems. Numerical methods have become preferable and extremely powerful for understanding the dynamic characteristics of structures in comparison with the experimental modal analysis in which the number of testing scenarios are limited.

The ability to investigate the dynamic characteristics of structures numerically allows structures to be designed economically and competitively. However, the accomplishment must not be at the expense of safety, reliability and durability which highly depend on the dynamic characteristics of structures. Numerical models, particularly the finite element models, are, in fact, constructed based on assumptions about the model and material properties of structures. The best way to develop confidence in the numerical models is to compare its predicted results with measured results on actual hardware. The discrepancies between the numerical results and experimental results drive a process in which the numerical models are systematically adjusted to become a closer representation of the tested structures. The chief expectation from the systematic adjustment process is a better reconciliation between both models.

The systematic process of reconciling the numerical results with the experimental results systematically is called model updating. Updating finite element models of complex structures that consist of a large number of substructures often presents unsatisfactory results in comparison with updating the individual components. This is the chief issue that is addressed in this work. The significant contributions to the

difficulties in obtaining a satisfactory level of accuracy of the results are the complexity of joint types, the uncertainties in boundary conditions, the presence of initial stress and also the inaccurate description of the interactions between substructures.

The configuration of structures as described in the preceding paragraph, for example a car body-in-white is an assembly of a number of substructures which are formed from many components. The components are made from thin metal sheets and are assembled together by thousands of joints. Resistance spot weld (RSW) is one of the joint types that are widely used in automotive engineering. As the paramount contributors of a car's dynamic characteristics, spot welds are highly required to be properly modelled. However because many automotive components are designed and analysed in parallel, different CAE engineer teams supply components with dissimilar meshes. This has lead to a difficulty in modelling the spot welds which is cumbersome, time-consuming and error prone. As a result, the confidence in the correlation between the numerical and experimental results of the global assembled structures is questionable.

It is imperative that model updating needs to be performed to address the effects of the different modelling assumptions on the resulting discrepancies of the correlation. In this study, the welded structure which is an assembly of five substructures made from thin metal sheets and joined together by eighty resistance spot welds, is used for investigating the dynamic characteristics and also for demonstrating superelement based model updating (SEMU) of the structure. On top of that this study also reveals two significant findings (bending moment of inertia ratio and branch elements) which have not been used for superelement based model updating and also been reported in any other research work.

In this work, several unfamiliar technical and non-technical terms have been used for describing certain modelling scenarios. The following items account for the definition of:

1.1.1 Superelement

Superelement is a combination of several particular regular finite elements into a single unit form of element in which part of the degrees of freedom is condensed out for computational and modelling purposes. Superelement and substructure are interchangeable terms in this work.

1.1.2 Residual structure

Residual structure is, by definition, the substructure in which the condensation of matrices is not performed. It is the substructure in which the condensed matrices of superelements are combined and solved. The substructure which is totally represented in physical coordinates. Furthermore the residual structure is also the substructure in which the design space such as model updating and optimization process are carried out.

1.1.3 Boundary nodes

Boundary nodes are the interchangeable term for interface nodes. They are best described as those that are retained for further analysis and those to which the matrices of superelements are reduced and also those that connect a superelement with another superelement or a residual structure.

1.1.4 Bending moment of inertia ratio ($12I/T^3$)

Bending moment of inertia ratio is the ratio of the actual bending moment inertia of the shell element, I, to the bending moment of inertia of a homogeneous shell element, $T^3/12$. MSC NASTRAN is a unit less code, however, if SI system of units is used then $12I/T^3$ would have the units of meters. The I is the second moment of area of the cross section of the shell, which is by definition rectangular if the thickness at all GRID points is the same. T is the thickness of the shell and has units of meters. The default value of $12I/T^3$ is 1.0 for a homogeneous shell element and the value can be systematically manipulated in NASTRAN SOL 200.

$$I = \left(WT^3\right)/12$$

Where:

W = section width (the width of the element)

T = section height (the thickness of the element)

The unit of $12I/T^3$ is meter.

1.1.5 Interior nodes

The nodes that can be thought of as those that are condensed out during the superelement processing. All nodes that are not boundary nodes can be regarded as interior nodes.

1.1.6 CEEF

It stands for CWELD elements in ELPAT format. This is the format that is used to represent the eighty spot welds on the welded structure after CWELD elements in ALIGN format have failed to demonstrate good predictive models for the spot welds.

1.1.7 Branch elements

Branch elements, in context of this work, are a group of elements surrounding CWELD elements in ELPAT format (CEEF). Using ELPAT format, additional support nodes are automatically generated and evenly positioned on different elements, up to 3x3. The surrounding elements namely branch elements may be included into the modelling spot weld, instead of only one element.

1.1.8 SEMU

Superelement based model updating or SEMU is a combination of two methods between superelement and model updating. It is an efficient method for substructuring and model updating for large, complex structures in which spot welds are used to join their substructures. SEMU is chiefly constructed and used for efficiently assisting in the development of reliable predictive models of structures, in particular involving very large complex structures and also spot welds assembled structures.

1.2 Research goal and objectives

The chief goal of this research is to present an efficient method for the identification and reconciliation of the dynamic characteristics of finite element model. The proposed method is effectively valuable for large, complex structures in which spot welds are the joint interfaces. Four objectives are identified and they are:

1. To perform finite element modelling and modal testing on a structure which is an assembly of substructures made from thin metal sheets and joined by a number of spot welds
2. To perform model updating of the above-mentioned welded structure in order to improve the accuracy of finite element model.
3. To construct and apply superelement based model updating to the welded structure
4. To validate the accuracy and efficiency of superelement based model updating
    - Performing modal testing on the tested substructures and welded structure
    - Performing comparative study for identifying the most reliable CWELD elements in modelling physical spot welds
    - Performing normal modes analysis on finite element models of substructures and welded structure
    - Performing sensitivity analysis for identifying the most potential updating parameters
    - Performing model updating on the full finite element models of substructures and welded structure
    - Performing superelement based model updating on welded structure
    - Performing comparison of finite element derived modal parameters and physical derived modal parameters

1.3 Research scope

The scope of this research includes the following steps:

1. Finite element modelling and modal testing are performed on substructures and the welded structure. The first ten modes are investigated numerically and experimentally.
2. Model updating is divided into two phases. The first phase is performed on finite element models of substructures. The Young Modulus, thickness and boundary conditions are among the updating parameters used. The second phase is carried out on finite element model of the welded structure in which a parameter (bending moment of inertia ratio), CWELD elements and boundary conditions are used as the updating parameters. In this work, updating boundary conditions refer to updating the properties of NASTRAN CELAS elements used to represent the four sets of suspension springs and nylon strings to approximate free-free boundary conditions of the modal tests of the bent floor and the welded structure (see Figure 3.14 page 70 and Figure 3.17 page 75).
3. Construction of superelement based model updating is based on the Craig-Bampton fixed interface methods and the application of NASTRAN Optimizer SOL 200 and also of specially designed branch elements. While application of superelement based model updating is to show the efficiency of the method in the reconciliation of the finite element model with the tested structure and also to assist effectively in the development of a reliable predictive model for structural dynamic investigations.
4. Validation of the accuracy and efficiency of superelement based model updating is carried out from three sets of results of natural frequencies and mode shapes derived from full finite element model, experiment and superelement based model updating. On top of that the expenditure of CPU time is taken into consideration in the validation as well.

1.4 List of publications

- ABDUL RANI, M. N. A., STANCIOIU, D., YUNUS, M. A., OUYANG, H., DENG, H. & JAMES, S. 2011. Model Updating for a Welded Structure Made from Thin Steel Sheets. *Applied Mechanics and Materials*, vol. 70, pg. 117-122.

- YUNUS, M. A., RANI, M. N. A., OUYANG, H., DENG, H. & JAMES, S. 2011. Identification of damaged spot welds in a complicated joined structure. *Journal of Physics: Conference Series*, vol. 305, no. 1, pg. 1-10.

1.5 Thesis outline

This thesis consists of seven chapters covering introduction, literature review, experimental modal analysis of structure, finite element modelling and model updating of the substructures, finite element modelling and model updating of the welded structure, substructuring method based model updating of the welded structure, conclusions and future work.

Chapter 1 gives an overview of the introduction, the goal, objectives and scope of research.

Chapter 2 reviews previous work in the field of finite model updating, substructuring modelling schemes, superelement model updating, modelling spot welds, model updating of spot welds and also the effect of initial curvatures and initial stress towards the accuracy of natural frequencies.

Chapter 3 covers comprehensive experimental modal analyses of substructures and the welded structure in which experimentally derived results, natural frequencies in particular are used for updating the finite element models. These include addressing the problems encountered in characterising the natural frequencies and modes shapes of substructures and of the welded structure and also highlighting several important factors in ensuring the accuracy of the results calculated such as the number of measuring points and accelerometers, the weight of accelerometers, method of support and method of excitation have been briefly discussed and are successfully used.

Chapter 4 presents the finite element modelling and model updating procedures. These include elaborating the formulation used in finite element method, model updating and the description of Design Sensitivity and Optimization SOL200 provided in NASTRAN. This chapter also covers the development of finite element models of the substructures through which model updating methods are performed to minimise the errors introduced in the finite element models. Iidentifying the source of discrepancies is the most challenging aspect of the updating process. This chapter reveals that the inclusion of the PELAS as one of the updating parameters could result in a dramatic reduction in the first frequencies of the bent floor. This chapter also discusses that the consideration of the thickness reduction in the backbone leading to more representative models of the stoppers for model updating process.

Chapter 5 discusses the work of finite element modelling and model updating of the welded structure. The construction of the finite element model of the welded structure is based on the updated finite element models of the substructures (structural components). This chapter also discusses how the combination between the sensitivity analysis, the inputs of the technical observation and engineering judgment has proved to be a powerful tool for localizing the main sources of the errors which are the boundary conditions and initial stress. The combination has led to the significant reduction in the discrepancies, dropping from 26.44 to 7.30 percent in total error, between measured and predicted frequencies. The outstanding capability of CWELD elements in ELPAT format over ALIGN format in representing spot welds is elaborated and demonstrated in this chapter. Another significant finding in this chapter is that a methodology which is using bending moment of inertia ratio is proposed for model updating in the presence of initial stress and initial curvatures on the structure.

Chapter 6 elaborates the construction and the use of substructuring or superelement based model updating (SEMU) in an attempt to reconcile the finite element model with the tested structure. Apart from that it discusses the problem of linking the superelements together using the nodes that define CWELD elements (branch element) as the boundary nodes that connect a substructure with another

substructure or a residual structure, a process which gives modal solution for the structure. This chapter also stresses that the use of normal procedure for assembling superelements together via the nodes of CWELD elements in ELPAT format as the boundary nodes fails in arriving at a satisfactory solution. On top of that this chapter reveals that SEMU has been successfully used for the reconciliation of the finite element model with the tested structure of the welded structure and stresses the use of branch elements, the efficient settings and the augmentation (using residual vectors) in SEMU is of the essence of the success. Another outstanding findings in this chapter is that SEMU has proven capability of accurately minimizing the uncertainties in the finite element model in comparison with the full finite element model and SEMU has also shown better efficiency in dealing with the analysis involving a large number of iterations.

Chapter 7 presents the overall conclusions, suggestions and recommendations for future study. This includes suggestions of the type of structures and joints to be used and also of another substructuring modelling scheme to be considered for the future work.

Chapter 2

Literature Review

2.1 Introduction

The efficient methods for the numerical prediction of dynamic characteristics of large, complex structures have been the subject of much investigation in the scientist and engineer communities. The finite element method has become the predominant method for numerically predicting structural behavior and the results obtained are very useful for virtual product development. Nonetheless, constructing accurate finite element models for modern structures which are usually large and complex is not an easy task (Friswell and Mottershead, 1995). This is because the sort of structures requires a very large number of degrees of freedom to be accurately modeled and the accuracy of the methods improves as more elements are used (Cook, 1989).

A large number of research works, among them (Walz et al. 1969; Good and Marioce, 1984; Mares and Mottershead, 2002; Burnett and Young, 2008 and Weng, 2011) revealed that the detailed finite element models were not capable of demonstrating the behaviour of the tested structures. This is because the approach of the finite element predictions to the characteristics of the tested structures is governed by the initial assumptions used in the construction of the mathematical models. In other words, the accuracy of the finite element results highly depends on the reliability of the assumptions which have different sources of errors. Thus, totally relying on the predicted results in advancing the investigation of designated solutions of structures would only decrease the confidence in the study. Therefore, validation and improvement in the accuracy of the predicted results should be carried out with the respect to the experimental results.

For the predicted results of finite element models to correlate as closely as possible with the measured results, systematic adjustments must be made to minimise the errors introduced to the models. The finite element model updating method has become the accepted method for the reconciliation. Structural model updating methods (Mottershead and Friswell, 1993) have been proposed to reconcile the finite element results with the measured results. There are many different methods of model updating, and the most predominant one is the iterative method so is the direct method.

The method has the advantage of allowing the updating parameters of finite element models to be updated during the reconciling process at every iteration. However, the optimisation algorithm (which is a gradient based method) used in the model updating in this project requires repeated computations of the finite element models. Using these conventional methods, the number of reanalyses during the solution process may be reduced but it is necessary to calculate repeatedly the response derivatives or the sensitivity coefficients. Therefore, when these conventional methods are applied to a modern engineering structure which is in the form of an assembly of several large substructures that consists of a very large number of components, with many unknowns, obviously, these methods are often perceived to be inefficient and computationally burdensome.

Substructuring synthesis schemes have been widely used for model reduction purposes. The application of the schemes in improving the computing efficiency, especially the structural dynamic analysis, has been successfully demonstrated in several high- profile engineering fields such as aerospace, automotive and civil engineering (Craig and Chang, 1977; Bennur, 2009 and Weng et al., 2011). In the schemes, large, complex structures are treated as assemblies of substructures by dividing the main structures into several substructures. This allows the investigations of the individual substructures to be carried out separately either by different design groups or different collaborating companies.

The substructuring schemes are obviously outstanding in a situation in which optimisation is merely required for a particular substructure. This distinct advantage is clearly seen when modifications are only performed on the particular substructure. Only the system matrices of the affected substructure are to be reanalysed while other substructures' system matrices remain intact (Perera and Ruiz, 2008). This leads to tremendous reduction in the expenditure of computational time in comparison with the conversional method of optimization in which full finite element models are used.

In this chapter, previous works in the domains of structural modelling, finite element model updating methods, structural joint modelling and substructuring schemes are reviewed and discussed especially those associated with the most popular methods for model updating, substructuring and spot weld modelling. At the end of this chapter the type of model updating, spot weld modelling and substructuring that have been studied in this work are drawn with concise conclusions.

2.2 Structural modelling

Rigorous mathematical solutions of engineering problems are not always possible available. In fact, analytical solutions can be obtained only for certain simplified scenarios. For problem involving complex material properties, loading, and boundary conditions, the engineer introduces assumptions and idealizations deemed necessary to make the problem mathematically manageable, but still capable of providing sufficiently approximate solutions and satisfactory results from the point of safety and economy. The link between the real physical system and the mathematically feasible solution is provided by the mathematical model which is the symbolic designation for the idealised system including all the assumption imposed on the physical problem.

An approximate approach involving discretisation of structures into a potentially large number of elements, whose behaviour is known, came to prominence in the late fifties (Kamal et al., 1985). The approach which is so called the finite element method (FEM) allows the stiffness and mass distribution of a structure to be described in matrix terms with rows and columns representing the active degrees of freedom. The term finite element was firstly used by Clough (1960) in 1960. The finite element method has become the predominant method of analysing structural performance. However, this method offers many choices that require engineers to make the decision in the construction of finite element models.

The estimation of the properties of material and geometric performed by engineers usually has a high tendency towards the use of textbook values and the initial design rather than the measured data. As such, therefore, the predictions of structural performance based on the finite element models are not flawless. In fact Maguire (1995) discovered that large variations in the predicted results of structural dynamic behaviour obtained from a number of finite element models of the same structure constructed by different engineers. The same issue of the inaccuracy of the predictions was elaborated by Ewins and Imregun (1986). Actually there are several factors that can be identified as being responsible for the inaccuracy of predictions in structural dynamic behaviour. These principally include:

- mis-estimation of structural material properties
- inaccurate modelling of structural geometry
- inaccurate modelling boundary conditions and loads
- poor choice of element type and quantity required
- difficulty in modelling complex structural systems, the most common and widespread being the pitfalls in the modelling of structural joints

Further errors in the prediction of dynamic characteristics of finite element models can arise due to model reduction. This is undertaken for finite element models of large, complex structural systems with very large numbers of degrees of freedom to reduce the size of the matrices of mass and stiffness.

2.3 Finite element model updating

The elimination of some errors in the finite element models seems to be impossible even though well rounded selection of data including the use of practical and measured parameters in the process of constructing the finite element models is used. For the success of construction of reliable finite element models, comparative evaluation of both the predicted results and measured results is vital because the results of the comparison provides some insights into the likely sources of errors in the finite element models. The requirement to improve the finite element models derived results with respect to those obtained from the tested models is a part of the model correlation process. There are many techniques that have been developed through which the finite element models of structures are adjusted by varying the parameters of numerical models to fit the experimentally measured data.

In this day and age, the reconciliation of finite element models with tested structure has become universally accepted method for constructing reliable finite element models through which the dynamic behaviour of structures can be fully investigated and significantly improved. The process of adjusting finite element models exits in a range of techniques. The simplest one can be performed by simply changing the values of model parameters of the finite element model, re-running the analysis and comparing the updated results with the measured results. These repetitive processes may be stopped once a required correlation has been achieved. Nevertheless, this type of finite element model adjustment significantly poses a challenge to the engineer not only to assess the level of improvement in the finite element model but also to ensure the rationale behind the changes made to the finite element model. On top of that, this trial and error approach seems to be inefficient because firstly a large of amount of unnecessary repetitive processes is required for the correlation and secondly this approach highly depends on the individual skills and intuition in the classification of the source of errors in the finite element model.

In an era dominated by high technology, demands on the accuracy in predicting structural dynamic performance of large and complex structures, in particular in automotive and aerospace industry for safety and economic benefits, are surging. With increasing size and complexity of the structures involved, as a result, model updating has become more difficult to efficiently perform. Therefore systematic and efficient approaches are necessary. In the past few decades, vigorous effort has been made in order to improve the correlation between analytical model of structures and measured data through the application of modal data. One of the earliest attempts was published by Rodden (1967) who identified the structural influence coefficients via the application of measured natural frequencies and mode shapes of an effectively free-free ground vibration test. While Berman and Flannelly (1971) were among the first authors who presented a systematic approach through which the improvement of stiffness and mass characteristics of a finite element model was performed. The improvement was only achieved through the mass matrix, but not through the stiffness matrix because in this case it did not resemble a true stiffness matrix.

Assuming that the mass matrix is correct in his proposed method, Baruch (1978) used Lagrange multipliers to update the stiffness matrix by minimising the discrepancy between the updated and analytical stiffness matrices. The same approach was employed by Berman and Nagy (1983) to updated the mass matrix of a large analytical model. However for the updated stiffness matrix, two additional constraint equations were included. Wei (1980) and Caesar (1986) used the same approach proposed by Berman and Nagy (1983), for the investigation of the robustness of variations of these methods including looking into the possibility of the methods to be used to affect structural changes and the applicability to be used in small and banded matrices only. It appears that all the aforementioned methods require no iteration in order to satisfy the desired matrices to all the constraint equations.

The initiation of the development of model updating algorithms began in the 1970s as a results of increasing reliability and confidence in measurement technology. The iterative methods through which analytical models can be reconciled with measured data have become of interest to researchers since. Collins et al. (1974) formulated and demonstrated a method for the statistical identification of a structure. Through the proposed method they maintained the specific finite element character of the model and used values of the structural properties originally assigned to model by the engineer as the starting point. The original property values were modified to make the model characteristics conform to the experimental data.

Chen and Garba (1980) considered more measurements than parameters in computing the new eigenvalues and eigenvectors of the spacecraft structure by introducing extra constraints to turn the parameter estimation problem into an over-determined set of equations. Dascotte and Vanhonacker (1989) discussed and demonstrated the results of the updated analytical model that achieved through the application of the eigensensitivity approach using weighted least square solutions. The drawback of the suggested approach is that engineering intuition and judgement are required to determine the proper value of the weights.

In recent years, modal updating based on optimisation scheme has become one of the predominant approaches used in automotive industry. This approach allows a number of model parameters to be systematically adjusted with respect to the measured modal parameters in order to minimise the objective function defined. The adjustment of the model parameters are performed iteratively in which perturbation to the model parameters is altered at each iteration with respect to the objective function. While the objective function is defined in the form of the differences in modal parameters between the predicted and measured results. There are several papers that extensively discussed and demonstrated the results obtained from model updating using optimization approach.

For example Zabel and Brehm (2009) suggested that the selection of appropriate optimization algorithm for particular analysis problem is essential. This is to avoid presenting the issue of local extrema in the objective function defined. On top of that, they also concluded that the objective function has to be sensitive to updating parameters which requires a certain smoothness. Model updating based optimisation scheme was tested by Bakira et al. (2007) on a finite element model of actual residential multi-storey building in Turkey and successfully used the scheme to detect and localise the damage on the building.

Generally, frequency-domain model updating can be mathematically categorised in two groups, firstly direct methods and secondly iterative methods. Usually the former tends to have low computational expenditure, however, the updated models do not always represent physically meaningful results (Friswell and Mottershead, 1995). On the other hand, the latter requires higher computational effort due to repeated solutions. The updated models via iterative methods will always represent physically meaningful if their convergence is achieved (Caesar, 1987). A good introduction on the subject was presented by Imregun, (1992), including a discussion of practical bounds of the algorithms in general terms. Furthermore mathematical approach and comprehensive surveys, were presented by Natke (1998), Imregun and Visser (1991), Mottershead and Friswell (1993); Natke et al. (1995). The latest survey was given by (Mottershead et al., 2010). Meanwhile a comprehensive textbook on finite element model updating is available in Friswell and Mottershead (1995).

2.3.1 Direct methods of finite element model updating

The earliest generation of algorithms produced the methods often referred to as direct methods. These methods can be directly employed by taking derivatives with respect to structural system matrices to be updated and the updated system matrices are obtained in a single step. The resulting updated structural system matrices will reproduce the measured data exactly and lead to imperfect analysis results if the updated model is used for succeeding analysis. The unavoidable phenomenon

happens because the updated system matrices lose their original characters from being sparse and only contain non zero elements in a band along the leading diagonal to a fully populated and also reflected little physical meaning. None of the direct methods, however, gives particularly satisfactory results as the updated structural system matrices have little practical value. Baruch (1978) and Berman and Nagy (1983) are the first advocates who employed these methods. However, Mottershead and Friswell (1993) in their survey mentioned that Berman concluded that it is impossible to identify a physically meaningful model through a direct approach.

On top of that, these methods require a very high quality of experimental data which seems to be completely difficult to achieve for complex structures. Therefore iterative methods or optimization methods have great advantages that outweighs all the drawbacks of direct methods. The following section outlines iterative methods which are the methods used in this research work. None of direct methods have received general acceptance, due to certain shortcomings, although many have been successfully applied to specific problems. A review of the previous research and existing procedures can be found in Allemang and Visser (1991); Maia and Silva (1997) and Dascotte (2007).

2.3.2 Iterative methods of finite element model updating

The main idea of iterative methods is to use sensitivity based methods in improving the correlation between the predicted and measured eigenvalues and eigenvectors. This is because sensitivity based methods have capability of reproducing the correct measured modal parameters. Almost all sensitivity based methods compute a sensitivity matrix by considering the partial derivatives of modal parameters with respect to structural parameters via truncated Taylor's expansion (Imregun and Visser, 1991). The variation of analytical response due to parameter variations can be expressed as a Taylor's series expansion limited to the first two terms

$$\mathbf{Z}_m = \mathbf{Z}_j + \mathbf{S}_j \left(\boldsymbol{\theta}_{j+1} - \boldsymbol{\theta}_j \right) \tag{2.1}$$

where $\mathbf{Z}_m$ is the vector of measured data involving eigenvalues or eigenvectors, $\mathbf{Z}_j$ is the vector of analytical response at j^{th} iteration and $\boldsymbol{\theta}$ is the vector of structural updating parameters which probably belong to one of these: geometrical and material properties or boundary conditions. The application of structural updating parameters has been thoroughly discussed and demonstrated in chapter 4, chapter 5 and chapter 6. $\mathbf{S}$ in Equation (2.1) are the eigenfrequency sensitivities which can be calculated from Equation (2.2).

$$\frac{\partial \lambda_i}{\partial \theta_j} = \boldsymbol{\phi}_i^{\mathrm{T}} \left(\frac{\partial \mathbf{K}}{\partial \theta_j} - \lambda_i \frac{\partial \mathbf{M}}{\partial \theta_j} \right) \boldsymbol{\phi}_i \tag{2.2}$$

The solution vector in Equation (2.1) is obtained by solving the vector of structural updating parameters $\boldsymbol{\theta}$. The resulting parameter changes are used to calculate the structural system matrices of mass and stiffness yielding a new eigensolution which matches the measured data more closely. The calculation is iteratively carried out until the target modal properties are satisfactorily achieved.

The relative merits of iterative methods of finite element model updating when used in practical application examples was demonstrated by Dascotte (1990) in which real-life structural dynamic problems were solved by characterising and optimising the properties of material and geometry. Link (1990) presented the classification of possible error sources in analytical models and discussed their influence on the accuracy of predicted results. In addition, he also presented the guidelines for identifying the source and the location of errors prior to performing model updating. David-West et al. (2010) applied the method for updating a thin wall enclosure and the updated model showed good correlation with the experimentally derived data.

Joints, that are used for joining structural components of a body-in-white are not only important for the integrity and rigidity of the assembled structural system but they are also highly susceptible to damage because of operational and environmental issues. The capability of iterative methods based model updating in damage identifications was demonstrated by Fritzen et al. (1998), Abu Husain et al. (2010a) and Yunus et al. (2011) . However, uncertainties in finite element models and measured data could limit the success of the method (Friswell et al., 1997). Model updating of joints was studied by Palmonella et al. (2003); Abu Husain et al. (2010b) and also Abdul Rani et al. (2011) in which the results and discussion of the latest updated model can be referred from chapter 4, 5 and 6.

It is imperative to stress that the structure identification and damage detection of joints require updating local information. Therefore, whatever type of design parameters representing local features, especially those of large, complex structures, the conventional iterative methods are very difficult to be utilised to reconcile the finite element model with tested structure. In these particular problems, Component Mode Synthesis (CMS) has always superseded the conventional model updating methods that use, in practice, full finite element models.

2.4 Structural joint modelling

Whatever types of joints are used for joining automotive structural components, the significant effect of joints on structural stiffness and the consequent dynamic characteristics on the other hand are the issues of chief concern to engineers. These important issues can be due to a variety of structural design considerations. For example, a fundamental design consideration for an automobile is the overall dynamic behaviour in bending and torsion (Kamal et al., 1985).

Experience has shown (Maloney et al., 1970 and Ewins et al., 1980) that many of the joints commonly used on structures to serve design requirements can result in substantial and often unpredictable reductions in the stiffness of the primary structure. On top of that, in the absence of reliable analysis methods for estimating joint effects on structural stiffness and dynamics, a common practice is to rely on experimental data for definition of the joint properties. The shortcoming of this approach, however, is that data obtained for a particular type of joints on a given structure often cannot be confidently extrapolated in different structure designs or even, in many cases, to a different location on the same structure. Therefore, simple and reliable modelling of joints that are be able to deliver accurate results of any analysis interest is necessary.

A recent advancement in technological changes has made the automotive component modelling easier and faster. However, developing a simple and reliable model of joints is one of the chief difficulties in constructing a concept model of a vehicle. A simple and reliable model of joints is crucially required by engineers in order to construct complex structures that usually have a large number of joints. Realising this issue which has been of central important since 1970, a large effort has been made either by creating new methods or improving and enhancing theoretically the existing methods or applying the available methods with the combination of other methods systematically.

2.4.1 Bolted joint modelling

Bolted joints are one of the joint types for connecting structural components. Being easily dissembled, maintained and inspected has made bolted joints become one of the prevailing joint types in practical work of engineering industry. On the other hand, this type of joints has many complexities such as pretension, nonlinear frictional behaviour, etc., which are very difficult to investigate and compute yet important for joints (Ouyang et al., 2006). As a result, bolted joint modelling will be a major challenging problem for engineers. A large amount of research work on joints has been carried out by scientist and engineer communities since 1970. They

have tried to understand the characteristics of joints and to simulate their findings into analytical modelling. Whatever findings they have made so far, in fact, one point is certain that, joints are the important components on assembled structural systems because they significantly affect, in some cases or even dominate the static and dynamic behaviour of structures.

Attempts to understand and investigate the behaviour of joints have been carried out by several authors. Among them, Chang (1974) demonstrated and discussed the importance of joint flexibility on the structural response analysis. Through the static analysis, he discovered that the structural response was significantly sensitive to the level of joint stiffness. On the modelling work, Rao et al. (1983) had improved modelling techniques and determined joint stiffness based on an instantaneous centre of rotation approximation. While Moon et al. (1999) developed a method for modelling joints and calculating the stiffness value of joints by using static load test data. In the investigation carried out by Rao et al. (1983) and Moon et al. (1999) they used rigid and rotational spring joints, however, good dynamic analysis results were achieved through the latter. Friction behaviour that is inherent in bolted joints is complicated and is a nonlinear phenomenon. To try to have understanding of the phenomenon at reasonable computational work load, Oldfield et al. (2005) used Jenkins element or the Bouc-Wen model to represent the dynamic response of finite element model. The results calculated from the proposed simplified models showed very good agreement with those calculated from a detailed 3D finite element model.

For the friction laws of bolted joints and modelling issues of bolted joints Gaul and Nitsche (2001) provided an extensive source of information. Kim et al. (2007) investigated a modelling techniques for structures with bolted joints by introducing four types of finite element models which are a solid bolt model, a coupled bolt model, a spider bolt model and lastly is a non-bolt model. The comparison of analysis was performed with the consideration of pretension effect and also contact behaviour. It was found that the most accurate model was the solid bolt model and the most efficient model was the coupled model. Another good source of comprehensive information on bolted joints, particularly in the issues pertaining to

structural dynamics with bolted joints, such as the energy dissipation of bolted joints, linear and non-linear identification of the dynamic properties of the joints, parameter uncertainties and relaxation, and active control of the joint preload were reviewed by Ibrahim and Pettit (2005). On top of that, they also covered the issues relating to design of fully and partially restrained joints, sensitivity to variations of joint parameters, and fatigue prediction for metallic and composite joints.

A common observation made in the studies of bolted joints was that the complexities of behaviour that are inherent in joints such as frictional contact, damping, energy dissipation, etc have made it difficult to ascertain and replicate them in finite element modelling. As a result, bolted joints are not always practical. The size and shape make them unsuitable for some structures for example a body-in white.

2.4.2 Welded joint modelling

Resistance spot welding (RSW) is one of the weld techniques. RSW was invented in 1877 by Elihu Thomson and has been widely used since then as a manufacturing process for joining sheet metal. RSW welding has been used for over 100 years in various industrial applications for joining a large variety of metals. RSW has a reputation for superior assembly technique over other joining methods, because it is faster and easier to operate, adaptable to automation and is also idealistic for mass production. RSW has been a dominant method for joining structural components, in particular in automotive industry. However, the process often produces high variability in weld strength and quality mainly due to current levels, electrode force, surface condition, material type and material thickness. It was found (Nied, 1984) that the variation of nugget size is greatly dependent on the material type and surface condition, while the variation of surface indentation is mainly due to the material and current. The nugget size and indentation increase with increasing current level. Decreasing the electrode force increases the nugget size but has no significant effect on the indentation. Figure 2.1 illustrates the resistance spot weld process.

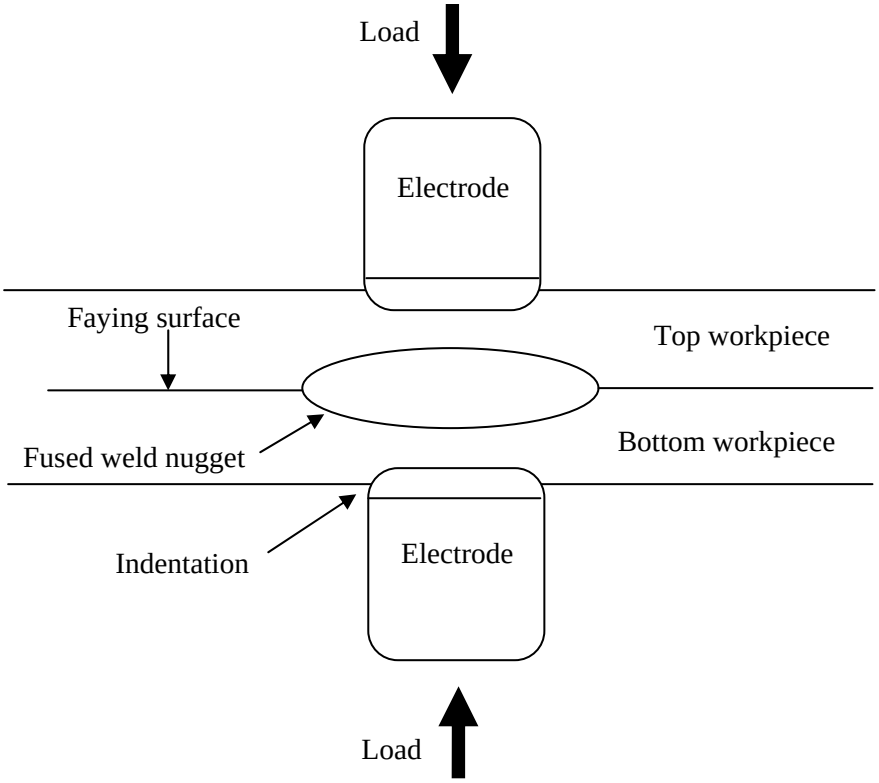

Figure 2.1: Illustration of resistance spot welding process

The dominance of RSW in the automotive structural assemblies can be seen on a typical body-in-white which contains a very large number of spot welds. Therefore, the reliability of the spot welds hence determines the structural performance of a body-in-white. Nevertheless, liked bolted joints, thorough characterization of spot weld behaviour is important and always of concern owing to the fact that the inherent behaviour of spot welds such as geometrical irregularities, residual stresses, material inhomogeneity and defects are difficult to replicate in finite element modelling (Mottershead et al., 2006). However, because of a large number of spot welds in automobile structures, it is often impractical to model each or every spot weld joint in details. Therefore reliable procedures and methods that could be used to represent spot weld joints in automobile structures in the simplest way have been of interest for the last few decades. In other words the simplified models should be able to deliver reliable results of any analysis interest.

In years before the 1980s, theoretical modelling of spot weld was not mature. For example, publications of theoretical modelling of the resistance spot welding in the decade of 1967 to 1977 were sparse (Nied, 1984). Consequently, most of research work on spot welded structures was carried out experimentally. By and large, the work was mainly focused either on the fatigue and the static strength of spot welds (Jourmat and Roberts, 1955 ; Orts, 1981 and Rossetto, 1987). However, since early 1990s numerous attempts have been progressively made to improve the previous approach by adopting numerical techniques for modelling spot welds. There is a large number of people who worked on this subject and some of them are Lim et al. (1990); Vopel and Hillmann (1996); Blot (1996); Heiserer et al. (1999); Palmonella et al. (2003); De Alba et al. (2009); Abu Husain et al. (2010b) and etc.

Modelling work associated with spot welds can be categorised into two major groups. The first category belongs to models for limit capacity analysis (Deng et al., 2000) and the second one belongs to models for dynamic analysis (Fang et al., 2000) which the application of ACM2 and CWELD model was reported to be the predominant approach for dynamic analyses in automotive industry (Palmonella et al., 2004). Due to the fact of the complexity of spot weld behaviour, the former requires a very detailed models which are important to capture stress concentrations and hence particular emphasis is placed on modelling sudden geometry changes.

On the other hand, these features are not all that important in models for dynamic analysis where the overall stiffness and mass play a much more important role in the determination of structural characteristics. Although the models for limit capacity analysis is an important issue in spot welds, however the topic will not be thoroughly reviewed as it is not the objective of this research work that focuses on spot weld modelling for dynamic analysis. Detailed information on the topic of models for limit capacity was elaborated and presented in several papers such as Chang et al. (1999); Chang et al. (2000); Deng et al. (2000); Radaj (1989); Radaj and Zhang (1995); Zang and Richter (2000);and Xu and Deng (2004); Roberto (2008) and Pal and Chattopadhyay (2011).

Study of dynamic characteristics of structures is usually treated as a global issue rather than a local issue owing to the fact that eigenproblem is typically a function of the structural mass and stiffness and of the boundary conditions as well. However, when it comes to investigating eigenproblem of welded structures, emphasis should not only be on modelling work of the structure but also be on spot weld modelling. This is because the properties and characteristics of spot welds play a significant role in the dynamic behaviour of welded structures. In other words, dynamic characteristics of numerical models of welded structures highly depend on the quality and reliability of spot weld model. The well accepted alternative method for modelling spot welds in the past few decades was to use coincident nodes approach through which the nodes were coincident at boundary between the welded components (Lardeur et al., 2000). However, since early 1990s single beam models have been commonly used in modelling spot welds in industries. Rigid bar and elastic rod element are categorised into these single beam models. They are used to connect between two nodes of adjoining meshed sheets and their descriptions of connection and usage are available in (MSC.2., 2010).

The advantages of single beam models are that they are more flexible in connecting nodes of congruent meshes and of non-congruent meshes. Pal and Cronin (1995) used rigid bars and elastic rod elements to model spot welds on a simple welded beam for investigating the effects of spot welds spacing on the dynamic behaviour of the welded beam that consists of hat and box welded together. They compared the finite element results with those experimentally observed. The results calculated from the former were unsatisfactory, while better improvement was seen in the results obtained from the latter. However, large deviations from the elastic rod elements based model were still observed in the comparison. Consequently, they used elastic solid element namely CHEXA for representing the spot welds and also concluded that the CHEXA element based model produced the best results of comparison to the experimental data of the welded beam. However, the model of the simple beam to which the CHEXA elements were connected, was developed using congruently meshed model which would become the necessary requirement if the type of element was chosen to represent spot welds.

Further demonstration of the application of single beam elements in representing resistance spot welds was performed by Vopel and Hillmann (1996) and Blot (1996). It was then followed by Lardeur et al. (2000) who also used single beam elements in studying the best predictive spot weld model for vibrational behaviour of automotive structure. The Investigation on spot weld modelling using single beam elements was continued by Fang et al. (2000). They demonstrated the numerical problems with spot weld connections modelled with single beam elements.

Meanwhile, Donders et al. (2005) particularly in one of the sections of their paper, discussed the accuracy of results calculated from spot weld connections modelled as single beam elements. However, none of the aforementioned attempts to use single beam elements to model spot welds had produced satisfactory results of dynamic behaviour of welded structures. Common conclusions made in their studies were that spot weld connections modelled as single beam elements would only produce unsatisfactory results in comparison with those experimentally observed and the drawbacks of single beam elements representing the physical spot welds lie in several factors. The factors were summarised by Heiserer et al. (1999) as follows:

- Shell elements with rotational stiffness are not strong enough to resist the rotations introduced by elements such as beams or springs. A singularity is introduced in the shell area. The model does not run without PARAM, K6ROT and PARAM, SNORM.

- Beam elements, or even worse, bar elements are used whose diameter is approximately 5 times bigger than their length. The main problem, besides the ill conditioned matrices, is the neglect of finite elements whose formulation is based on the assumption that their axial dimension is much bigger than their radial dimension.

CQUAD4 and CTRIA3 shell elements, only have five degrees of freedom, the sixth degree of freedom which is the rotational degree of freedom (R3) about a vector normal to the shell element at each GRID point (sometimes called the drilling degree of freedom), has zero stiffness. Therefore, PARAM, K6ROT defines a multiplier to a fictitious stiffness to be added to the out of plane rotation stiffness of CQUAD4 and CTRIA3 elements. For linear solutions (all solution sequences except SOLs 106 and 129), the default value for K6ROT is equal to zero and it can be defined in NASTRAN as PARAM, K6ROT, 0. In most instances, the default value should be used.

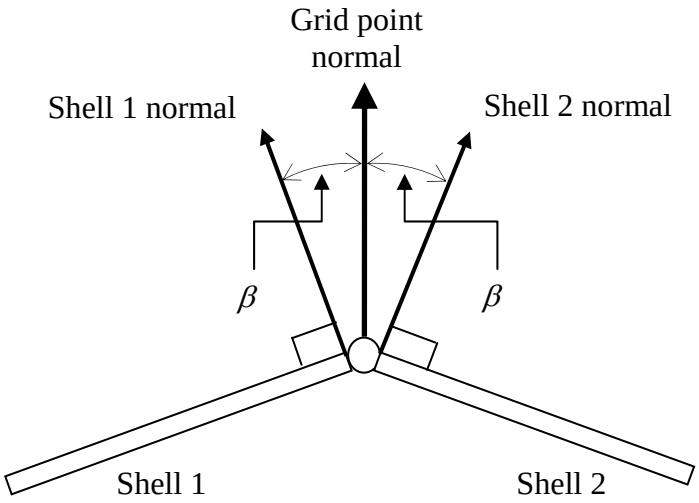

Figure 2.2: Unique grid point normal for adjacent shell elements

PARAM, SNORM defines a unique direction for the rotational degrees of freedom of all adjacent elements (CQUAD4 and CTRIA3). A shell normal vector is created by averaging the normal vectors of the attached elements. In this example, shell normals are used if the actual angle, β, between the local element normal and the unique grid point normal is less than 20 degrees (see Figure 2.2).

In linear solution sequences, the values of PARAM, K6ROT, 0 and PARAM, SNORM, 20 are recommended (MSC.5., 2004).

The pitfalls had attracted attention of a number of people to come out better ways of representing numerically physical spot welds. Heiserer et al. (1999) proposed another type of spot weld model namely Area Contact Model 2 (ACM2). The surface contact model was constructed based on HEXA solid element and RBE3 interpolation elements that were used to link the HEXA model with the nodes of shell elements. The advantages of this spot weld model is that it can be used for both limit capacity analysis and dynamic analysis. Another beneficial gain from the model is that it allows the model to be used for congruent and non-congruent component meshes.

The advantages of the model in several aspects have caused an attention to a large number of the people either from academia or industry to use it in their research and development work. For example, Lardeur et al. (2000) successfully used ACM2 to represent physical spot welds and predicted the dynamic behaviour of both academic welded structure and automotive welded structure in comparison with the measured results. Another good example of using ACM2 in predicting the dynamic behaviour of welded structure was performed by Palmonella et al. (2003). Apart from using ACM2 to represent the spot welds, they also demonstrated model updating work on the spot weld model and the effect of considering patch as updating parameter on the accuracy of the updated model. Meanwhile a compressive overview of ACM2 in term of the application of the model in NVH and durability analysis in automotive industry was give by Donders et al. (2005) and Donders et al. (2006). The effect of refinement of the welded structure meshes on the accuracy of the analysis results calculated from ACM2 was elaborated and presented by Torsten and Rolf (2007).

In contrast to ACM2 which was represented by HEXA solid element and RBE3, CWELD element that was proposed by Fang et al. (2000) and then was introduced by MSC. NASTRAN in 2001, is a type of spot weld model whose element is represented by a sheer flexible Timoshenko type element with two nodes at the end of element and 12 degrees of freedom. The properties of CWELD element that are required to be defined in representing physical spot welds are the diameter and the Young's modulus of spot welds. Since no additional material is involved in the spot

welding process, therefore the Young's modulus of parent material is used for that of CWELD element. Apart from being able to be used for connecting both congruent and non-congruent meshes, CWELD element also can be defined in three types of connections with five different formats:

- A Point to Point connection, where an upper and lower shell grid are connected. This type of connection can be defined with ALIGN format

- A Point to Patch connection; where a grid point of a shell is connected to a surface patch. This connection can be defined with format in ELEMID and GRID

- A Patch to Patch connection, where a spot weld grid GS is connected to an upper and lower surface patch. It can be defined with PARTPAT, ELPAT, ELEMID and GRID. However, ELPAT or PARTPART is the most flexible format in comparison with the other two.

It seems to be unnecessary for detailing something that can be easily obtained from and that is already available in the open literature. As such, the detailed explanation of CWELD element is available in Fang et al. (2000), MSC.5 (2004) and MSC.2. (2010). However, it is imperative to discuss which candidate of the three connections would produce more fruitful predictive spot weld models in NVH analyses in particular. Fang et al. (2000) demonstrated the application of three types of CWELD element connections in investigating the numerical problems with the modelling techniques of spot welds. They applied the modelling techniques of spot welds to two different types of connections which are a point to a point connection and a patch to a patch connection. They concluded that the former and latter connection had fulfilled two basic requirements for spot weld modelling. Both types of connections could be used for connecting non-congruent meshes and they also took the area of spot weld into account proving the ratio between the diameter of spot weld model and the size of mesh should be less than one. In other words, in order to avoid the stiffness of connection being underestimated, the diameter of spot weld model should not be bigger than the size

of patch which is normally 3x3 elements per patch. The same spot weld modelling technique was used by Palmonella et al. (2003) ; Palmonella et al. (2004) and Palmonella et al. (2005) for investigating and improving dynamic behaviour of a welded beam that is comprised of a hat and a plate welded together by twenty spot welds. CWELD elements with the type of connection of patch to patch were used to model the spot welds. The discrepancies between the initial model of the welded beam and the tested structure were assumed to be due to the invalid assumptions of the parameters of spot welds. In the investigation, they concluded that CWELD modelling technique showed a high capability of and the simplest method for representing spot welds. On top of that, the optimum size and also the Young's modulus of patch of CWELD element had play a significant role in improving the accuracy of the predicted results through the application of model updating.

The requirement of detailed finite element models highly depends on the type of analysis concerned. The more detailed the finite element models are the more elements on the models would there be and the much longer computational time is required. Therefore, the detail of finite element models is a trade-off between accuracy and expenditure of computational time. Owing to the fact, it is always to be a high desire for CAE engineers in automotive industry to have the same finite element model mesh for durability, crashworthiness and NVH analysis. However, the sort of the analyses, in practice, requires different finite element model meshes, especially crashworthiness analysis that needs detailed finite element models.

The key to good CWELD modelling is to have a reasonable degree of mesh refinement in the spot weld area. The size of mesh should not be too coarse or too fine as shown in Figure 2.3. For example in Figure 2.3 (a) the size of mesh is too large when compared with the size of the spot weld. In this case, CWELD cannot do any better because it only has one element either side to which to connect. Therefore, this configuration might be better with the ALIGN option with one pair of nodes of the elements moved to the centre of the spot weld. However, if the size of mesh is too fine as shown in Figure 2.3 (b), it is going to be problematic as well. This is because if the PARTPAT option is used, the CWELD search logic looks for elements of the same property in a bounding box defined by the diameter of the

spot weld (the D on the PWELD entry). Furthermore, if the ELPAT option is used to model the spot welds, the CWELD search logic looks for any elements connected to the elements that are defined on SHIDA/SHIDB which is in a bounding box defined by the diameter of the spot weld. However, the CWELD only ever connects a mesh of maximum 3 x 3 elements by expanding the search from the GA/GB intersection point with the shell mesh. This means that only a few elements in the centre of the patch as shown in Figure 2.3 (c) will be connected irrespective of the diameter defined on the PWELD entry.

As a result the correct stiffness of the spot weld cannot be obtained. This can be clearly seen in Figure 2.3(d) in which the red blob in the middle does not represent the correct stiffness of the spot weld. Meanwhile, Figure 2.3(e) shows the correct stiffness of the spot weld in which the red blob fills the circle with a much better fit than the one shown in Figure 2.3(d).

If ELPAT option is chosen to model the spot welds, the suitable ratio between the diameter of spot weld and the mesh size will be somewhere between two and three elements across the diameter of the spot weld as illustrated in Figure 2.3(e). However, it is imperative to stress that no more than 3 x 3 elements will be connected irrespective of the diameter.

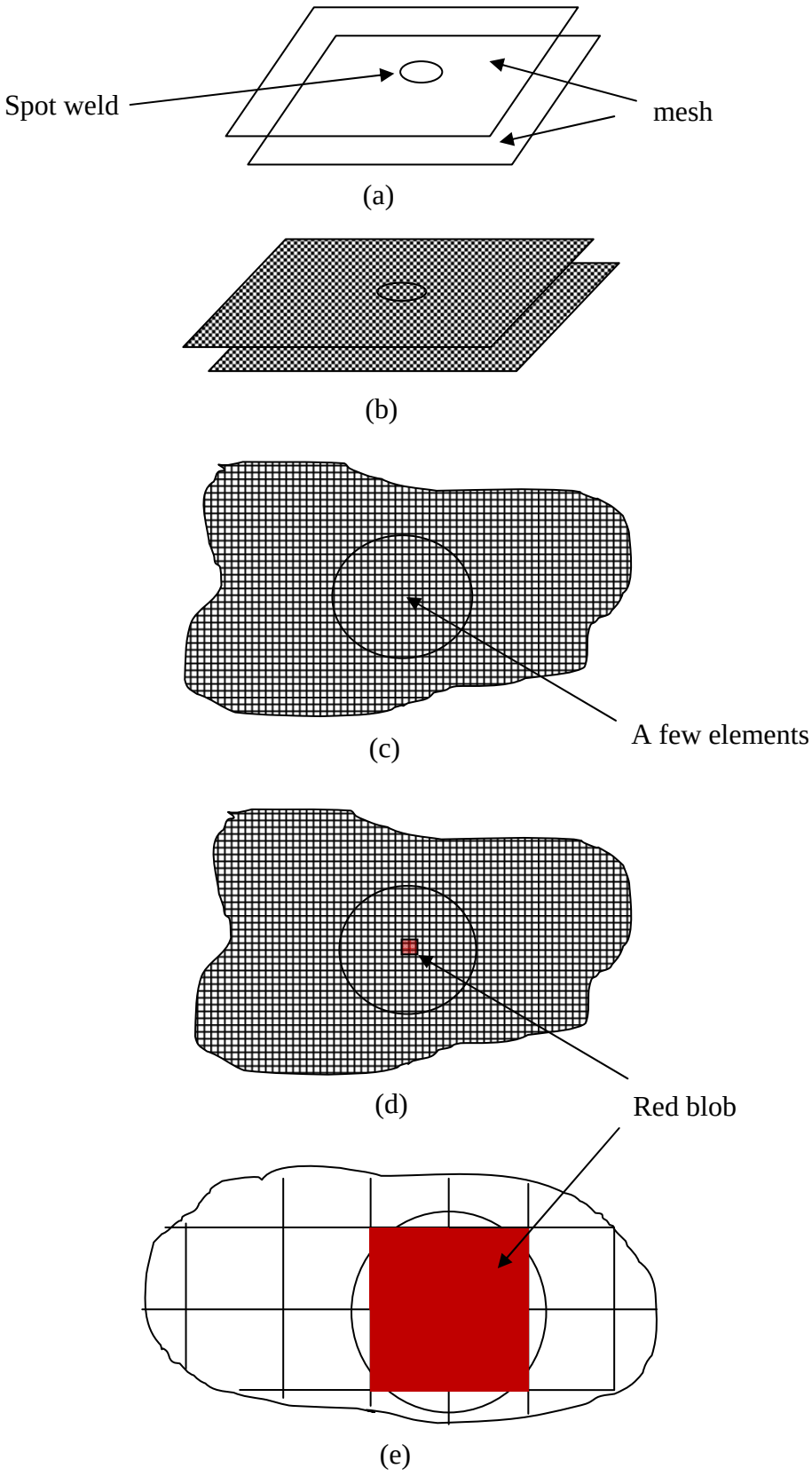

Figure 2.3: The size of mesh for CWELD element

Torsten and Rolf (2007) used a Volvo sidemember panel that has a significant contribution for crash safety for investigating the efficiency of CWELD element and ACM2 when the refinement of finite element model mesh of sidemember panel was taken into account. Three different sizes of finite element model meshes of 10mm, 5mm and 2.5mm were studied. The investigation revealed that CWELD element model was not applicable for the model mesh smaller than 5mm due to its functional limitation. On the other hand, ACM2 model had no additional loss of bending stiffness when the model was used for the patch area of model mesh of 10mm.

The work related to using CQUAD4 and CWELD elements in the development of finite element models was reported in Horton et al. (1999); Palmonella et al. (2004); Mares et al. (2005) and Palmonella et al. (2005). These papers merely dealt with model updating procedures for minimising the errors introduced in finite element models which are mainly due to the inaccurate assumptions of the properties of materials, elements and patches. However, a structure with a large surface area of a thin metal sheet is susceptible to initial curvature due to its low flexible stiffness or manufacturing or assembling errors. A survey of the literature on model updating shows that no work has been done which addresses big errors in finite element models due to initial curvature and/or initial stress.

Initial stress can arise when components are assembled either by means of welded or bolted joints. For a structure with a large surface of low thickness with initial curvature, stiffeners can be intentionally added to remove it and they may also unintentionally remove it. When the initial curvature is suppressed after addition of stiffeners, initial stress arises (Abdul Rani et al., 2011). Initial stress can also arise as a result of fabrication and heat treatment. However, such initial stress is very difficult to estimate by theoretical analysis or to measure, unless the unstressed configuration is first measured in the latter case, which is very rare in reality. In general, initial stress state is rarely completely known (de Faria and de Almeida, 2006). The influence of initial curvature and initial stress on the natural frequencies of structures was investigated and was found to be noticeable in Leissa and Kadi (1971), Fong (2003) and Yu et al. (1994).

Furthermore work on the effect of initial curvature was carried out in Yu et al. (1994). It was also pointed out (Yu et al., 1994) that finite element commercial software treats membrane and bending deformation as being independent and this approximation is only reasonable for structures with a small initial curvature and small deflection, however, for a moderate initial curvature and a small deflection the interaction between membrane and bending deformations should not be neglected. In order to minimise the discrepancies between the predicted results of the welded structure and experimentally observed, Abdul Rani et al. (2011) expounded the idea of including initial curvature and/or initial stress (which have a large effect on natural frequencies) as an updating parameter for improving the performance of the finite element model of a structure made from thin steel sheets with a large surface area.

In Abdul Rani et al. (2011) the investigation revealed that the key parameters, namely the properties of materials, elements and patches that have been widely used by many researchers for the improvement in the finite element models were found to be insufficient for improving the initial finite element model in the study. The cause for the discrepancy was discovered to be the initial stress arising in the welding process and a new updating parameter was used successfully in the end to produce very good results by the updated finite element model. They also suggested that structures with large spans (walls or floors for example) made from thin metal sheets are susceptible to initial curvature and/or initial stress and they should be accounted for in updating the finite element models of these structures.

Modelling work on bolted and welded joints has been reviewed in the present and preceding section. However, the review has been performed by focusing more on the topics of welded joints, especially resistance spot weld joints. The reviewing work reveals that the application of resistance spot weld joints has been a dominant method for joining components in comparison with bolted joints, especially in automotive industry due to flexibility, robustness and high speed of process combined with very high quality joints at very low cost.

Consequently, several modelling techniques of spot welds have been proposed in the past few decades. Among the modelling techniques of spot welds such as coincident nodes, single beam models, brick models, umbrella and ACM1 models, 1st Salvani model and 2nd Salvani model that have been proposed and tested (Palmonella et al., 2003), however, ACM2 and CWELD element models are the predominant spot weld modelling technique in industry (Palmonella et al., 2004). Those two models were either merely used for modelling or purposely used for updating welded structures as reported in the aforementioned publications. However, model updating work which requires the parameters of finite element model to be update in order to match with tested structure, will lead to, in practice, a dramatic increase in computational cost if the conventional updating method is used. Therefore, if the properties of spot welds and patches and also initial stresses / curvatures which are regarded as the local properties, are the only chosen updating parameters in updating finite element model, substructuring schemes are perceived to be an efficient technique for the aforementioned problem.

2.5 Dynamic substructuring and component mode synthesis

Analysis of internal loads is highly required for ensuring the successful design of structures, especially when the structure is placed in its operating environment. A vital part of this endeavour is the modal analysis of structural finite element models. Generally, in practice, normal modes and static analysis are performed directly from the finite element model. However, when it comes to analysing large, complex structures whose components are often designed and produced by different companies, it is often difficult to assemble the whole finite element model in a timely efficient manner. In addition, the finite element model of a large, complex structure which contains a very large number of degrees of freedom, can lead to a dramatic effect on computational time. Therefore, substructures of finite element models can be one of the efficient ways of solving the aforementioned issues.

Dynamic substructuring and component mode synthesis (CMS) have been recognized as powerful methods and they have been effectively used for analysing large, complex structures. The theory of the topic and its applications are contained in many references too numerous to list. However, the work by De Klerk et al. (2008) who comprehensively reviewed the topic, Craig (1981); Qu (2004) and Craig and Kurdila (2006) who wrote textbooks on the topic are good sources of references. Other interesting reviews, in particular of CMS methods are available in O'Callahan (2000) and Craig Jr (2000).

In practice, whatever type of analysis concerned using substructuring and CMS methods, a common observation made in these methods are :

- It permits the investigation of dynamic characteristics of large, complex structures that contain a number of substructures to be independently carried out either by different groups of engineers or different companies.

- It permits the dynamic local behaviour of substructures to be more easily and quickly identified than when the whole structure is analysed. This advantage is useful for optimisation work because only the modified substructures are to be re-analysed while the other substructures remain intact. In addition, optimisation work would be computationally expensive if the whole structure is considered. Performing optimisation work using substructuring and CMS techniques with the attempt to minimise the discrepancies between finite element model and tested structure is one of the chief objectives of this study.

- It permits the combination between numerical or analytical models and experimentally determined models.

- It permits the combination of substructures from different groups of engineers or different companies .

It is learnt that the papers in Hurty (1960) and Hurty (1965) had activated the idea of developing dynamic substructuring as reduction techniques. In between the years of 1960 and 1965, Gladwell (1964) developed a method namely branch mode method in which a number of components may be divided into several branches and the branches are formed into two main stages. These aforementioned methods were analogous to and soon known under the name of component mode synthesis (De Klerk et al., 2008). The efficiency and effectiveness of dynamic substructuring and component mode synthesis, particularly in dealing with analyses involving large, complex structures were noticed by the scientific and engineering communities. The topic soon become an interesting topic in the field of structural dynamics. A large effort was taken by the communities for the development of the existing techniques. In the late 1960s and 1970s some chief developments were seen in the existing techniques. Craig and Bampton (1968) suggested that all constraints at the boundary degrees of freedom could be regarded as boundary constraints and there was no need to identify rigid-body modes specifically in comparison with the procedure proposed in Hurty (1965) that required a sharp distinction between determinate and indeterminate constraints. The procedure proposed by Hurty (1965) was difficult to apply as the boundary degrees of freedom were required to be partitioned accordingly. Therefore, Craig and Bampton (1968) method in which reduced matrices are nearly diagonal so that it leads to an efficient implementation in finite element, has remained the most popular and widely used for substructuring technique in structural dynamics (De Klerk et al., 2008).

In Craig and Bampton (1968) method, the constraint modes were defined as the mode shapes due to successive unit displacements at the boundary degrees of freedom, all other boundary degrees of freedom being totally constrained. In addition, they discussed the substructure in terms of a finite element model, instead of a distributed one, which permitted a ready identification of the constraint displacements as nodal displacements at the boundaries. On the other hand, the interior modes were simply the normal modes of the substructure with totally constrained boundary degrees of freedom.

MacNeal (1971); Rubin (1975) and Craig and Chang (1976) introduced free-interface methods in which attachment modes including residual flexibility attachment modes and inertia relief attachment modes were to represent the internal dynamics of the substructures. Substructuring synthesis techniques that use modes to represent the dynamic behaviour of substructures, have gained popularity among the engineering communities as a reduction technique for finite element models. However, there are a lot of methods that have been developed for representing the modes. The variants of substructuring synthesis techniques differ in the procedures adopted in defining component modes which are used to approximate the physical space. For example, using different component modes to establish reduction basis which can be used for better approximating the dynamics of substructures have been proposed by many authors.

Gladwell (1964) proposed branch method in which the complete problem was divided into two stages. At first, certain sets of constraints were imposed on the system and certain sets of principal modes of the constrained systems were calculated. In the second stage the calculated modes were used in a Rayleigh-Ritz analysis of the whole system. Shyu et al. (1997) and Shyu et al. (2000) who employed quasi static modes in replace of static modes for capturing inertial effects of the truncated modes. The method was ideally suited for mid band frequency analysis in which both high frequency and low frequency modes were omitted.

Because there are a number of difficulties associated with fixed boundary modal testing, in some cases making the approach impractical to be adopted, Chandler and Tinker (1997) introduced a method for measuring and computing the substructure. The method required known mass additive to be attached to interface of the substructure. The proposed method worked very well for a system with nearly determinate substructures and relatively stiff interface support structures. However it didn't work well for a structural system having flexible and highly indeterminate component interfaces.

Craig and Hale (1988) employed a new method which is based on the concept of a block-Krylov subspace for generating component normal modes of substructures. The new Krylov vectors were found to require less computation than component normal modes. However, because of the disturbability and observability properties, the proposed method was claimed to be particularly suited to applications requiring high-fidelity reduced-order models. One such application area was that of large space structures.

Recently scientist and engineering communities have realised that the great potential of extending modal truncation vector (MTV) in a dynamic substructuring technique which is particularly the use of MTV in Craig-Bampton model. The theoretical work and technical discussions on this topic can be found in Dickens and Stroeve (2000) and Rixen (2001). The application of MTV in Craig-Bampton model of a large structure was presented in Rixen (2002b). He concluded that the resulting reduced matrices exhibited the same quasi-diagonal topology as in the standard Craig-Bampton method. In addition, the application of MTV led to significant reduction in the force residual associated with the global eigenmodes of the reduced model and also provided more accurate stresses when used in dynamic analysis.

It is imperative to note that the application of component mode synthesis techniques for reducing large, complex structures into new computationally and experimentally manageable substructures as demonstrated in Hurty (1960), Hurty (1965) and Craig and Chang (1977). The important spinoffs of the techniques can be effectively extended to modal updating methods particularly iterative model updating methods which normally employ optimization techniques that are used to calculate eigensolutions and associated sensitivity matrices of the finite element models iteratively (Bakira et al., 2007).

The economical benefits of component mode synthesis techniques in model updating work have attracted the scientist and engineering communities (Zhang and Natke, 1991; Link, 1997 Biondi and Muscolino, 2003; Masson et al., 2006; Cerulli et al., 2007) to use the coupling techniques in the reconciliation between the

finite element models and the tested structures. The substructuring synthesis techniques discussed and presented in the preceding paragraphs basically have the same general ideas, however, in fact, substantive differences exist. Therefore, the chief aspect of the success of substructuring technique application is the selection of modes and its effect on the eigenvalue error. The Craig-Bampton component mode synthesis methods which have become the most popular and been widely used by a large number of scientists and engineers for structural dynamic characterisation was reported to possess the better capability of dealing with a complex assembled system that consists of a large number of substructures (Vorst, 1991). In addition, the Craig-Bampton CMS models which are based on fixed boundary modes and constraint boundary modes are straightforward formulating procedure and easy to be efficiently used in computer resources. The most attractive idea of the Craig-Bampton CMS is that it uses essentially reduced order superelements. Its capability has already been formularised in MSC. NASTRAN (MSC.4., 2001).

The application of the Craig-Bampton CMS methods in structural performance investigations in aerospace, automotive and civil engineering fields were reported by many authors (Cerulli et al., 2007; Bennur, 2009; Papadioti and Papadimitriou, 2011 and Liu et al., 2008) and the types of structures and analyses involved and of concern in their investigations, in practice, are large and complex ones. In addition, those types of structures that consist of a number of substructures, usually have a very large number of joints which have a significant contribution to the stiffness and dynamic behaviour of the structures. It was reported that in structural dynamic analysis, the issues associated with the inaccuracy of modelling work on joints due to the invalid assumptions in the initial models, could be efficiently dealt with using substructuring schemes (Good and Marioce, 1984 and Link, 1998). These schemes allow to be incorporated with model updating and their combination offers high capability of correcting the invalid assumptions of the initial models by concentrating on certain affected areas of substructures rather than the whole structure. However, most of the works on substructuring schemes described in the open literature have been directed to proposing and investigating new component modes of substructures. On top of that most modelling work via the application of

the schemes has only been directed to assembling the substructures using the nodes of the model elements rather than the nodes of joint elements. In fact, in practice, most of large, complex structures are the assemblages of substructures in which joints (regardless of what types) (welded, bolted and riveted joints) are used as the means for assembling the substructures. In all the publications cited (for example, Good and Marioce, 1984; Link, 1998; Cerulli et al., 2007 and Bennur, 2009), the nodes of elements of the substructure models were selected as the interface nodes, while the nodes of joint elements which have a high potential to be the alternative interface nodes were completely neglected.

In certain practical cases, where the confidential and proprietary issues of modelling work are of concern between the collaborating companies, in which the finite element models of the substructures could not be revealed and only the condensed matrices of the substructures are used instead, the areas of the substructures having fewer number of interface nodes would always be the first choice as the interface nodes. For welded structures, therefore, the nodes in the vicinity of spot weld element models are few and hence are usually taken as the interface nodes for connecting substructures. However, the present MSC. NASTRAN superelement model reduction procedures are known not allow the nodes of CWELD elements to be the interface nodes of substructure.

Prior to the present study, no work appears to have been done to use the nodes of CWELD elements as the interface nodes of substructures in the investigation of dynamic behaviour of welded structures. In this work, the application of branch elements as the interface elements of substructure are proposed and tested. Prior to the present study, there also appears to have been no work done concerning the adjustment of the finite element model of the welded structure by including the effects of initial curvatures, initial stress and spot welds that are attributed to the modelling errors, via the combination between the Craig-Bampton CMS and model updating. The results calculated from the application of branch elements and the combination between the Craig-Bampton CMS and model updating have been presented and discussed in Chapter 6.

2.6 Conclusions

Modelling work on structures, bolted joints, welded joints, model updating methods, substructuring synthesis schemes has been reviewed in this chapter. It appears that the versatility of the finite element method has made it the most popular numerical method used for structural performance analysis. However, in all cases, the results calculated from the method which is developed based on assumptions, may produce a large discrepancy from experimentally observed results. For the predicted results of finite element models to correlate as closely as possible with the measured results, systematic adjustments must be made to minimise the errors introduced to the models. The finite element model updating method has become the accepted method for the reconciliation.

There are two major groups of frequency domain of model updating methods: the first is direct model updating methods and the second is iterative model updating methods. However the latter has superseded the former because the physically meaning updating parameters can be directly identified and then used for further applications. In addition, the iterative methods can benefit from optimisation techniques which are readily available in commercial software like MSC. NASTRAN.

Most iterative model updating methods require a high number of iterations for computing the eigensolutions and associated sensitivity matrices of large, complex structures which usually consist of a very large number of degrees of freedom. The use of the conventional method for model updating purposes in which non-reduced finite element models are reconciled with tested structures, has been reported to be inefficient and impractical for this problem.

The difficulties in attaining the required accurate dynamic predictions of assembled systems, in most cases, highly lie in the deficiency of joint modelling approaches in representing the complexity of physical joint behaviour. In case of welded structures, ACM2 and CWELD element have been the most popular elements for modelling spot welds in the scientist and engineering communities. However, in terms of the number of degrees of freedom that would be introduced to and the

simplicity of application in a welded large complex structure, CWELD element seems to be better in comparison with ACM2 model which introduces more degrees of freedom to the complete structure model and also poses tedious work.

The Craig-Bampton CMS scheme which uses fixed interface modes and constraints modes has been reported to be the most reliable and accurate for predicting low frequency modes in comparison with other substructuring synthesis schemes. On the other hand, the low frequency modes are often modes of interest to be investigated because they can be accurately experimentally observed. However, to the author's best knowledge no research work has yet made use of the Craig-Bampton CMS formulations in model updating of welded structures by considering the nodes of joint model elements as the interface nodes of substructures instead of the nodes of model elements.

Chapter 3

Experimental Modal Analysis of the Substructures and the Welded Structure

3.1 Introduction

Experimental modal analysis (EMA) is a very useful vibration analysis tool, providing an understanding of structural characteristics, operating conditions and performance criteria that enable designing for optimal dynamic behaviour or solving structural dynamics problems in existing designs.

Experimental modal analysis involves three constituent phases; test preparation, frequency response measurements and modal parameter identification. Test preparation involves selection of a structure's support, type of excitation force(s), location(s), of excitation, hardware to measure force(s) and responses; determination of a structural geometry model which consists of points of response to be measured; identification of mechanisms which could lead to inaccurate measurement. During the test, a set of FRF data is measured and stored which is then analysed to identify modal parameters of the tested structure.

In this chapter, modal testing to measure frequencies and model shapes of the welded structure comprising of five substructures namely side wall 1, side wall 2, stopper 1, stopper 2 and bent floor is discussed and presented. An introductory overview of modal experimental analysis procedure of a typical model test is covered as well. Furthermore many technical issues encountered during the tests such as the selection of a testing method and hanging orientation for thin sheets based structures are investigated and discussed.

3.2 Experimental modal analysis

3.2.1 Introduction

In this section, an introductory overview of experimental modal analysis is presented. Most structures (vehicles, machines and buildings) in operation are subjected to dynamic forces that cause vibrations in the structures. These vibrations can cause noise and durability problems when it exceeds the maximum levels of vibration tolerated by a given structure. In order to study these vibrations it is necessary to know the response of the structure studied.

In order to determine the characteristics of a structure, it is necessary to know the relationship between the forces applied to the structure in a particular point and the structural response in another point (vibration). The frequency response function or FRF gives this relationship. Knowing the FRF of the structure in several points, an image of its response can be visualised when it is excited by a given force in a particular point. This process is known as experimental modal analysis.

3.2.2 Basics of experimental modal analysis

Any forced response of a system can be broken down to a sum of different vibration modes.

Each vibration mode is defined by its modal properties. These are:

- Modal frequency (resonance frequency)
- Modal damping
- Modal Shape

The repossession of these parameters for each resonance of the system allows creating a mathematical model of a system. These modes of vibration will determine the intrinsic characteristics of the free systems (system with no force). Therefore experimental modal analysis is the process of obtaining these parameters that permits a dynamic mathematical model to be created. The applications of the created mathematical model include the following typical:

- knowledge of the natural frequencies
- qualitative analysis of the mode shapes, in order to get better knowledge of the dynamic structural behaviour in cases of problem solving
- correlation with analytical models (FEM). Whatever modal analysis carried out, it is necessary to have a correlation between the analytical and experimental model
- computer simulation, based on the modal experimental model to develop better quality prototype more quickly, as well as faster problem-solving

3.2.3 Modal testing

The process of experimentally extracting the modal model of a structure is called modal testing. The theoretical basis of the process is secured upon establishing the relationship between the vibration response at one location and excitation at the same or another location as a function of excitation frequency. This relationship which is often a complex mathematical function is known as frequency response function or FRF. In other words, the practice of modal testing involves measuring the FRFs or impulse responses of a structure.

Modal testing allows the dynamic properties of a structure to be determined quickly without the difficulties and possible inaccuracies of formulating an analytical model. Although the modal model of a structure can be obtained either by mathematical modelling or modal testing, however, generally the term of modal analysis is used to refer to the process of extracting modal parameters from the test data rather than analytically.

Initial assessment of measured FRF data

Since the quality of the modal analysis relies critically on the quality of the measured FRF data, the assessment on the quality of measured FRF data becomes fundamentally essential for experimental modal analysis. The assessment of measured FRF data is basically to ascertain two things: (1) the structure satisfies the assumptions modal analysis requires; and (2) human and system errors are minimized or eliminated. Basically, the structure needs to comply with reciprocity, time invariance and linearity so that consistent modal properties exist in the measured FRF data which can be revealed by the subsequent analysis.

- **Reciprocity check of the measured FRF data:** A linear and time-invariant structure honours reciprocity property. For a single input, this means that the FRF data from a measurement should be identical if we exchange the locations of force and response. The reciprocity property of the FRF can be used to assess the reliability and accuracy of the measured FRF data.
- **Repeatability check of the measured FRF data:** This is mainly to ensure that the structure's dynamic behaviour and the whole measurement set-up system are time-invariant. For selected force input and response locations, a linear structure should yield identical FRF curves for every measurement.
- **Linearity check of the measured FRF data:** Perhaps the most important assumption of modal analysis is that the structure measured for FRF data behaves linearly. The ultimate check of linearity is to ensure that the FRF data are independent of excitation amplitudes. This can be achieved either qualitatively or quantitatively. For the former, FRF data from the same locations can be measured repeatedly with different but uncontrolled changes of excitation amplitudes. The measured FRF data can be overlaid to verify the uniformity of the curves. For the latter, controlled measurement is used to understand the nonlinearity existing in the structure. For example, an FRF measurement with constant response amplitude has the capacity to linearize nonlinearity.

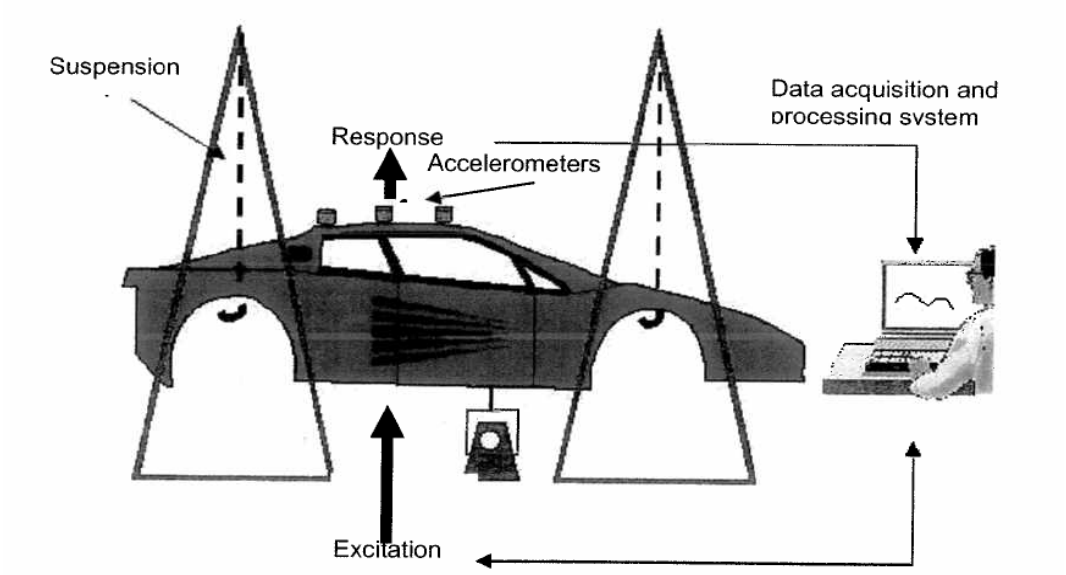

Figure 3.1: Typical modal analysis test (Cerulli et al., 2007)

The test engineer should have knowledge of the modal theory and the modal experimental analysis process. Therefore the correct choice of instrumentation and method necessary for modal test is also of vital importance. The outline of a typical modal analysis test is presented in Figure 3.1. In the procedure of a modal test, a variable force is applied to the structure. A shaker or an impact hammer creates the excitation. The vibration transducers measure the responses of the system. All the measured signals from the transducers are digitised and processed by an analysis system for the estimation of the FRF. This procedure is repeated for different combinations of excitation and response. During the next stage, the modal characteristics (poles of the system, vectors of modal shapes, etc) of the structure will be determined based on the measured FRF. The modal deformations can be simulated by means of graphic animation tools.

3.2.4 Force and vibration transducers

The excitation force (input) applied to the system and the produced vibrations (outputs) are measured with force and vibration transducers. Vibration transducers measure the displacement, velocity or acceleration of the different measurement points in the system. Most transducers used in modal analysis tests use piezoelectric crystals. However the most widely used accelerometers in automotive NVH operation is the piezoelectric accelerometer.

The choice of accelerometers necessary for a modal test is crucial. Characteristics such as weight, frequency range or temperature will define the type needed for a particular application. A very important factor is the weight of the accelerometer. Depending on the structure that is going to be tested, the weight of the accelerometer will modify the dynamic characteristics (especially the resonance frequency) of the structure substantially. Therefore the accelerometer or accelerometers used in a test should not exceed 10 percent (Heylen et al., 1998 and IDIADA, 2005) of the weight of the structure to be measured, especially for a structure made from thin steel sheets and has a large flat surface used in this research. The specific series of accelerometers used in this research are depicted in Figure 3.2.

Figure 3.2: Accelerometer (Kristler 8728A)

3.2.5 Acquisition and analysis systems

Data acquisition equipment permits the recording and processing of the measurement data of vibration. Analysis systems carry out the processing of the acquired FRF's to obtain the modal parameters. There is a very wide variety of acquisition and analysis equipment on the market. The important aspects that determine the choice of the type of systems are the number of acquisition channels, bandwidth, accuracy, processing speed, portability and etc. LMS SCADAS III analyser with 12 channels was used in this research to process the load and response signals.

3.2.6 Method of support

The structures to be tested must be supported by in some manner by surrounding environment. Although theoretical boundary conditions such as fixed support or hinges may seem easier to construct, in reality, this is generally not true. Practical experience showed that it is very difficult to construct a nearly perfect clamping (Heylen et al., 1998). The limitations on the construction of a clamping boundary often cause significant frequency and mode shape differences. As consequence of that, very frequently free conditions are used because they are normally easy to approximate experimentally than fixed boundary conditions (Carne et al., 2007). There are a few good publications discussing the importance of selecting the right support to be used in modal testing to ensure the accuracy of the results measured. The effects of support stiffness and mass on the modal frequencies have been discussed at length by Bisplinghoff (1955). Meanwhile Ewins (2000) elaborated the issue of the location of suspensions for free boundary conditions.

The first step in setting up a structure for frequency response measurement is to consider the fixture mechanism necessary to obtain the desired boundary conditions. This is a key step in the process as it affects the overall structural characteristics, particularly for subsequent analyses such as finite element correlation. Analytically, boundary conditions can be specified in a completely free

or completely constrained sense. In testing practise, however, it is generally not possible to fully achieve these conditions. The free condition means that the structure is floating in air with no connections to the ground and exhibits rigid body behaviour at zero frequency. Physically this cannot be realised, so the structure must be supported in some manner.

In order to approximate a free system, the structure can be suspended from very soft elastic cords or placed on a very soft cushion. By doing this, the structure will be constrained to a degree and the rigid body modes will no longer have zero frequency. However the rigid body frequencies will be much lower than the frequencies of the flexible modes and thus have negligible effect if a sufficiently soft support system is used. The rule of thumb for free support is that the highest rigid body mode frequency must be less that 10% of the first flexible mode (Wolf Jr, 1984). If this criterion is met, rigid body modes will have negligible effect on flexible modes.

3.2.7 Method of excitation

There are two common methods that the structure can be excited. In one method a shaker is connected to the structure that provides the necessary excitation force based on the specified input voltage. A schematic test set up for shaker excitation is shown in Figure 3.3. Three different types of signal inputs are normally produced by shakers and they are sinusoidal, random and periodic chirp. Since the joining of the shaker to the structure will modify the mass, damping and stiffness of the structure, therefore the connection between the shaker and the structure should be stiff in the direction of the measurement and very flexible in the other directions. A stinger which is stiff in the measuring direction is used to connect between the structure and shaker.

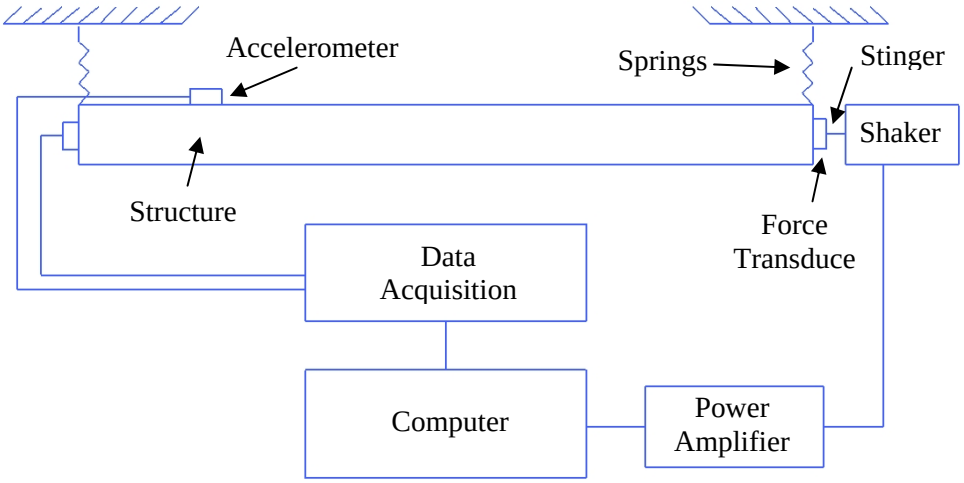

Figure 3.3: Schematic diagram of shaker excitation test set up

Another method which is a popular excitation technique and relatively simple way of exiting the structure is impact testing (Maia and Silva, 1997). The method is adopted in this research and the set up of the method is shown in the schematic diagram in Figure 3.4. The convenience of this technique is attractive because it requires less hardware and provides shorter measurement time. The method of applying the impulse includes a hammer, an electric gun or a suspended mass. However a hammer as shown in Figure 3.5 is the most common used device.

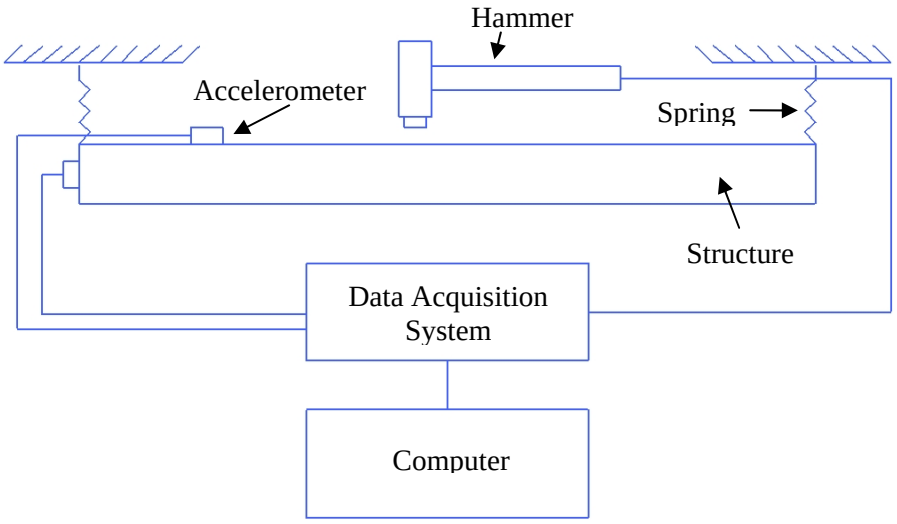

Figure 3.4: Schematic diagram of hammer excitation test set up

Since the force is an impulse, the amplitude level of the energy applied to the structure is a function of the mass and the velocity of the hammer. It is difficult to control the velocity of the hammer, so the force level is usually controlled by varying the mass. This can be done by adding mass to or removing mass from most hammers, making them useful for testing objects of varying sizes and weights.

The frequency content of the energy applied to the structure is a function of the stiffness of the contacting surfaces and, to a lesser extent, the mass of a hammer. The stiffness of the contacting surfaces affects the shape of the force pulse, which in turn determines the frequency content. Therefore it is not feasible to change the stiffness of the structure; the frequency content is controlled by varying the stiffness of the hammer tip. The harder the tip, the shorter the pulse duration and thus the higher the frequency content.

Figure 3.5: PCB impact hammer

3.2.8 Measuring points (degrees of freedom)

The number and position of the measuring points, the response of the structure to be measured must be carefully chosen. The number of measuring points will depend on the frequency range under study, the number of available transducers and the available test time. The wavelength of the modes at high frequency is relatively small. Therefore sufficient point density is required if these modes are to be observed. For those parts of structure that to be studied in more detail more measuring points have to be deployed.

The distribution of the measuring points must be equally spread throughout the tested structure. This reduces the probability of losing any mode and also getting a suitable mesh for the animated visualisation of modes. The way of the accelerometers are installed decisively influences the accuracy of the test results and also the frequency range cover by the test, especially for a structure made from thin steel sheets used in this research, the number of accelerometers used on the tested structure should not be in a large amount. This reduces the chance of increasing in mass and changing in the local stiffness of the structure. Therefore the accelerometer or accelerometers used in a test should not exceed 10 percent of the weight of the structure to be measured (Heylen et al., 1998). Another important factor to be considered is that the locations of accelerometer attachments should be far out from the nodes of vibration modes. This minimises the chance of missing modes and generally results in decent wire frame. The final one is considering the type of accelerometer attachment to use on the test. There are several methods such as fixed installation, waxing, magnetic, adhesive and cementable bases. In comparison waxing method offers quick measurement of vibration and also the simplest attachment through which measurement method is used in this research.

3.3 Modal test of the substructures of the welded structure

The structure under investigation is a welded structure made from 1.5mm-thick steel sheets. It consists of five substructures welded together as shown in Figure 3.6. There is the U-shaped floor (bent floor no. 1), two side walls each with three flanges (side wall no. 2 and 3) and two hut-like stiffeners (stoppers no. 4 and 5). They are clearly shown in Figure 3.6 with numbering. There are in total eighty spot welds on the structure.

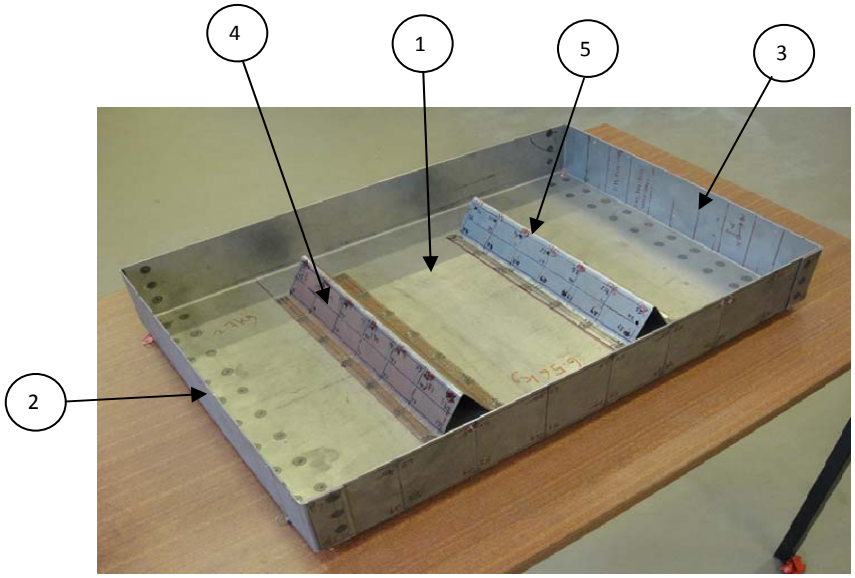

Figure 3.6: The welded structure

Due to the complexity of the original sub-structure which is called NGV compartment and also the fabrication costs of the sub-structure which is very expensive, a simplified structure was used in this study. The original structure which is one of the sub-structures of an automotive body-in-white is shown in Figure 3.7.

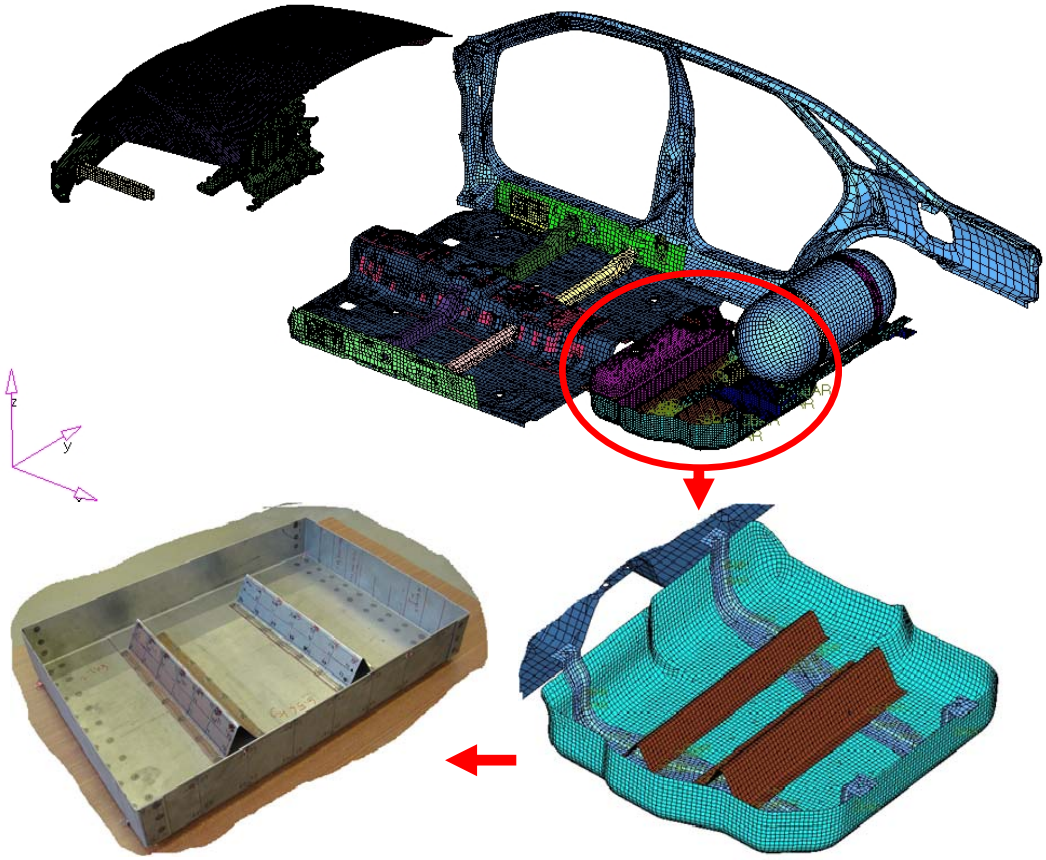

Figure 3.7: A truncated body-in-white

Figure 3.7 shows a truncated automotive body-in-white through which the welded structure is conceptualised and replicated in this research.

Modal testing was carried out for each individual substructure before all were assembled together by a number of spot welds to form the structure which is called the welded structure in this work. The tests were performed by following the procedures highlighted in the previous sections. The substructures were tested in free-free boundary conditions for the first ten modes of the frequency range from 0 to 1000 Hz. Springs and nylon strings were used to simulate the free-free boundary conditions. An impact hammer and roving accelerometers were used in the investigation of the dynamic behaviour of the test models of the substructures and the welded structure.

The details of test set ups and experimental data of the substructures and the welded structure are presented and discussed in the following sections.

3.3.1 Thin steel sheets

In this study, thin steel sheets are used to fabricate the substructures and the welded structure. The material properties of steel sheets are tabulated in Table 3.1.

Table 3.1: Nominal values of mild steel material properties of side wall 1 and side wall 2

Material Properties	Nominal Values
Young's modulus (E)	210 GPa
Shear modulus (G)	81 GPa
Poisson's ratio (ν)	0.3
Mass density (ρ)	7850 kg/m^3

3.3.2 Modal test of side wall 1 and side wall 2

This section describes the way modal test on side wall 1 and side wall 2 was carried out. Since both side wall 1 and side wall 2 have the same geometrical design and were tested using the same procedures, it would be better to describe the procedures of the test based on one of them.

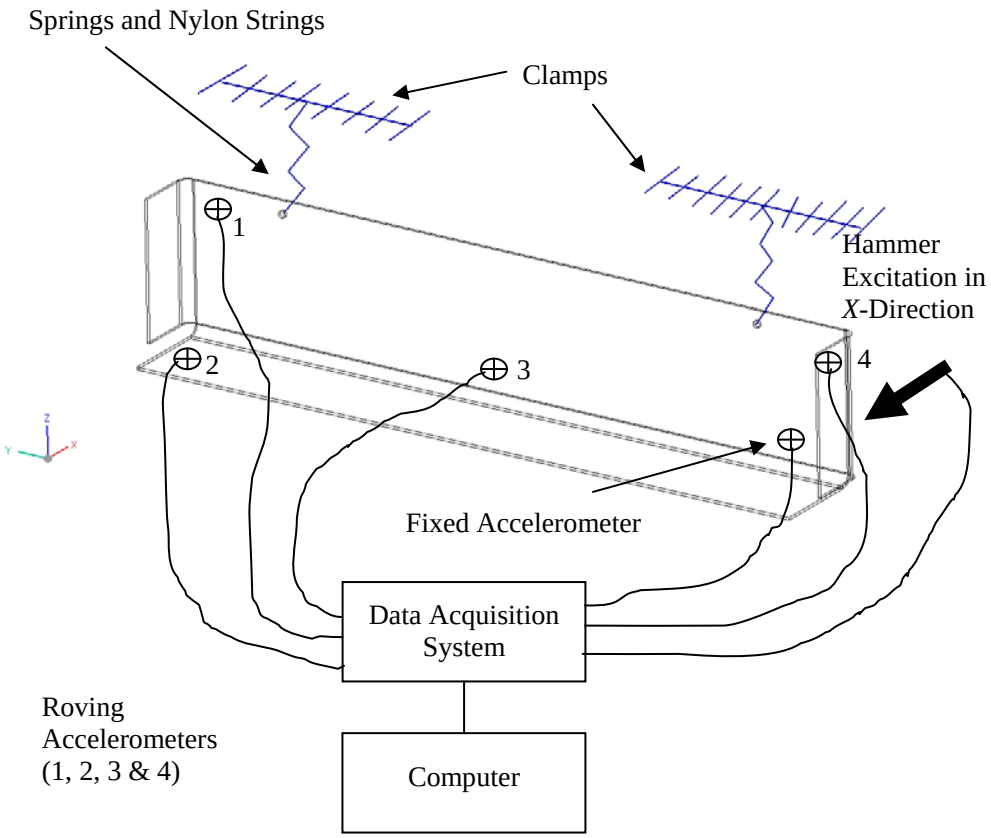

Figure 3.8: Schematic diagram of the side wall test set up

The type of modal test used for the substructure was free-free boundary conditions. Two sets of springs and nylon strings were used to simulate the free-free boundary condition by attaching them to the holes on the substructure and to the rigid clamps as show in Figure 3.8. The side wall was divided into 37 measuring points as shown in Figure 3.9 (a), (b) and (c). Five sets of accelerometers were used in the test by allowing four of them roving over the substructure and another one was fixed in the opposite direction of the excitation point. Based on the schematic

diagram of the test set up, the surface of the accelerometer which was chosen to be a fixed accelerometer was attached to the substructure in the *X* direction. This is because the direction of the excitation was in the (-ve) *X* direction. In other words the surface of the fixed accelerometer must be always in the opposite direction of the force induced by the impact hammer. Meanwhile the way of attaching the accelerometers to be roving over the substructure could be carried out in two options by either waxing the surfaces in the same direction of the hammer excitation or in the opposite direction of it. Neither approach will affect the accuracy of the results measured. Since waxing method offers quick measurement of vibration and the simplest attachment, it was used to attach the accelerometers to the substructure.

The details of the accelerometers arranged over the substructure were depicted in Table 3.2 in which the first column represents the number of FRF measurements at every measuring point. Meanwhile the second, third and fourth columns indicate the number of accelerometers used in the measurement of the responses and also the measurement directions. The last column is the point at which the hammer was used to excite the substructure.

Numerical analyses were performed on side wall 1 and side wall 2 beforehand in order to predict the natural frequencies and mode shapes of the substructures. The numerical results were used in the test as an indicator for the determination of the excitation and measuring points in order to ensure all the modes of interest could be calculated. This is a very important factor that needs to be implemented and considered before carrying out any modal testing. The LMS PolyMAX curve-fitting procedures were used to extract the responses calculated from the measuring points of 37 (52 degrees of freedom) and they are tabulated in Table 3.2 and Table 3.3.

(a)

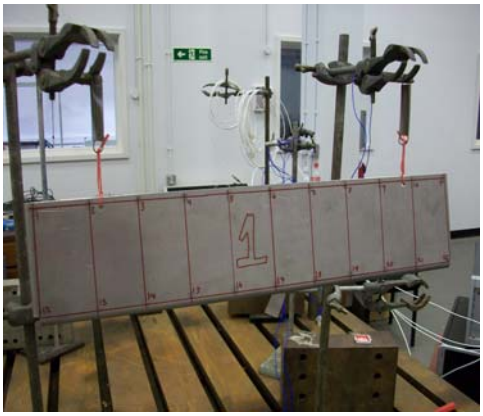

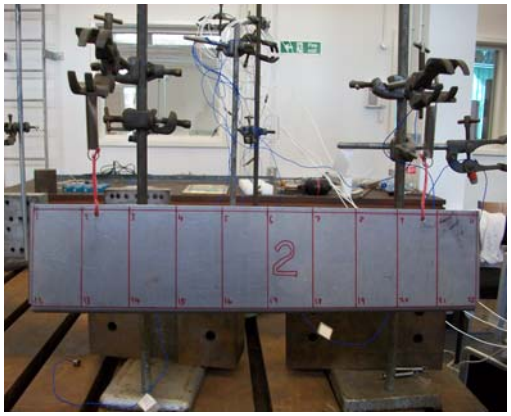

(b) (c)

Figure 3.9: Side wall 1 and side wall 2 test set up

Table 3.2: Number of measuring points and measuring directions of side wall 1 and side wall 2

Run	Accelerometers (Kistler)				
	2008881 (1)	2008882 (2)	2008891 (3)	2008879 (4)	2007226 (Fixed)
1	1 in *X*	12 in *Z*	27 in *Z*	33 in *Z*	13 in *X*
2	2 in *X*	32 in *Z*	11 in *Y*	12 in *X*	13 in *X*
3	3 in *X*	14 in *Z*	12 in *Y*	14 in *X*	13 in *X*
4	4 in *X*	15 in *Z*	22 in *Y*	15 in *X*	13 in *X*
5	5 in *X*	16 in *Z*	34 in *Y*	16 in *X*	13 in *X*
6	6 in *X*	17 in *Z*	35 in *Y*	17 in *X*	13 in *X*
7	7 in *X*	18 in *Z*	36 in *Y*	18 in *X*	13 in *X*
8	8 in *X*	19 in *Z*	37 in *Y*	19 in *X*	13 in *X*
9	9 in *X*	20 in *Z*	23 in *Z*	20 in *X*	13 in *X*
10	10 in *X*	21 in *Z*	24 in *Z*	21 in *X*	13 in *X*
11	31 in *Z*	22 in *Z*	25 in *Z*	22 in *X*	13 in *X*
12	26 in *Z*	1 in *Y*	28 in *Z*	29 in *Z*	13 in *X*
13	30 in *Z*	11 in *X*	13 in *Z*		13 in *X*

Table 3.3: Experimental and numerical frequencies of side wall 1 and side wall 2

Mode	Experimental Side wall 1 (Hz)	Experimental Side wall 2 (Hz)	Numerical Side wall 1 & 2 (Hz)
1	96.55	96.74	94.54
2	138.84	138.99	137.01
3	222.87	222.91	219.39
4	315.61	315.91	310.22
5	360.25	361.90	358.96
6	376.95	377.76	375.12
7	418.61	419.31	415.86
8	442.13	442.48	434.90
9	527.14	527.05	519.46
10	555.29	555.23	544.87

3.3.3 Modal test of stopper 1 and stopper 2

Modal tests were performed on stopper 1 and stopper 2 with free-free boundary conditions. The free conditions were approximated by using spring and nylon string as shown that were attached to the substructure and clamp as shown schematically in Figure 3.10 and physically depicted in Figure 3.11 and also in Figure 3.12. Five sets of accelerometers were used in the measurement of the vibrational responses. Four of them which are accelerometer 1, 2, 3 and 4 were roved over the substructure, while another one was fixed to one particular point for every run. The details of the arrangement of the accelerometers in the test can be seen from Table 3.4 in which there are 70 measuring points with 82 degrees of freedom and also 18 runs to complete the measurement.

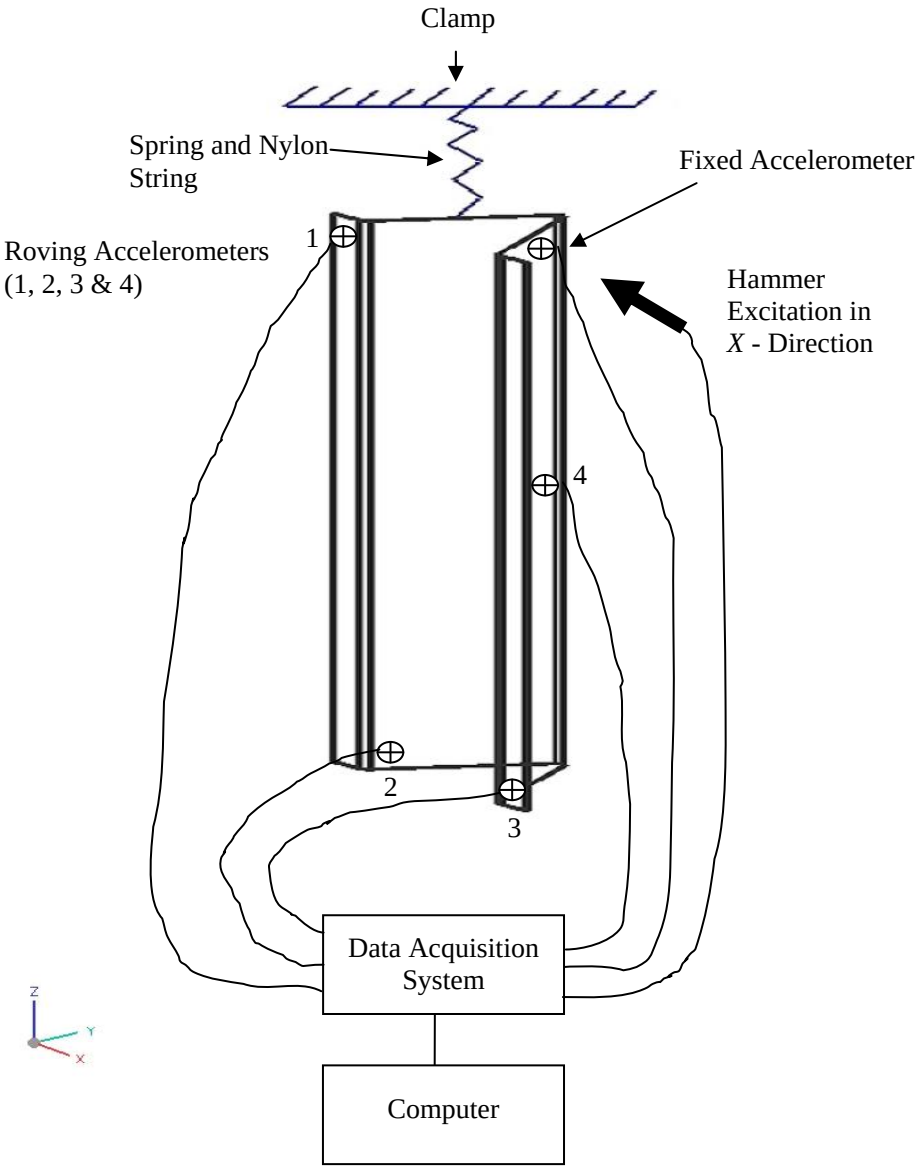

Figure 3.10: Schematic diagram of the stopper test set up

Figure 3.11: Stopper 1 test set up

Figure 3.12: Stopper 2 test set up

Table 3.4: Number of measuring points and measuring directions of stopper 1 and stopper 2

Run	Accelerometers (Kistler)				
	2008881 (1)	2008882 (2)	2008891 (3)	2008879 (4)	2007226 (Fixed)
1	1 in *Y*	46 in *X*	38 in *X*	35 in *Y*	45 in *X*
2	2 in *Y*	47 in *X*	37 in *X*	34 in *Y*	45 in *X*
3	3 in *Y*	48 in *X*	36 in *X*	33 in *Y*	45 in *X*
4	4 in *Y*	49 in *X*	42 in *X*	32 in *Y*	45 in *X*
5	5 in *Y*	43 in *X*	41 in *X*	31 in *Y*	45 in *X*
6	6 in *Y*	44 in *X*	40 in *X*	30 in *Y*	45 in *X*
7	7 in *Y*	64 in *X*	39 in *X*	29 in *Y*	45 in *X*
8	8 in *Y*	18 in *X*	54 in *X*	22 in *Y*	45 in *X*
9	9 in *Y*	19 in *X*	55 in *X*	23 in *Y*	45 in *X*
10	10 in *Y*	20 in *X*	56 in *X*	24 in *Y*	45 in *X*
11	11 in *Y*	21 in *X*	50 in *X*	25 in *Y*	45 in *X*
12	12 in *Y*	65 in *X*	57 in *X*	26 in *Y*	45 in *X*
13	13 in *Y*	66 in *X*	58 in *X*	27 in *Y*	45 in *X*
14	14 in *Y*	67 in *X*	59 in *X*	28 in *Y*	45 in *X*
15	68 in *X*	21 in *X*	51 in *X*	60 in *Y*	45 in *X*
16	69 in *X*	15 in *X*	52 in *X*	63 in *Y*	45 in *X*
17	70 in *X*	16 in *X*	53 in *X*	62 in *Y*	45 in *X*
18	17 in *X*	61 in *X*			45 in *X*

Table 3.5: Experimental and numerical frequencies of stopper 1 and stopper 2

Mode	Experimental Stopper 1 (Hz)	Experimental Stopper 2 (Hz)	Numerical Stopper 1 & 2 (Hz)
1	139.57	139.32	136.29
2	221.94	221.83	228.62
3	256.20	257.13	262.71

The natural frequencies and mode shapes of both stoppers were calculated using NASTRAN and the frequencies are shown in Table 3.5. The modes were used to determine the measuring points and also the excitation point of the substructures. It is imperative to study modes shapes in order to ensure the accelerometers are not placed on the nodes of the modes. The range of the frequency of interest for both stoppers is from 1 to 500 Hz. The first three frequencies are calculated and tabulated in Table 3.5. It shows that the experimental natural frequencies of both substructures in particular the first mode is higher than the numerical frequency.

3.3.4 Modal test of the bent floor

Since the bent floor is fabricated from a thin steel sheet and has a large flat surface area, the number of accelerometers, the distribution of them over the substructure and also the excitation point must be carefully studied and considered before performing the test. This is to avoid mass loading and double impacts issue which affect the accuracy of the experimental results.

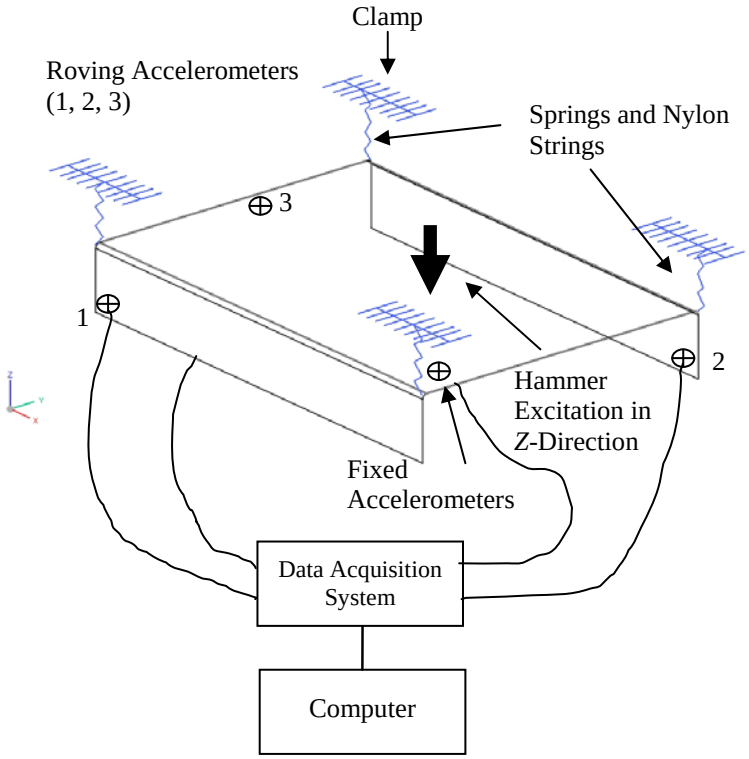

Figure 3.13: Schematic diagram of the bent floor test set up

Therefore, numerical results as shown in the 3rd column in Table 3.6 were used to determine the excitation point, measurement points and number of accelerometers used in the test. Four sets of accelerometers were used through which three of them (no 1, 2 and 3) were roving over the substructure and another one was fixed right underneath the point of the hammer excitation as shown in Figure 3.13. Four sets of springs coupled with nylon strings were used to hang the bent floor to the clamps to approximate free-free boundary conditions.

In order to avoid double impact issues during the exciting processes and also to produce good experimental results, the excitation point and its direction were chosen to be as nearest as possible to the one of the four corners where the substructure is hung. The details of the test set-up are illustrated schematically in Figure 3.13 and Figure 3.14. Meanwhile Table 3.7 presents the arrangements of the accelerometers over the bent floor. There are 63 measuring points representing 82 degrees of freedom that were used to calculate the vibrational responses of the bent floor. The first ten frequencies calculated from the test within the frequency range of interest from 1 to 200 Hz are tabulated in the 2nd column in Table 3.6. The overall comparison shows that the experimental frequencies are higher than those calculated numerically presented in the 3rd column.

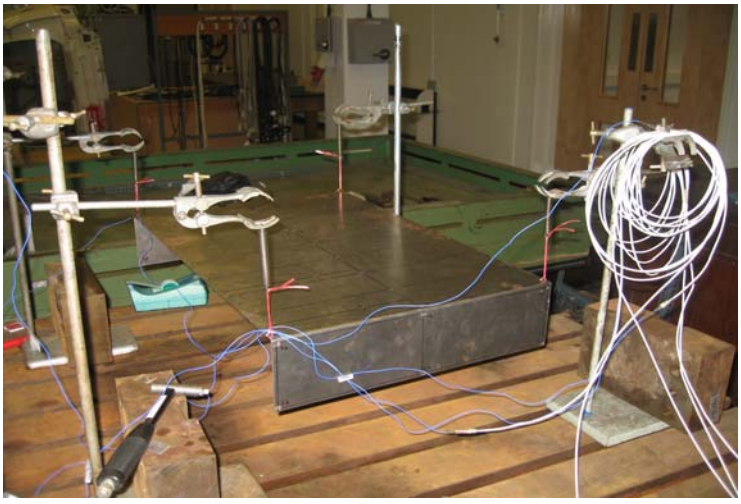

Figure 3.14: Bent floor test set up

Table 3.6: Experimental and numerical frequencies of the bent floor

Mode	Experimental Bent floor (Hz)	Numerical Bent floor (Hz)
1	16.59	15.56
2	29.14	28.94
3	45.34	44.58
4	57.09	56.74
5	74.85	73.94
6	86.16	85.95
7	98.12	97.27
8	109.26	108.73
9	114.88	113.60
10	119.94	118.87

Table 3.7: Number of measuring points and measuring directions of the bent floor

Run	Accelerometers (Kistler)			
	2008881 (1)	2008882 (2)	2008891 (3)	2007226 (Fixed)
1	1 in *Y*	63 in *Z*	45 in *Y*	39 in *Y*
2	6 in *Y*	62 in *Z*	40 in *Y*	39 in *Y*
3	11 in *Z*	61 in *Z*	35 in *Y*	39 in *Y*
4	16 in *Z*	60 in *Z*	30 in *Y*	39 in *Y*
5	21 in *Y*	59 in *Z*	25 in *Y*	39 in *Y*
6	26 in *Y*	58 in *Z*	20 in *Y*	39 in *Y*
7	31 in *Y*	57 in *Z*	15 in *Y*	39 in *Y*
8	36 in *Y*	56 in *Z*	10 in *Y*	39 in *Y*
9	41 in *Y*	55 in *Z*	5 in *Y*	39 in *Y*
10	2 in *Y*	3 in *Z*	44 in *Y*	39 in *Y*
11	7 in *Y*	8 in *Z*	34 in *Y*	39 in *Y*
12	12 in *Y*	13 in *Z*	29 in *Y*	39 in *Y*
13	17 in *Y*	18 in *Z*	24 in *Y*	39 in *Y*
14	22 in *Y*	23 in *Z*	19 in *Y*	39 in *Y*
15	27 in *Y*	28 in *Z*	14 in *Y*	39 in *Y*
16	32 in *Y*	33 in *Z*	9 in *Y*	39 in *Y*
17	37 in *Y*	38 in *Z*	4 in *Y*	39 in *Y*
18	42 in *Y*	43 in *Z*	44 in *Z*	39 in *Y*
19	2 in *Z*	54 in *Y*	39 in *Z*	39 in *Y*
20	7 in *Z*	53 in *Y*	34 in *Z*	39 in *Y*
21	12 in *Z*	52 in *Y*	29 in *Z*	39 in *Y*
22	17 in *Z*	51 in *Y*	24 in *Z*	39 in *Y*
23	22 in *Z*	50 in *Y*	19 in *Z*	39 in *Y*
24	27 in *Z*	49 in *Y*	14 in *Z*	39 in *Y*
25	32 in *Z*	48 in *Y*	9 in *Z*	39 in *Y*
26	37 in *Z*	47 in *Y*	4 in *Z*	39 in *Y*
27	42 in *Z*	46 in *Y*		39 in *Y*

3.4 Modal test of the welded structure

In this section, the procedures used to calculate the experimental data of vibrational responses of the welded structure and the results are presented. The welded structure used in this study is already shown in Figure 3.6 and briefed in section 3.3. The procedures of modal testing of the substructures used to form the structure were already covered in the previous sub-sections. Upon completion of the tests of the substructures, they were taken for spot welding in the Core Services Department of the University of Liverpool. The process was performed manually by the staff of the department as depicted in Figure 3.15.

Free-free configurations are commonly used in modal testing as reported in Carne et al. (2007). This is because it is easy to achieve this type of configuration in practice. In a free-free test configuration, the structure is supported from a suspension system designed so as to ensure that the rigid body frequencies are at least an order of magnitude lower than the fundamental frequency of the structure.

The experimental set up is shown in Figure 3.16. The welded structure is suspended from the clamps by four sets of springs and nylon strings to approximate free-free boundary conditions. Five accelerometers were used to measure the vibrational responses at 91 measuring points with 127 degrees of freedom. The details of the accelerometer arrangements are highlighted in Table 3.8. Four of them were roving over and another one was fixed at one point which is considered as the excitation point. This is due to a large flat surface on the test model and also it is made from thin steel sheets. The impact hammer was used to excite the structure in the *Z* direction.

Meanwhile the dynamic data of the excited structure was acquired by the accelerometers. The load and response signals were processed by LMS SCADAS III analyser. The numerical analysis results as shown in the 3rd column in Table 3.9 were used to provide guidance on determining the frequency bandwidth of the testing, the locations of the excitation points, excitation directions and also response measurement points. Based on a few tests carried out beforehand it lends

credence to the view that the quality of the particular test data could sometimes significantly depend on hanging orientation of the test model and also the excitation directions and points. As a result the test model was set up in the way as shown schematically in Figure 3.16 and physically in Figure 3.17.

Figure 3.15: Spot welding process

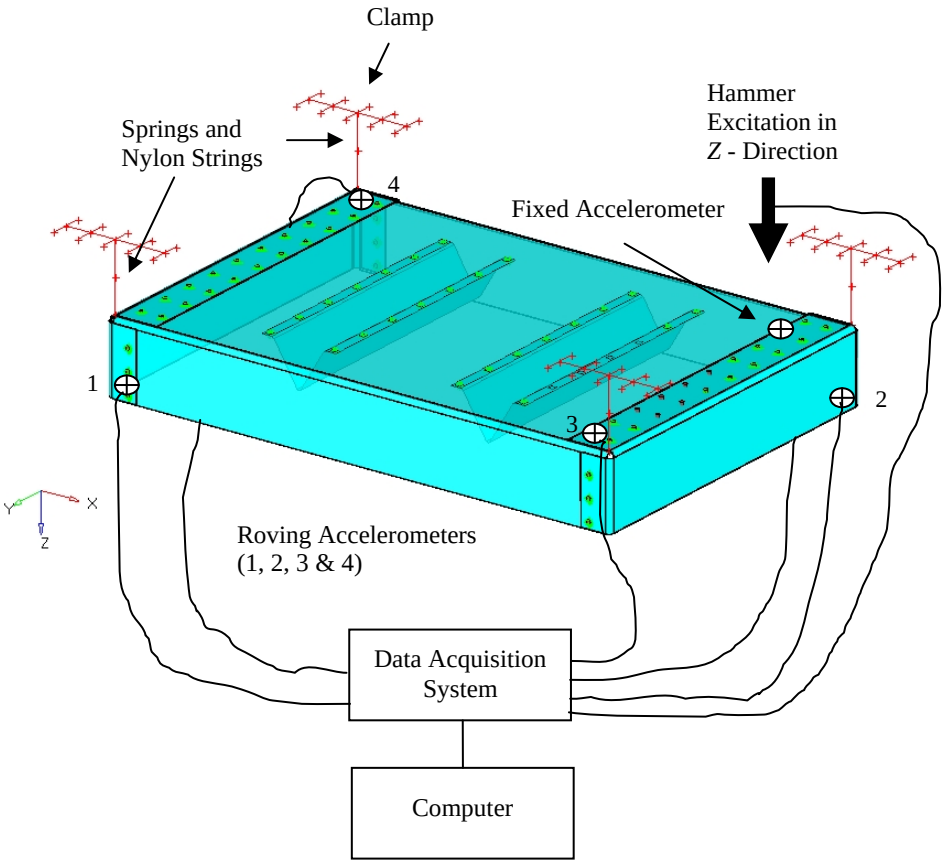

Figure 3.16: Schematic diagram of the welded structure test set up

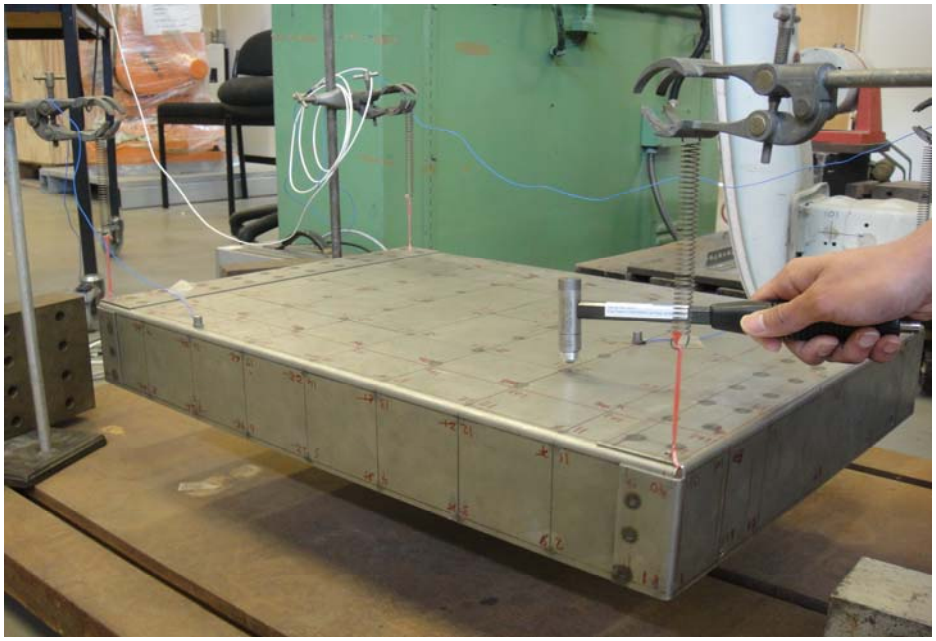

Figure 3.17: The test set up of the welded structure

Table 3.8: Number of measuring points and measuring directions of the welded structure

Run	Accelerometers (Kistler)				
	2008881 (1)	2008882 (2)	2008891 (3)	2008879 (4)	2007226 (Fixed)
1	1 in *Y*	63 in *Y*	110 in *Z*	109 in *Z*	102 in *Z*
2	2 in *Y*	62 in *Y*	111 in *Z*	108 in *Z*	102 in *Z*
3	3 in *Y*	61 in *Y*	112 in *Z*	107 in *Z*	102 in *Z*
4	4 in *Y*	60 in *Y*	113 in *Z*	106 in *Z*	102 in *Z*
5	5 in *Y*	59 in *Y*	114 in *Z*	105 in *Z*	102 in *Z*
6	6 in *Y*	58 in *Y*	115 in *Z*	104 in *Z*	102 in *Z*
7	7 in *Y*	57 in *Y*	116 in *Z*	103 in *Z*	102 in *Z*
8	8 in *Y*	56 in *Y*	117 in *Z*	101 in *Z*	102 in *Z*
9	9 in *Y*	55 in *Y*	118 in *Z*	27 in *Z*	102 in *Z*
10	10 in *Y*	54 in *Y*	37 in *Z*	26 in *Z*	102 in *Z*
11	11 in *Y*	53 in *Y*	38 in *Z*	25 in *Z*	102 in *Z*
12	12 in *Y*	52 in *Y*	39 in *Z*	24 in *Z*	102 in *Z*
13	13 in *Y*	51 in *Y*	40 in *Z*	23 in *Z*	102 in *Z*
14	14 in *Y*	50 in *Y*	41 in *Z*	22 in *Z*	102 in *Z*
15	15 in *Y*	49 in *Y*	42 in *Z*	21 in *Z*	102 in *Z*
16	16 in *Y*	48 in *Y*	43 in *Z*	20 in *Z*	102 in *Z*
17	17 in *Y*	47 in *Y*	44 in *Z*	19 in *Z*	102 in *Z*
18	18 in *Y*	46 in *Y*	45 in *Z*	63 in *X*	102 in *Z*
19	18 in *Z*	46 in *Z*	36 in *Z*	122 in *X*	102 in *Z*
20	17 in *Z*	47 in *Z*	35 in *Z*	64 in *X*	102 in *Z*
21	16 in *Z*	48 in *Z*	34 in *Z*	65 in *X*	102 in *Z*
22	15 in *Z*	49 in *Z*	33 in *Z*	66 in *X*	102 in *Z*
23	14 in *Z*	50 in *Z*	32 in *Z*	121 in *X*	102 in *Z*
24	13 in *Z*	51 in *Z*	31 in *Z*	9 in *X*	102 in *Z*
25	12 in *Z*	52 in *Z*	30 in *Z*	54 in *X*	102 in *Z*
26	11 in *Z*	53 in *Z*	29 in *Z*	118 in *X*	102 in *Z*
27	10 in *Z*	54 in *Z*	28 in *Z*	45 in *X*	102 in *Z*
28	55 in *X*	46 in *X*	109 in *X*	36 in *X*	102 in *Z*
29	120 in *X*	110 in *X*	18 in *X*	27 in *X*	102 in *Z*
30	69 in *X*	37 in *X*	101 in *X*	27 in *X*	102 in *Z*
31	67 in *X*	28 in *X*	10 in *X*		102 in *Z*
32	119 in *X*	19 in *X*	1 in *X*		102 in *Z*

Table 3.9: Experimental and numerical frequencies of the welded structure

Mode	Experimental Welded Structure (Hz)	Numerical Welded Structure (Hz)
1	29.48	26.26
2	76.58	78.17
3	101.07	102.44
4	110.86	109.55
5	121.91	126.10
6	140.46	144.16
7	147.50	144.31
8	159.77	160.86
9	187.51	187.02
10	199.65	196.19

The experimental and numerical frequencies are presented in Table 3.9. The 1st column indicates the mode numbers. Meanwhile the experimental frequencies calculated from the test are informed in the 2nd column and the last column highlights the numerical frequencies calculated from the finite element analysis.

3.5 Conclusions

Experimental modal analysis has been explained and discussed in this chapter. Several important factors in ensuring the accuracy of the experimental results calculated such as the number of measuring points and accelerometers, the weight of accelerometers, method of support and method of excitation have been discussed and were successfully used. The measured frequencies and mode shapes of the substructures are shown in a number of sets starting from Figure 3.18 to 3.25. Meanwhile the experimental frequencies and mode shapes of the welded structure are depicted from Figure 3.26 to 3.27.

Systematic approaches to perform modal testing for a welded structure made from thin steel sheets and that has a large flat surface have been discussed and demonstrated.

To increase the chances of successful tests, a series of finite element analyses were conducted and the results were used to aid in determining the number and location of measuring points of the tested substructures and the welded structure.

It is clearly shown that there are big discrepancies between the experimental and numerical results of the welded structure in particular. This is due to the assumptions made in the finite element models based on the nominal values which are insufficient to represent the real tested model.

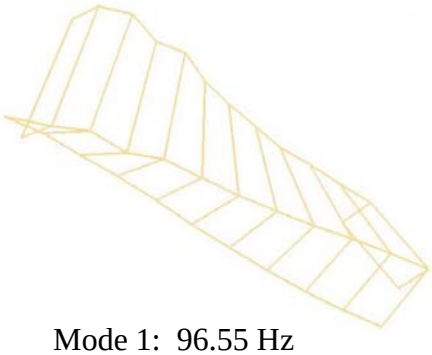

Mode 1: 96.55 Hz

Mode 2: 138.84 Hz

Mode 3: 222.87 Hz

Mode 4: 315.61 Hz

Mode 5: 360.25 Hz

Mode 6: 376.95 Hz

Figure 3.18: 1st, 2nd and 3rd pair of measured modes of side wall 1

Mode 7: 418.61 Hz

Mode 8: 442.13 Hz

Mode 9: 527.14 Hz

Mode 10: 555.29 Hz

Figure 3.19: 4^{th} and 5^{th} pair of measured modes of side wall 1

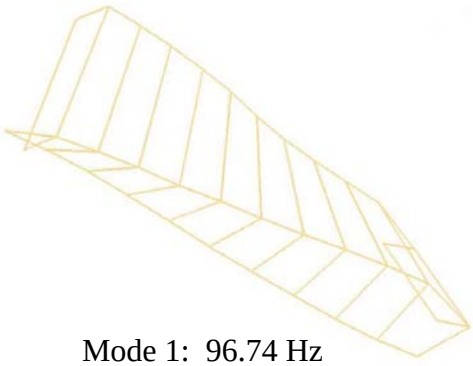

Mode 1: 96.74 Hz

Mode 2: 138.99 Hz

Mode 3: 222.91 Hz

Mode 4: 315.91 Hz

Mode 5: 361.90 Hz

Mode 6: 377.76 Hz

Figure 3.20: 1st, 2nd and 3rd pair of measured modes of side wall 2

Mode 7: 419.31 Hz

Mode 8: 442.48 Hz

Mode 9: 527.05 Hz

Mode 10: 555.23 Hz

Figure 3.21: 4th and 5th pair of measured modes of side wall 2

Mode 1: 139.57 Hz

Mode 2: 221.94 Hz

Mode 3: 256.20 Hz

Figure 3.22: 1st, 2nd and 3rd measured mode of stopper 1

Mode 1: 139.32 Hz

Mode 2: 221.83 Hz

Mode 3: 257.13 Hz

Figure 3.23: 1st, 2nd and 3rd measured mode of stopper 2

Mode 1: 16.59 Hz

Mode 2: 29.14 Hz

Mode 3: 45.34 Hz

Mode 4: 57.09 Hz

Mode 5: 74.85 Hz

Mode 6: 86.16 Hz

Figure 3.24: 1st, 2nd and 3rd pair of measured modes of the bent floor

Mode 7: 98.12 Hz

Mode 8: 109.26 Hz

Mode 9: 114.88 Hz

Mode 10: 119.94 Hz

Figure 3.25: 4th and 5th pair of measured modes of the bent floor

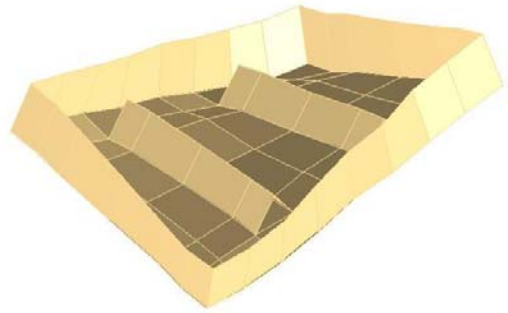

Mode 1: 29.48 Hz

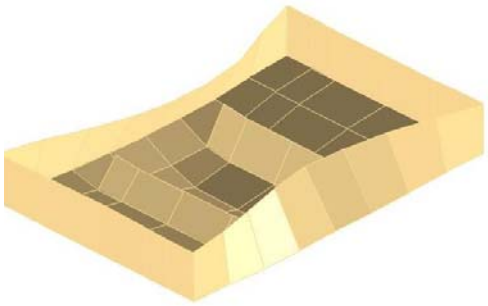

Mode 2: 76.58 Hz

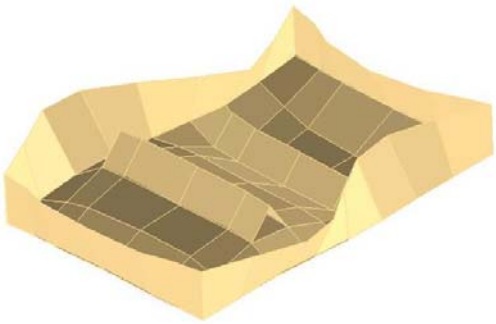

Mode 3: 101.07 Hz

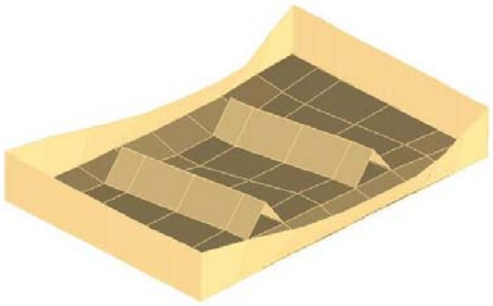

Mode 4: 110.86 Hz

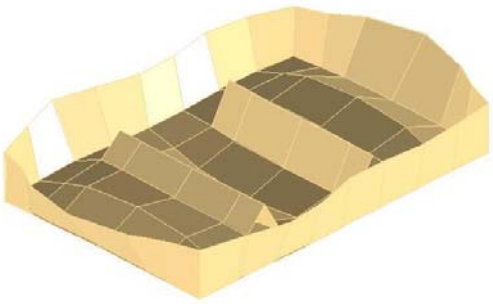

Mode 5: 121.91 Hz

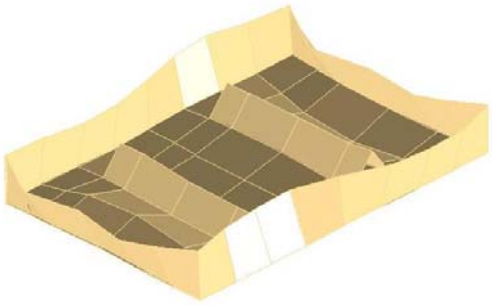

Mode 6: 140.46 Hz

Figure 3.26: 1st, 2nd and 3rd pair of measured modes of the welded structure

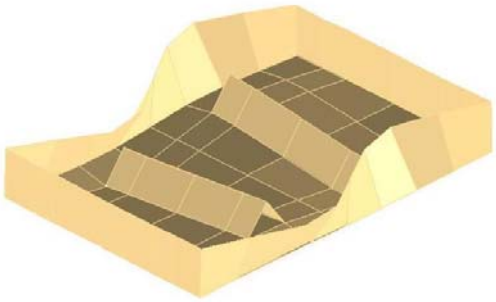

Mode 7: 147.50 Hz

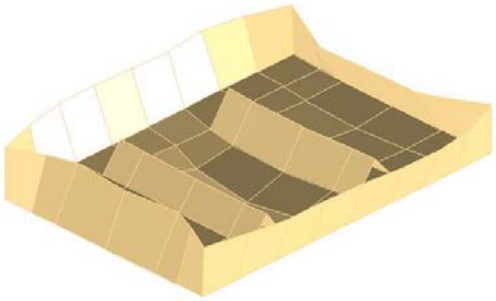

Mode 8: 159.77 Hz

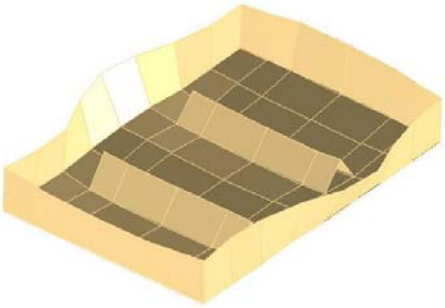

Mode 9: 187.51 Hz

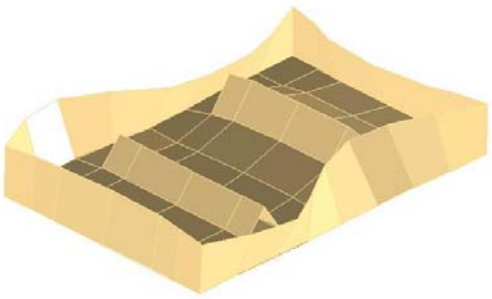

Mode 10: 199.65 Hz

Figure 3.27: 4th and 5th pair of measured modes of the welded structure

Chapter 4

FE Modelling and Model Updating of the Substructures

4.1 Introduction

Structural analyses continue to present a major concern for a very wide range of engineering products today. However, the procedures and methods for modelling and analysing structures have been the subject of much investigation for the last four decades. In the past, structural vibration analyses were based on experience, extensive laboratory testing, and finally, proving ground evaluation and development. Analytical methods, though available, were extremely difficult if not impossible to apply to the complex structural analyses, in particular automobile structures. Emphasis therefore was on experimental determination of structural behaviour and performance. The demands on the structures designer increased and changed rapidly, first to meet new safety requirements and later to reduce weight in order to satisfy economy requirements. Experience could not be extended to new structure sizes, and performance data on the new criteria was not available. Mathematical modelling was therefore a logical avenue to explore and investigate.

However, during the past five decades, owing to the advent of digital computers, computer simulation and numerical methods have become very popular for solving complex problems. The procedures and methods have been widely used by researchers and engineers throughout the world. The finite element method which is one of the numerical methods has become universally accepted and routine numerical tools for analysing any complex product geometries (Kamal et al., 1985).

Finite element analysis has been a powerful and practical tool for simulating structural behavior for some decades, however creating accurate finite element models that are frequently required in large number of applications such as optimization, design, damage identification, structural control and health

monitoring (Mottershead and Friswell, 1993) is not an easy task. A very large number of degrees of freedom are required to model large complex structures. This absolutely leads to computational burden. Therefore simplifications and assumptions on geometrical and material properties, boundary conditions and also those of joints during the construction of FE models are necessary required in order to keep the order of the models computationally manageable.

Since the finite element method is a numerical method-based analysis which relies on the initial assumptions in the development of the mathematical model, therefore validation between FE data and experimental data must be performed in order to ensure the reliability of the FE models. Significant discrepancies between the FE data and experimental data due to modal properties and boundary conditions were reported by Mottershead et al. (2000) ; Palmonella et al. (2003) and Ahmadian et al. (2001). Therefore model updating is a tool for the preparation of reliable FE models through which the invalid assumptions of the initial values of FE models are corrected by processing the experimental data. In other words model updating is a process of attempting to correct the errors in FE models by using measured data such as natural frequencies, damping ratios, mode shapes and frequency response functions which can be usually obtained from vibration tests (Yueh et al., 2009).

The finite element model updating methods that are well elaborated in Mottershead and Friswell (1993), have been intensively used for the past decades in order to minimise the discrepancies in the finite element models in comparison with the experimental results which are commonly natural frequencies and mode shapes. However it is imperative note that experimental results are always partial (Kenigsbuch and Halevi, 1998), these arise as a result of all vibration modes being impossible to measure during the experiment, in particular for large and complex structures (Ewins, 2000; Friswell and Mottershead, 1995).

This chapter presents the finite element modelling and model updating procedure. These include elaborating the formulation used in finite element method, model updating and also the description of Design Sensitivity and Optimisation SOL200

provided in NASTRAN. This chapter also covers the development of finite element models of the substructures through which model updating methods are performed to minimise the errors introduced in the finite element models. The numerical results obtained from the initial and updated finite element models which are natural frequencies and mode shapes are then compared with those measured from the experiment as described in chapter 3. Meanwhile the same procedures and methods would be used in the construction of the finite element model of welded structures. The details of the work, results and discussion are covered in the next chapter.

The main objective of this chapter is presenting and discussing the systematic approaches of modelling of the substructures (side wall 1, side wall 2, stopper 1, stopper 2 and bent floor). This includes considering the effect of boundary conditions and also the thickness reduction in the bending areas on the accuracy of the results which is one of the significant findings in this research study.

4.1.1 FE method and model updating

Due to lack of viable computational methods to handle distributed parameters systems through which vibrating systems such as automotive structures and buildings are usually described, the finite element method that has evolved into one of the most powerful and widely used techniques for finding approximate solutions to the differential equations is generally used to discretize such systems to a finite element model, namely a second order differential equation.

$$\mathbf{M}\ddot{\mathbf{q}}(t)+\mathbf{C}\dot{\mathbf{q}}(t)+\mathbf{K}\mathbf{q}(t)=\mathbf{f}(t) \tag{4.1}$$

where **M**, **C** and **K** are symmetric matrices of mass, damping and stiffness. Meanwhile $\ddot{\mathbf{q}}$, $\dot{\mathbf{q}}$ and $\mathbf{q}$ are the $n \times 1$ vector of accelerations, velocities and displacements respectively and $\mathbf{f}(t)$ is $n \times 1$ vector of external forces.

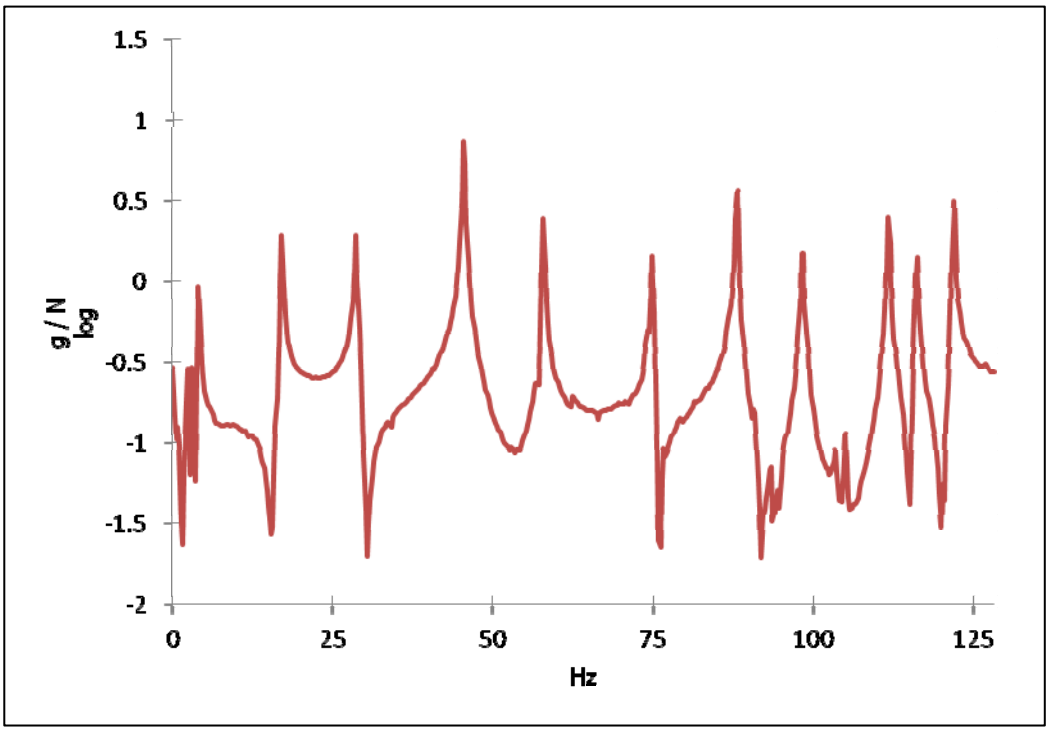

(a)

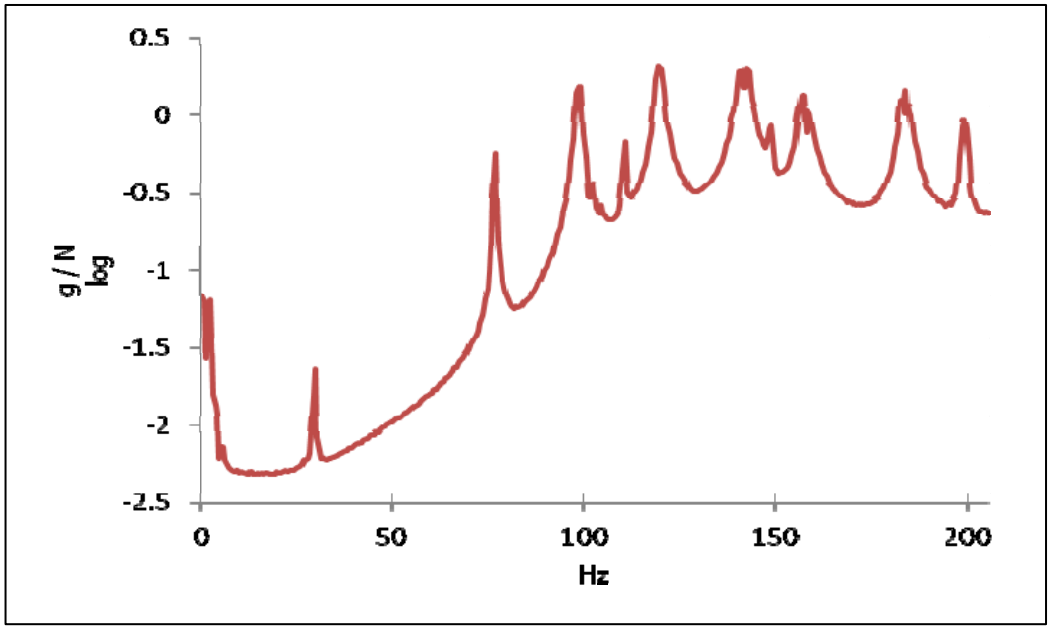

(b)

Figure 4.1: FRFs of the substructure (a) and the welded structure (b)

Since lightly damped modes show very narrow peaks in the frequency response functions, therefore, in this work, the substructures and the welded structure are considered having light damping and the effect of damping can be theoretically neglected in the FE modelling. The frequency response functions of the substructure and the welded structure are shown in Figure 4.1.

In undamped free vibration analysis, the equation of motion (4.1) reduces to

$$\mathbf{M}\ddot{\mathbf{q}}(t)+\mathbf{K}\mathbf{q}(t)=0 \tag{4.2}$$

To solve Eq. (4.2) assume a harmonic solution of the form

$$\mathbf{q}=\boldsymbol{\phi}\sin\omega t \tag{4.3}$$

where $\boldsymbol{\phi}$ and ω are is the mode shape and frequency of the system

If differentiation of the assumed harmonic solution is performed and substituted into Eq. 4.1, yields the following

$$-\omega^2\mathbf{M}\boldsymbol{\phi}\sin\omega t+\mathbf{K}\boldsymbol{\phi}\sin\omega t=0 \tag{4.4}$$

and it can be further simplified

$$(\mathbf{K}-\omega^2\mathbf{M})\boldsymbol{\phi}=0 \tag{4.5}$$

Eq. (4.5) has the form of an algebraic eigenvalues problem or it is usually termed as eigenproblem through which the eigensolutions are calculated computationally by commercially available FEM commercial software. In this study, Lanczos method which is probably the most common algorithm used for computing free vibration modes (Rixen, 2002) and the method is also available in many commercial computer codes. NASTRAN SOL103, in particular is used to predict

the dynamic behaviour of the substructures and also the welded structure. The numerical natural frequencies and mode shapes calculated from different sets of model configurations are then compared with those obtained from the experimental results.

In order to quantify the correlation between experimental mode shapes and numerical counterparts, it is commonplace to use the Modal Assurance Criterion (MAC) introduced by Allemang (2003) and deduced originally in a linear regression setting. It is calculated as

$$\mathrm{MAC} = \left(\boldsymbol{\phi}_a, \boldsymbol{\phi}_e\right) = \frac{\left|\boldsymbol{\phi}_a^H \boldsymbol{\phi}_e\right|^2}{\left(\boldsymbol{\phi}_a^H \boldsymbol{\phi}_a\right)\left(\boldsymbol{\phi}_e^H \boldsymbol{\phi}_e\right)} \tag{4.6}$$

where $\boldsymbol{\phi}_a$ is predicted mode shapes and $\boldsymbol{\phi}_e$ is measured mode shapes. MAC takes values between 0 and 1; the closer to 1, the higher correlation, while the closer to 0 means that those modes are not orthogonal or independent.

4.1.2 FE model updating

Due to uncertainties in the geometry, material properties, joints and boundary conditions as a result of the simplifications and assumptions, the dynamic behaviour of structures predicted by finite element models usually differs from the experimental results. For example, Mares et al. (2002) used finite element model to predict the frequencies of GARTEUR SM-AG19. In the investigation the first fourteen modes of the initial finite element model were found to be not in good agreement with the total error of 32 % in comparison with experimental results. In another study Li (2002) reported that the discrepancy between the test and the finite element frequencies of a simple beam structure was 28.9 % for the first five modes. While Schedlinski et al. (2004) reported that the errors in the frequency predictions of the body-in-white deviated less than 30% from the test counterparts and MAC value were larger than 50% for the first seven modes.

Burnett and Young (2008) used FEM to construct and study the dynamic behaviour of a body-in-white with hundred thousands of degrees of freedom and the element sizes of approximately of 3mm. The discrepancies between the first four modes of the test and the prediction observed in their studies were reported to be 25%. Therefore the issues of large deviations between the test and finite element results as reported beforehand clearly show that an effective and feasible method is necessary in order to obtain reliable finite element models for further analyses. Thus modal updating as elaborated in Friswell and Mottershead (1995) which aims to correct the invalid assumptions of the analysis model properties of the finite element models is a viable method to be considered.

The finite element model updating method that was explained in Mottershead and Friswell (1993) has been a subject of great importance for and widely used in mechanical and aerospace structures since the 1990s. Model updating methods which are model-based technique involving a hybrid use of experimental data and finite element model results can be broadly classified into two categories: the direct method or one-step method and the penalty method or iterative method (Li, 2002 and Weng et al., 2011). The former directly solves a set of characteristic equations that typically consist of the stiffness and mass matrices of the finite element models. While the latter is based on modifying the parameters of the finite element models iteratively to minimise some kind of error norms or modal properties (frequencies and mode shapes) that are used to evaluate the discrepancies between the experimental and finite element results. An appreciable amount of research using finite element model updating has been performed for structural dynamics has increased in recent years. Kim et al. (1989) successfully applied the latter method to a tool-holder system with a taper joint to identify the joint stiffness and damping characteristics. The same method was used by Arruda and Santos (1993) to identify the stiffness and damping properties of the mechanical joints.

4.1.3 Iterative methods of FE model updating

These methods are based on sensitivity methods. It requires the determination of the sensitivity of a set of updating parameters to differences in dynamic behaviour between analytical and experimental dynamic data. The techniques yield an expression of the form

$$\Delta \mathbf{Z} = \mathbf{S}\,\Delta\boldsymbol{\theta} \tag{4.7}$$

where $\Delta\mathbf{Z}$ are a set of differences in dynamic behaviour between an theoretical model and experimental model, while $\Delta\boldsymbol{\theta}$ is the vector of perturbations in the updating parameters and $\mathbf{S}$ is the sensitivity matrix and the first derivative of eigenvalues with respect to the updating parameters. The sensitivity coefficient denotes the rates of change of eigenvalues and eigenvectors due to the perturbations in updating parameters.

The rate of change of the i^{th} eigenvalues (λ_i) with respect to the j^{th} parameters, (θ_j) can be derived as follows (Friswell and Mottershead, 1995).

$$\mathbf{S}_{ij} = \frac{\partial \lambda_i}{\partial \theta_j} = \boldsymbol{\phi}_i^{\mathrm{T}} \left[\frac{\partial \mathbf{K}}{\partial \theta_j} - \lambda_i \frac{\partial \mathbf{M}}{\partial \theta_j} \right] \boldsymbol{\phi}_i \tag{4.8}$$

4.1.4 FE model updating via MSC NASTRAN (SOL200)

There are two ways of updating a model in order to minimise the discrepancies. The refinement process can be implemented in an inefficient or efficient manner. The inefficient way is by trial-and-error in which simply changing one or more parameters, rerunning the analysis, and comparing the new numerical results with the experimental ones. If the discrepancies are reduced enough, then the process is stopped. However the repeated processes of changing the parameters and rerunning

the analysis are required if it is not close enough. Apparently, the process is very inefficient and time consuming for a complex structure with a large number of parameters. An efficient way is using MSC NASTRAN to compute the response sensitivities directly. In this work, MSC NASTRAN's design sensitivity and optimization (SOL200) is used for model updating process of the substructures and the welded structure in order to match with the experimental results.

In MSC NASTRAN's design sensitivity and optimization (SOL200), an objective function can be defined via a user-written equation. The objective function used in this work is to minimise the error between the numerical and experimental frequencies and it is defined by

$$F = \sum_{i=1}^{n} w_i \left(\frac{\lambda_i^{FE}}{\lambda_i^{EXP}} - 1 \right)^2 \tag{4.9}$$

where λ_i^{FE} is the i^{th} numerical eigenvalue obtained from the finite element model and λ_i^{EXP} is the i^{th} experimental eigenvalues calculated from the tested model. While w_i represents the weighting coefficient through which certain modes that need more attention are assigned to. However in this work, the weighting coefficient is not assigned to any modes of interest. Attention is paid to other areas for improving the accuracy of the finite element models. While design variables (geometric and material properties) are defined as side constraints (upper and lower bounds on the design variables) and performance constraints (minimum and maximum allowable response values, such as an eigenvalue limit).

The optimizer in MSC NASTRAN which is based on the Modified Method of Feasible Direction is used to find the set of updated parameters that minimizes the error as defined in Eq. (4.9). In the procedure which is elaborated in Muira (1988), the parameters are automatically updated until the numerical results match the experimental results. The minimum of the error calculated from the objective function gives a good correlation between the numerical and experimental results. The optimizer uses response sensitivities and approximate analysis to select new

parameters for each iteration in the process. This iterative process continues automatically until convergence is achieved by a lack of change in the parameters or the objective function between consecutive iterations.

4.2 Suspension effects on test structures

The use of soft springs to approximate a free-free state of the structure is often used in modal testing because the effect of soft springs on the test structure is negligible. However, for flexible and thin structures, the lowest elastic mode may interfere with the stiffness of the soft springs. On the other hand, even soft springs could introduce stiffness and damping into the system. This added stiffness and damping of the springs may significantly alter the lowest elastic mode of the test structure. Therefore the effect of the stiffness of the springs on the lowest elastic mode of the test structure must also be considered in finite modelling and model updating.

The effect of suspension stiffness on the modal parameters of test structures has been of interest and concern for the last few decades. Bisplinghoff (1955) discussed the effects of support stiffness and mass on modal frequencies, based on Rayleigh's results. Wolf Jr (1984) investigated effects of support stiffness with regard to modal testing of a car. Initially, he analytically studied the effects of a spring to ground on a simple 2 DOF system. He concluded that to minimise the influence of the suspension system, the support system should be attached to the most massive portion of the test system. He also reported that the rule of thumb to simulate free-free boundary conditions is to design the support system so that the rigid body modes are no more than one-tenth of the frequency of the lowest elastic mode.

Carne and Dohrmann (1998) studied the effects of the support stiffness and damping on measured modal frequencies and damping ratios. They developed the model used by Wolf by including damping in the supporting system of the model. It was shown that for a lightly-damped structure even when the rigid body modes are no more than one-tenth of the frequency of the lowest elastic mode, the measured damping can be far from the true damping. investigated the effects of

suspension stiffness on a beam using different shock cord lengths and thicknesses. A perturbation study was done to determine what effects suspension stiffness would have on the mode shapes of the beam and optimization routines were used to achieve a minimal difference between the analytical mode shapes and the experimental mode shapes. Carne and Dohrmann (1998) also suggested that to obtain meaningful updates, strict control must be exercised over which parameters were varied and for the beam suspended with shock cords, the only part of the system that was not known with confidence was the suspension. In their work, updates were only performed on the equivalent stiffnesses representing the suspension. It can be concluded that suspension springs which are quite often used to simulate free-free boundary conditions in a test may have serious effects on the measurement of modal parameters of a structure. Therefore, the stiffness of suspension springs which, in practice, can be measured must be included in the FE modelling of the structure.

In this study the investigation of the effect of the stiffness of the springs and strings on the modal properties (frequencies and mode shapes) of the substructures and the welded structure is demonstrated and discussed. Furthermore the effect is also considered in the finite element modelling and model updating of the substructures (only the bent floor) and the welded structure in the attempt to achieve minimal discrepancies between the experimental and numerical results.

4.3 FE modelling and model updating of the substructures

4.3.1 FE modelling and model updating of side wall 1 and side wall 2

The geometrical design of side wall 1 and side wall 2 with three flanges and radii was initially constructed using a CAD system, where the tools for handling complex geometries are normally much well developed than those in the pre-processors of the finite element systems. The CAD models of both substructures are shown in Figure 4.2(a). One of the central important requirements of constructing finite element models through 2D- elements is using mid-surface

abstraction models. Therefore the mid-surfaced models of the substructures were then created using mid-surfacing tools in PATRAN. The mid-surface representation models are shown in Figure 4.2 (b).

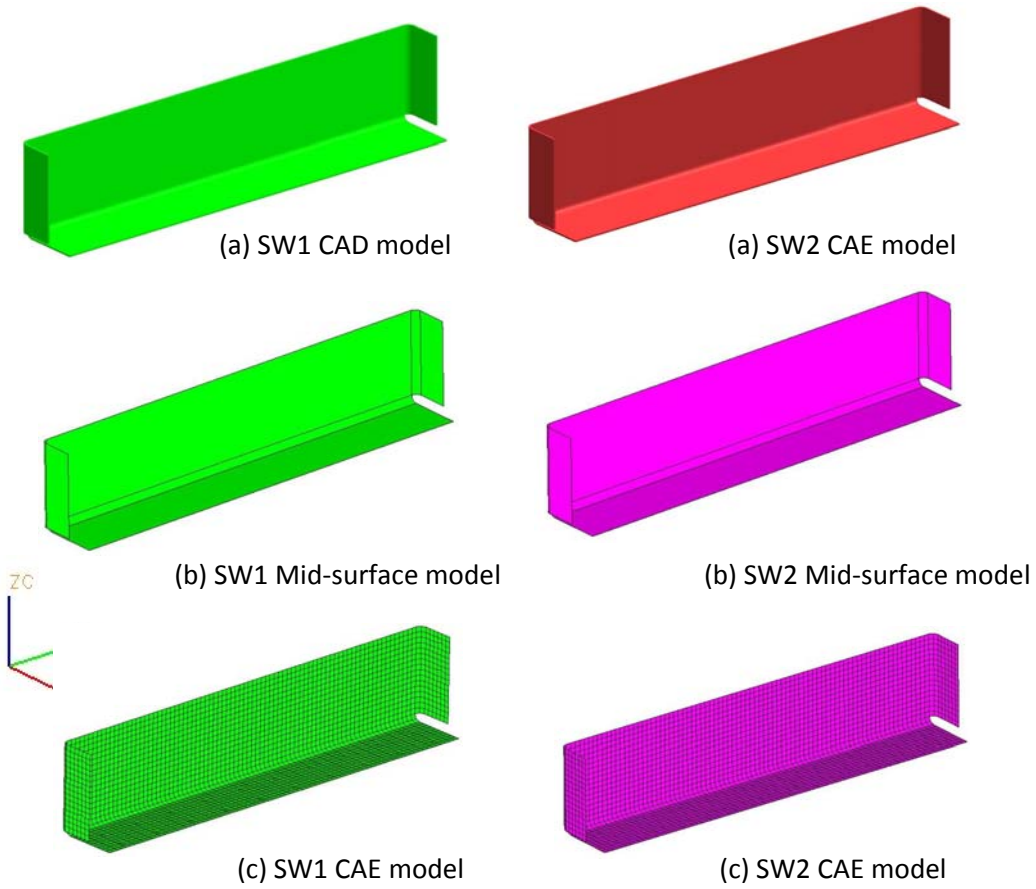

Figure 4.2: Visual models of side wall 1 (SW1) and side wall 2 (SW2)

PATRAN which is widely used as pre/post-processing package for NASTRAN was then used to construct the finite element models of both side wall 1 and side wall 2 with a total of 2524 CQUAD4 shell elements on each model. The CQUAD4 elements based finite element models are depicted in Figure 4.2 (c). The nominal values as tabulated in Table 4.1 are used for the material properties of the finite element models.

Table 4.1: Nominal values of mild steel material properties of side wall 1 and side wall 2

Material Properties	Nominal Values
Young's modulus (E)	210 GPa
Shear modulus (G)	81 GPa
Poisson's ratio (ν)	0.3
Mass density (ρ)	7850 kg/m^3

NASTRAN codes for normal modes analysis are developed and used for the calculation of the frequencies and mode shapes of side wall 1 and side wall 2. The computed frequencies of side wall 1 and side wall 2 are shown in Table 4.2 and 4.3 respectively, while the mode shapes of the former and latter are depicted in Figure 4.4 to Figure 4.5.

The first ten frequencies calculated from the finite element models which are termed initial finite element models are compared with the experimental counterparts. The comparisons of the results for both side wall 1 and side wall 2 are found to be not in good agreement with the total error of being 13.13 percent and 14.43 percent respectively. The comparison results which are calculated in a relative error between the initial finite element and experimental are shown in the column (III) of Table 4.2 and 4.3 accordingly. The dissonant results reveal that the initial finite element models need to be updated in order to minimise the errors.

Table 4.2: Comparison of results between the tested and initial FE model of side wall 1

Mode	I Experimental Side Wall 1 (Hz)	II Initial FE Side Wall 1 (Hz)	III Error (%) |I-II/I|	IV Initial FE MAC
1	96.55	94.54	2.08	0.95
2	138.84	137.01	1.31	0.97
3	222.87	219.39	1.56	0.92
4	315.61	310.22	1.71	0.97
5	360.25	358.96	0.36	0.95
6	376.95	375.12	0.48	0.93
7	418.61	415.86	0.66	0.91
8	442.13	434.90	1.64	0.97
9	527.14	519.46	1.46	0.91
10	555.29	544.87	1.88	0.92
Total Error			13.13	

Table 4.3: Comparison of results between the tested and initial FE model of side wall 2

Mode	I Experimental Side Wall 2 (Hz)	II Initial FE Side Wall 2 (Hz)	III Error (%) |I-II/I|	IV Initial FE MAC
1	96.74	94.54	2.28	0.95
2	138.99	137.01	1.42	0.94
3	222.91	219.39	1.58	0.93
4	315.91	310.22	1.80	0.98
5	361.90	358.96	0.81	0.95
6	377.76	375.12	0.70	0.94
7	419.31	415.86	0.82	0.90
8	442.48	434.90	1.71	0.98
9	527.05	519.46	1.44	0.91
10	555.23	544.87	1.87	0.95
Total Error			14.43	

The parameterisation for model updating of side wall 1 and side wall 2 is performed through a series of sensitivity analyses in which several potential parameters such as the thickness, Young's modulus, density, Poisson's ratio and shear modulus are listed down in the section of design model data of the NASTRAN SOL200 code (Muira, 1988). The coefficients of design sensitivity which are tabulated in Table 4.4 are defined as the rate of change of the frequencies with respect to a change in the parameters. In other words, the higher the coefficient, the more sensitive to the parameter the frequencies are. From the table, it is found that the highest coefficient appears to be the thickness, which is then followed by the Young's modulus and Poisson's ratio. The frequencies are shown much less sensitive to the shear modulus and density.

Table 4.4: Summarised results of the sensitivity analysis of side wall 1 and side wall 2

Mode	Frequency	Parameters				
		Thickness	Poisson's Ratio	Young's Modulus	Shear Modulus	Density
1	9.45E+01	9.40E+01	1.00E+01	4.70E+01	2.40E-01	-4.73E+01
2	1.37E+02	1.35E+02	1.09E+01	6.82E+01	3.51E-01	-6.85E+01
3	2.19E+02	2.16E+02	9.52E+00	1.09E+02	5.34E-01	-1.10E+02
4	3.10E+02	3.04E+02	1.39E+00	1.55E+02	6.08E-01	-1.55E+02

Since the parameterisation for model updating must reflect a physical meaning, therefore the thickness which is quite easily quantifiable is not considered as updating parameter. Technically the thickness correction is often made to finite element models manually rather than include it as updating parameter. This is to avoid being ended up with an unreasonable updated thickness that leads to no physical meaning to the structure. Therefore there is only one updating parameter which is the Young's modulus used for both finite element models of side wall 1 and side wall 2. The initial value of the Young's modulus is set to be 210 GPa and it is merely allowed to vary from 190 GPa to 220 GPa in which the range of Young's modulus of mild steel is standardised.

As a result of considering the Young's modulus as the updating parameter in the attempt to minimise the error introduced into the initial finite element model of side wall 1, the relative total error of 13.13 percent as shown in the column (III) of Table 4.5 obtained from the comparison between the experimental and the initial finite element models is significantly reduced to 4.95 percent (column V). This clearly shows that the chosen parameter which is the Young's modulus in the updating procedure is appropriate for improving the correlation between the tested and finite element models. Furthermore the use of the updating parameter helps to maintain the excellent correlation of mode shapes between the finite element model and tested model which is quantified in MAC values presented in column (VI) of the Table 4.5.

The updating procedure of side walls 1 and 2 is performed by minimising the objective function as shown in Equation 4.9 and the first four experimentally observed frequencies are used in updating the finite element models of side walls 1 and 2. In Tables 4.5 and 4.7, the 5th to 10th natural frequencies have not been used in the objective function and may be used to assess the model quality. Those five frequencies have improved significantly and show as expected that the updated models represent the measured model well.

Table 4.5: Three comparisons of results between the tested and FE models of side wall 1

Mode	I Experimental Side Wall 1 (Hz)	II Initial FE Side Wall 1 (Hz)	III Error (%) |I-II/I|	IV Updated FE Side Wall 1 (Hz)	V Error (%) |I-IV/I|	VI Updated FE MAC
1	96.55	94.54	2.08	96.14	0.42	0.95
2	138.84	137.01	1.31	139.33	0.36	0.97
3	222.87	219.39	1.56	223.11	0.11	0.92
4	315.61	310.22	1.71	315.48	0.04	0.97
5	360.25	358.96	0.36	365.06	1.33	0.95
6	376.95	375.12	0.48	381.49	1.20	0.93
7	418.61	415.86	0.66	422.90	1.03	0.91
8	442.13	434.90	1.64	442.27	0.03	0.97
9	527.14	519.46	1.46	528.25	0.21	0.91
10	555.29	544.87	1.88	554.11	0.21	0.92
Total Error			13.13		4.95	

Table 4.6 shows the increment of 3.43 percent in the initial value of the Young's modulus after undergoing the updating process. Meanwhile the convergence of the updating parameter starting from the initial normalised value to the convergent value is depicted in Figure 4. 3.

Table 4.6: Updated value of parameter of side wall 1

Parameter	Initial value	Updated value	Unit
Young's Modulus	210000	217203	MPa

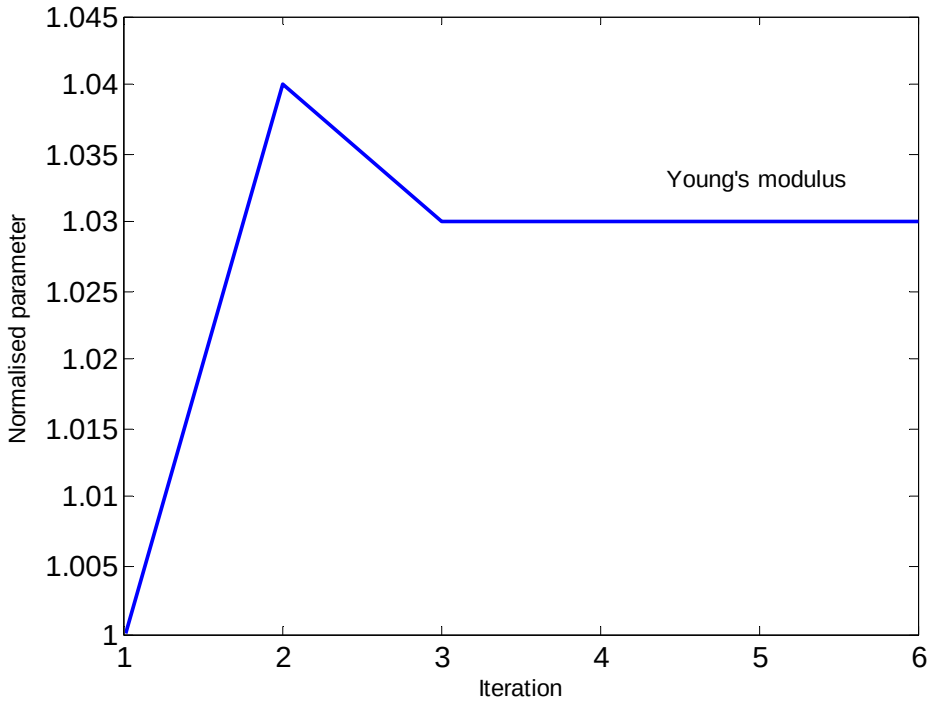

Figure 4.3: The convergence of the updating parameter of side wall 1

Even though the tested model of both side wall 1 and side wall 2 is almost identical visually in appearance and geometry, however the experimental results of the substructures as shown in the column (I) of Table 4.5 and 4.7 respectively have revealed the invalidity of the visual assumption. Furthermore the total error of 14.43 percent shown in the column (III) of Table 4.7 has given additional information on the need of the substructures to be independently tested experimentally and numerically.

The same updating parameter which is the Young's modulus is used for matching the initial finite element model of side wall 2 to the tested model. The decision to use the same updating parameter as used in side wall 1 is due to the identical results of sensitivity analysis obtained. The total error of 14.43 percent has been successfully reduced to 4.61 percent with MAC value of 0.9 above as depicted in the column (V) and (VI) respectively in Table 4.7.

Table 4.7: Three comparisons of results between the tested and FE models of side wall 2

Mode	I Experimental Side Wall 2 (Hz)	II Initial FE Side Wall 2 (Hz)	III Error (%) |I-II/I|	IV Updated FE Side Wall 2 (Hz)	V Error (%) |I-IV/I|	VI Updated FE MAC
1	96.74	94.54	2.28	96.24	0.52	0.95
2	138.99	137.01	1.42	139.48	0.35	0.94
3	222.91	219.39	1.58	223.34	0.19	0.93
4	315.91	310.22	1.80	315.80	0.03	0.98
5	361.90	358.96	0.81	365.44	0.98	0.95
6	377.76	375.12	0.70	381.88	1.09	0.94
7	419.31	415.86	0.82	423.34	0.96	0.90
8	442.48	434.90	1.71	442.73	0.06	0.98
9	527.05	519.46	1.44	528.80	0.33	0.91
10	555.23	544.87	1.87	554.69	0.10	0.95
Total Error			14.43		4.61	

The initial value and updated value of the Young's modulus are tabulated in Table 4.8 with the increment of 3.65 percent from the initial value. Meanwhile the convergence of the updating parameter of side wall 2 starting from the initial normalised value to the convergent value is depicted in Figure 4. 4.

Table 4.8: Updated value of parameter of side wall 2

Parameter	Initial value	Updated value	Unit
Young's Modulus	210000	217665	MPa

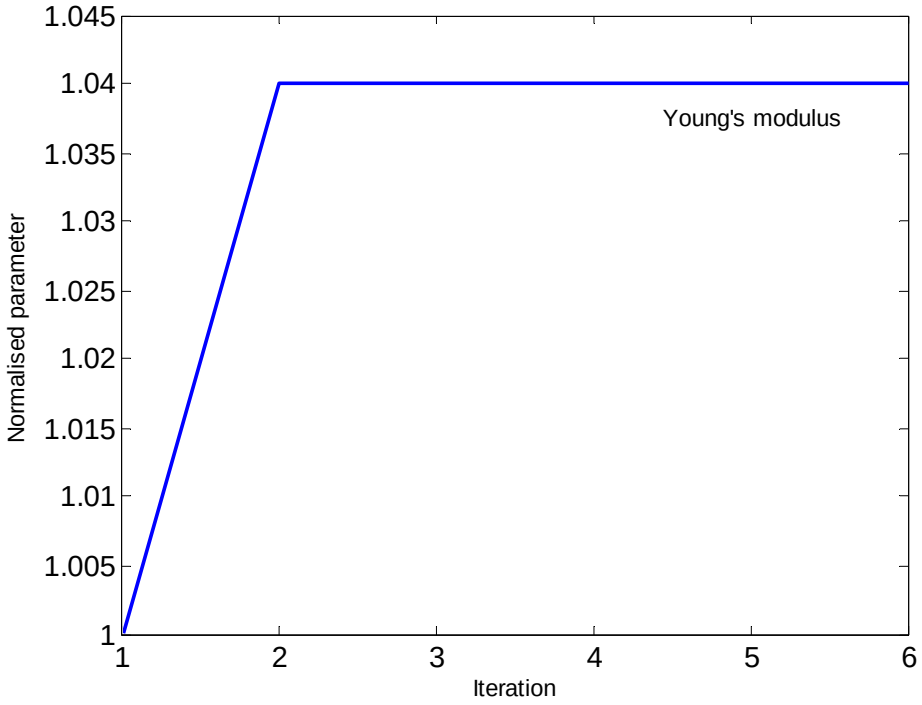

Figure 4.4: The convergence of the updating parameter of side wall 2

Tables 4.9 up to 4.12 show the comparisons of the results of side walls 1 and 2 calculated based on the different number of the measured frequencies defined in the objective function as shown in Equation 4.9. Column I and II represent for the experimental results and the results calculated from the initial finite element model respectively, while columns III to XII are the results calculated from the updated finite element model. NoMF stands for the number of measured frequencies and VoOF is the sum of the objective function value. From the tables, it is shown that the larger the number of measured frequencies used in the objective function, the better the results are obtained. However, in this study, only four measured frequencies are used in the objective function. This is because there is no much difference between the value of objective function (VoOF) calculated from before or after NoMF 4 as shown in columns V, VI and VII in Tables 4.9 and 4.11 respectively.

Table 4.9: The comparisons of results calculated from different number of measured frequencies (NoMF) of side wall 1 - 1st to 5th

Mode	I Exp (Hz)	II Initial FE (Hz)	III NoMF 1 (Hz)	IV NoMF 2 (Hz)	V NoMF 3 (Hz)	VI NoMF 4 (Hz)	VII NoMF 5 (Hz)
1	96.55	94.54	96.55	96.17	96.13	96.14	95.88
2	138.84	137.01	139.93	139.38	139.32	139.33	138.96
3	222.87	219.39	224.06	223.18	223.08	223.11	222.51
4	315.61	310.22	316.83	315.58	315.43	315.48	314.63
5	360.25	358.96	366.62	365.18	365.01	365.06	364.08
6	376.95	375.12	383.12	381.61	381.43	381.49	380.46
7	418.61	415.86	424.71	423.04	422.85	422.90	421.77
8	442.13	434.90	444.16	442.42	442.21	442.27	441.08
9	527.14	519.46	530.50	528.42	528.18	528.25	526.83
10	555.29	544.87	556.48	554.30	554.04	554.11	552.62
VoOF		0.20539	0.09644	0.04947	0.04596	0.04692	0.03464

Table 4.10: The comparisons of results calculated from different number of measured frequencies (NoMF) of side wall 1 - 6th to 10th

Mode	I Exp (Hz)	II Initial FE (Hz)	VIII NoMF 6 (Hz)	IX NoMF 7 (Hz)	X NoMF 8 (Hz)	XI NoMF 9 (Hz)	XII NoMF 10 (Hz)
1	96.55	94.54	95.73	95.65	95.71	95.73	95.79
2	138.84	137.01	138.74	138.62	138.71	138.74	138.83
3	222.87	219.39	222.16	221.97	222.10	222.16	222.30
4	315.61	310.22	314.14	313.87	314.05	314.14	314.33
5	360.25	358.96	363.51	363.19	363.41	363.51	363.74
6	376.95	375.12	379.87	379.54	379.76	379.87	380.11
7	418.61	415.86	421.11	420.75	420.99	421.11	421.37
8	442.13	434.90	440.40	440.02	440.28	440.40	440.67
9	527.14	519.46	526.01	525.56	525.87	526.01	526.34
10	555.29	544.87	551.76	551.28	551.61	551.76	552.11
VoOF		0.20539	0.03417	0.03600	0.03459	0.03417	0.03377

Table 4.11: The comparisons of results calculated from different number of measured frequencies (NoMF) of side wall 2 - 1st to 5th

Mode	I Exp (Hz)	II Initial FE (Hz)	III NoMF 1 (Hz)	IV NoMF 2 (Hz)	V NoMF 3 (Hz)	VI NoMF 4 (Hz)	VII NoMF 5 (Hz)
1	96.74	94.54	96.74	96.32	96.24	96.23	96.05
2	138.99	137.01	140.21	139.59	139.48	139.46	139.21
3	222.91	219.39	224.50	223.52	223.34	223.32	222.90
4	315.91	310.22	317.45	316.06	315.80	315.77	315.18
5	361.90	358.96	367.35	365.74	365.44	365.40	364.72
6	377.76	375.12	383.87	382.19	381.88	381.84	381.13
7	419.31	415.86	425.54	423.69	423.34	423.30	422.51
8	442.48	434.90	445.04	443.09	442.73	442.68	441.86
9	527.05	519.46	531.54	529.23	528.79	528.74	527.76
10	555.23	544.87	557.58	555.14	554.69	554.63	553.60
VoOF		0.23254	0.09846	0.04240	0.03624	0.03554	0.02697

Table 4.12: The comparisons of results calculated from different number of measured frequencies (NoMF) of side wall 2 -6tht to 10th

Mode	I Exp (Hz)	II Initial FE (Hz)	VIII NoMF 6 (Hz)	IX NoMF 7 (Hz)	X NoMF 8 (Hz)	XI NoMF 9 (Hz)	XII NoMF 10 (Hz)
1	96.74	94.54	95.91	95.82	95.87	95.87	95.92
2	138.99	137.01	139.00	138.88	138.94	138.95	139.02
3	222.91	219.39	222.57	222.37	222.48	222.49	222.60
4	315.91	310.22	314.71	314.44	314.58	314.60	314.75
5	361.90	358.96	364.17	363.85	364.02	364.04	364.22
6	377.76	375.12	380.56	380.23	380.40	380.43	380.61
7	419.31	415.86	421.88	421.51	421.70	421.73	421.93
8	442.48	434.90	441.20	440.81	441.01	441.05	441.26
9	527.05	519.46	526.97	526.51	526.75	526.79	527.04
10	555.23	544.87	552.77	552.28	552.53	552.57	552.84
VoOF		0.23254	0.02509	0.02608	0.02538	0.02530	0.02507

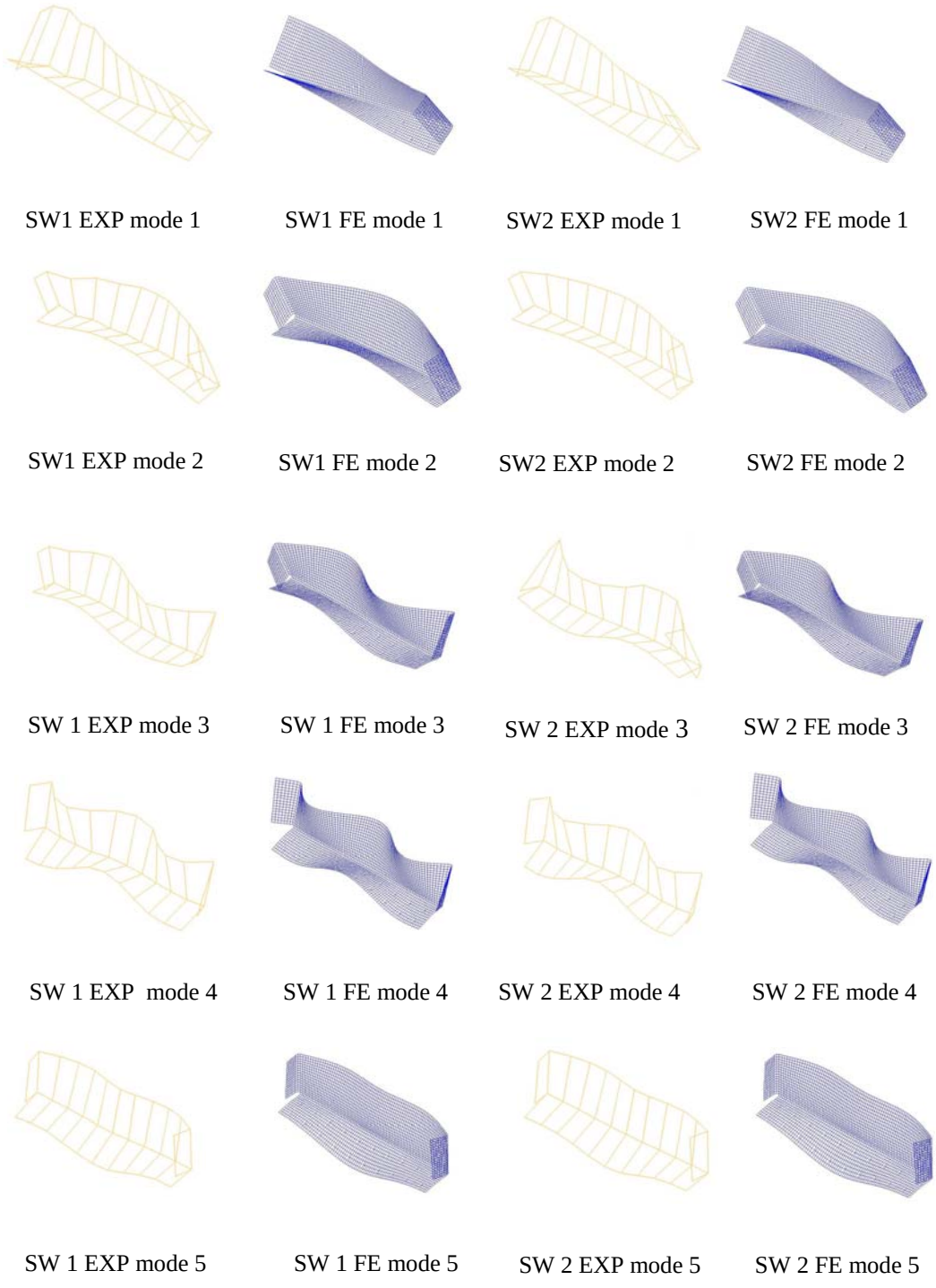

Figure 4.4: 1st, 2nd, 3rd, 4th and 5th pair of experimental (EXP) and updated FE modes of side wall 1 (SW1) and side wall 2 (SW2)

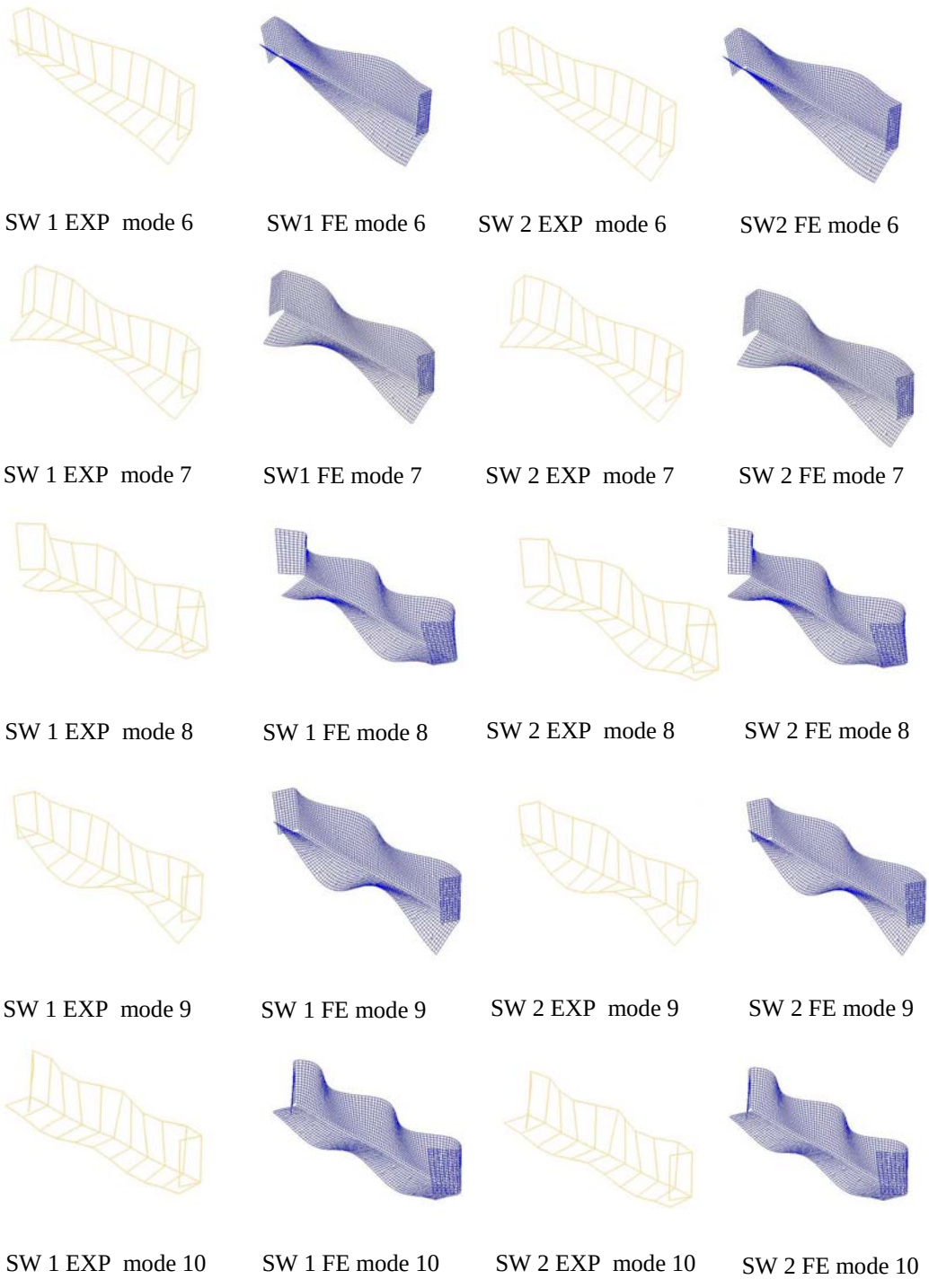

Figure 4.5: 6^{th}, 7^{th}, 8^{th}, 9^{th} and 10^{th} pair of experimental (EXP) and updated FE modes of side wall 1 (SW1) and side wall 2 (SW2)

4.3.2 FE modelling and model updating of stopper 1 and stopper 2

This section presents the finite element modelling of stopper 1 and 2 using the same procedures elaborated in the preceding section. 4800 CQUAD4 elements were used to construct the finite element models and they are shown in Figure 4.7. There are two models which are called 1st and 2nd model that have been used in the attempt to match the finite element model with the tested model. Two measured frequencies are used in the objective function (Equation 4.9) in order to update the finite element models of stoppers 1 and 2.

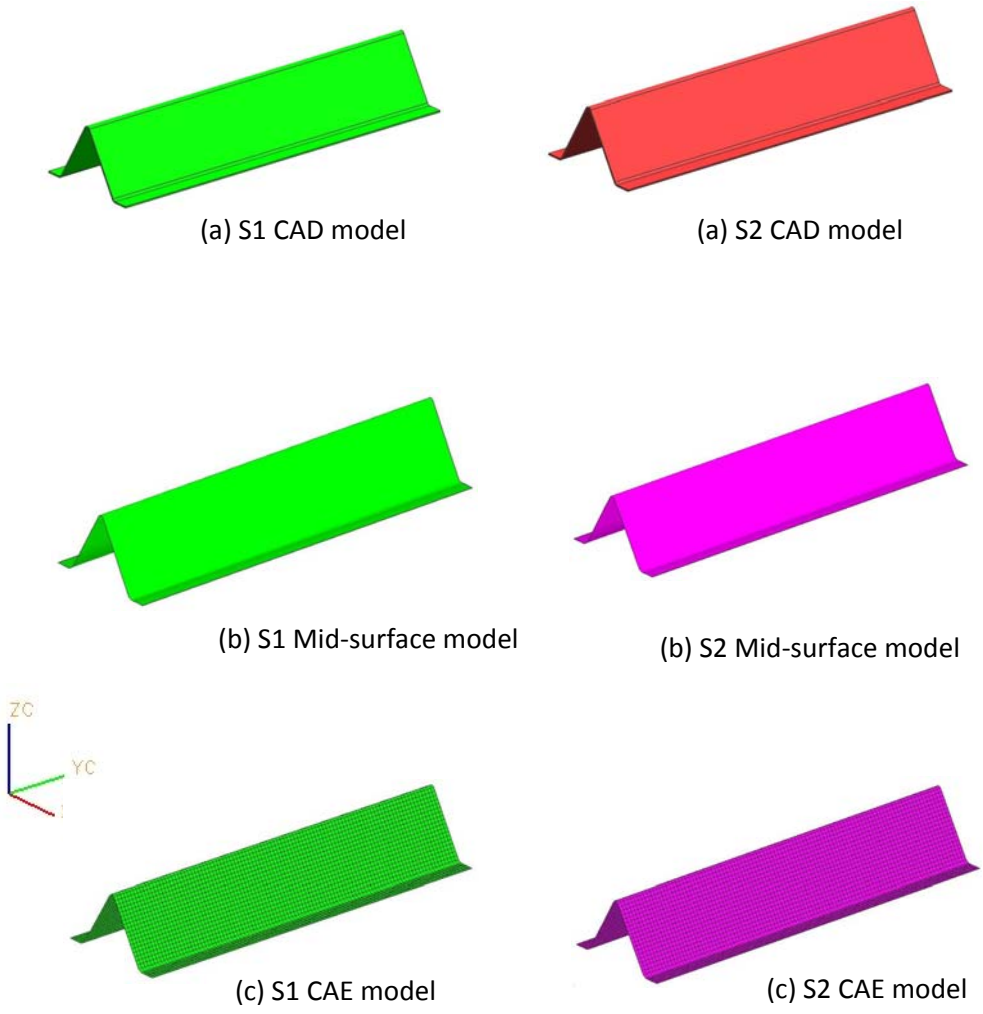

Figure 4.7: Visual models of stopper 1 (S1) and stopper 2 (S2)

Tables 4.13 and 4.14 show the initial finite element results of stoppers 1 and 2 calculated based on the nominal values of mild steel material properties with the uniform thickness of 1.2mm. From the tables it can be seen that the total error of both substructures is 7.90 and 7.40 percent respectively.

Table 4.13: Comparison of results between the tested and initial FE model of stopper 1

Mode	I Experimental Stopper 1 (Hz)	II Initial FE Stopper 1 (Hz)	III Error (%) |I-II/I|	VI Initial FE MAC
1	139.57	136.29	2.35	0.95
2	221.94	228.62	3.01	0.94
3	256.20	262.71	2.54	0.92
Total Error			7.90	

Table 4.14: Comparison of results between the tested and the initial FE model of stopper 2

Mode	I Experimental Stopper 2 (Hz)	II Initial FE Stopper 2 (Hz)	III Error (%) |I-II/I|	VI Initial FE MAC
1	139.32	136.29	2.17	0.95
2	221.83	228.62	3.06	0.93
3	257.13	262.71	2.17	0.91
Total Error			7.40	

The results of the 1st updated finite element model to match those with the tested model are tabulated in Table 4.15 and 4.16 respectively. The Young's modulus is used as the updating parameter and it is found to be no significant reduction in the total error of both substructures. In addition, from both Tables, it can be observed that the predicted 1st frequency in particular has become far away from the measured frequency. This clearly suggests that the use of that updating parameter alone is not enough to reduce the error and there must be something amiss in the finite element models that should be looked into.

Table 4.15: Comparison of results between the tested and the 1st updated FE model of stopper 1

Mode	I Experimental Stopper 1 (Hz)	II 1st Updated FE model Stopper 1 (Hz)	III Error (%) |I-II/I|	VI Updated FE MAC
1	139.57	134.78	3.43	0.95
2	221.94	226.06	1.86	0.94
3	256.20	259.78	1.40	0.92
Total Error			6.69	

Table 4.16: Comparison of results between the tested and the 1st updated FE model of stopper 2

Mode	I Experimental Stopper 2 (Hz)	II 1st Updated FE mode Stopper 2 (Hz)	III Error (%) |I-II/I|	VI Updated FE MAC
1	139.32	134.85	3.21	0.95
2	221.83	226.18	1.96	0.93
3	257.13	259.92	1.08	0.91
Total Error			6.25	

The 2nd updated FE models of the substructures are about considering the reduction in the thickness of the tested models in the finite element models. The tested models of the stoppers are scrutinised and they are found to have a reduction of 0.2mm in the thickness of the backbone area in particular. The reduction is a result of bending process during the fabrication. A different collector is introduced in the finite element models in order to represent the area where the thickness reduction took place. The area naming backbone is graphically shown in Figure 4.8. In this attempt two different collectors are used to represent two different types of model properties which are backbone (red) and non-backbone (green). The details of the two different collectors of the finite element models are shown in Table 4.13.

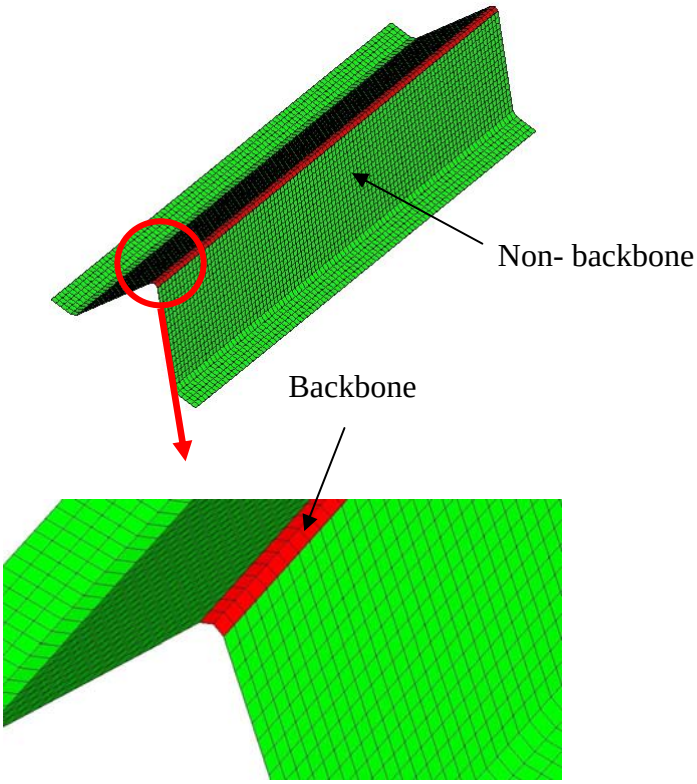

Figure 4.8: Backbone of stopper 1 and stopper 2

Table 4.17: The details of the two different collectors of FE models of the stopper 1 and stopper 2

Description	Thickness (mm)	Young's Modulus (GPa)	Poisson's Ratio	Density (kg/m^3)
Backbone Collector	1.0	210	0.3	7850
Non-Backbone Collector	1.2	210	0.3	7850

From Table 4.17 it can be seen that the nominal values of the mild steel material properties are used for both collectors. The two collectors differ in firstly the thickness and secondly the Young's modulus of the non backbone which is set to be the updating parameter and is permitted to vary 210 GPa to 220 GPa. The new set up of the model properties has reduced the error for both stopper 1 and stopper 2. From Tables 4.15, 4.16 and 4.18, it can be observed that a significant reduction in the second and third modes. This clearly reveals that the consideration of the reduction in the backbone thickness from 1.2 mm to 1 mm which reflects the actual thickness of the tested models has helped to reduce the geometrical uncertainties of the finite element models before the models undergoing model updating process.

Table 4.18: The FE results of stopper 1 and stopper 2 due to the change in the backbone thickness (BT)

Mode	I Experimental Stopper 1 (Hz)	II BT FE Stopper 1 (Hz)	III Error (%) |I-II/I|	IV Experimental Stopper 2 (Hz)	V BT FE Stopper 2 (Hz)	VI Error (%) |IV-V/I|
1	139.57	135.65	2.81	139.32	135.65	2.63
2	221.94	219.24	1.22	221.83	219.24	1.17
3	256.20	253.60	1.01	257.13	253.60	1.37
Total Error			5.04			5.17

Tables 4.19 and 4.20 present the updated value of the Young's modulus. It clearly shows that there is an increment in the initial value of the Young's modulus of stopper 1 and stopper 2. While the convergence of the updating parameter of stopper 1 and stopper 2 is depicted in Figures 4.9 and 4.10 accordingly.

Table 4.19: The updated value of the updating parameter of stopper 1

Parameter	Initial value	Updated value	Unit
Young's Modulus of	210000	218589	MPa

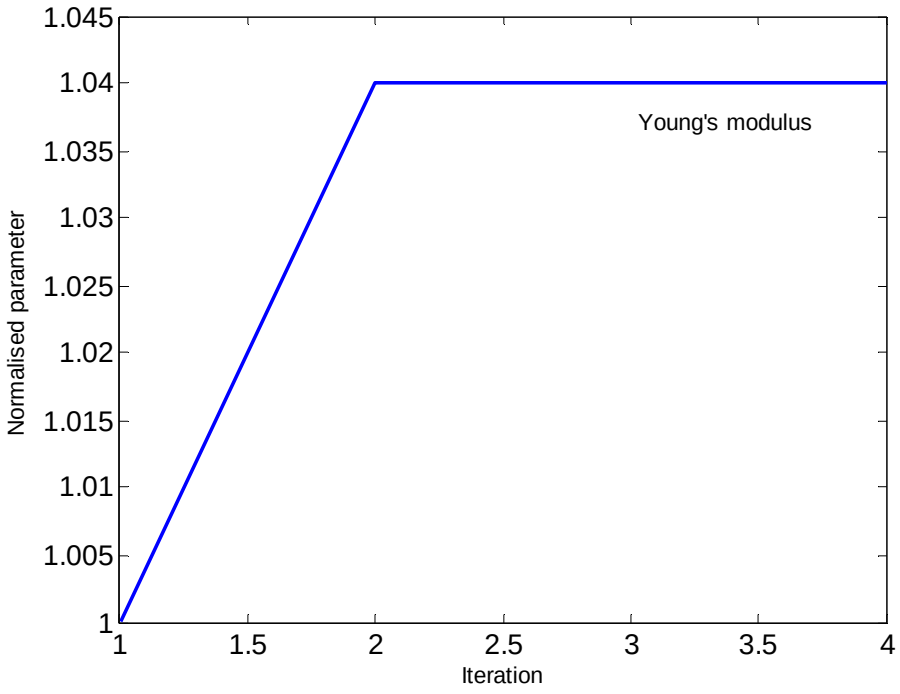

Figure 4.9: The convergence of the updating parameter of stopper 1

Table 4.20: The updated value of the updating parameter of stopper 2

Parameter	Initial value	Updated value	Unit
Young's Modulus of	210000	218778	MPa

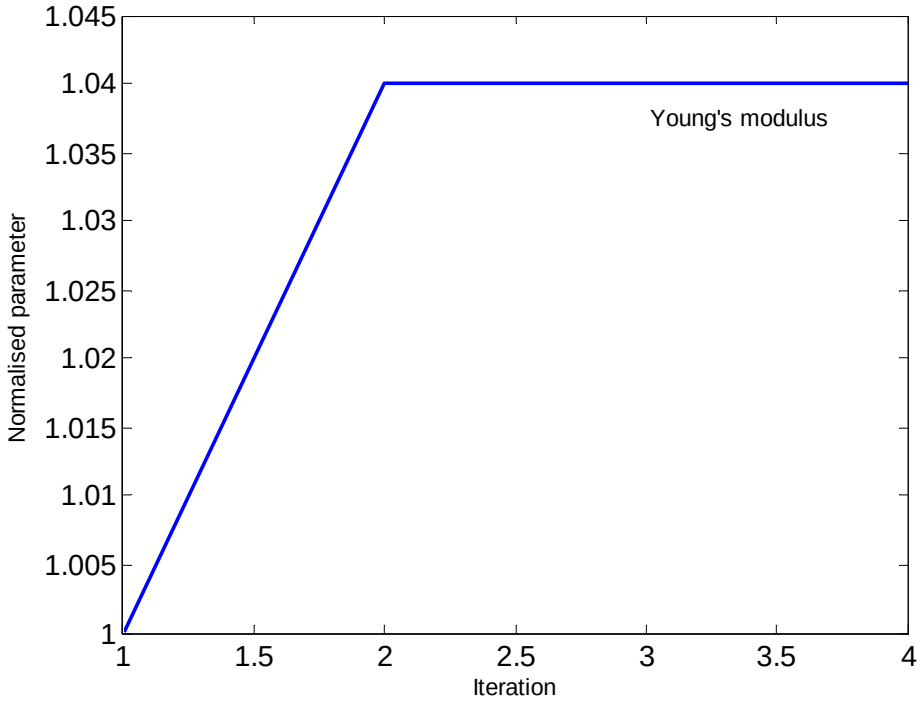

Figure 4.10: The convergence of the updating parameter of stopper 2

From Tables 4.21 and 4.22, it can be observed that the total error between the tested and FE models of stopper 1 and stopper 2 are significantly reduced from 7.90 to 1.93 percent (column III & V) and 7.40 to 1.43 percent (column III & V) accordingly. The achievement of the improvement is a result of introducing the thickness reduction and also using the Young's modulus as the updating parameter. While the comparison of three pairs of mode shapes between the measured and the improved finite element model is shown in Figure 4.11.

Table 4.21: Three comparisons of results between the tested and FE models of stopper 1

Mode	I Experimental Stopper 1 (Hz)	II Initial FE Stopper 1 (Hz)	III Error (%) |I-II/I|	IV 2nd Updated FE Stopper 1 (Hz)	V Error (%) |I-IV/I|	VI Updated FE MAC
1	139.57	136.29	2.35	138.33	0.89	0.97
2	221.94	228.62	3.01	222.79	0.38	0.98
3	256.20	262.71	2.54	257.87	0.65	0.94
Total Error			7.90		1.93	

Table 4.22: Three comparisons of results between the tested and FE models of stopper 2

Mode	I Experimental Stopper 2 (Hz)	II Initial FE Stopper 2 (Hz)	III Error (%) |I-II/I|	IV 2nd Updated FE Stopper 2 (Hz)	V Error (%) |I-IV/I|	VI Updated FE MAC
1	139.32	136.29	2.17	138.39	0.67	0.97
2	221.83	228.62	3.06	222.87	0.47	0.98
3	257.13	262.71	2.17	257.97	0.33	0.95
Total Error			7.40		1.46	

The updating procedure of stoppers 1 and 2 is performed by minimising the objective function as shown in Equation 4.9 and the first two experimentally observed frequencies are used in updating the finite element models of stoppers 1 and 2. In Tables 4.21 and 4.22, the 3rd natural frequencies has not been used in the objective function and may be used to assess the model quality. In addition, the 3rd natural frequency of the stoppers is out of the frequency range of interest in this work which is between 0 to 200Hz. However, the 3rd natural frequency produced by the updated parameter has improved significantly and show as expected that the updated models represent the measured model well.

Table 4.23: The comparisons of results calculated from different number of measured frequencies (NoMF) of stopper 1- 1st to 3rd

Mode	I Exp (Hz)	II Initial FE (Hz)	III NoMF 1 (Hz)	IV NoMF 2 (Hz)	V NoMF 3 (Hz)
1	139.57	136.29	138.92	138.80	138.33
2	221.94	228.62	223.57	223.42	222.79
3	256.20	262.71	258.81	258.62	257.87
VoOF		0.21038	0.01794	0.0164	0.01363

Table 4.24: The comparisons of results calculated from different number of measured frequencies (NoMF) of stopper 2 - 1st to 3rd

Mode	I Exp (Hz)	II Initial FE (Hz)	III NoMF 1 (Hz)	IV NoMF 2 (Hz)	V NoMF 3 (Hz)
1	139.32	136.29	138.92	138.62	138.39
2	221.83	228.62	223.57	223.18	222.87
3	257.13	262.71	258.81	258.34	257.97
VoOF		0.18808	0.01125	0.0084	0.00772

Tables 4.23 and 4.24 show the comparisons of the results of stoppers 1 and 2 calculated based on the different number of the measured frequencies defined in the objective function as shown in Equation 4.9. Columns I and II represent for the experimental results and the results calculated from the initial finite element model, while columns III to V are the results calculated from the updated finite element model. NoMF stands for the number of measured frequencies and VoOF is the sum of the objective function value. It is shown that the more number of measured frequencies used in the objective function, the better the results are obtained as shown in columns V in Table 4.23 and 4.24 respectively.

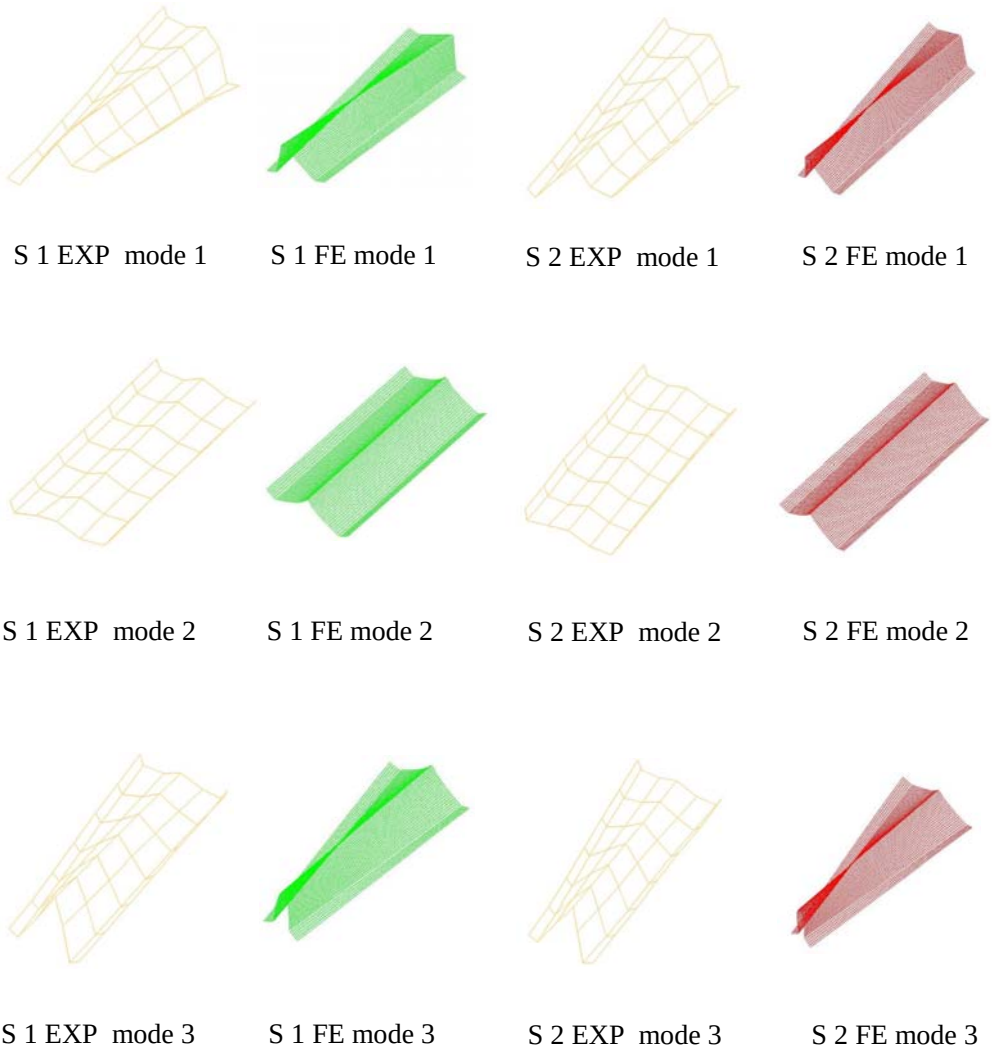

Figure 4.11: 1st, 2nd and 3rd pair of the experimental (EXP) and the 2nd updated FE modes of stopper 1 (S1) and stopper 2 (S2)

4.3.3 FE modelling and model updating of the bent floor

This section discusses the procedures and approaches used in the finite element modelling and model updating of the bent floor. The same procedures as discussed in section 4.3.1 are used in the construction of the finite element model of the bent floor in which it begins with CAD model and ends with finite element model as shown in Figure 4.12. However, different approaches of finite element modelling of bent floor are adopted in this section. These include considering the effect of the stiffness of the springs and strings used to simulate free-free boundary conditions in the tests into the finite element modelling and model updating of the bent floor. The decisions of considering the stiffness are firstly due to the incapability of the common updating parameters used by many researchers (Burnett and Young, 2008 and Abu Husain et al., 2010b) and such as Young's modulus, shear modulus, Poisson's ratio and density to reconcile the finite element model with the tested model. While the second reason is that the first mode shape of the bent floor is a torsional mode and it appears to be very sensitive to the stiffness.

There are three different finite element models of the bent floor that have been used in the attempt to minimise the discrepancies between the experimental and numerical results. The first model which is named the initial finite element model uses the nominal values of mild steel properties. The second model uses the updated parameter of Young's modulus based model. While the last model is based on the inclusion of the effect of the boundary conditions coupled with the updated Young's modulus. In reconciling the finite element model of the bent floor with the tested model, four experimental frequencies are used in the objective function (Equation 4.9).

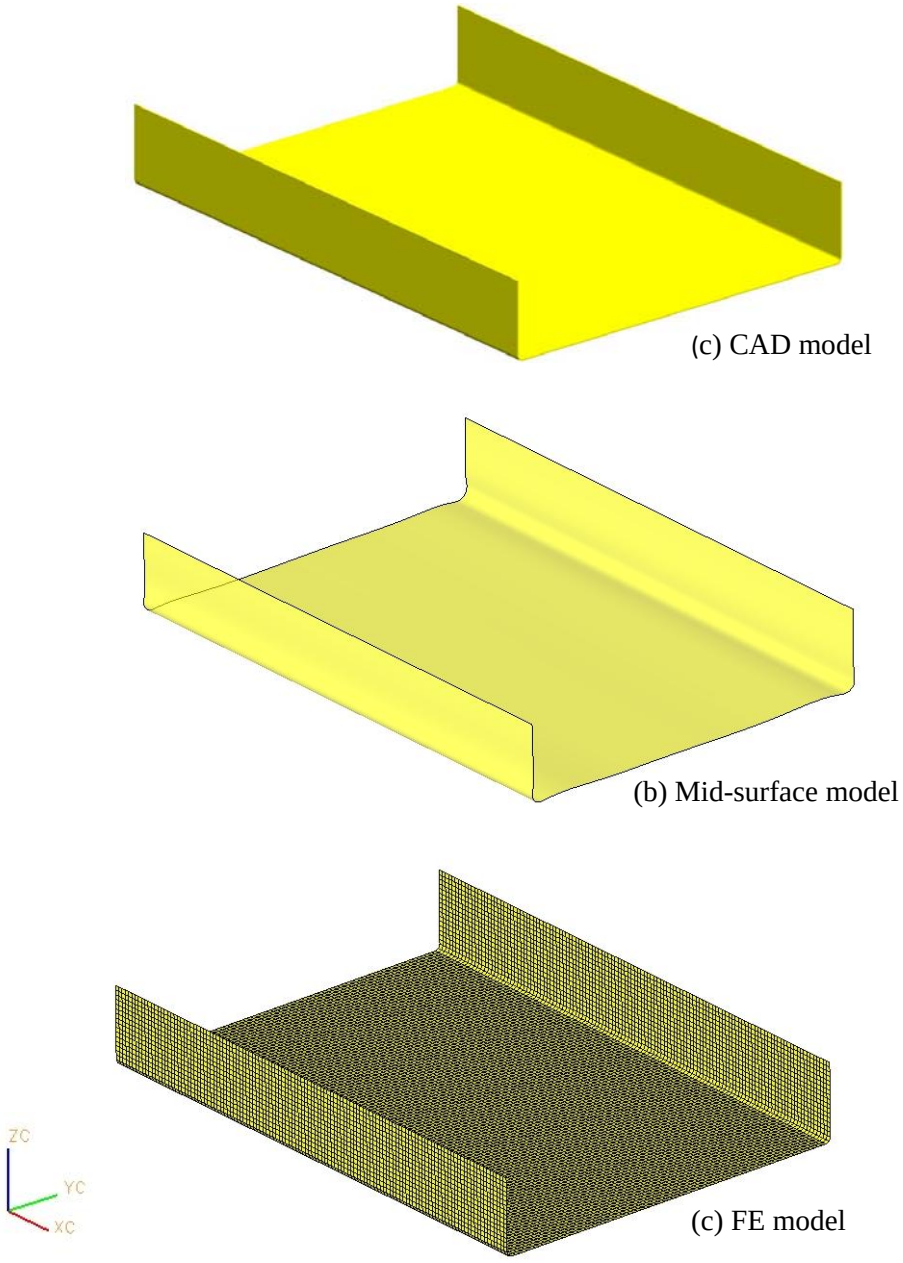

Figure 4.12: Visual models of the bent floor

The results of the nominal values of mild steel properties based initial finite element model are presented in Table 4.25. It can be seen that the total error is 13.99 percent in which the major contributor to the figure comes from the first mode of 6.21 percent. This gives an insight into the use of the nominal values in the finite element modelling of the bent floor is not good enough to bring the numerical model close to the tested model. Therefore the application of model updating is necessarily required in order to minimise the discrepancies between the two types of models.

Table 4.25: Comparison of results between the tested and initial FE model of the bent floor

Mode	I Experimental Bent floor (Hz)	II Initial FE Bent floor (Hz)	III Error (%) |I-II/I|	IV Initial FE MAC
1	16.59	15.56	6.21	0.90
2	29.14	28.94	0.67	0.97
3	45.34	44.58	1.68	0.94
4	57.09	56.74	0.61	0.91
5	74.85	73.94	1.22	0.98
6	86.16	85.95	0.24	0.96
7	98.12	97.27	0.87	0.79
8	109.26	108.73	0.48	0.84
9	114.88	113.60	1.11	0.82
10	119.94	118.87	0.90	0.87
Total Error (%)			13.99	

As a result of the finite element modelling uncertainties in the bent floor, an attempt to minimise the uncertainties is performed through model updating process and the Young's modulus is used as the updating parameter. The results of model updating process are summarised in Table 4.26. It can be seen that the third, fifth, ninth and the tenth mode are well matched with the experimental results. However the first and the second mode are not close. While the updated value of the updating parameter is shown in Table 4.27 which shows the initial value of the Young's modulus has increased for about 4.5 percent.

Table 4.26 Comparison of results between the tested and updated Young's modulus (UYM) based FE model of the bent floor

Mode	I Experimental Bent floor (Hz)	II UYM FE Bent floor (Hz)	III Error (%) |I-II/I|
1	16.59	15.84	4.52
2	29.14	29.46	1.10
3	45.34	45.37	0.07
4	57.09	57.74	1.14
5	74.85	75.23	0.51
6	86.16	87.45	1.50
7	98.12	98.99	0.89
8	109.26	110.51	1.14
9	114.88	115.59	0.62
10	119.94	120.83	0.74
Total Error (%)			12.23

Table 4.27: The updated value of the updating parameter of the bent floor

Parameter	Initial value	Updated value	Unit
Young's Modulus	210000	219408	MPa

The results calculated from the updated Young's modulus based finite element model are still not good enough to match the test results, particularly the first and second mode. Therefore there is a need to systematically investigate other areas of the finite element model that potentially may contribute to the remaining discrepancy, particularly the effect of boundary conditions. CELAS elements which are available in MSC NASTRAN are used to simulate the boundary conditions of the bent floor test as elaborated in 3.3.4. The finite element modelling of the bent floor considering the effect of the boundary conditions is depicted in Figure 4.13.

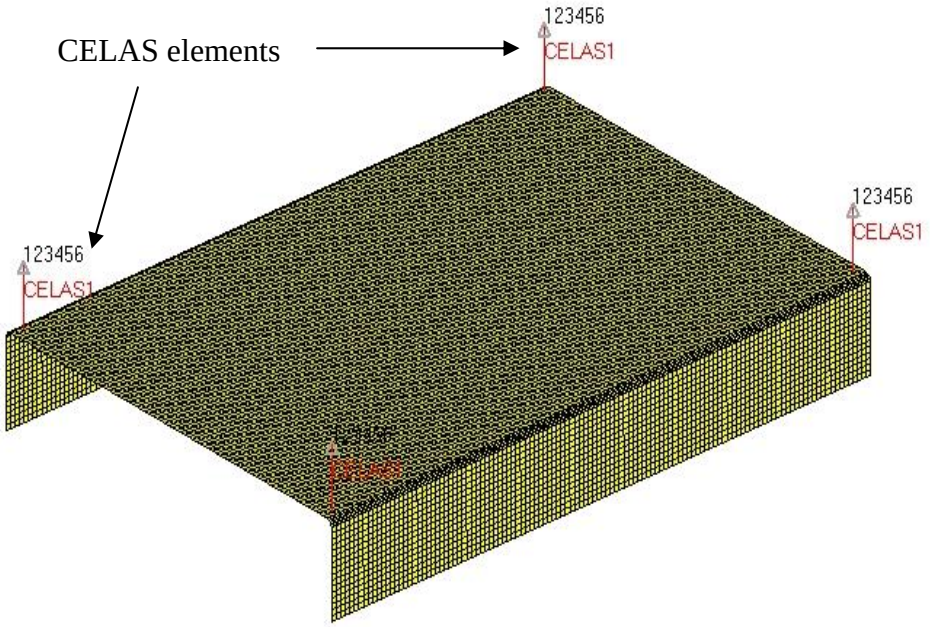

Figure 4.13: FE modelling of the bent floor considering the effect of boundary conditions

In order to determine the sensitivity parameters, a sensitivity analysis with five parameters is performed. The results of the sensitivity analysis are summarised in Table 4.28. From the table it is noticed that the coefficient of the Young's modulus indicates high sensitivity, while PELAS (the property of CELAS elements) is merely influential to the first frequency as compared with other frequencies. Therefore among the five parameters, only two of them which are the Young's modulus and PELAS are taken as updating parameters in the finite element model updating of the bent floor. It is decided not to include the thickness as a potential updating parameter because technically it can be measured directly from the tested model.

Table 4.28: Summarised results of the sensitivity analysis of the bent floor

Mode	Frequency	Parameters				
		Thickness	Young's Modulus	Density	Shear Modulus	PELAS
1	1.40E+01	9.58E+00	5.53E+00	-7.01E+00	6.44E-03	1.48E+00
2	2.33E+01	2.29E+01	1.15E+01	-1.16E+01	7.76E-04	1.37E-01
3	3.59E+01	3.51E+01	1.77E+01	-1.80E+01	2.22E-02	2.66E-01
4	4.54E+01	4.52E+01	2.27E+01	-2.27E+01	2.81E-02	5.77E-03
5	5.92E+01	5.92E+01	2.96E+01	-2.96E+01	2.91E-03	1.16E-03

The results calculated from the updated Young's modulus and PELAS based finite element model (UYMP FE) are summarised in column (IV) of Table 4.23. The comparison of results between the experimental and UYMP finite element results are tabulated in column (V). From the column it can be observed that a significant improvement is made in the first mode reducing from 6.21 percent to 0 percent. While the total error of 13.99 percent calculated from the initial finite element model has dropped to 3 percent as a result of considering the effect of the boundary conditions and the Young's modulus to be the updating parameters. Furthermore the individual MAC values of UYMP FE model are improved in comparison with those calculated from the initial finite element model.

The updating procedure is carried out on the basis of the first four measured frequencies of the bent floor and two updating parameters. The discrepancies between the measured frequencies and the frequencies produced by the updated parameters are significantly improved and the improvement can be seen in the first four frequencies shown in Table 4.29. Meanwhile, the 5th up to 10th natural frequencies have been significantly improved as well, giving confidence in the quality of the updated model.

Table 4.29: Three comparisons of results between the tested, the initial FE and the updated Young's modulus and PELAS (UYMP) based FE model of the bent floor.

Mode	I Experimental Bent floor (Hz)	II Initial FE Bent floor (Hz)	III Error (%) |I-II/I|	IV UYMP FE Bent floor (Hz)	V Error (%) |I-IV/I|	VI UYMP FE MAC
1	16.59	15.56	6.21	16.59	0.00	0.93
2	29.14	28.94	0.67	29.25	0.38	0.97
3	45.34	44.58	1.68	45.07	0.60	0.95
4	57.09	56.74	0.61	57.18	0.16	0.91
5	74.85	73.94	1.22	74.50	0.47	0.98
6	86.16	85.95	0.24	86.61	0.52	0.98
7	98.12	97.27	0.87	98.02	0.10	0.80
8	109.26	108.73	0.48	109.52	0.24	0.88
9	114.88	113.60	1.11	114.48	0.36	0.92
10	119.94	118.87	0.90	119.74	0.17	0.91
Total Error (%)			13.99		3.00	

The updated values of the updating parameters used in the finite element model updating of the bent floor are shown in Table 4.30 and the convergence of the parameters can be seen in Figure 4.14. To summarise, the initial value of the Young's modulus has increased for about 1.59 percent and two iterations are required to converge. Meanwhile the PELAS in which the stiffness of springs and strings are defined has dropped from 1.6 to 1.44 with three iterations taken to converge.

The comparison in pairs of mode shapes of the bent floor between the tested and UYMP FE model is presented in Figure 4.15 accordingly. It can be clearly seen that the mode shapes calculated from the UYMP FE model are graphically very similar to those obtained from the test.

Table 4.30: The updated values of the updating parameters of the bent floor

Parameter	Initial value	Updated value	Unit
Young's Modulus	210000	213339	MPa
CELAS element stiffness (PELAS)	0.0016	0.00144	N/m

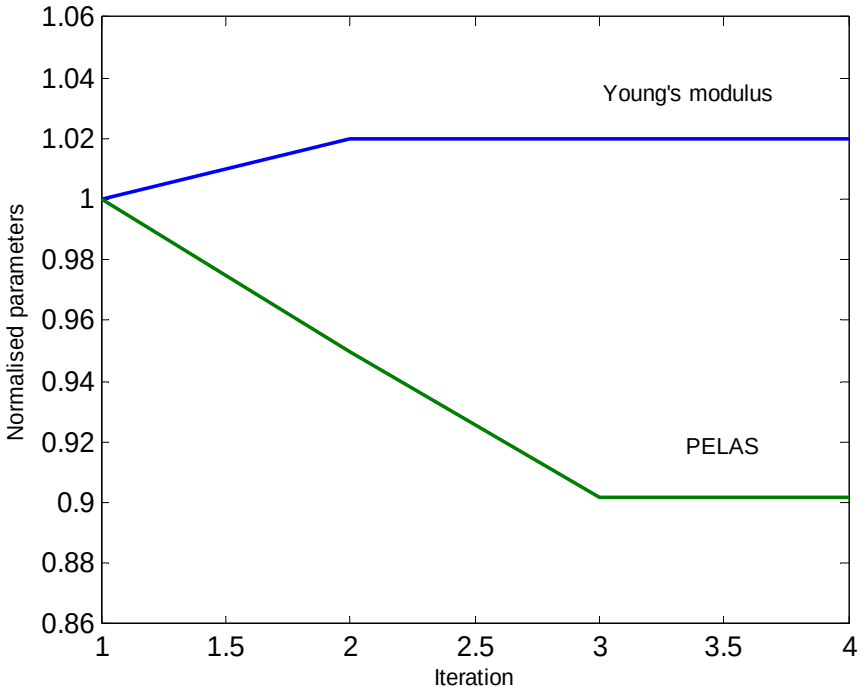

Figure 4.14: The convergence of the updating parameter of the bent floor

Tables 4.31 and 4.32 show the comparisons of the results of bent floor calculated based on the different number of the measured frequencies defined in the objective function as shown in Equation 4.9. Columns I and II represent for the experimental results and the results calculated from the initial finite element model respectively, while columns III to XII are the results calculated from the updated finite element model. NoMF stands for the number of measured frequencies and VoOF is the sum of the objective function value. From the tables, it is shown that the larger the number of measured frequencies used in the objective function, the better the results are obtained. However, in this study, only four measured frequencies are used in the objective function. The rest of the measured frequencies (the 5th to 10th) are used to confirm the good predictability of the updated model.

Table 4.31: The comparisons of results calculated from different number of measured frequencies (NoMF) of the bent floor - 2nd to 5th

Mode	I Exp (Hz)	II Initial FE (Hz)	III NoMF 2 (Hz)	IV NoMF 3 (Hz)	V NoMF 4 (Hz)	VI NoMF 5 (Hz)
1	16.59	15.56	16.59	16.59	16.60	16.59
2	29.14	28.94	29.14	29.28	29.25	29.28
3	45.34	44.58	44.91	45.12	45.08	45.13
4	57.09	56.74	56.96	57.24	57.18	57.25
5	74.85	73.94	74.22	74.58	74.51	74.60
6	86.16	85.95	86.29	86.70	86.62	86.72
7	98.12	97.27	97.65	98.12	98.03	98.15
8	109.26	108.73	109.13	109.62	109.53	109.65
9	114.88	113.60	114.05	114.59	114.49	114.62
10	119.94	118.87	119.31	119.85	119.75	119.88
VoOF		0.46763	0.02711	0.01236	0.01213	0.01267

Table 4.32: The comparisons of results calculated from different number of measured frequencies (NoMF) of the bent floor - 6th to 10th

Mode	I Exp (Hz)	II Initial FE (Hz)	VII NoMF 6 (Hz)	VIII NoMF 7 (Hz)	IX NoMF 8 (Hz)	X NoMF 9 (Hz)	XI NoMF 10 (Hz)
1	16.59	15.56	16.59	16.59	16.59	16.59	16.59
2	29.14	28.94	29.25	29.25	29.24	29.26	29.26
3	45.34	44.58	45.07	45.08	45.06	45.08	45.09
4	57.09	56.74	57.18	57.19	57.17	57.20	57.20
5	74.85	73.94	74.50	74.52	74.49	74.53	74.54
6	86.16	85.95	86.61	86.62	86.60	86.64	86.65
7	98.12	97.27	98.02	98.04	98.00	98.05	98.06
8	109.26	108.73	109.51	109.53	109.50	109.55	109.56
9	114.88	113.60	114.47	114.49	114.46	114.51	114.53
10	119.94	118.87	119.73	119.75	119.71	119.77	119.78
VoOF		0.46763	0.01224	0.01211	0.01237	0.01207	0.01204

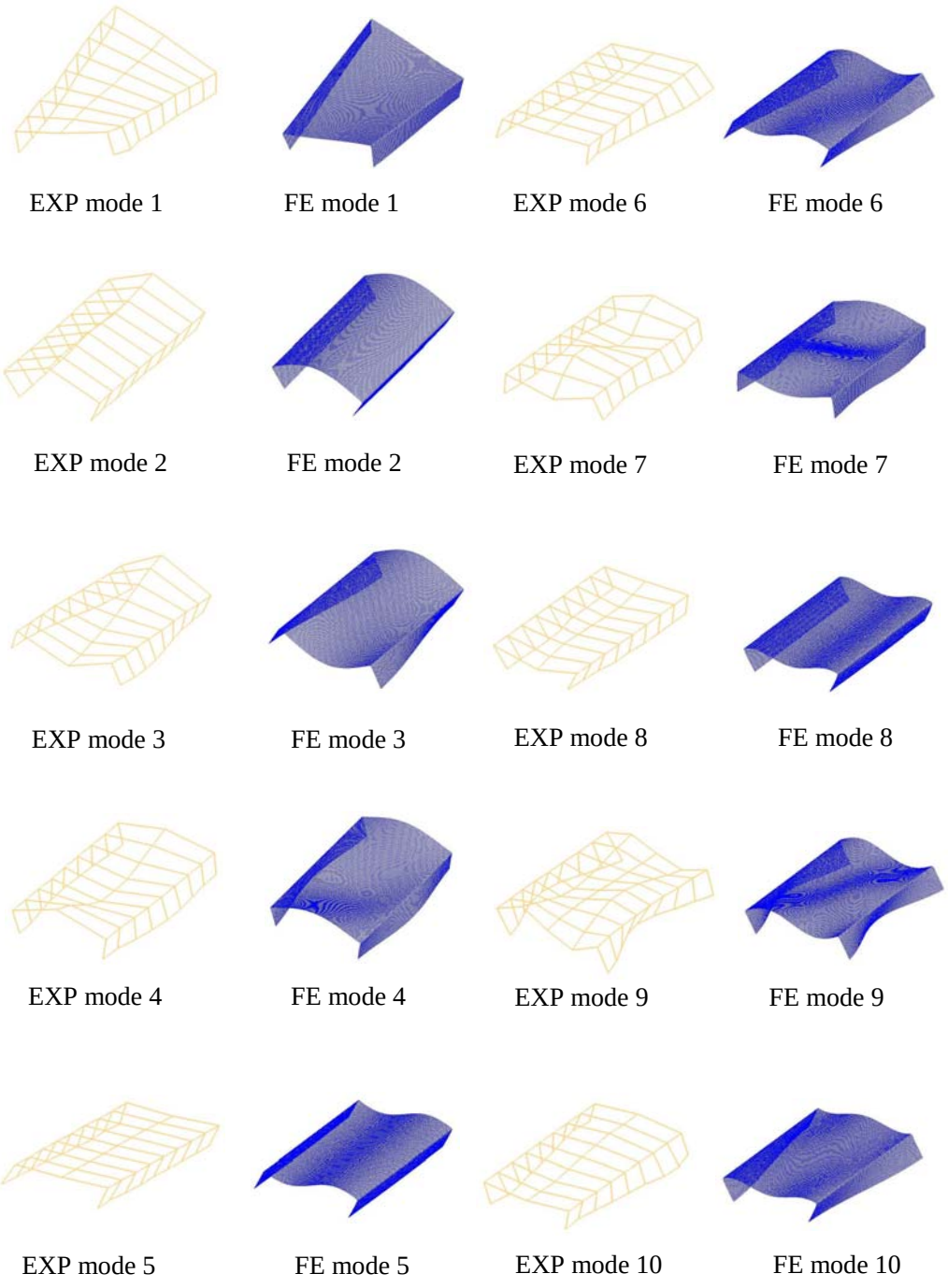

Figure 4.15: Comparison ten pairs of the experimental (EXP) and the UYMP FE modes of the bent floor

4.4 Conclusions

Finite element modelling and model updating process of the substructures have been demonstrated technically and discussed theoretically. The discrepancies between measured and predicted results of every individual substructure which are calculated in total error have been successfully reduced below 5 percent.

The work has revealed that identifying the source of discrepancies is the most challenging aspect of the updating process. The differences can be caused by global effects such as geometry errors (thickness), exclusion of significant substructures from the model, local effects, mismatch in boundary conditions, incorrect material modelling and other factors.

It should be apparent that the inclusion of the PELAS which specifies the stiffness coefficient of CELAS element used to represent the stiffness of the spring suspensions as one of the updating parameters could result in a big reduction in the first frequencies of the bent floor. While the consideration of the thickness reduction in the backbone leading to more representative models of the stoppers for model updating process.

Chapter 5

FE Modelling and Model Updating of the Welded Structure

5.1 Introduction

The main objective of finite element model updating elaborated in the previous chapter is to improve the accuracy and enhance the quality of analytical or finite element models of structures using modal test data. Extensive work has been carried out by many researchers and engineers in the last two decades to attain the objective. While a vast amount of literature related to the use of model updating exists, however the use of model updating method applied to solve practical problems is relatively little.

In this chapter the work of FE modelling and model updating of the welded structure is presented and the frequency range of interest is between 0 to 200Hz. The construction of the FE model of the welded structure is based on the updated FE models of the structural components. They are assembled together by eighty CWELD elements which are used to represent the physical spot welds on the structure.

This chapter also presents the analysis results calculated from different FE models through which the effects of the potential parameters on the accuracy of the predicted modal parameter are investigated. In particular the accuracy of the predicted frequencies based on two different CWELD elements which are format in ALIGN and ELPAT is elaborated and discussed.

Five different configurations of FE model are used in the investigation of the modal properties (frequencies and mode shapes) of the welded structure and also for the minimisation of the discrepancies between the measured and predicted results. They are summarised as follows:

1) Initial FE model based on the nominal values of material properties of mild steel and CWLED element ALIGN format (CEAF).

2) Initial FE model based on the nominal values of material properties of mild steel and CWLED element ELPAT format (CEEF).

3) The first updated FE model based on the diameter of spot welds.

4) The second updated FE model based on the diameter of spot welds and the Young's modulus of patches.

5) The third updated FE model based on the diameter of spot welds, the Young's modulus of patches and also the effect of the support stiffness as the updating parameters.

6) The fourth updated FE model based on the effect of the initial stress and the support stiffness.

7) The fifth updated FE model based on the diameter of spot welds, the effect of the initial stress and the support stiffness.

5.2 FE modelling of the welded structure

Since the geometrical design of welded structure is fairly complex with two side walls and stoppers attached to the bent floor with eighty spot welds, thus the use of CAD system is necessary, in which the tools for handling complex geometrical designs are normally much well developed and streamlined than those in the pre-processors of the FE systems. Furthermore the indicators of spot weld locations are much easier to define in CAD systems rather than FE systems. In automotive industry, having the pre-defined indicators of spot welds in CAD models from the designers before sending them to CAE engineers for the construction of FE models is compulsorily required. This helps the CAE engineers to easily identify the locations and also develop the models of spot welds efficiently.

Therefore in this study, the pre-defined locations of spot welds that have already been identified in the CAD model as shown in Figure 5.1 (a) and (b) are used for the FE model construction of the welded structure. A total of 28680 CQUAD elements and 80 CWELD elements have been used to construct the FE model of the welded structure as illustrated in Figure 5.1 (c).

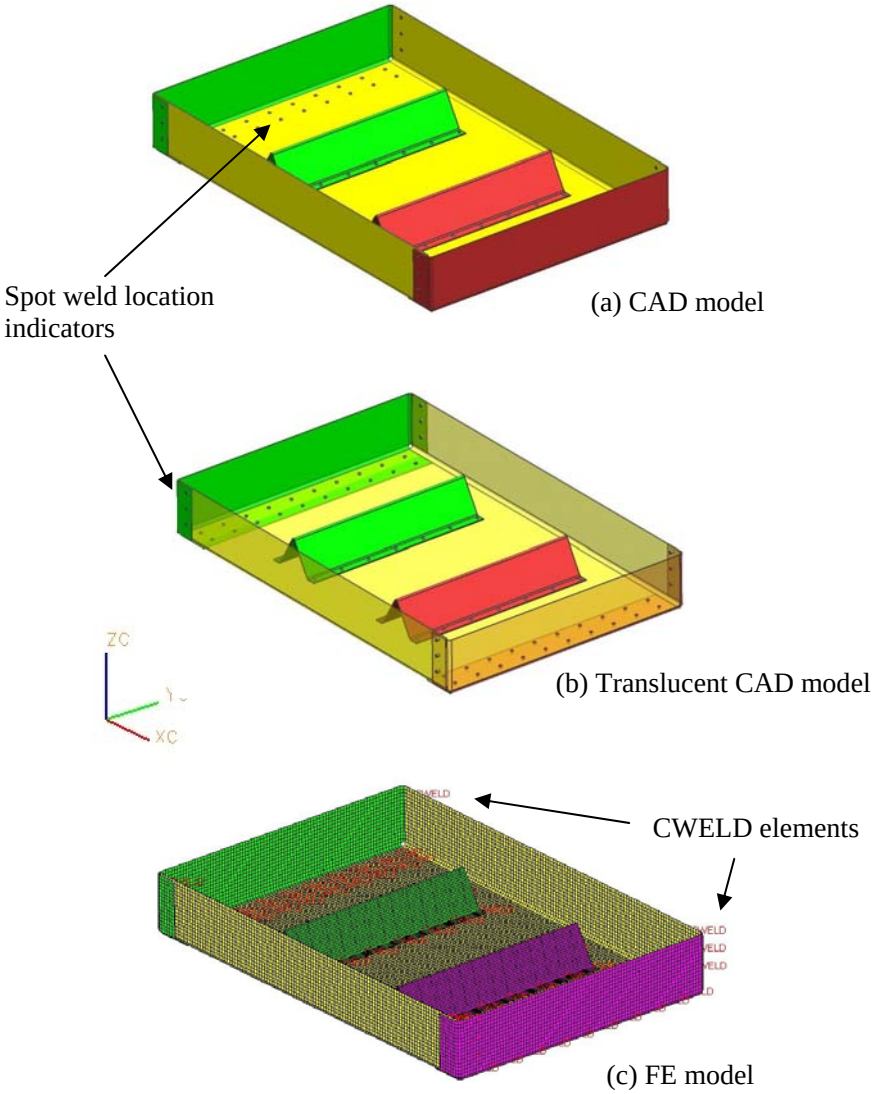

Figure 5.1: Visual models of the welded structure

5.2.1 CWELD element ALIGN format (CEAF)

Due to uncertainties such as geometrical irregularities, material inhomogeneities, residual stress and defects that are inherent during spot welding process, the work of modelling spot welds on account of the uncertainties is always difficult and challenging for CAE engineers in automotive industry. In addition to these, due to a large number of spot welds in automobile structures reliable procedures and methods that are capable of representing spot welds in the simplest way is of interest and concern in this study.

CWELD element ALIGN format which is available in MSC NASTRAN and its capability of representing spot welds on a complicated structure were already demonstrated and discussed in Yunus et al. (2011) is also used to represent the eighty spot welds on the welded structure. The ALIGN format defines a point to point connection, as shown in Figure 5.2, GA and GB. They must be existing vertex nodes of shell elements that make up the steel sheets connected by welds. For the other format, GA and GB are not required. Two shell normal to the direction GA-GB are generated at GA and GB respectively.

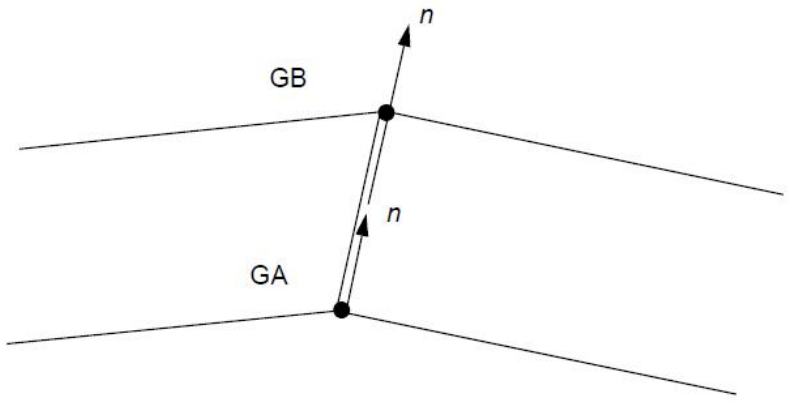

Figure 5.2: Point to point connection defined with ALIGN format

The numerical results of ten modes calculated from the CWLED elements ALIGN format (CEAF) based finite element model are compared with those obtained from the experiment and they are summarised in Table 5.1.

Table 5.1: Comparison of results between the tested and the CEAF FE model of the welded structure

Mode	I Experiment (Hz)	II CEAF FE model (Hz)	III Error (%) |I-II|/I
1	29.48	25.10	14.85
2	76.58	75.17	1.84
3	101.07	98.20	2.84
4	110.86	106.92	3.55
5	121.91	121.95	0.04
6	140.46	139.54	0.66
7	147.50	141.02	4.39
8	159.77	157.44	1.46
9	187.51	181.21	3.36
10	199.65	192.04	3.81
Total Error (%)			36.80

From Table 5.1 large discrepancies can be observed between the CEAF finite element model and the tested model. The total error of 36.80 percent with the largest contributor partly from the first mode which is 14.85 percent, it clearly suggests that the CEAF finite element model is not capable of representing the dynamics of the physical joints of the welded structure.

5.2.2 CWELD elements ELPAT format (CEEF)

The ELPAT format defines a connection of two shell element patches A and B with shell element identification numbers SHIDA and SHIDB as shown in Figure 5.3. Depending on the location of the piercing points GA, GB and the size of the diameter *D*, the number of connected elements per patch may range from a single element up to 3x3 elements. For this option, shell element patches A and B are allowed to share a common grid.

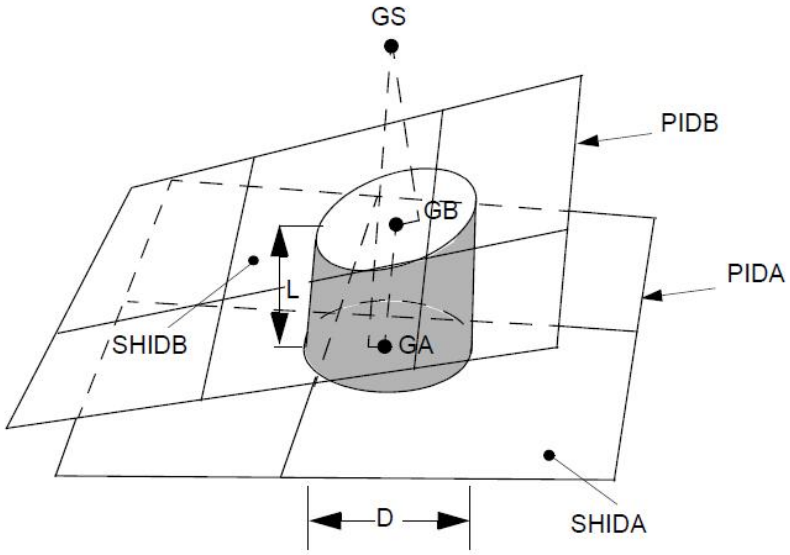

Figure 5.3: Patch to patch connection defined with ELPAT format.

The frequencies of the first ten modes calculated from the CWELD element ELPAT format (CEEF) based finite element model are given in column (II) of Table 5.2. The discrepancies between the tested and CEEF finite element model quantified in relative errors are given in column (III) of the table 5.2. The total error calculated from the CEEF finite model in comparison with the tested model is 26.44 percent. The comparison also reveals that the maximum error of the numerical frequencies decreases to 10.92 percent which is contributed from the first mode and this is followed by the errors of 3.43 percent and 2.64 percent for the fifth and sixth modes respectively. However the CEEF finite element model shows better capability of representing the physical joints in comparison with the finite element model constructed with CEAF.

Table 5.2: Comparison of results between the tested and the CEEF FE model of the welded structure

Mode	I Experiment (Hz)	II CEEF FE model (Hz)	III Error (%) |I-II|/I
1	29.48	26.26	10.92
2	76.58	78.17	2.07
3	101.07	102.44	1.36
4	110.86	109.55	1.18
5	121.91	126.10	3.43
6	140.46	144.16	2.64
7	147.50	144.31	2.16
8	159.77	160.86	0.68
9	187.51	187.02	0.26
10	199.65	196.19	1.73
Total Error (%)			26.44

5.2.3 Results and discussion of CEAF and CEEF

The format of point to point connection is very different from the physical reality. This is because the nuggets of the spot welds which normally can be measured spread the connection load path over the connecting areas in the local area of the spot welds. This is a significant difference between the CEAF configuration and the physical spot welds. Apart from that, point to point connections which technically require congruent meshes are numerically very difficult to implement for complex automobile structures.

Meanwhile as expected the results obtained from the CEEF finite element model are stiffer than CEFA FE model because the format ELPAT connects more material which is up to 3 x 3 meshes of elements within the diameter of the PWELD specification. This clearly suggests that the CWLED elements format ELPAT shows better capability of representing the physical spot welds in comparison with the CWELD elements ALIGN format.

Basically, if the CWELD configuration does not represent the physical connection well, then modifying some of the CWELD parameters such as the Young's modulus, density, Poisson's ratio and diameter may be necessary to obtain the correct stiffness of the spot welds.

5.3 FE model updating of the welded structure

Since the CWELD element ELPAT format shows better capability of representing the physical spot welds on the welded structure, therefore this format is used instead of the other format (ALIGN) for the finite element modelling and model updating of the welded structure. The same constructed finite element model namely initial finite element model is used in the attempt to correct the large error as shown in column (V) of Table 5.2, arising from the uncertainties of the CWELD element configurations (Palmonella et al., 2004).

In a series of attempts to update the finite element model of the welded structure using different types of parameters, the first eight measured frequencies are used in the objective function (Equation 4.9) defined in NASTRAN SOL 200. The finite element model is updated until the predicted frequencies match the measured counterparts well enough by minimising the objective function.

In the first attempt to update the model, sensitivity analysis is initially run to identify the most sensitive parameters to the frequencies. The potential parameters listed down in SOL200 are those of the CWELD element properties such as the diameter, Young's modulus, density, shear modulus and Poisson's ratio. The results of the sensitivity analysis are given in Table 5.3. It is observed that the frequencies are only sensitivity to the diameter of the CWELD and the parameter is used in the updating process.

Table 5.3: Summarized results of the sensitivity analysis of the welded structure using the updating parameters of the CWELD element properties

Mode	Frequency	Parameters		
		Diameter	Young's Modulus	Shear Modulus
1	26.35	0.7441	0.0203	0.0700
2	78.31	1.4812	0.1032	0.1370
3	102.70	2.2633	0.1292	0.2271
4	109.74	1.4714	0.0844	0.1800
5	126.44	2.4542	0.1153	0.2528
6	144.51	2.5266	0.1601	0.2600
7	144.62	2.2498	0.1034	0.3260
8	161.09	2.0185	0.1248	0.2007

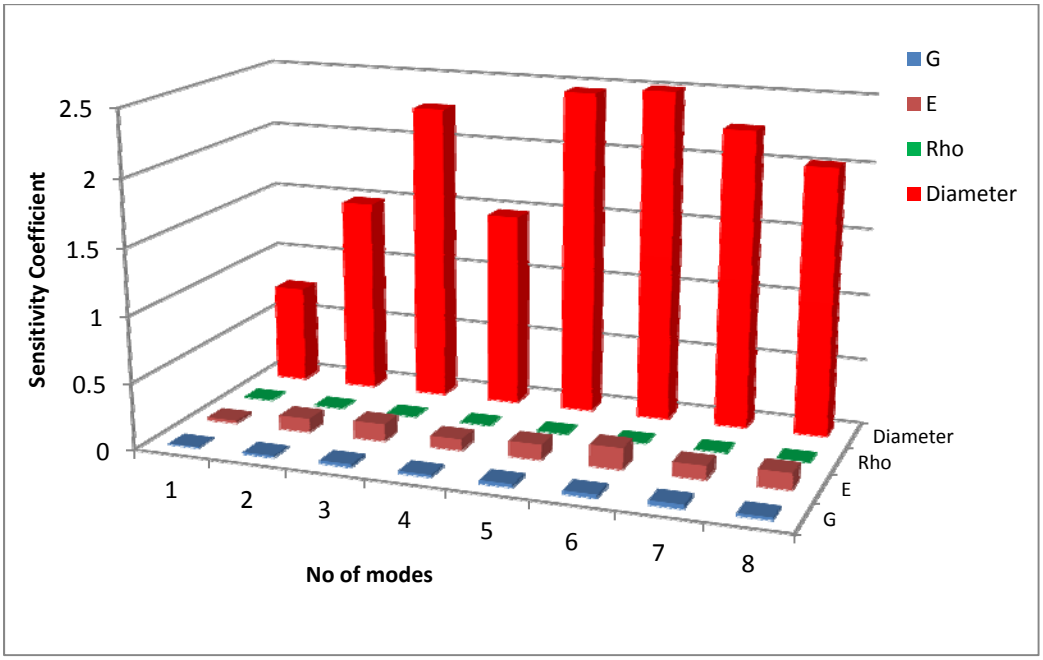

Figure 5.4: The results of sensitivity analysis of CWELD properties

From Table 5.3 and also Figure 5.4, it is noticeable that the first frequency up to the eighth frequency is merely sensitive to the diameter of spot welds instead of other parameters. Therefore the diameter of CWELD is only used for updating process by excluding the non-sensitivity parameters in order to avoid ill-condition problems.

Table 5.4: Comparison of results between the tested and the 1st updated FE model of the welded structure

Mode	I Experiment (Hz)	II Initial FE model (Hz)	III Error (%) |I-II|/I	IV 1st Updated FE model (Hz)	V Error (%) |I-IV|/I
1	29.48	26.26	10.92	26.31	10.74
2	76.58	78.17	2.07	78.35	2.31
3	101.07	102.44	1.36	102.70	1.61
4	110.86	109.55	1.18	109.71	1.03
5	121.91	126.10	3.43	126.20	3.52
6	140.46	144.16	2.64	144.14	2.62
7	147.50	144.31	2.16	144.57	1.99
8	159.77	160.86	0.68	161.00	0.77
9	187.51	187.02	0.26	187.30	0.11
10	199.65	196.19	1.73	196.53	1.56
Total Error (%)			26.44		26.27

Table 5.4 shows the results of updated finite element model of the welded structure as a result of using the diameter of CWELD element as the updating parameter in the attempt to minimise the error introduce the FE model. From Table 5.4 it is observed that the reduction in the total error as shown in column (V) is merely 0.17 percent which is very small improvement in the FE model.

On top of that the updated diameter of the CWELD which is 5.5mm as shown in Table 5.5 does not reflect the real average value of the physical nugget diameter of the spot welds of 3.75mm as depicted in Figure 5.5. This clearly indicates that the usage of the diameter of the CWELD as the updating parameters has proved to be incapable of reducing the large discrepancy between the measured and predicted frequencies.

Table 5.5: Updated value of parameter of CWELD diameter

Parameter	Initial value	Updated value	Unit
CWELD diameter	6	5.5	mm

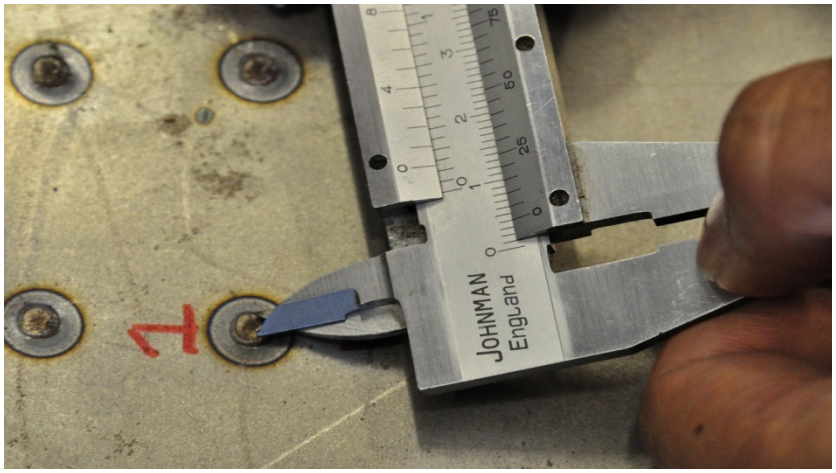

Figure 5.5: The measurement of the diameter of physical spot weld

The second attempt to improve the predicted frequencies is introducing patches on the FE model of welded structure as elaborated and used by Palmonella et al. (2004) and Abu Husain et al. (2010b). Eighty pairs of squared patches are constructed with the dimension of 10mm x 10mm to represent the heat-affected zone of the spot welds. Different model properties such as the Young's modulus, density, shear modulus and Poisson's ratio are assigned to the patches. The organization and arrangement of patches on the FE model of the welded structure are shown in Figure 5.6.

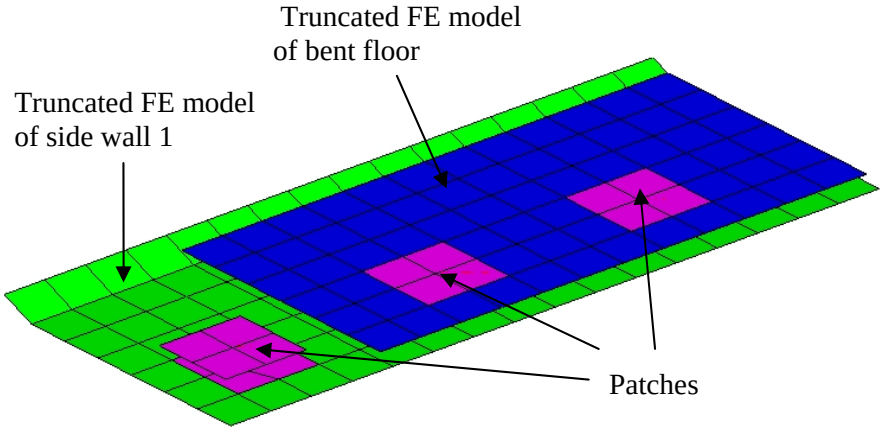

Figure 5.6: FE model of patches from the truncated FE model of the welded structure

Having different properties from other components' as mentioned earlier means the patches are readily available to be considered as the updating parameters on top of the diameter of CWELD element. From the results of sensitivity analysis as shown in Figure 5.7, it is clearly shown than the eight modes are sensitivity to the Young's modulus of patches and the diameter of CWELD element in comparison with other parameters. The model updating procedures considering the results of the sensitivity analysis are performed on the welded structure and the results of the procedures are tabulated in column (IV) of Table 5.7. The updated values of the updating parameters used in updating the finite element model are shown in Table 5.6 below.

Table 5.6: Updated values of parameters of the 2nd updated FE model of the welded structure

Parameter	Initial value	Updated value	Unit
Patches' Young's Modulus	210000	252000	MPa
CWELD diameter	5	5.5	mm

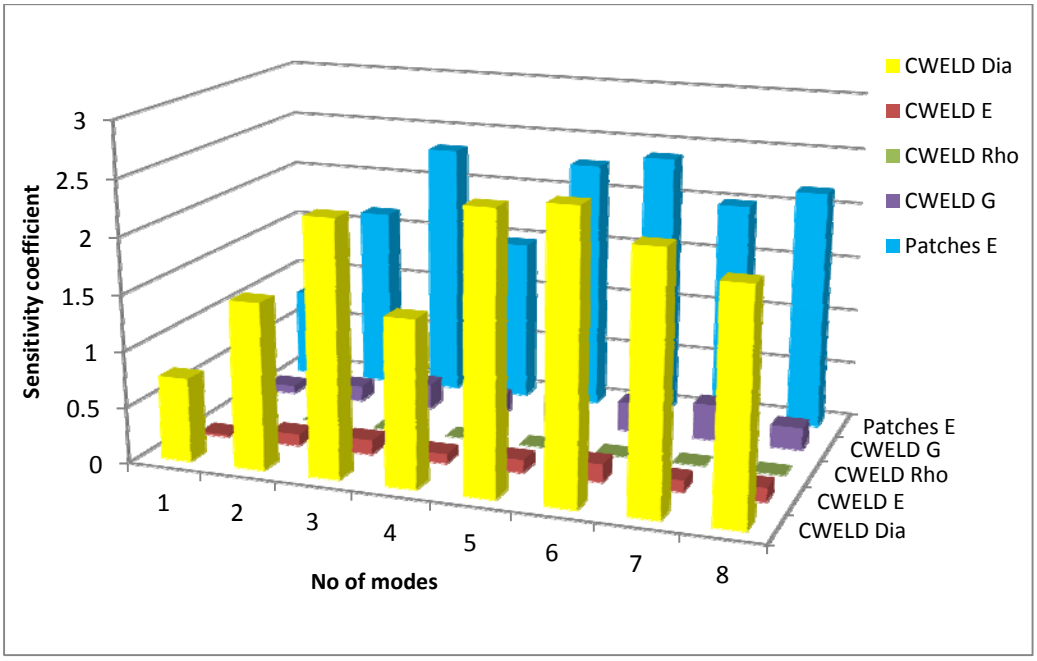

Figure 5.7: The results of sensitivity analysis of CWELD properties and the Young's modulus of patches

Table 5.7: Comparison of results between the tested and the 2nd updated FE model of the welded structure

Mode	I Experiment (Hz)	II Initial FE model (Hz)	III Error (%) |I-II/I|	IV 2nd Updated FE model (Hz)	V Error (%) |I-IV/I|
1	29.48	26.26	10.92	26.44	10.33
2	76.58	78.17	2.07	78.61	2.65
3	101.07	102.44	1.36	103.05	1.96
4	110.86	109.55	1.18	109.95	0.82
5	121.91	126.10	3.43	126.52	3.78
6	140.46	144.16	2.64	144.48	2.87
7	147.50	144.31	2.16	144.87	1.78
8	159.77	160.86	0.68	161.33	0.98
9	187.51	187.02	0.26	187.77	0.14
10	199.65	196.19	1.73	196.92	1.37
Total Error (%)			26.44		26.67

There is no significant improvement that can be seen from the 2nd updated FE model especially in the lowest modes. The first mode has only dropped by 0.59 percent, while the percentage of error increments is seen in the second, third, fifth and sixth mode. Furthermore the total error has increased from 26.44 to 26.67 percent as a result of the combined updating parameters of the Young's modulus of patches and the diameter of CWELD element. To summarise, the initial value of the Young's modulus of patches has increased by 20 percent, while 10 percent increment is seen in the initial value of the diameter of CWELD. Five iterations are required to converge.

Upon the two unsuccessful attempts at minimising the discrepancies between the measured and predicted frequencies of the welded structure, the model reconciliation was then carried on by considering more potential updating parameters. In this work, sensitivity analysis was used to identify the parameters and the results are shown in Figure 5.8 below.

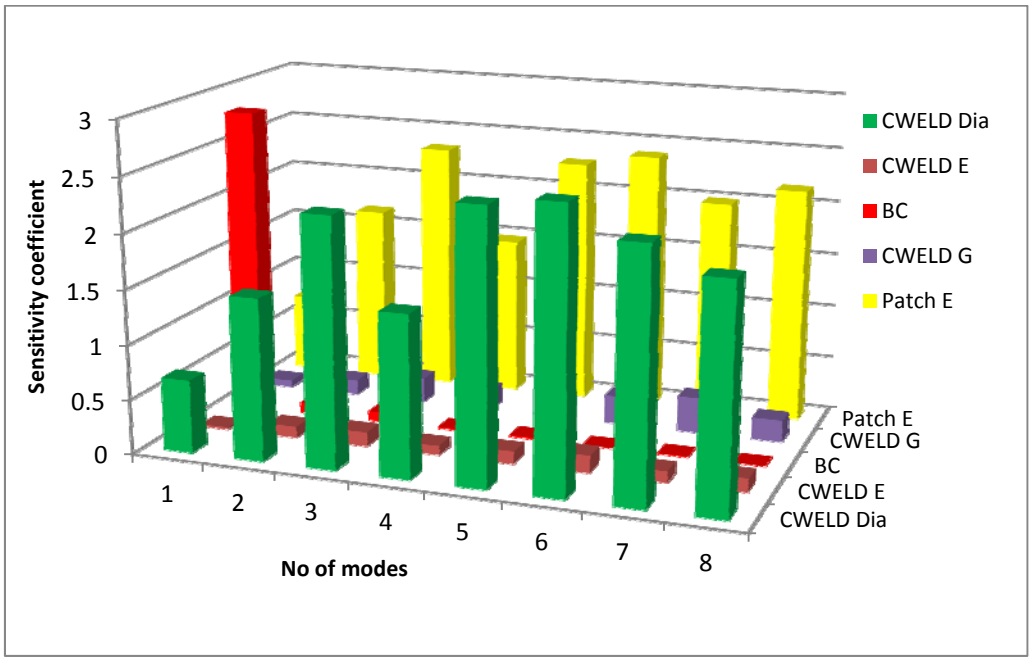

Figure 5.8: The results of sensitivity analysis of CWELD properties, the Young's modulus of patches and the boundary conditions (BC)

The sensitivity analysis results as shown in Figure 5.8 reveals that the first mode which is a torsional mode is very sensitive to the boundary conditions as compared with other parameters. The results clearly suggest that the boundary conditions have a significant contribution towards the first frequency. This happens because the springs and nylon strings that were used to simulate free-free boundary conditions in the test were not taken into account in the initial FE model of the welded structure. Meanwhile other frequencies from the second to the eighth mode are only sensitive to the diameter of CWELD element and the Young's modulus of patches. Therefore the updating parameters used in the third attempt to minimise the error are the diameter of CWELD element, the Young's modulus of patch and the boundary conditions. The results of the updated FE model are tabulated in column (IV) of Table 5.8. The results also reveal that a big improvement in the first mode of the updated FE model and also a drastic reduction in the total error as shown in column (V).

Table 5.8: Comparison of results between the tested and the 3rd updated FE model of the welded structure

Mode	I Experiment (Hz)	II Initial FE model (Hz)	III Error (%) |I-II/I|	IV 3rd Updated FE model (Hz)	V Error (%) |I-IV/I|
1	29.48	26.26	10.92	29.47	0.02
2	76.58	78.17	2.07	77.65	1.40
3	101.07	102.44	1.36	101.62	0.54
4	110.86	109.55	1.18	109.00	1.68
5	121.91	126.10	3.43	125.07	2.59
6	140.46	144.16	2.64	143.04	1.84
7	147.50	144.31	2.16	143.55	2.68
8	159.77	160.86	0.68	160.04	0.17
9	187.51	187.02	0.26	185.86	0.88
10	199.65	196.19	1.73	195.24	2.21
Total Error (%)			26.44		14.01

Table 5.9: Updated values of the updating parameters of the 3rd updated FE model of the welded structure

Parameter	Initial value	Updated value	Unit
Patches' Young's Modulus	210000	189000	MPa
CWELD diameter	5	4.0	mm
CELAS element stiffness	2.2	2.59	N/mm

The updated values of the updating parameters used in the finite model updating of the 3rd updated FE model are shown in Table 5.9. It can be seen that the initial value of the Young's modulus of patches and the diameter of CWELD have decreased by 10 percent and 20 percent respectively. Meanwhile the initial values of CELAS element in which the stiffness of springs and strings are defined has increased by about 18 percent. Five iterations are required to converge.

5.4 FE model updating of the welded structure considering initial stress and the effect of boundary conditions

The preceding section presents the results of the investigation of using different types of parameters in the updating process. The section also covers the sensitivity analysis through which the selection of the updating parameters is carried out. The investigation reveals that not all parameters seem to be capable of improving the veracity of the prediction. However one of the major findings from the study is the effectiveness of the boundary conditions in altering the first mode of the predicted frequency which has led to a significant improvement and also a big reduction in the total error. The reason is likely to be that the four suspension springs liking the four corners the welded structure provide some stiffness to the first mode which torsion. Nevertheless there is a room for improvement on the predicted results. Therefore a further investigation into the sources of the errors is required and it should be systematically performed. In this work, more potential updating parameters are listed down and included in sensitivity analysis so that sensitive parameters can be used in the updating process.

This section presents and discusses how the large discrepancy between the measured and predicted frequencies are minimised through the application of sensitivity analysis and model updating process. Apart from that it also covers the procedure used to identify and include the initial stress in the FE model of welded structure arising from the assembly due to the clamp load applied to the spot welds during welding and cooling process and also the clamp load applied to the components.

The finite element model of welded structure was rearranged to become a new configuration after the three attempts to reconcile the model led to the unsatisfactory results. The model rearrangement is illustrated in Figure 5.9. The reasons for having the new configuration as depicted in Figure 5.9 (b) lies in the fact that firstly there are no other possible sources of potential updating parameters that can be used in updating process since the level of the accuracy of the finite element models of components remains essentially unsettled. Secondly the rejuvenation of the model allows the bending moment of inertia ratio $(12I/T^3)$ which is available in NATRAN code to be systematically and efficiently used to represent initial stress in the finite element model. The details of the work are explained in the next following paragraphs and also are illustrated in Figure 5.9, while the explanation of the bending moment of inertia ratio $(12I/T^3)$ is available on pages 3 to 4.

In this work, the initial FE model of a welded structure, in particular the bent floor was specially divided into three major sections namely Wall, Centre Floor and End Floor in which $(12I/T^3)$ is introduced. They are called new updating parameters. The detail of the FE model is shown in Figure 5.9 (c). This allows every section to have its own model properties such as the Young's modulus, density, shear modulus, Poisson's ratio and thickness. In other words the more new sections are introduced into the FE model, the larger the number of updating parameters is available to be considered. However the aforementioned parameters are no longer useful to be considered as the potential updating parameters in the updating process of welded structure. This is due to firstly the sensitivity of the model properties of the bent floor was already studied and used in updating process of the model.

Secondly not all the properties could help reduce the error in the model as discussed and presented in Chapter 4. Repeated investigations allow to identify a new quantity came to attention, which is the bending moment of inertia ratio ($12I / T^3$). It is used as a new updating parameter and it turns out to be very effective in reducing the large error mentioned before. The ratio can be used to represent the effect of the initial stress which is believed to arise as a result of the assembly of substructures. During the assembly process, clamps are used to position the substructures before they are welded together. As a result the load associated with the clamping process is permanently passed on to the structure after it is completely built-up. The inherent initial stress can be represented and simulated by using and adjusting the parameter. This work can be performed by coding NASTRAN SOL200 and the truncated input file of the NASTRAN SOL200 code is shown as follows:

```
$  End Floor
DESVAR,1,E_Floor,1.,.02,5.5,.01
DVPREL1,1,PSHELL,17,6
,1,1.0
$ Centre Floor
DESVAR,2,C_Floor,1.,.02,5.5,.01
DVPREL1,2,PSHELL,20,6
,2,1.0
$ Boundary Conditions
DESVAR,3,PELAS_1,1.,.2,5.5,.01
DVPREL1,3,PELAS,1,K1
,3,2.2
$ Wall
DESVAR,4,Wall,1.,.02,5.5,.01
DVPREL1,4,PSHELL,29,6
,4,1.0
$ Diameter SPOT WELD
DESVAR,5,Dia,1.,.75,2.5,.01
DVPREL1,5,PWELD,71,D
,5,5.0
```

The code clearly shows that the three sections have their own properties of the bending moment of inertia ratio ($12I / T^3$) and it is represented by no. 6 in the 5th field of DVPREL1. Meanwhile the value of ratio is calculated based on the value given in the 3rd field of the 2nd row of DVPREL1. The initial value used in the analysis is 1.

Sensitivity analysis is used to gauge the sensitivity of the potential updating parameters. In this work, six parameters were used with eight frequencies and the results are depicted in Figure 5.10. They clearly show that the first mode which is the poorest predicted frequency is obviously sensitive to the boundary conditions (BC) in comparison with other parameters. This means that the stiffness of the springs and strings used in the test must be considered in the FE model. While the second poorest prediction which is the fifth mode is more sensitive to the section of centre floor and end floor as compared with the wall section. In general all frequencies are more sensitive to the specially designed sections except the first mode. Furthermore the Young's modulus of the CWELD element has again proved to be less capable as an updating parameter. This has been demonstrated by the results that none of the frequencies are sensitive to the parameter.

Since the sectioning process of the finite element model as shown in Figure 5.9 is based on the observation and engineering judgement, therefore the feasibility of the process should be assessed and validated. This can be performed through the sensitivity analysis which would find the sensitive design variables used to represent the sections.

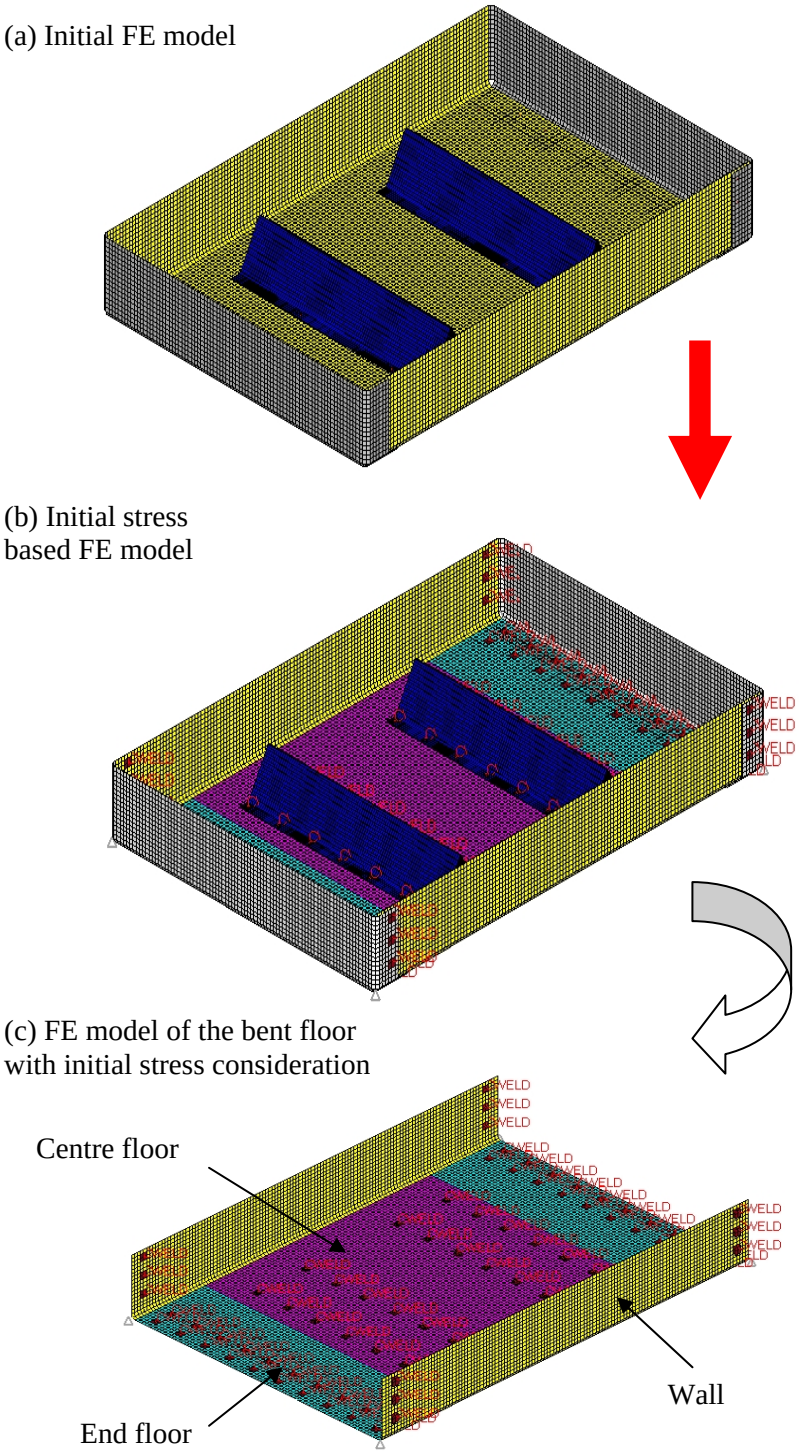

Figure 5.9: Characterisation of initial stress on the FE model of the welded structure

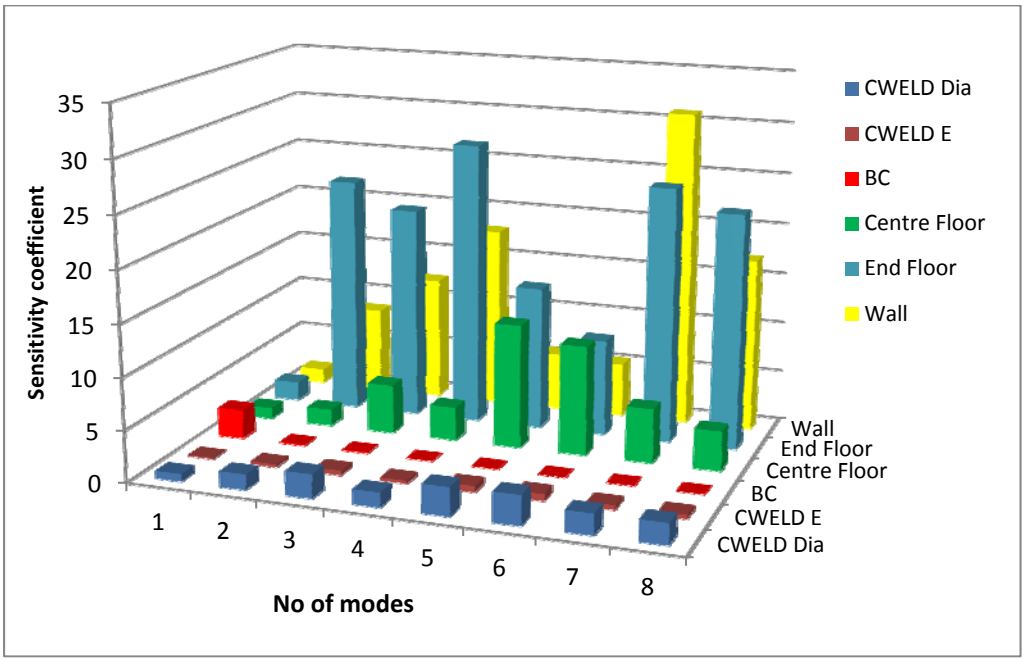

Figure 5.10: The results of sensitivity analysis of CWELD properties, the Young's modulus of patches and the boundary conditions (BC)

In order to prove the accuracy of the sensitive analysis results, only the most sensitive parameters are used in the updating process. There are two versions of updated FE model using different number of the updating parameters. The first version, namely, the 4th updated FE model is constructed, excluding the Young's modulus and diameter of CWELD element and the results are shown in column (IV) of Table 5.10. The updated values of the updating parameters of the 4th updated FE model are tabulated in Table 5.11.

Meanwhile, the second version which is called the 5th updated FE model containing only five updating parameters including the diameter of CWELD element, BC and the three new parameters. The results are tabulated in column (IV) of Table 5.12. The updated values of the updating parameters of the 5th updated FE model are shown in Table 5.13.

Table 5.10: Comparison of results between the tested and the 4th updated FE model of the welded structure

Mode	I Experiment (Hz)	II Initial FE model (Hz)	III Error (%) |I-II/I|	IV 4th Updated FE model (Hz)	V Error (%) |I-IV/I|
1	29.48	26.26	10.92	29.48	0.01
2	76.58	78.17	2.07	77.13	0.72
3	101.07	102.44	1.36	101.84	0.76
4	110.86	109.55	1.18	109.27	1.44
5	121.91	126.10	3.43	121.91	0.00
6	140.46	144.16	2.64	140.25	0.15
7	147.50	144.31	2.16	147.61	0.07
8	159.77	160.86	0.68	159.99	0.14
9	187.51	187.02	0.26	191.87	2.32
10	199.65	196.19	1.73	203.46	1.91
Total Error (%)			26.44		7.53

Table 5.11: Updated values of the updating parameters of the 4th updated FE model of the welded structure

Parameter	Initial value	Updated value	Unit
CELAS element stiffness represents Boundary conditions	0.0022	0.00294	N/m
$12I / T^3$ at Wall section	1	0.00131	m
$12I / T^3$ at Center floor section	1	0.00072	m
$12I / T^3$ at End floor section	1	0.00088	m

From the comparison of the results shown in Table 5.10, it is noticeable that the reduction in the total error highly depends on the stiffness of CELAS element and the three new parameters ($12I / T^3$ at the designated sections as shown in Figure 5.9). The total error has dropped from 26.44 to 7.53 percent which is a massive reduction of the discrepancies between the two types of model of the welded structure.

Table 5.12: Comparison of results between the tested and the 5th updated FE model of the welded structure

Mode	I Experiment (Hz)	II Initial FE model (Hz)	III Error (%) |I-II/I|	IV 5th Updated FE model (Hz)	V Error (%) |I-IV/I|	VI Updated FE model MAC
1	29.48	26.26	10.92	29.48	0.00	0.95
2	76.58	78.17	2.07	77.09	0.66	0.97
3	101.07	102.44	1.36	101.66	0.58	0.92
4	110.86	109.55	1.18	109.44	1.28	0.97
5	121.91	126.10	3.43	121.99	0.07	0.95
6	140.46	144.16	2.64	140.19	0.19	0.93
7	147.50	144.31	2.16	147.67	0.12	0.91
8	159.77	160.86	0.68	159.99	0.14	0.97
9	187.51	187.02	0.26	191.69	2.23	0.91
10	199.65	196.19	1.73	203.70	2.03	0.92
Total Error			26.44		7.30	

The updating procedure is carried out using the first eight measured frequencies of the welded structure and five updating parameters as shown in Table 5.13. The reasons for using the first eight frequencies in the updating lie in firstly this case has more measured data quantities than unknown parameters, secondly, the discrepancies between the measured frequencies and the frequencies produced by the updated parameters are significantly improved and the improvement can be seen in the first eight frequencies shown in Table 5.12. Meanwhile, the 9th and 10th natural frequencies have been significantly improved as well, giving confidence in the quality of the updated model.

Meanwhile Table 5.12 shows the reduction in total error as a result of the inclusion of the diameter of CWELD element as a updating parameter. The total error has decreased from 26.44 to 7.30 percent which is merely 0.23 percent different from the results obtained from the 4th updated FE model. Therefore there are two conclusions can be drawn from the findings. Firstly CWELD element ELPAT format has shown a good capability for representing spot welds in the prediction of the dynamic characteristics of the welded structure in comparison with CWELD element ALIGN format (see Tables 5.1 and 5.2). Secondly the dynamic behaviour

of the structure is less affected by the properties of the CWELD element in comparison with the ratio ($12I / T^3$).

In updating the finite element model of the welded structure, eight iterations are required to converge. The convergence of the updating parameters of finite element model of the welded structure is depicted in Figure 5.11. The updated values of the updating parameters are shown in Table 5.13. To summarise, the initial value of $12I / T^3$ at the section of centre floor and wall have started converging at the seventh iteration, while there are no rapid changes in the initial value of the CWELD diameter and $12I / T^3$ at the section of end floor after the sixth iteration. The increment rate of the initial value of boundary conditions has become totally flat right after the eighth iteration.

Meanwhile the measured and predicted mode shapes are shown in Figure 5.12 and 5.13. The qualitative results of the mode shapes calculated from the updated FE model are summarised in column (VI) of Table 5.12. In general the MAC value of the individual mode shapes of the structure is above 0.9 which is a good achievement for a complex structure.

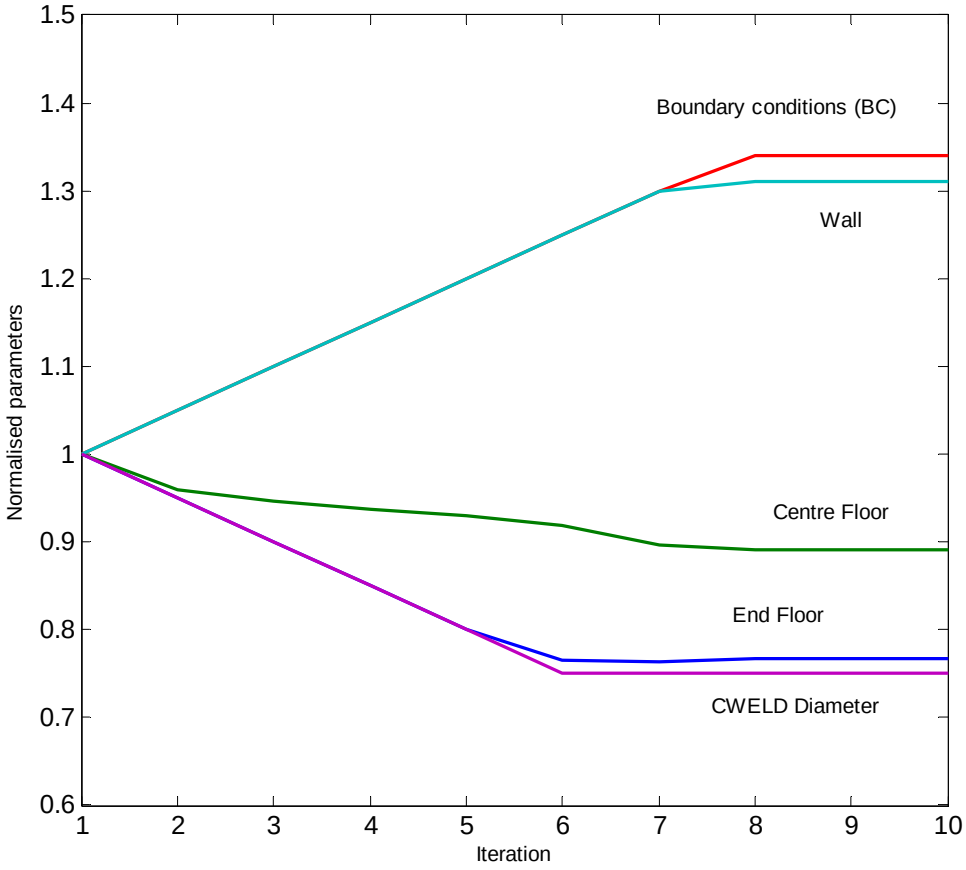

Figure 5.11: The convergence of the updating parameters of the 5th updated FE model of the welded structure

Table 5.13: Updated values of the updating parameters of 5th updated FE model of the welded structure

Parameter	Initial value	Updated value	Unit
CELAS element stiffness represents Boundary conditions	0.0022	0.002940	N/m
$12I / T^3$ at Wall section	1	0.001307	m
$12I / T^3$ at Center floor section	1	0.000767	m
$12I / T^3$ at End floor section	1	0.000891	m
CWELD diameter	0.005	0.00375	m

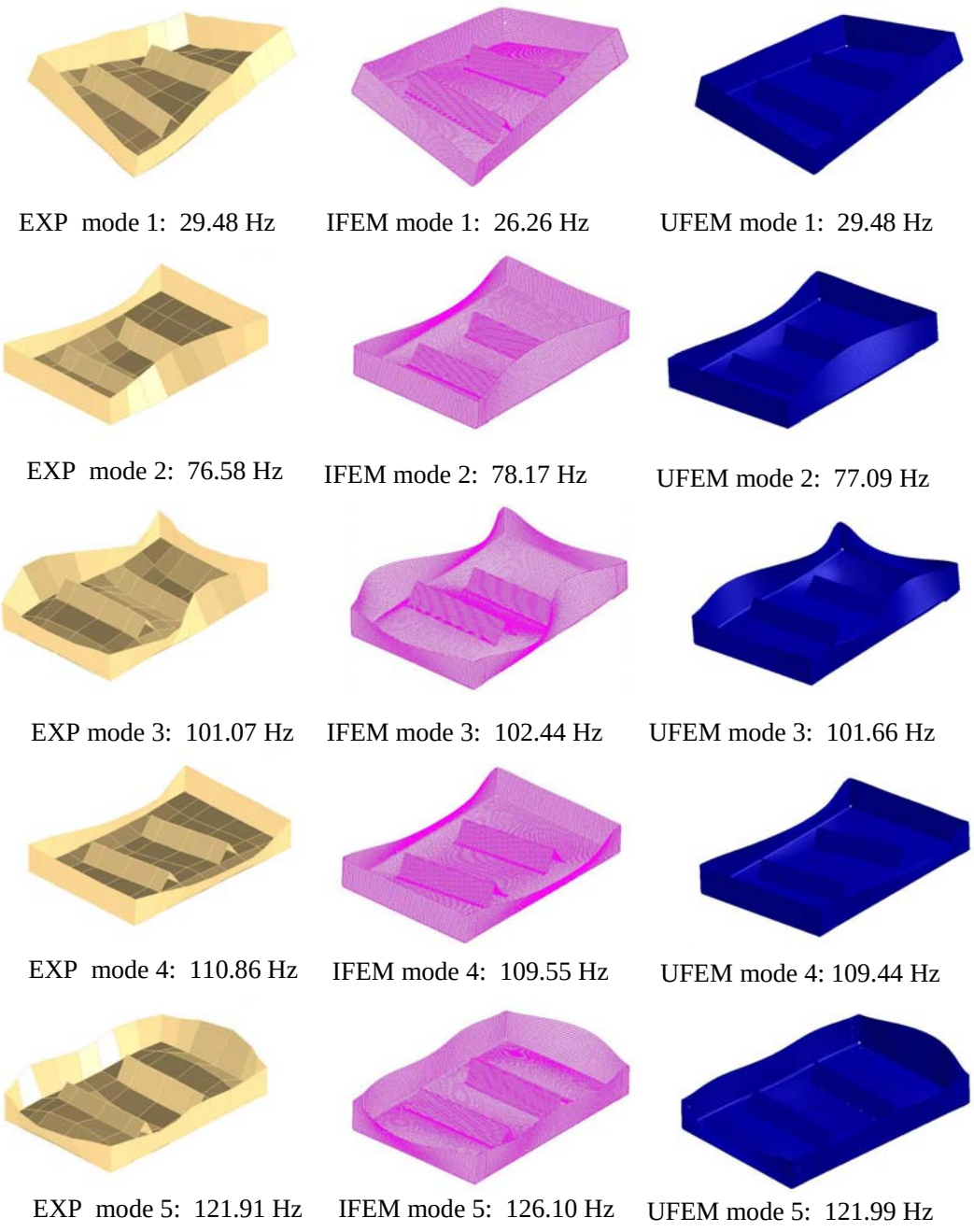

Figure 5.12: 1st, 2nd, 3rd, 4th and 5th pair of mode shapes of the welded structure calculated from experiment (EXP), initial FE model (IFEM) and updated FE model (UFEM)

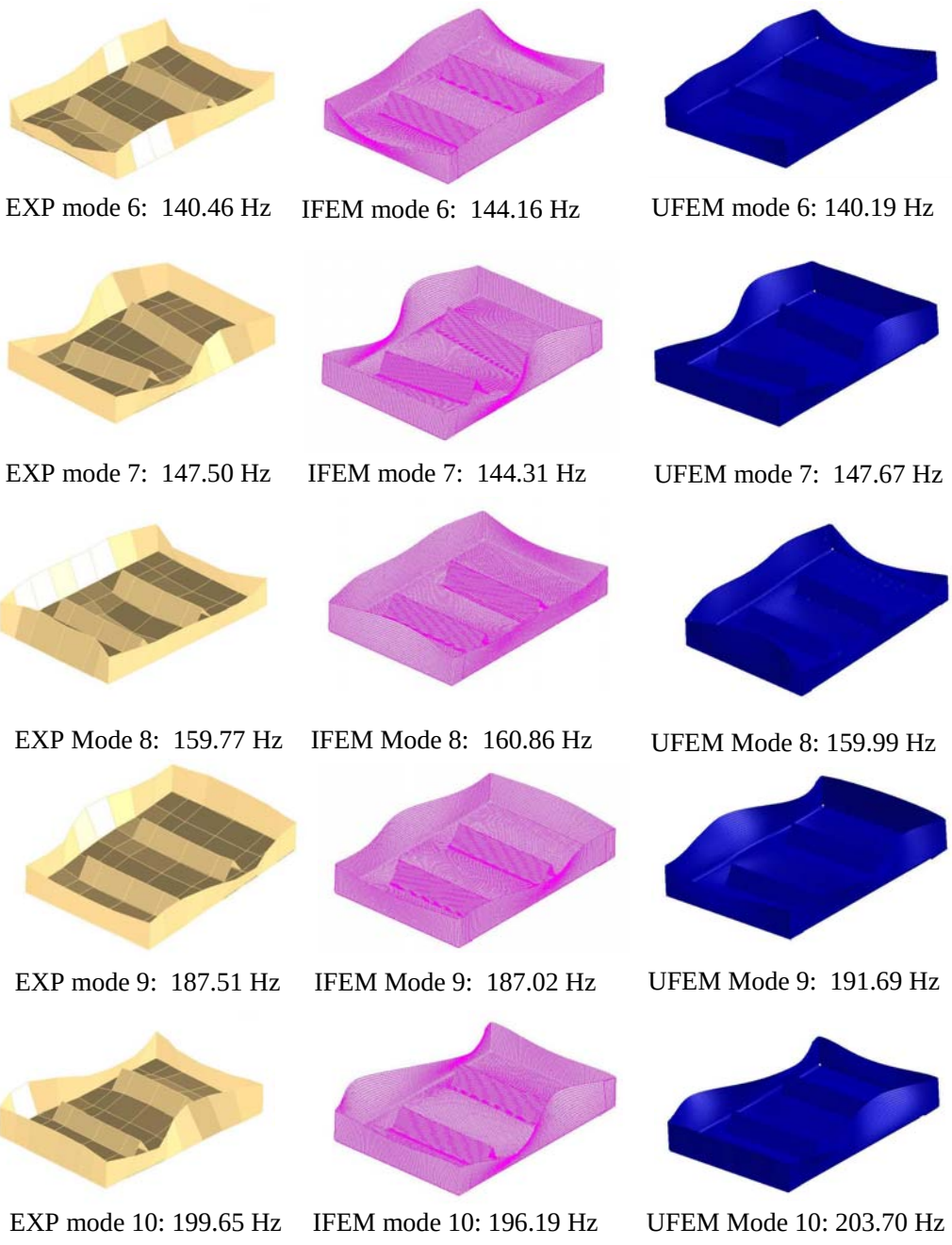

Figure 5.13: 6^{th}, 7^{th}, 8^{th}, 9^{th} and 10^{th} pair of mode shapes of the welded structure calculated from experiment (EXP), initial FE model (IFEM) and updated FE model (UFEM)

5.5 Conclusions

In this chapter, FE modelling and model updating process of the welded structure have been systematically demonstrated and elaborated. The large discrepancies between the measured and predicted frequencies have been successfully reduced from 26.44 to 7.30 percent (Table 5.12).

The achievement has been successfully achieved through the investigation of the sources of the errors in the FE model in which the inputs of the technical observation and engineering judgment coupled with the sensitivity analysis are systematically ustilised.

In this work, the sensitivity analysis has proved to be a powerful tool for localizing the sources of the error that are believed to arise as a result of excluding the effects of the boundary conditions and initial stress. However, the sensitivity analysis alone definitely would not have been able to be used to achieve the satisfactory reduction in the discrepancies without supporting by the inputs of the technical observation and engineering judgment.

This work also reveals that the three new parameters ($12I/T^3$) and CELAS element representing the stiffness suspensions of the springs (boundary conditions) are the very influential parameters in updating the finite element model of the welded structure.

Chapter 6

Substructuring Scheme based Model Updating

6.1 Introduction

The use of the full finite element model based model updating for correcting the discrepancies between the finite element and experimental results arising from invalid assumptions in the FE model of the welded structure was already discussed and presented in the previous chapter. In this present chapter, attention is focused on using substructuring or superelement based model updating (SEMU) in an attempt to reconcile the finite element model with the tested structure. Another concentration is given to the problem of linking the superelements together using the nodes of CWELD elements in form of branch elements, a process which gives modal solution for the structure. It is imperative to highlight here, the assembly of the superelements is only achieved at the superelement boundary nodes. Specifically, normal procedure for assembling superelements together via the nodes of CWELD elements in ELPAT format as the boundary nodes fails in arriving at a satisfactory solution.

This issue has been a topical subject in MSC. NASTRAN Community (MSC.6., 2011). However to the author's best knowledge there is no publication and evidence available in open literature on the use of the nodes of CWELD elements in ELPAT format for representing the boundary nodes of the superelement method.

The chief objectives of the present chapter are to show and discuss how:

- The superelements and the residual structure are organised, constructed and implemented in the context of updating the welded structure made from thin metal sheets

- The method of using the nodes that define CWELD elements (branch element) as the boundary nodes that connect a substructure with another substructure or a residual structure is specially designed and effectively used in SEMU

- The superelement method is incorporated into model updating procedure through the application of NASTRAN SOL200 and NASTRAN superelement code

- The augmentation of the Craig-Bampton transformation matrix (residual vectors) and the number of fixed-boundary component modes play an important role in improving the accuracy of the SEMU derived modal parameters (natural frequencies and mode shapes)

- The expenditure of CPU time which is the important criterion when large, complex structures are analysed using the finite element method, is calculated from the SEMU and the full finite element model.

In this work, the Craig-Bampton fixed boundary method is preferred over free boundary method because it is one of the most straightforward and accurate methods of component mode synthesis (Craig and Bampton, 1968; Craig and Kurdila, 2006 and Hinke et al., 2007). Therefore only the fixed boundary method and all its attendant theoretical procedures are covered.

6.2 Component mode synthesis (CMS)

Component mode synthesis (CMS) is one of the popular model reduction techniques for large structural models. A good introduction to the subject of CMS methods and the definition of varies types of component modes can be found from Craig (1981), Wijker (2004) and Craig and Kurdila (2006). Generally this technique involves the following four steps:

1) The complete structure is divided into a number of separate components or substructures
2) The finite element method or other schemes are utilized to formulate a discrete model for each component. In this stage each model is represented by a reduced model that consists of partial physical coordinates of the full model and a set of generalized coordinates
3) All the reduced models are assembled to formulate a global model for the complete structure. In this way, the global model has a much smaller size than the model directly obtained from the finite element method. All the structural analyses may be performed on the reduced global model
4) The responses in the physical coordinates may be computed using back-substitution

The component mode synthesis may be classified as a fixed-boundary method (Hurty, 1965 and Craig and Bampton, 1968), free-interface method (Goldman, 1969 and Hou, 1969) and hybrid method (MacNeal, 1971) depending upon whether the mode shapes, used to define substructure coordinates, are obtained with fixed or free master degrees of freedom or a combination of them. One feature of component mode synthesis is that partial modal coordinates are used in place of the physical coordinates to represent the substructures.

These modal coordinates must be transformed to physical coordinates in order to assemble the substructure matrices into global matrices by means of equilibrium and compatibility conditions. Comprehensive research has been performed during the past four decades, and a large number of component mode synthesis methods have been developed (Craig, 1995 and Craig, 2000).

The component mode synthesis has several advantages:

1) The computational effort and computer storage can be saved significantly. With the application of the component mode synthesis, a large-size dynamic problem can be divided into several smaller-size dynamic problems.

2) The component mode synthesis technique makes it possible that different components of a structural system may be analyzed by different groups, at different places, and at different times. This feature is especially important for a large model of structure such as the space station.

3. Structural dynamic modification and optimization become easier. Usually a structural modification of a structure is local. These local modifications only have an effect on the corresponding components. The repeated computation of other components can be avoided.

4. The technique allows a hybrid modeling scheme to be implemented. In some situations some components of a structural system are too complex to be modeled using any analytical method. For these components an experiment-based method may be used. Using the component mode synthesis, the global model can be obtained by assembling all the models from different modeling schemes.

6.3 CMS- Fixed boundary method based substructures

Figure 6.1 shows a structural system consisting of two substructures that are connected together by spot welds. The system is divided into two parts, the substructure and the residual structure, as depicted in Figure 6.1 (a). These two substructures are discretized using the finite element method and the full finite element model of each substructure is shown in Figure 6.1 (b). Each substructure has the boundary nodes connecting to other substructures and the internal nodes which are independent from other substructures. In dynamic analysis of complex structures with a large number of degrees of freedom, the Craig Bampton method is a well known method to significantly reduce the overall number of degrees of freedom. Therefore the same method is applied to the full finite element models of the substructures and the arrangement of the reduced substructures is schematically shown in Figure 6.1 (c) for one substructure and residual structure.

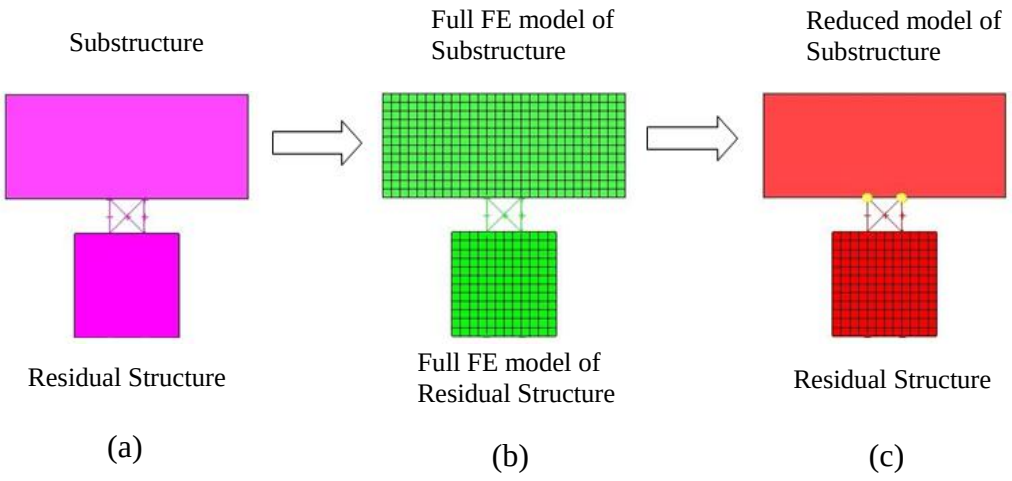

Figure 6.1: Schematic diagram of substructuring process

The residual structure

The residual structure (Figures 6.1 and 6.2) which is totally represented in physical coordinates is a non-reduced substructure and the last substructure to be processed. The residual structure contains the degrees of freedom on which the equations of motion (statics, dynamics, eigenvalues, buckling, aeroelastics, etc.) are solved. Therefore, there has to be at least one degree of freedom in the residual structure, otherwise there is no problem to solve. Superelements are just a method of representing substructures/components of the complete structure by reduced matrices. This might just be static condensation, but can also involve dynamic reduction using CMS with augmented shapes (static correction vectors) through which it is used in this work. The substructures/components can even be represented by matrices that come from an external source – any external source – another NASTRAN job, another finite element code, MATLAB, or even test. Subsequently, these reduced matrices of the substructures are linked together and finally connected to the residual structure, leading to considerable reduction in computational work.

For NASTRAN SOL 200, design parameters (updating parameters) are required and they may change as a result of trying to minimise some objective function. However, any design parameters are not necessarily required to be only placed in the residual structure, and all the design parameters can be placed in superelements as well. However, placing any design parameters in superelements will lead to an inefficiency. The advantage of superelements is that the reduced models can be attached many times (each design cycle for example). Although design parameters can be put in the superelements, normally, in CAE communities this practice rarely happens. This is because each time design parameters are updated, the superelements in which that design parameters are located must be re-reduced. Sometimes, however design parameters in the superelements are unavailable, especially for large complex structures. In addition, the residual structure is needed, not because NASTRAN SOL 200 needs it but because NASTRAN always has to have a residual structure. Basically, there are not any

elements that are required at all in the residual structure and the residual structure can even be just a modal model, but there must be one.

The advantage of using superelements would be much clearly seen if the user thinks ahead when defining superelements. In other words, on restarts this advantage is magnified by the need to process only the parts of the structure directly affected by the change. This means that it is possible to achieve performance improvements on the order of anywhere from 2 to 30 times faster than non-superelement methods.

Branch elements (patch)

The area in which the branch elements are located, in general, is directly defined by the NASTRAN's users. When a CWELD with the ELPAT option is defined, one shell element on each of the 2 parts to connect with the CWELD is specified. It is the MSC NASTRAN program that will then detect which elements constitute the branch elements (patch).

This means that all the elements that might be chosen as the branch elements must be present either in the superelement or in the residual. MSC NASTRAN doesn't allow some elements to be in the superelement and some in the residual, therefore, in order to have a good set of branch elements, all possible candidates for the branch elements should be placed in the residual structure and let MSC NASTRAN decide which elements it will finally select for the complete CWELD elements.

The details of procedure on how the elements are selected to be the branch elements and how the residual structure is decided are presented in section "the arrangement of branch elements, superelements and residual structure" starting from page 188 to 192.

The corresponding degrees of freedom of each substructure are called boundary degrees of freedom and internal degrees of freedom respectively. Therefore the dynamic equation of motion for the S^{th} undamped substructure can be expressed as

$$\mathbf{M}^S \ddot{\mathbf{X}}^S + \mathbf{K}^S \mathbf{X}^S = \mathbf{F}^S \tag{6.1}$$

where the superscript S relates to the S^{th} substructure and $\mathbf{M}^S$, $\mathbf{K}^S$, $\mathbf{X}^S$ and $\mathbf{F}^S$ are the S^{th} substructure's mass matrix, stiffness matrix, displacement vector and force vector respectively.

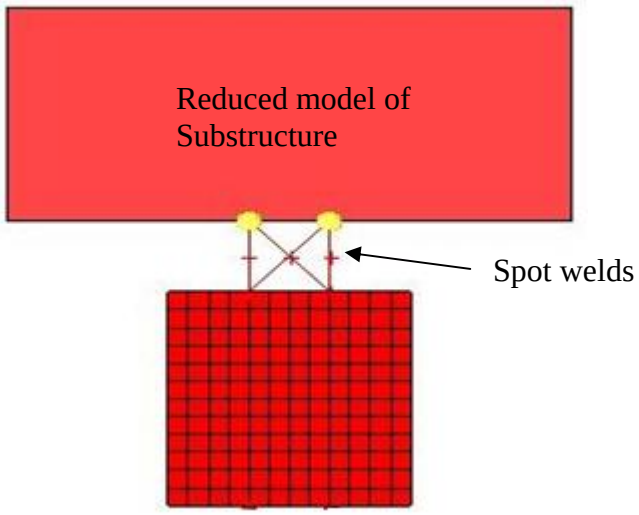

Figure 6.2: Schematic diagram of reduced model

Since the Craig-Bampton method requires the use of the component modes which are constraint modes and normal modes, it is convenient to partition the total degrees of freedom of the S^{th} substructure into the boundary and internal degrees of freedom as follows

$$\mathbf{X}^S = \begin{Bmatrix} \mathbf{X}_B^S \\ \mathbf{X}_I^S \end{Bmatrix} \tag{6.2}$$

Therefore the equation of motion (6.1) can be partitioned as

$$\begin{bmatrix} \mathbf{M}_{BB}^S & \mathbf{M}_{BI}^S \\ \mathbf{M}_{IB}^S & \mathbf{M}_{II}^S \end{bmatrix} \begin{Bmatrix} \ddot{\mathbf{X}}_B^S \\ \ddot{\mathbf{X}}_I^S \end{Bmatrix} + \begin{bmatrix} \mathbf{K}_{BB}^S & \mathbf{K}_{BI}^S \\ \mathbf{K}_{IB}^S & \mathbf{K}_{II}^S \end{bmatrix} \begin{Bmatrix} \mathbf{X}_B^S \\ \mathbf{X}_I^S \end{Bmatrix} = \begin{Bmatrix} \mathbf{F}_B^S \\ \mathbf{F}_I^S \end{Bmatrix} \tag{6.3}$$

where the superscript B and I indicates boundary and interior degrees of freedom, respectively. In order to reduce the size of the S^{th} substructure, the Craig-Bampton transformation matrix for the substructure is defined as

$$\mathbf{X}^S = \begin{Bmatrix} \mathbf{X}_B^S \\ \mathbf{X}_I^S \end{Bmatrix} = \begin{bmatrix} \mathbf{I} & \mathbf{0} \\ \mathbf{\Phi}_B & \mathbf{\Phi}_I \end{bmatrix} \begin{Bmatrix} \mathbf{X}_B^S \\ \mathbf{q}_m \end{Bmatrix} = \begin{bmatrix} \mathbf{\Psi}_B & \mathbf{\Psi}_I \end{bmatrix} \begin{Bmatrix} \mathbf{X}_B^S \\ \mathbf{q}_m \end{Bmatrix} \tag{6.4}$$

Note that the physical displacements of the interior points are computed by

$$\mathbf{X}_I^S = \mathbf{\Psi}_B \, \mathbf{X}_B^S + \mathbf{\Psi}_I \, \mathbf{q}_m \tag{6.5}$$

The Craig-Bampton transformation matrices $\boldsymbol{\Psi}_B$ and $\boldsymbol{\Psi}_I$ can be partitioned as

$$\boldsymbol{\Psi}_B = \begin{bmatrix} \mathbf{I} \\ \boldsymbol{\Phi}_B \end{bmatrix} \qquad \boldsymbol{\Psi}_I = \begin{bmatrix} \mathbf{0} \\ \boldsymbol{\Phi}_I \end{bmatrix} \tag{6.6}$$

Equation (6.4) clearly shows that the dimension of $\mathbf{X}_I^S$ is that of all of the interior coordinates of the substructure, whereas the dimension of $\mathbf{q}_m$ is that of the selected normal modes of the interior of the substructure. The matrix, $\boldsymbol{\Psi}_B$ is usually referred to as the boundary node functions or constraint modes. It is obtained by setting all interior forces of the substructure in Equation (6.3) equal to zero, which gives

$$\mathbf{K}_{IB}^S \mathbf{X}_B^S + \mathbf{K}_{II}^S \mathbf{X}_I^S = \mathbf{0} \tag{6.7}$$

From Equation (6.7), the following Equation can be derived

$$\mathbf{X}_I^S = -\mathbf{K}_{II}^{S\,-1} \mathbf{K}_{IB}^S \mathbf{X}_B^S = \boldsymbol{\Phi}_B \mathbf{X}_B^S \tag{6.8}$$

where

$$\boldsymbol{\Phi}_B = -\mathbf{K}_{II}^{S\,-1} \mathbf{K}_{IB}^S \tag{6.9}$$

Therefore the full set of displacements merely considering constraint modes can be formed as

$$\begin{bmatrix} \mathbf{X}_{\mathrm{B}}^{S} \\ \mathbf{X}_{\mathrm{B}}^{S} \end{bmatrix} = \begin{bmatrix} \mathbf{I} \\ -\mathbf{K}_{\mathrm{II}}^{S\,-1}\mathbf{K}_{\mathrm{IB}}^{S} \end{bmatrix} \begin{bmatrix} \mathbf{X}_{\mathrm{B}}^{S} \end{bmatrix} = \begin{bmatrix} \mathbf{I} \\ \boldsymbol{\Phi}_{B} \end{bmatrix} \begin{bmatrix} \mathbf{X}_{\mathrm{B}}^{S} \end{bmatrix} = \begin{bmatrix} \boldsymbol{\Psi}_{B} \end{bmatrix} \begin{bmatrix} \mathbf{X}_{\mathrm{B}}^{S} \end{bmatrix} \qquad (6.10)$$

It consists of two sub-matrices which are $\mathbf{I}$ that has B rows and B columns and $\boldsymbol{\Phi}_{B}$ that has I rows and B columns. This matrix clearly represents rigid body modes of a substructure at the I degrees of freedom due to successive unit displacement at one of the B degrees of freedom.

The matrix of $\boldsymbol{\Psi}_{I}$ which is usually referred to as the fixed boundary modes or component normal modes, is shown in Equation (6.4) and (6.6). It represents displacements on the internal degrees of freedom relative to the boundaries. Each column represents a mode function is calculated with all boundary nodes all fixed. In principle, as many independent modes can be calculated from this matrix because there are internal degrees of freedom and it may be a square matrix. However the novelty of modal synthesis methods lies in the fact that useful solutions can be obtained from the selection of the number of the fixed boundary modes. Practically this matrix is constructed using normal modes of vibration of the substructure with the boundary degrees of freedom fixed. Therefore only a subset of these modes is used. The resulting matrix consists of two sub-matrices

$$\boldsymbol{\Psi}_{I} = \begin{Bmatrix} \mathbf{0} \\ \boldsymbol{\Phi}_{I} \end{Bmatrix} \qquad (6.11)$$

The matrix $\mathbf{0}$ is a mathematical statement with B rows and m columns, while the matrix $\mathbf{\Phi}_I$ with I rows and m columns is a transformation matrix between modal coordinates and the physical coordinates of the internal degrees of freedom, $\mathbf{X}_I^S$. This matrix can be derived from the equation of motion by setting the boundary degrees of freedom and the forces acting on the interior degrees of freedom zero as

$$\ddot{\mathbf{X}}_B^S, \mathbf{X}_B^S, \mathbf{F}_I^S = \mathbf{0} \tag{6.12}$$

Equation (6.3) reduces to

$$\mathbf{M}_{II}^S \ddot{\mathbf{X}}_I^S + \mathbf{K}_{II}^S \mathbf{X}_I^S = \mathbf{0} \tag{6.13}$$

Assuming harmonic response for the interior degrees of freedom, leads to

$$\mathbf{X}_I^S = \boldsymbol{\phi}_I \mathbf{q}_m e^{\mathrm{i}\omega t} \tag{6.14}$$

Substituting Equation (6.14) into Equation (6.13) and simplifying yields the expression

$$\left[\mathbf{K}_{II}^S - \omega^2 \mathbf{M}_{II}^S\right] \boldsymbol{\phi}_I = \mathbf{0} \tag{6.15}$$

The number of the fixed boundary modes in Equation (6.15) is calculated by user input on NASTRAN, EIGRL entry (MSC.2., 2010) or some other computer program for the eigensolutions. Then the fixed boundary modes are concatenated with the constrained modes in Equation (6.10) to form the coordinate transformation matrix and Equation (6.4) may be rewritten as

$$\mathbf{X}^S = \begin{Bmatrix} \mathbf{X}_B^S \\ \mathbf{X}_I^S \end{Bmatrix} = \begin{bmatrix} \mathbf{I} & \mathbf{0} \\ \boldsymbol{\Phi}_B & \boldsymbol{\Phi}_I \end{bmatrix} \begin{Bmatrix} \mathbf{X}_B^S \\ \mathbf{q}_m \end{Bmatrix} = \begin{bmatrix} \boldsymbol{\Psi}_B & \boldsymbol{\Psi}_I \end{bmatrix} \begin{Bmatrix} \mathbf{X}_B^S \\ \mathbf{q}_m \end{Bmatrix} = \mathbf{T}\mathbf{p}^S \tag{6.16}$$

The component mode matrix $\mathbf{T}$ is the coordinate transformation matrix relating component physical coordinates $\mathbf{X}^S$ to component generalized coordinates $\mathbf{p}^S$ which consists of the boundary degrees of freedom and modal coordinates of the substructure. Substituting Equation (6.16) into Equation (6.1) leads to equations of motion in terms of truncated generalized coordinates

$$\mathbf{M}^S \mathbf{T}\ddot{\mathbf{p}}^S + \mathbf{K}^S \mathbf{T}\mathbf{p}^S = \mathbf{F}^S \tag{6.17}$$

Multiply Equation (6.17) with the transpose of the component mode matrix, $\mathbf{T}^T$ to yield

$$\mathbf{T}^T\mathbf{M}^S \mathbf{T}\ddot{\mathbf{p}}^S + \mathbf{T}^T\mathbf{K}^S\mathbf{T}\mathbf{p}^S = \mathbf{T}^T\mathbf{F}^S \tag{6.18}$$

Equation (6.18) may be written as

$$\begin{bmatrix} \hat{\mathbf{M}}_{BB}^{S} & \hat{\mathbf{M}}_{Bm}^{S} \\ \hat{\mathbf{M}}_{mB}^{S} & \hat{\mathbf{M}}_{mm}^{S} \end{bmatrix} \begin{Bmatrix} \ddot{\mathbf{X}}_{B}^{S} \\ \ddot{\mathbf{q}}_{m} \end{Bmatrix} + \begin{bmatrix} \hat{\mathbf{K}}_{BB}^{S} & \hat{\mathbf{K}}_{Bm}^{S} \\ \hat{\mathbf{K}}_{mB}^{S} & \hat{\mathbf{K}}_{mm}^{S} \end{bmatrix} \begin{Bmatrix} \mathbf{X}_{B}^{S} \\ \mathbf{q}_{m} \end{Bmatrix} = \begin{Bmatrix} \hat{\mathbf{F}}_{B}^{S} + \boldsymbol{\Psi}_{B}^{\mathrm{T}} \hat{\mathbf{F}}_{I} \\ \boldsymbol{\Psi}_{I}^{\mathrm{T}} \hat{\mathbf{F}}_{I} \end{Bmatrix} \tag{6.19}$$

The submatrices of the reduced mass matrix are

$$\begin{aligned} \hat{\mathbf{M}}_{BB}^{S} &= \boldsymbol{\Psi}_{B}^{\mathrm{T}} \mathbf{M}^{S} \boldsymbol{\Psi}_{B} = \begin{bmatrix} \mathbf{I} \\ \boldsymbol{\Phi}_{B} \end{bmatrix}^{\mathrm{T}} \begin{bmatrix} \mathbf{M}_{BB}^{S} & \mathbf{M}_{BI}^{S} \\ \mathbf{M}_{IB}^{S} & \mathbf{M}_{II}^{S} \end{bmatrix} \begin{bmatrix} \mathbf{I} \\ \boldsymbol{\Phi}_{B} \end{bmatrix} \\ &= \mathbf{M}_{BB}^{S} + \mathbf{M}_{BI}^{S} \boldsymbol{\Phi}_{B} + \boldsymbol{\Phi}_{B}^{\mathrm{T}} \mathbf{M}_{IB}^{S} + \boldsymbol{\Phi}_{B}^{\mathrm{T}} \mathbf{M}_{II}^{S} \boldsymbol{\Phi}_{B} \end{aligned} \tag{6.20}$$

$$\begin{aligned} \hat{\mathbf{M}}_{Bm}^{S} &= \boldsymbol{\Psi}_{B}^{\mathrm{T}} \mathbf{M}^{S} \boldsymbol{\Psi}_{I} = \begin{bmatrix} \mathbf{I} \\ \boldsymbol{\Phi}_{B} \end{bmatrix}^{\mathrm{T}} \begin{bmatrix} \mathbf{M}_{BB}^{S} & \mathbf{M}_{BI}^{S} \\ \mathbf{M}_{IB}^{S} & \mathbf{M}_{II}^{S} \end{bmatrix} \begin{bmatrix} \mathbf{0} \\ \boldsymbol{\Phi}_{I} \end{bmatrix} \\ &= \mathbf{M}_{BI}^{S} \boldsymbol{\Phi}_{I} + \boldsymbol{\Phi}_{B}^{\mathrm{T}} \mathbf{M}_{II}^{S} \boldsymbol{\Phi}_{I} \end{aligned} \tag{6.21}$$

$$\begin{aligned} \hat{\mathbf{M}}_{mB}^{S} &= \boldsymbol{\Psi}_{I}^{\mathrm{T}} \mathbf{M}^{S} \boldsymbol{\Psi}_{B} = \begin{bmatrix} \mathbf{0} \\ \boldsymbol{\Phi}_{I} \end{bmatrix}^{\mathrm{T}} \begin{bmatrix} \mathbf{M}_{BB}^{S} & \mathbf{M}_{BI}^{S} \\ \mathbf{M}_{IB}^{S} & \mathbf{M}_{II}^{S} \end{bmatrix} \begin{bmatrix} \mathbf{I} \\ \boldsymbol{\Phi}_{B} \end{bmatrix} \\ &= \boldsymbol{\Phi}_{I}^{\mathrm{T}} \mathbf{M}_{IB}^{S} + \boldsymbol{\Phi}_{I}^{\mathrm{T}} \mathbf{M}_{II}^{S} \boldsymbol{\Phi}_{B} \end{aligned} \tag{6.22}$$

$$\hat{\mathbf{M}}^S_{mm} = \boldsymbol{\Psi}_I^{\mathrm{T}}\,\mathbf{M}^S\boldsymbol{\Psi}_I = \begin{bmatrix}\mathbf{0}\\ \boldsymbol{\Phi}_I\end{bmatrix}^{\mathrm{T}}\begin{bmatrix}\mathbf{M}^S_{BB} & \mathbf{M}^S_{BI}\\ \mathbf{M}^S_{IB} & \mathbf{M}^S_{II}\end{bmatrix}\begin{bmatrix}\mathbf{0}\\ \boldsymbol{\Phi}_I\end{bmatrix}$$

$$= \boldsymbol{\Phi}_I^{\mathrm{T}}\,\mathbf{M}^S_{II}\,\boldsymbol{\Phi}_I = \mathbf{I}^S_{mm} \tag{6.23}$$

Similarly, the submatrices of the reduced stiffness matrix are

$$\hat{\mathbf{K}}^S_{BB} = \boldsymbol{\Psi}_B^{\mathrm{T}}\,\mathbf{K}^S\,\boldsymbol{\Psi}_B = \begin{bmatrix}\mathbf{I}\\ \boldsymbol{\Phi}_B\end{bmatrix}^{\mathrm{T}}\begin{bmatrix}\mathbf{K}^S_{BB} & \mathbf{K}^S_{BI}\\ \mathbf{K}^S_{IB} & \mathbf{K}^S_{II}\end{bmatrix}\begin{bmatrix}\mathbf{I}\\ \boldsymbol{\Phi}_B\end{bmatrix}$$

$$= \mathbf{K}^S_{BB} + \mathbf{K}^S_{BI}\,\boldsymbol{\Phi}_B + \boldsymbol{\Phi}_B^{\mathrm{T}}\left[\mathbf{K}^S_{IB} + \mathbf{K}^S_{II}\,\boldsymbol{\Phi}_B\right] \tag{6.24}$$

$$\hat{\mathbf{K}}^S_{Bm} = \boldsymbol{\Psi}_B^{\mathrm{T}}\,\mathbf{K}^S\boldsymbol{\Psi}_I = \begin{bmatrix}\mathbf{I}\\ \boldsymbol{\Phi}_B\end{bmatrix}^{\mathrm{T}}\begin{bmatrix}\mathbf{K}^S_{BB} & \mathbf{K}^S_{BI}\\ \mathbf{K}^S_{IB} & \mathbf{K}^S_{II}\end{bmatrix}\begin{bmatrix}\mathbf{0}\\ \boldsymbol{\Phi}_I\end{bmatrix}$$

$$= \mathbf{K}^S_{BI}\boldsymbol{\Phi}_I + \boldsymbol{\Phi}_B^{\mathrm{T}}\,\mathbf{K}^S_{II}\boldsymbol{\Phi}_I \tag{6.25}$$

$$\hat{\mathbf{K}}^S_{mB} = \boldsymbol{\Psi}_I^{\mathrm{T}}\,\mathbf{K}^S\boldsymbol{\Psi}_B = \begin{bmatrix}\mathbf{0}\\ \boldsymbol{\Phi}_I\end{bmatrix}^{\mathrm{T}}\begin{bmatrix}\mathbf{K}^S_{BB} & \mathbf{K}^S_{BI}\\ \mathbf{K}^S_{IB} & \mathbf{K}^S_{II}\end{bmatrix}\begin{bmatrix}\mathbf{I}\\ \boldsymbol{\Phi}_B\end{bmatrix}$$

$$= \boldsymbol{\Phi}_I^{\mathrm{T}}\mathbf{K}^S_{IB} + \boldsymbol{\Phi}_I^{\mathrm{T}}\,\mathbf{K}^S_{II}\boldsymbol{\Phi}_B \tag{6.26}$$

$$\hat{\mathbf{K}}_{mm}^{S} = \boldsymbol{\Psi}_{I}^{\mathrm{T}} \mathbf{K}^{S} \boldsymbol{\Psi}_{I} = \begin{bmatrix} \mathbf{0} \\ \boldsymbol{\Phi}_{I} \end{bmatrix}^{\mathrm{T}} \begin{bmatrix} \mathbf{K}_{BB}^{S} & \mathbf{K}_{BI}^{S} \\ \mathbf{K}_{IB}^{S} & \mathbf{K}_{II}^{S} \end{bmatrix} \begin{bmatrix} \mathbf{0} \\ \boldsymbol{\Phi}_{I} \end{bmatrix}$$

$$= \boldsymbol{\Phi}_{I}^{\mathrm{T}} \mathbf{K}_{II}^{S} \boldsymbol{\Phi}_{I} = \boldsymbol{\Lambda}_{mm}^{S} \tag{6.27}$$

The equations of motion for the reduced model of the S^{th} substructure stated in Equation (6.17) and restated in Equation (6.19) can be rewritten simply as

$$\begin{bmatrix} \hat{\mathbf{M}}_{BB}^{S} & \hat{\mathbf{M}}_{Bm}^{S} \\ \hat{\mathbf{M}}_{mB}^{S} & \hat{\mathbf{I}}_{mm}^{S} \end{bmatrix} \begin{Bmatrix} \ddot{\mathbf{X}}_{B}^{S} \\ \ddot{\mathbf{q}}_{m} \end{Bmatrix} + \begin{bmatrix} \hat{\mathbf{K}}_{BB}^{S} & \hat{\mathbf{0}}_{Bm} \\ \hat{\mathbf{0}}_{mB} & \boldsymbol{\Lambda}_{mm}^{S} \end{bmatrix} \begin{Bmatrix} \mathbf{X}_{B}^{S} \\ \mathbf{q}_{m} \end{Bmatrix} = \begin{Bmatrix} \hat{\mathbf{F}}_{B}^{S} \\ \mathbf{0} \end{Bmatrix} \tag{6.28}$$

It can clearly be shown that only the matrices $\hat{\mathbf{M}}_{Bm}^{S}$ and $\hat{\mathbf{M}}_{mB}^{S}$ are coupled, while the matrices $\hat{\mathbf{K}}_{BB}^{S}$ and $\boldsymbol{\Lambda}_{mm}^{S}$ are uncoupled as indicated in Equation (6.28). This is due, essentially to the fact that the modes obtained from the boundary degrees of freedom fixed. The first global step of the Component Mode Synthesis is used to divide the structure into the residual structure and substructure(s) which is shown in Equation (6.1) and Equation (6.3). The calculation for a set of component modes which are constraint modes and fixed boundary modes for each substructure is shown in Equation (6.4) to (6.16). The second step is stated in Equation (6.17) to Equation (6.28), in which the component modes are used to reduce the substructure model. The combination of the reduced substructure models with the non-reduced substructure to form global reduced model through which further finite element analyses are, in practice, performed, is the final step of the Component Mode Synthesis.

The residual structure is, by definition, the non-reduced substructure and also the substructure to which all the reduced substructures are assembled. The residual structure also is always the last substructure to be processed and is the one on which the assembly level analysis is performed. After partitioning the matrices of stiffness and mass of the residual structure with respect to the displacement vector

$\mathbf{X}_{II}^{RS}$ and the boundary vector $\mathbf{X}_{B}^{S}$, the assembly of the reduced model of the S^{th} substructure shown in Equation (6.28) with the residual structure can be performed as usual, in practice, by adding the submatrices at the boundary degrees of freedom, which the equation of motion of the coupled system

$$\begin{bmatrix} \mathbf{M}_{II}^{RS} & \mathbf{M}_{BI}^{RS} & \mathbf{0} \\ \mathbf{M}_{IB}^{RS} & \mathbf{M}_{BB}^{RS} + \hat{\mathbf{M}}_{BB}^{S} & \hat{\mathbf{M}}_{Bm}^{S} \\ \mathbf{0} & \hat{\mathbf{M}}_{mB}^{S} & \hat{\mathbf{I}}_{mm}^{S} \end{bmatrix} \begin{Bmatrix} \ddot{\mathbf{X}}_{II}^{RS} \\ \ddot{\mathbf{X}}_{B}^{S} \\ \ddot{\mathbf{q}}_{m}^{S} \end{Bmatrix} + \begin{bmatrix} \mathbf{K}_{II}^{RS} & \mathbf{K}_{BI}^{RS} & \mathbf{0} \\ \mathbf{K}_{IB}^{RS} & \mathbf{K}_{BB}^{RS} + \mathbf{K}_{BB}^{S} & \mathbf{0} \\ \mathbf{0} & \mathbf{0} & \mathbf{\Lambda}_{m}^{S} \end{bmatrix} \begin{Bmatrix} \mathbf{X}_{II}^{RS} \\ \mathbf{X}_{B}^{S} \\ \mathbf{q}_{m}^{S} \end{Bmatrix} = \begin{Bmatrix} \mathbf{F}_{II}^{RS} \\ \mathbf{F}_{B}^{S} \\ \mathbf{F}_{m}^{S} \end{Bmatrix} \tag{6.29}$$

where *RS* indicates the residual structure. This equation is formulated based on the Craig-Bampton method or Craig-Bampton superelement which is the component modes are constraint modes and fixed boundary normal modes. The method is frequently used for substructure coupling analysis due to the accuracy and robustness of the results obtained and its accuracy is governed by the number of the fixed-boundary modes shown in Equation (6.15). On top of that it is clearly shown that the mass and stiffness of the residual structure is totally described by the physical quantities, while the counterparts of the substructure are expressed in modal coordinates.

In the absence of the external force, Equation (6.29) can be rearranged and simplified to be eigenequations of motion as,

$$\left(\hat{\mathbf{K}} - \omega^2 \hat{\mathbf{M}}\right)\boldsymbol{\varphi} = \mathbf{0} \tag{6.30}$$

where

$$\boldsymbol{\varphi} = \begin{Bmatrix} \mathbf{X}_{II}^{RS} \\ \mathbf{X}_{B}^{S} \\ \mathbf{P}_{m}^{S} \end{Bmatrix} \tag{6.31}$$

and $\hat{\mathbf{K}}$ and $\hat{\mathbf{M}}$ are the matrices of the complete assembly of stiffness and mass in Equation (6.29). While corresponding to each natural frequency ω_i is an eigenvector $\boldsymbol{\varphi}_i$ representing the participation of the displacement coordinates.

The stiffness of CWELD element $\mathbf{K}^{CW}$ can be written as follows

$$\left[\mathbf{K}^{CW}\right]\begin{Bmatrix}\mathbf{X}_{GA}\\ \mathbf{X}_{GB}\end{Bmatrix}=\begin{Bmatrix}\mathbf{F}_{GA}\\ \mathbf{F}_{GB}\end{Bmatrix} \tag{6.32}$$

and Equation (6.32) can be re-written in a partition form, yields

$$\begin{bmatrix}\mathbf{K}_{BB}^{CW} & \mathbf{K}_{BI}^{CW}\\ \mathbf{K}_{IB}^{CW} & \mathbf{K}_{II}^{CW}\end{bmatrix}\begin{Bmatrix}\mathbf{X}_{GA}\\ \mathbf{X}_{GB}\end{Bmatrix}=\begin{Bmatrix}\mathbf{F}_{GA}\\ \mathbf{F}_{GB}\end{Bmatrix} \tag{6.33}$$

where $\mathbf{X}_{GA}$ and $\mathbf{X}_{GB}$ are expressed in terms of nodal displacement vector of the element containing *GA* and *GB* using shape function matrix. $\mathbf{F}_{GA}$ and $\mathbf{F}_{GB}$ are expressed in terms of distributed to nodal force vector of the element containing *GA* and *GB*

If *GA* and *GB* are not on the nodes which means the meshes are incongruent, Equation (6.33) needs to be cast as below

$$\begin{bmatrix}\bar{\mathbf{K}}_{BB}^{CW} & \bar{\mathbf{K}}_{BI}^{CW}\\ \bar{\mathbf{K}}_{IB}^{CW} & \bar{\mathbf{K}}_{II}^{CW}\end{bmatrix}\begin{Bmatrix}\bar{\mathbf{X}}_{GA}\\ \bar{\mathbf{X}}_{GB}\end{Bmatrix}=\begin{Bmatrix}\bar{\mathbf{F}}_{GA}\\ \bar{\mathbf{F}}_{GB}\end{Bmatrix} \tag{6.34}$$

where

$$\begin{bmatrix} \bar{\mathbf{K}}_{BB}^{CW} & \bar{\mathbf{K}}_{BI}^{CW} \\ \bar{\mathbf{K}}_{IB}^{CW} & \bar{\mathbf{K}}_{II}^{CW} \end{bmatrix} = \begin{bmatrix} \mathbf{N}_A^{\mathrm{T}} & 0 \\ 0 & \mathbf{N}_B^{\mathrm{T}} \end{bmatrix} \begin{bmatrix} \mathbf{K}_{BB} & \mathbf{K}_{BI} \\ \mathbf{K}_{IB} & \mathbf{K}_{II} \end{bmatrix} \begin{bmatrix} \mathbf{N}_A & 0 \\ 0 & \mathbf{N}_B \end{bmatrix}$$

$$\bar{\mathbf{X}}_{GA} = \begin{Bmatrix} \mathbf{X}_{GA1} \\ \mathbf{X}_{GA2} \\ \mathbf{X}_{GA3} \end{Bmatrix}$$

$$\bar{\mathbf{X}}_{GB} = \begin{Bmatrix} \mathbf{X}_{GB1} \\ \mathbf{X}_{GB2} \\ \mathbf{X}_{GB3} \end{Bmatrix}$$

$$\bar{\mathbf{F}}_{GA} = \begin{Bmatrix} \mathbf{F}_{GA1} \\ \mathbf{F}_{GA2} \\ \mathbf{F}_{GA3} \end{Bmatrix}$$

$$\bar{\mathbf{F}}_{GB} = \begin{Bmatrix} \mathbf{F}_{GB1} \\ \mathbf{F}_{GB2} \\ \mathbf{F}_{GB3} \end{Bmatrix}$$

$\bar{\mathbf{K}}_{BB}^{CW}$, $\bar{\mathbf{K}}_{BI}^{CW}$, $\bar{\mathbf{K}}_{IB}^{CW}$ and $\bar{\mathbf{K}}_{II}^{CW}$ should be added to the places in the global stiffness matrix corresponding to the $\bar{\mathbf{X}}_{GA}$ and $\bar{\mathbf{X}}_{GB}$ degrees of freedom.

$\mathbf{N}_A$ and $\mathbf{N}_B$ are the shape function matrices of points A and B in the top and bottom element connecting by CWELD element (Figure 6.3).

The sensitivity equation of the above eigensystem for the case of distinct eigenvalues can be expressed as the rate of change of the i^{th} eigenvalues (λ_i) with respect to the j^{th} parameters, (θ_j) as follows

$$\mathbf{S}_{ij} = \frac{\partial \lambda_i}{\partial \theta_j^{RS}} = \boldsymbol{\phi}_i^{\mathrm{T}} \left[\frac{\partial \hat{\mathbf{K}}}{\partial \theta_j^{RS}} - \lambda_i \frac{\partial \hat{\mathbf{M}}}{\partial \theta_j^{RS}} \right] \boldsymbol{\phi}_i \tag{6.35}$$

where $\hat{\mathbf{K}}$ and $\hat{\mathbf{M}}$ are the reduced matrices of the complete assembly of stiffness and mass of the structure and θ_j^{RS} represents the j^{th} parameters of the residual structure.

The way CWELD element is connected to branch elements (patches) is illustrated in Figure 6.3. It consists of a two node special shear flexible beam type element with 12 degrees of freedom (one node for 6 degrees of freedom). Each node is connected to a set of nodes from its corresponding branch elements (a group of shell elements connected to the CWELD element) with constraint from the Kirchhoff shell theory. All 6 degrees of freedom from each node GA are connected to three translational degrees of freedom of node GA_i, as follows.

$$\begin{Bmatrix} u \\ v \\ w \end{Bmatrix}_A = \sum \mathbf{N}_i \left(\xi_A, \eta_A \right) \begin{Bmatrix} u \\ v \\ w \end{Bmatrix}_i \tag{6.36}$$

$$\theta_x^A = \frac{\partial w}{\partial y} = \sum \mathbf{N}_{i,y} \, w_i \tag{6.37}$$

$$\theta_y^A = \frac{\partial w}{\partial x} = -\sum \mathbf{N}_{i,x} \, w_i \tag{6.38}$$

$$\theta_x^A = \frac{1}{2} \left(\frac{\partial v}{\partial x} - \frac{\partial u}{\partial y} \right) = \frac{1}{2} \left(\sum \mathbf{N}_{i,x} \, v_i - \sum \mathbf{N}_{i,y} \, u_i \right) \tag{6.39}$$

These equations are written in the local tangent system of the surface branch elements at point GA, where x and y are the tangent coordinates, $\mathbf{N}_{i,i}$ represents the parametric shape function matrix, ζ_A and η_A are the normalised coordinates, u , v and w are the displacement DOFs, and θ_x, θ_y and θ_z are rotational DOFs. Another set of similar equations (6.36 to 6.39) are written for node GB resulting in twelve constraint equations.

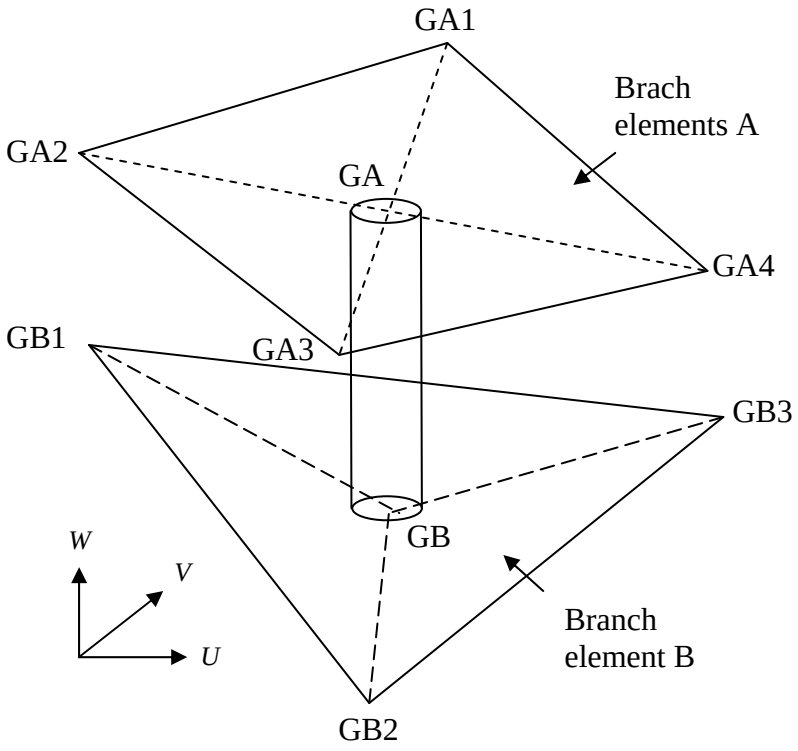

Figure 6.3: CWELD element connecting to branch elements (patches)

Augmentation of the Craig-Bampton transformation matrix

The normal modes which are calculated from the fixed-boundary modes $\mathbf{\Psi}_I$ as stated in Equation (6.4) are the modes of the lowest frequency and they are required in order to account for the inertia properties of the substructure. Therefore the larger the number of the normal modes is taken into account the better the representation of the inertia properties of the substructure. However the procedure, in practice, leads to great computational effort for calculating a large number of the normal mode and is totally diverged from the chief objective of the Craig-Bampton method in which the component mode set has to be truncated if any coordinate reduction is to be achieved. Generally the lower component modes which make the most significant contribution to the accuracy of the structural modes are kept and included in comparison with the higher component modes which are usually discarded.

The inertia-relief modes, $\mathbf{\Psi}_F$ based constraint mode method was proposed by Hintz (1975). It is calculated from the static response of a substructure due to rigid body motion with interfaces held fixed The constraint mode method is augmented with the constraint modes of the Craig-Bampton method as stated in Equation (6.40)

$$\begin{Bmatrix} \mathbf{X}_B^S \\ \mathbf{X}_I^S \end{Bmatrix} = \begin{bmatrix} \mathbf{I} & \mathbf{0} \\ \mathbf{\Phi}_B & \mathbf{\Phi}_F \end{bmatrix} \begin{Bmatrix} \mathbf{X}_B^S \\ \mathbf{q}_F \end{Bmatrix} \tag{6.40}$$

The inertia-relief modes, $\mathbf{\Psi}_F$ are obtained by applying a unit modal acceleration to each rigid body mode and imposing reaction forces to maintain zero displacement at the interface (Smith, 1993), yields

$$\begin{bmatrix} \mathbf{K}_{II}^S & \mathbf{K}_{BI}^S \\ \mathbf{K}_{IB}^S & \mathbf{K}_{II}^S \end{bmatrix} \begin{bmatrix} \mathbf{0} \\ \mathbf{\Phi}_F \end{bmatrix} = \begin{bmatrix} \mathbf{M}_{BB}^S & \mathbf{M}_{BI}^S \\ \mathbf{M}_{IB}^S & \mathbf{M}_{II}^S \end{bmatrix} \begin{bmatrix} \mathbf{\Phi}_B^R \\ \mathbf{\Phi}_I^R \end{bmatrix} + \begin{bmatrix} \mathbf{R}_B \\ \mathbf{0} \end{bmatrix} \tag{6.41}$$

Therefore the inertia-relief modes can be stated as

$$\boldsymbol{\Psi}_F = \begin{bmatrix} \mathbf{0} \\ \boldsymbol{\Phi}_F \end{bmatrix} = \begin{bmatrix} \mathbf{0} \\ \mathbf{K}_{II}^{A-1}\left(\mathbf{M}_{IB}^{S}\,\boldsymbol{\Phi}_B^{R} + \mathbf{M}_{II}^{S}\,\boldsymbol{\Phi}_I^{R}\right) \end{bmatrix} \tag{6.42}$$

It can be clearly shown in Equation (6.42) that the number of the initial-relief modes is equal to those of rigid body modes through which the component displacement field at low frequency can be enhanced. Therefore to improve the representation of component modes (Hintz, 1975; Rose, 1991 and Dickens and Stroeve, 2000), the Craig-Bampton transformation matrix may be augmented by adding the inertia-relief modes to Equation (6.4), yields

$$\begin{Bmatrix} \mathbf{X}_B^S \\ \mathbf{X}_I^S \end{Bmatrix} = \begin{bmatrix} \mathbf{I} & \mathbf{0} & \mathbf{0} \\ \boldsymbol{\Phi}_B & \boldsymbol{\Phi}_F & \boldsymbol{\Phi}_I \end{bmatrix} \begin{Bmatrix} \mathbf{X}_B^S \\ \mathbf{q}_F \\ \mathbf{q}_I \end{Bmatrix} \tag{6.43}$$

The augmentation procedure stated in Equation (6.43) can be manipulated by user input on NASTRAN RESVEC entry and full details of the procedure can be obtained from MSC.5. (2004) and MSC.2. (2010). The detailed theoretical explanation and discussion of the augmentation (residual vectors) is available in Wijker (2004), while the benefit of using the residual vectors in the dynamic analysis of a complex structure was discussed and demonstrated by Bennur (2009). However in this study, with the absence of the external loads, dynamic behaviour of the structure is investigated under free-free boundary conditions. By default the only option left to be used is INRLOD (MSC.5., 2004).

6.4 Description of the superelements and analysis

A three dimensional model of a welded structure is depicted in Figure 6.4. The substructuring scheme (superelement) is used in this study. The welded structure is divided into five substructures, comprising four Craig-Bampton superelements; side wall 1 (no. 1), side wall 2 (no. 2), stopper 1 (no. 3) and stopper 2 (no. 4) and a residual structure which is bent floor (no. 5). The arrangement of the substructuring scheme of the welded structure is shown in Figure 6.4. The relevant data regarding the superelements and residual structure can be found from Table 6.1.

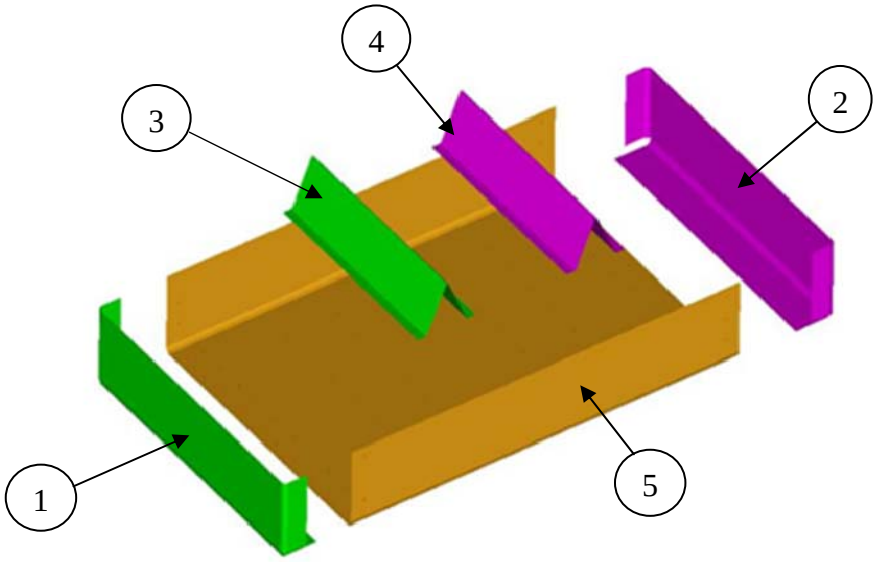

Figure 6.4: Superelement models of the welded structure

Table 6.1: Description of superelement and residual structure

DOFs	Superelement				Residual Structure
	Side Wall 1	Side Wall 2	Stopper 1	Stopper 2	Bent Floor
Total	15900	15900	29718	29718	84942
Boundary	624	624	336	336	N/A

Since the residual structure is the one to which the reduced matrices of all the superelements are assembled and also the one in which further analyses are carried out, the chief matter that needs to be taken into account by an engineer when defining a residual structure of a complete structural system is that the substructure is expected to change often due to uncertainties. In this study, the primary reasons of the bent floor is chosen to be the residual structure are

1. It is the primary substructure to which all substructures are to be assembled and also possesses the larger number of spot welds.

2. It is geometrically the most flexible substructures in comparison with others. Therefore, it is susceptible to local uncertainties such as initial curvatures, deformation and initial stress arising as a result of the assembling process.

3. It is highly expected to be the primary sources of the uncertainties in the finite element model. This was already proved and discussed at length in section 5.4 of Chapter 5.

4. It should technically have fewer number of degrees of freedom in comparison with other substructures. However this criterion would be relaxed if a large number of design variables are planned to be placed onto it.

The arrangement of branch elements, superelements and residual structure

In this work, branch elements (patches) are a set of adjacent elements through which CWELD elements are connected. For example elements ID 1 to 4 as shown in Figure 6.5 (b) are the branch elements of a particular CWELD element (Figure 6.5-d). The node ID of branch elements, particularly the nodes around the perimeter of the branch elements, starting from node ID 11 to ID 18 as shown in Figure 6.5 (c) are the boundary nodes from which the assembly of superelements is technically carried out and also through which the calculation of the constraints modes and fixed boundary modes is performed. In the application of the superelement method for a complex structure consisting of a large number of substructures connected to each other via spot welds, branch elements would be required if, CWELD elements in ELPAT format (CEEF) are chosen to represent the spot welds. This is because CEEF requires the elements per patch ranging up to 3 x 3 surrounding elements to be used to form the CWELD connection in which the elements have to be available at the time the CEEF logic runs to establish the connection based on the diameter on the PWELD entry (MSC.5., 2004). In other words a complete absence of branch elements on superelements, would definitely lead to a computational error in NASTRAN.

In this study, a number of branch elements is designed and introduced to superelements. The branch elements are then placed into the residual structure as shown in Figure 6.5 (a). As a result, these branch elements will no longer be inside the superelements and the boundary nodes to the superelements will be the nodes around the perimeter of branch elements or the perimeter of leftover branch elements (see Figure 6.5-c, Figure 6.6-b and Figure 6.7-b). Thus, there are no restrictions on what constitutes a boundary for a superelement. The arrangement of the branch elements for the residual structure, the branch elements themselves, the boundary nodes and also CWELD connection are depicted in Figure 6.5 (a), (b), (c) and (d) respectively.

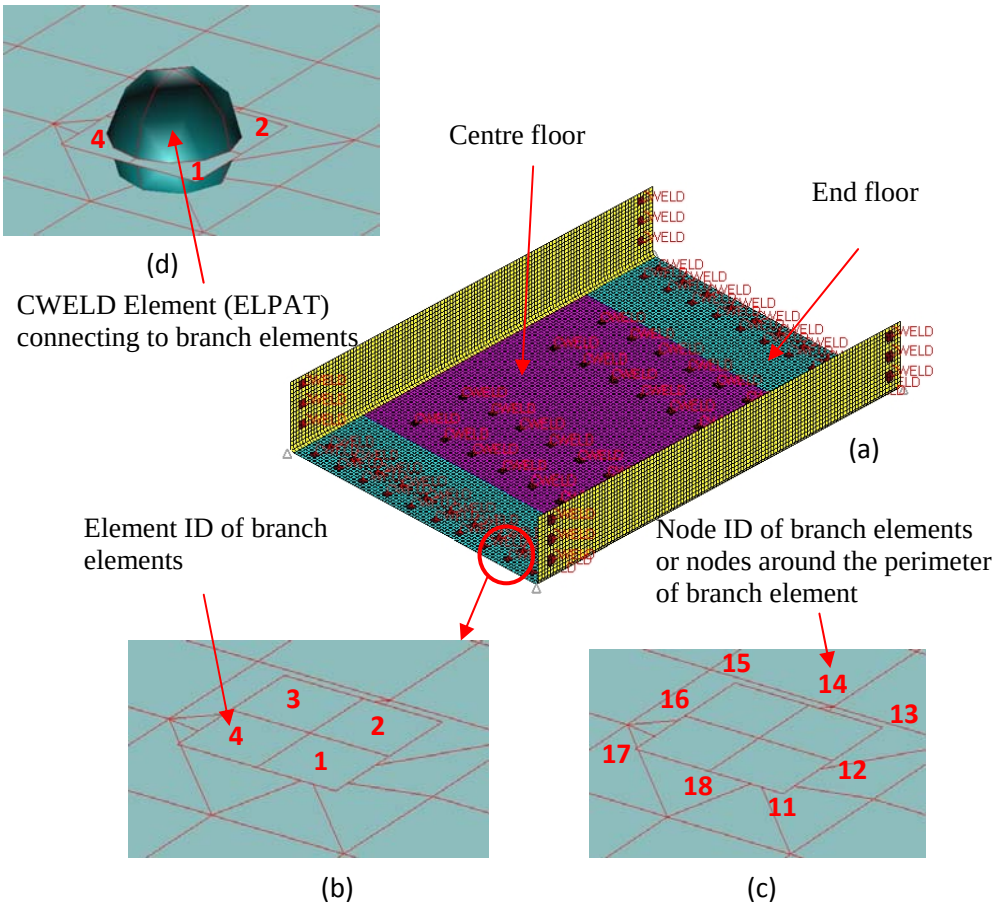

Figure 6.5: Residual structure and branch element sets

From Figure 6.5, it can be clearly seen that the constitution of the branch elements totally depends on the type of elements used to construct the finite element model. While the number of boundary nodes per superelement is the total number of nodes surrounding the perimeter of branch elements multiplied by the total number of the branch elements of a superelement. In other words, the more the branch elements, the more boundary nodes per superelement.

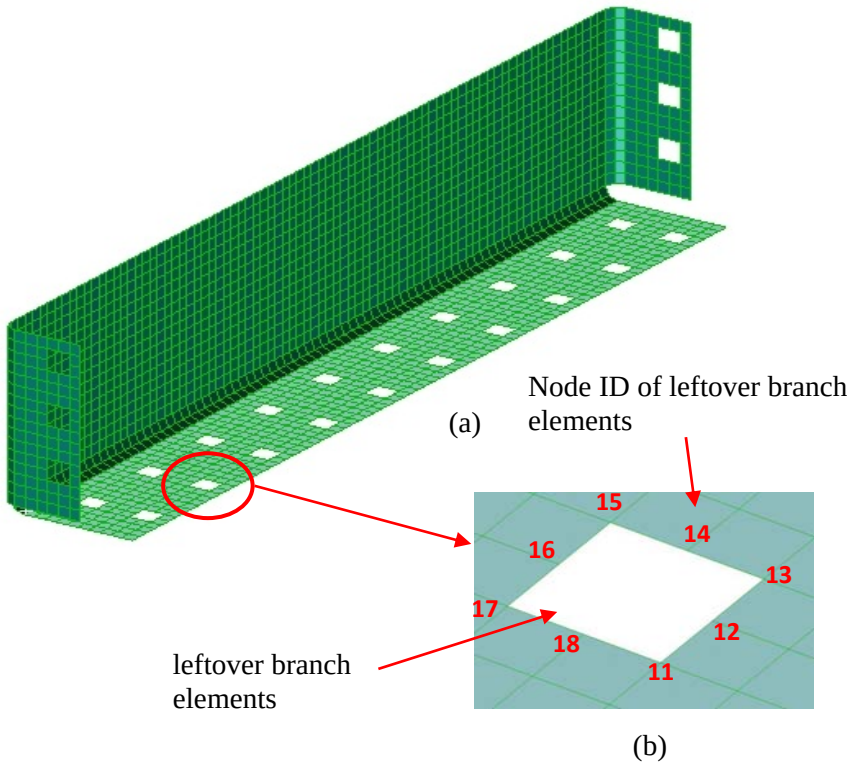

Figure 6.6: Superelement of side wall and branch element leftover

Figure 6.6 (a) and Figure 6.7 (a) respectively show the superelements of the side wall and stopper. There are a number of leftover branch element as a result of using the branch elements procedure for the construction of a superelement. The superelements that consist of a large number of nodes and the node IDs are automatically produced by NASTRAN. In this case, for example the node IDs surrounding the perimeter of the leftover branch element as shown in Figure 6.6 (b) and 6.7 (b) respectively, by default, would be having the same node IDs as the branch elements. This, in practice, would be a great advantage over the assembly process of superelements to the residual structure in which the automatic search logic in NASTRAN will identify and connect up the substructures that have the same entities.

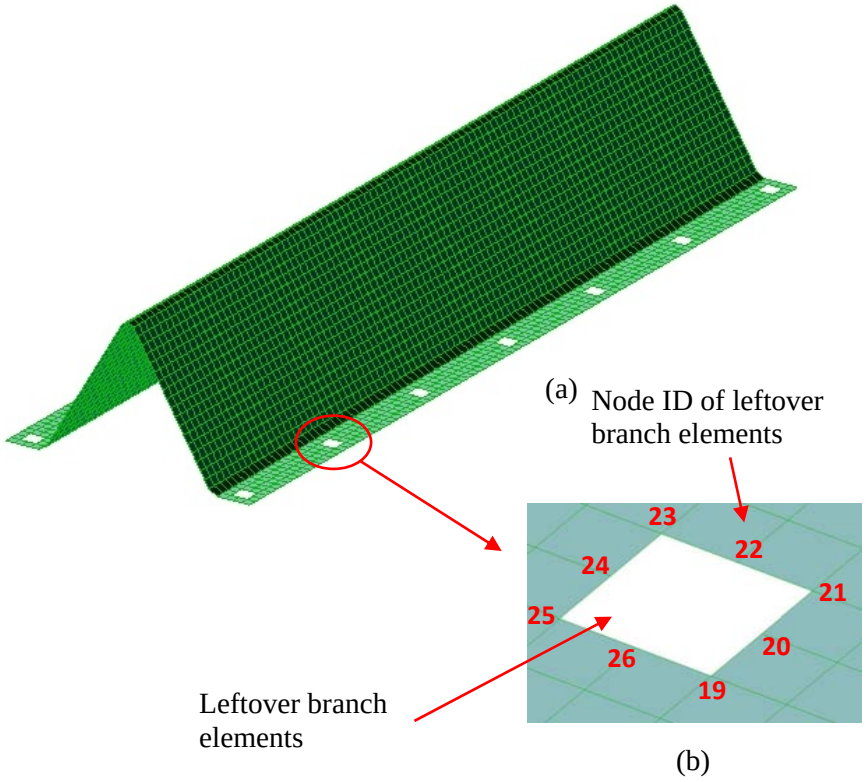

Figure 6.7: Superelement of stopper and branch element leftover

The number of branch elements depends on the number of spot welds on the superelements. The more the spot welds, the more branch elements need to be constructed. This can be clearly seen from Figure 6.6 (a) and Figure 6.7 (a), in which the superelement of the side wall possesses more branch elements in comparison with the superelement of the stopper that has fewer. This arises as a result of the number of spot welds on the tested substructure of the side wall being larger than that of the stopper. Sometimes, in real complex structures which consist of a large number of components or substructures, presence of an abundant number of spot welds on certain components is necessary and unavoidable.

In the characterization of dynamic behaviour of a complete structure, natural frequencies and mode shapes are the modal parameters of interest. There are two motivations for substructuring (superelement). The first is that the individual substructures may be designed, built and analysed by different subcontractors before they are physically assembled, therefore there is an incentive to analyse

them separately. The second is that the computational time may be conserved by dealing with separate subsystems during the analysis stage. In view of the common usage of substructuring scheme, particularly the first motivation in the context of using the branch elements as the boundary nodes, the question arises to how the proposed procedure can be used effectively between the two collaborating parties who have their own finite element substructure models.

In automotive industry, practically spot welds are used to connect two components or substructures and the regions where the spot welds are to be connected usually have already been pre-defined by CAD engineers before the CAD models are sent to the CAE engineers for analysis. The pre-defined locations of the spot welds are necessary because the components or substructures are normally modelled in parallel, different CAE engineer teams supply components with dissimilar meshes. However, the CAE engineers who are responsible for constructing the finite element models and superelements, have, in fact, already got a priori knowledge of where the spot welds are supposed to be. Thus, the selection of the branch elements of the superelements can be effectively devised by the engineers and then all the information can be passed to the engineers who manage the assembly process (the residual structure).

6.5 Results and discussion of the superelements

The method for selecting the boundary nodes of superelements and assembling superelements through the application of branch elements, has been thoroughly presented and discussed in the preceding section. It is clearly revealed that the proposed method (branch elements) is required for the application of superelement based model updating (SEMU).

This section presents the results calculated from the application of the proposed method in superelement based model updating (SEMU). This section also discusses the efficiency of SEMU in reconciling the finite element results with the experimental results of the welded structure by focussing on the accuracy of the

results and also the expenditure of CPU time. This section also covers the effect of the augmentation of the Craig-Bampton transformation matrix stated in Equation (6.43) in the calculation of the component modes for the superelements. On top of that this section shows and highlights the capability of SEMU to reduce the expenditure of CPU time. To demonstrate the capability of the proposed method and the augmentation to be used for SEMU, three case studies with different analysis set ups are carried out. In case study 1, six different analyses are performed. Each analysis has a different frequency range of component modes ranging from 500 Hz to 2000 Hz and it also has a different set up of the augmentation. The chief objectives of case study 1 are to investigate the effects of the augmentation and also the best frequency range of component modes for the improvement of the accuracy of the results. While the main objective of case study 2 is to investigate and demonstrate the capability of SEMU to reduce the expenditure of CPU time, especially a large number of iterations is required for convergence. In case study 3, its objective is to minimise the discrepancies between the finite element and experimental modal parameters. The analysis of case study 3 is performed within 200Hz which is the same range of frequency of interest determined in the experiment and ten modes are calculated.

Case study 1 - the effect of the augmented Craig-Bampton transformation matrix (residual vectors) and the frequency range of the component modes

In case study 1, a model of the welded structure shown in Figure 6.4 is used to investigate the augmentation effect towards the improvement of the component modes for the superelements, six analyses are performed by varying the frequency range of component modes and also by calculating the complete structure modes (residual structure) within 1000Hz. The results obtained from the six analyses are compared with those calculated from the full finite element model. The comparison of the results is shown in Figure 6.8. The set up of the superelements is tabulated in Table 6.2 in which the 1st column represents the superelements (SE 1 to SE 2), while the 2nd column defines the control card format for the real eigenvalue extraction data (EIGRL) and also the augmentation (RESVEC). Furthermore the

3rd to the 8th columns describe six different analysis set ups (RS_1 to RS_6) with different frequency ranges of component modes ranging from 500Hz to 2000Hz. The aforementioned columns also show the manipulation of the augmentation in the analyses by YES indicates that the augmentation is included, while NO means that the augmentation is excluded.

Table 6.2: The set up of the superelements for case study 1

Superelement Input		Analysis Set Ups					
		RS_1	RS_2	RS_3	RS_4	RS_5	RS_6
SE 1	EIGRL (Hz)	500	500	1000	2000	2000	1500
	RESVEC	YES	NO	YES	YES	NO	YES
SE 2	EIGRL (Hz)	500	500	1000	2000	2000	1500
	RESVEC	YES	NO	YES	YES	NO	YES
SE 3	EIGRL (Hz)	500	500	1000	1000	1000	1000
	RESVEC	YES	NO	YES	YES	YES	YES
SE 4	EIGRL (Hz)	500	500	1000	1000	1000	1000
	RESVEC	YES	NO	YES	YES	YES	YES

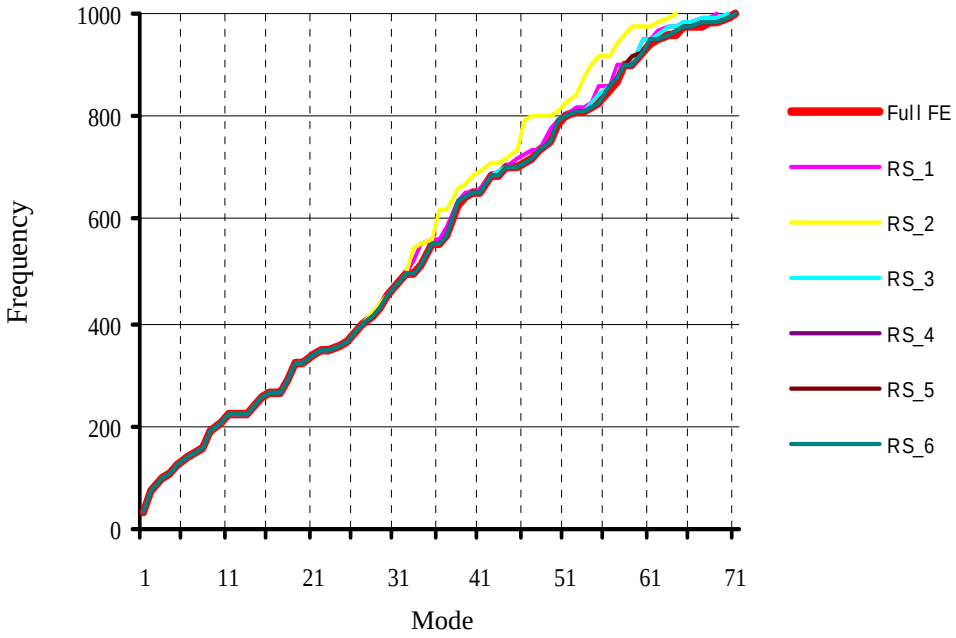

Figure 6.8: The combination of analysis results of the augmentation effect

The results obtained by exercising the superelements with different analysis set ups as tabulated in Table 6.3, demonstrate the effectiveness of the augmented Craig-Bampton transformation matrix (residual vectors) in improving the component modes of the superelements and also in predicting the natural frequencies of the welded structure. The significant residual vectors in improving the dynamic description of the superelements can be clearly seen in RS_1. The component modes in the analysis is merely calculated within 500 Hz, which is just half the frequency range of interest calculated in the residual structure (1000 Hz). However the accuracy of the dynamic behaviour of superelements in the higher modes is fairly close to the those calculated from the full finite element model. When a closer look is taken into the results obtained from RS_2, it is clear that the modes, especially those above 31th mode are not comparing well with the full finite element model. This arises as a result of excluding the residual vectors (RESVEC, NO) which is a powerful technique to mitigate against the effects of mode truncation in the analysis.

The effectiveness of the residual vectors in accounting for high frequency modes has already been presented and discussed in the previous paragraphs. It is concluded that in order to have enough component modes before they are attached to the residual structure, the frequency range of component modes should be within 1.5 to 2 times the frequency range of interest in the residual structure and the residual should be included in the analysis. The effectiveness of the suggested recommendation is shown in the results of RS_4, RS_5 and RS_6. The results obtained from the analyses are compared with the full finite element model and the discrepancies obtained from the comparisons are tabulated in Table 6.3 in the form of the truncated modes starting from the 33^{rd} to the 71^{th} modes. The reason of just looking into the specific modes is because the 1^{st} to the 32^{nd} modes of every analysis set up has shown very good agreement with the full finite element model which can be seen in Figure 6.8.

The total error is calculated in order to identify the efficient settings that should be used for model updating work of the welded structure which will be discussed in the next section. The results calculated from RS_1 and RS_2 reveal poor prediction of the frequencies, especially above the 32^{nd} mode. This arises as a results of calculating the component modes just within 500 Hz. The results also demonstrate that the application of residual vectors seems to be less effective in improving the accuracy of the dynamic characteristics of the welded structure. Another important revelation from the results is that a few modes are missing in the calculation. Further reduction in both the individual frequency error and the total error can be seen in RS_3 when additional component modes are added by increasing the frequency range of the component modes from 500 Hz to 1000 Hz with the residual vectors included as well. However this set up still suffers from missing modes. Tremendous improvement is seen in RS_4 in which all the modes are predicted well with frequency error of below 0.9 percent and the total error has dropped from 22.03 percent to 6.45 percent. Therefore the information presented in Table 6.2, Table 6.3 and Figure 6.8 reveals that the component modes of superelements should be calculated 1.5 to 2 times the frequency range of interest in the residual structure and the residual vectors should be included in the analysis.

Table 6.3: Percentage frequency error between the superelement model and the full FE model

Truncated Mode	Analysis Set Ups					
	RS_1	RS_2	RS_3	RS_4	RS_5	RS_6
33	5.89	10.75	0.07	0.01	0.01	0.02
34	8.09	9.01	0.03	0.01	0.01	0.01
35	0.18	0.75	0.06	0.05	0.06	0.05
36	0.39	11.27	0.05	0.04	0.04	0.04
37	3.16	9.81	0.08	0.04	0.04	0.05
38	0.57	4.63	0.04	0.01	0.01	0.03
39	1.83	4.25	0.04	0.01	0.02	0.02
40	0.18	4.12	0.11	0.04	0.06	0.05
41	1.42	5.85	0.11	0.04	0.05	0.04
42	0.15	3.70	0.11	0.02	0.15	0.02
43	1.21	3.66	0.48	0.05	0.05	0.06
44	0.35	2.61	0.14	0.10	0.10	0.10
45	1.96	4.70	0.03	0.02	0.03	0.02
46	2.10	11.60	0.18	0.05	0.06	0.06
47	2.73	11.51	0.37	0.06	0.06	0.06
48	0.97	9.29	0.11	0.05	0.06	0.05
49	3.70	7.45	0.07	0.03	0.07	0.04
50	1.08	3.02	1.08	0.87	0.88	0.87
51	0.16	2.93	0.10	0.08	0.14	0.09
52	1.32	4.38	0.09	0.06	0.09	0.07
53	1.23	7.94	0.40	0.13	0.13	0.13
54	1.03	10.30	1.01	0.56	0.62	0.56
55	3.18	10.97	1.20	0.06	0.07	0.14
56	1.01	8.39	0.98	0.76	0.77	0.77
57	3.31	8.55	0.19	0.09	0.11	0.09
58	0.48	6.34	0.19	0.07	0.50	0.08
59	0.11	7.77	0.10	0.07	1.13	0.09
60	3.10	5.65	3.05	0.04	0.06	0.10
61	1.07	3.70	1.02	0.78	0.80	0.86
62	1.90	3.40	1.43	0.41	0.41	0.44
63	1.53	2.94	1.50	0.09	0.09	0.09
64	1.85	3.81	1.65	0.45	0.50	0.51
65	1.13		1.10	0.21	0.34	0.22
66	1.18		1.17	0.29	0.29	0.45
67	1.50		1.05	0.19	0.33	0.19
68	1.27		0.87	0.21	0.21	0.33
69	1.31		0.79	0.17	0.23	0.17
70			0.98	0.15	0.20	0.15
71				0.06	0.07	0.07
Total Error	63.64	205.01	22.03	6.45	8.84	7.19

Superelement based model updating of the welded structure

In the preceding section, the results of case study 1 have been presented and discussed. The significant outcome of the case study is providing efficient settings for SEMU. The efficient settings in this work, means that the component modes of superelements should be calculated to 1.5 to 2 times the frequency range of interest in the residual structure and the residual vectors should be included in the analysis.

This section presents the superelement model updating (SEMU) in the reconciliation of the finite element model with the tested structure. The SEMU is enhanced with the proposed method which is the use of branch elements as the boundary nodes to connect the superelements. This work is performed through the application of NASTRAN SOL200 and also NASTRAN superelement code (see Appendix 1). In order to investigate the effectiveness of the SEMU in terms of the accuracy of results and also the CPU time expenditure, two sets of results obtained from two different case studies are presented and discussed. Both SEMU derived results of case study 2 and case study 3 are calculated from different sets of parameters. The numbers of measured frequencies and parameters are used for the analysis are seven for frequencies and five for parameters respectively. Case study 2 is performed for particularly demonstrating the effectiveness and capability of SEMU in solving the issue of analysis involving a large number of iterations.

The SEMU derived results of case study 3 are obtained based on the same parameters used and explained in section 5.4, with eight measured frequencies and five parameters. The SEMU derived frequencies and mode shapes are then compared with those from the experiment and also the full finite element model. The chief purposes of the comparison are first to evaluate the feasibility of the proposed method which is the use of the nodes of CWELD elements in form of branch element as the boundary nodes and then to assess the capability of the SEMU for reconciling the finite element model with the tested structure.

Table 6.4: The set up of the superelement model updating for case studies 2 and 3

Superelement Input		Analysis Set Ups	
		Case study 2	Case study 3
SE 1	EIGRL (Hz)	500	500
	RESVEC	YES	YES
SE 2	EIGRL (Hz)	500	500
	RESVEC	YES	YES
SE 3	EIGRL (Hz)	500	500
	RESVEC	YES	YES
SE 4	EIGRL (Hz)	500	500
	RESVEC	YES	YES

The efficient settings for the superelement (SE 1 to SE 4) inputs for both case study 2 and case study 3 are shown in Table 6.4. The frequency range of component modes is calculated within 500 Hz which is compliant with the recommendation of 2 times the frequency range of interest calculated in the residual structure. Furthermore the augmentation (residual vectors) as presented and discussed beforehand is used for all superelement inputs.

Three sets of results between the experiment, the full finite element and the SEMU are summarised in Table 6.5. The frequencies calculated from the experiment, the full finite element and the SEMU are shown in column (I), (II) and (IV) respectively. The comparison of results between the experiment and the full finite element method is given in column (III) with the total error of 15.23 percent. While the discrepancies between the tested structure and the SEMU are shown in column (V) with the total error of 15.91 percent. The purpose of these analyses is mainly to perform a comparative study of CPU time expenditure for two different methods of model updating so that the superior method can be fully utilised for reconciling the finite element model of the welded structure.

Both results calculated from the full finite element and the SEMU require 60 iterations to converge. However the SUME shows much better competency in the expenditure of the CPU time in comparison with the full finite element method. In addition the total error shown in the SEMU is pretty close to that of the full finite element method differing only by 0.68 percent. The significant reduction in the CPU time demonstrated in the SEMU is because the part of the model being optimised is small in comparison with the full finite element model and thus computer time saving is achieved through this method. The comparison of the two methods reveals two important things: first the proposed method by the branch elements can be used to connect the superelements and secondly the SEMU shows its superiority over the full finite element method in term of the expenditure of the CPU time by maintaining fairly good accuracy.

Table 6.5: The results of case study 2 for the full FE and superelement model updating

Mode	I Experiment (Hz)	II Full FE Method (Hz)	III Error (%) I-II	IV SEMU (Hz)	V Error (%) I-IV
1	29.48	29.48	0.02	29.49	0.02
2	76.58	77.09	1.94	78.09	1.97
3	101.07	101.66	0.53	101.89	0.81
4	110.86	109.44	2.66	107.73	2.82
5	121.91	121.99	0.21	121.99	0.07
6	140.46	140.19	0.10	139.95	0.37
7	147.50	147.67	0.43	146.94	0.38
8	159.77	159.99	0.34	159.33	0.28
9	187.51	191.69	2.84	182.31	2.77
10	199.65	203.70	6.16	186.83	6.42
Total Error (%)			15.23		15.91
CPU(s)			8607		4448

The main sources of the large discrepancies between the finite element model and the tested structure of the welded structure have already been discussed at great length in Chapter 5. They are technically believed to be a result of the modelling uncertainties, particularly the boundary conditions, spot welds and initial stress. Their parameters have already been proved to contribute the most to the response sensitivity as elaborated in section 5.4 and also shown in Figure 5.10 (page 155). Therefore the SEMU based sensitivity analysis seems to be unnecessary. In fact it can be simply performed in NASTRAN superelement code by using an additional control card in the Case Control . The main reasons for not redoing the sensitivity analysis are that firstly there are no other additional potential parameters that would influence the improvement of the finite element model and secondly it happens that all the parameters are from the bent floor, that is the residual structure, in the superelement method as depicted in Figure 6.4 (no.5)-page 186 and Figure 6.5 (a) - page 189.

Model updating is technically a process of modifying the potential parameters of a theoretical model iteratively upon the experimental data, as such the SEMU is used for modifying the parameters in the attempt to reconcile the finite element model of the welded structure with the tested structure. In the attempt the eight measured frequencies and the five parameters are defined in the DEQATN and DESVAR entry of NASTRAN superelement code (see Appendix 2). The accuracy of the SEMU derived frequencies is determined by comparing these results with those obtained from the full finite element model and the experiment. The comparison of the results is summarised in Table 6.6 in which columns (I), (II) and (IV) show the results from the experiment, the full finite element method and the superelement method respectively. The comparison of the results between the full finite element method and the experiment is given in column (III) with a total error of 7.30 percent. While the discrepancies between the SEMU derived frequencies and the experimental frequencies are shown in column (V) with a total error of 7.37 percent.

Table 6.6: The results of case study 3 for the full FE and superelement model updating (SEMU) using 8 measured frequencies in the objective function

Mode	I Experiment (Hz)	II Full FE Method (Hz)	III Error (%) I-II	IV SEMU 8 (Hz)	V Error (%) I-IV	VI SEMU MAC
1	29.48	29.48	0.00	29.48	0.00	0.95
2	76.58	77.09	0.66	77.09	0.67	0.97
3	101.07	101.66	0.58	101.66	0.58	0.92
4	110.86	109.44	1.28	109.44	1.28	0.97
5	121.91	121.99	0.07	121.99	0.07	0.95
6	140.46	140.19	0.19	140.20	0.19	0.93
7	147.50	147.67	0.12	147.68	0.12	0.91
8	159.77	159.99	0.14	159.99	0.14	0.97
9	187.51	191.69	2.23	191.84	2.26	0.91
10	199.65	203.70	2.03	203.85	2.06	0.92
Total Error (%)			7.30		7.37	
CPU (s)			1343		1282	

From the comparison of the results shown in Table 6.6, it is noticeable that the SEMU derived frequencies give a similar degree of accuracy to those obtained from the full finite element model based model updating. This can be clearly seen from the total error of the SEMU which is merely 0.07 percent different from that of the full finite element. This achievement suggests that in term of the accuracy of the updated results, SEMU has almost the same capability as the full finite element model has. However the performance of SEMU will be more outstanding when it is used in an analysis involving a large number of iterations.

The response sensitivities and approximate response analyses are required in NASTRAN SOL200 and they are iteratively used to arrive at better updated values of parameters in the process of minimising the discrepancies between the measured and numerical frequencies. Furthermore this process leads to repeated computation of the structural matrices which the size of the matrices totally depends on the number of degrees of freedom. The larger the size of structural matrices the bigger amount of computational time is required. Therefore the size of structural matrices

and the number of repeated computations, have a significant influence on the expenditure of computational time in the structural optimization. How to reduce the model to be processed in each finite element iteration, is a chief point of the reduction in computational time expenditure.

A method to maximize the modular characteristics of the superelement method in model updating work of the welded structure has been successfully used to both reduce the discrepancies and the expenditure of CPU time in comparison with the full finite element based model updating. Although there is not a huge difference between the SEMU and the full finite element in the context of the expenditure of CPU time as shown at the further bottom of Table 6.6, further reduction in the discrepancies is achieved from case study 3. It shows better reconciliation and the overall updating process merely requires eight iterations to converge in comparison with case study 2. The convergence is achieved at the sixtieth iteration. This reveals that the reduction in the expenditure of CPU time not solely depends on the size of superelement but also depends on the number of iterations requires in the analysis.

Table 6.7: Updated values of the updating parameters of SEMU of the welded structure

Parameter	Initial value	Updated value	Unit
CELAS element stiffness for boundary conditions	0.0022	0.002.936	N/m
$12I / T^3$ at Wall section	1	0.001309	m
$12I / T^3$ at Center floor section	1	0.000761	m
$12I / T^3$ at End floor section	1	0.000891	m
CWELD diameter	0.005	0.00375	m

The updated values of the updating parameters of SEMU of the welded structure are shown in Table 6.7 and the convergence of the updating parameters is depicted in Figure 6.9. To summarise, the initial parameter values of the centre floor and wall have started converging at the seventh iteration, while there are no rapid changes in the initial value of the CWELD diameter and end floor after the sixth iteration. The increment rate of the initial value of boundary conditions has become totally flat right after the eighth iteration.

The measured and predicted mode shapes are shown in Figure 6.10 and Figure 6.11. The qualitative results of the mode shapes calculated from the updated finite element model are summarised in column (VI) of Table 6.6. In general the MAC values of the individual mode shapes of the structure are above 0.9, which is a good achievement for a complex structure.

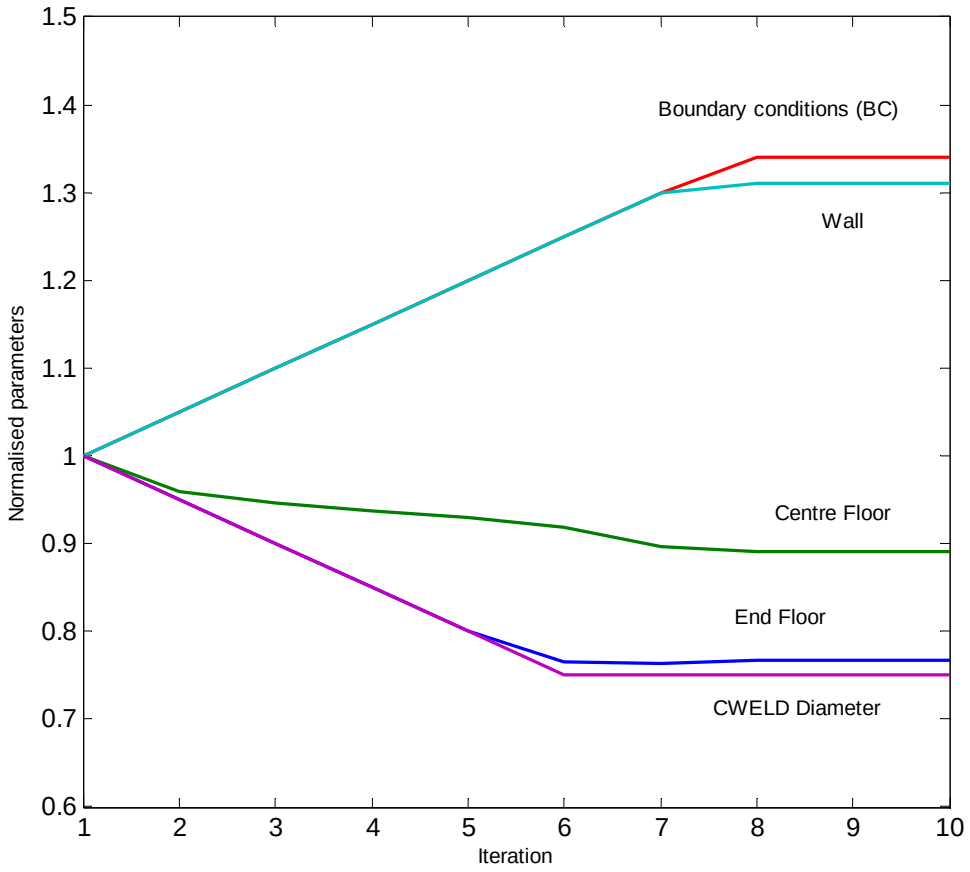

Figure 6.9: The convergence of the updating parameters of case study 3

Tables 6.8 and 6.9 show the comparisons of the results of the welded structure calculated based on the different number of the measured frequencies defined in the objective function as shown in Equation 4.9. Columns I and II represent for the experimental results and the results calculated from the initial finite element model respectively, while columns III to XI are the results calculated from the updated superelement model. NoMF stands for the number of measured frequencies and VoOF is the sum of the objective function value. From the tables, it is shown that the more the number of measured frequencies defined in the objective function, the better the results are obtained.

In this study, eight measured frequencies are used in the objective function. The rest of the measured frequencies (the 9th and 10th) are used to confirm the good predictability of the updated model. Using 8 measured frequencies in the objective function is a compromise between the quality and predictability of the updated model. It is found that the more measured frequencies used in the objective function the higher accuracy is achieved by the updated model. However, there would be fewer frequencies for this model to predict. 8 measured frequencies seem to make the best compromise.

Table 6.8: The comparisons of results calculated from different number of measured frequencies (NoMF) of SEMU - 2nd to 5th

Mode	I Exp (Hz)	II Initial FE (Hz)	III NoMF 2 (Hz)	IV NoMF 3 (Hz)	V NoMF 4 (Hz)	VI NoMF 5 (Hz)
1	29.48	26.26	29.24	29.29	29.48	29.48
2	76.58	78.17	76.57	76.58	77.15	77.06
3	101.07	102.44	100.86	100.99	101.57	101.84
4	110.86	109.55	106.76	106.90	109.59	109.57
5	121.91	126.10	125.99	126.30	119.86	121.79
6	140.46	144.16	140.32	140.69	137.99	140.00
7	147.50	144.31	144.34	144.72	148.88	148.60
8	159.77	160.86	158.30	158.54	159.36	159.95
9	187.51	187.02	182.08	182.50	193.50	192.80
10	199.65	196.19	189.86	190.51	205.06	204.98
VoOF		1.5375	0.6349	0.5843	0.2650	0.1811

Table 6.9: The comparisons of results calculated from different number of measured frequencies (NoMF) of SEMU - 6th to 10th

Mode	I Exp (Hz)	II Initial FE (Hz)	VII NoMF 6 (Hz)	VIII NoMF 7 (Hz)	IX NoMF 8 (Hz)	X NoMF 9 (Hz)	XI NoMF 10 (Hz)
1	29.48	26.26	29.47	29.48	29.48	29.47	29.49
2	76.58	78.17	77.07	77.11	77.09	77.17	77.29
3	101.07	102.44	101.82	101.66	101.65	101.33	101.28
4	110.86	109.55	109.55	109.46	109.44	109.19	109.20
5	121.91	126.10	122.00	122.00	121.97	122.15	122.10
6	140.46	144.16	140.21	140.22	140.21	140.41	140.36
7	147.50	144.31	148.34	147.68	147.68	146.17	145.75
8	159.77	160.86	160.02	160.02	159.99	159.94	159.95
9	187.51	187.02	192.48	191.75	191.74	189.91	189.42
10	199.65	196.19	204.66	203.72	203.72	201.28	200.47
VoOF		1.5375	0.1606	0.1175	0.1174	0.0610	0.0580

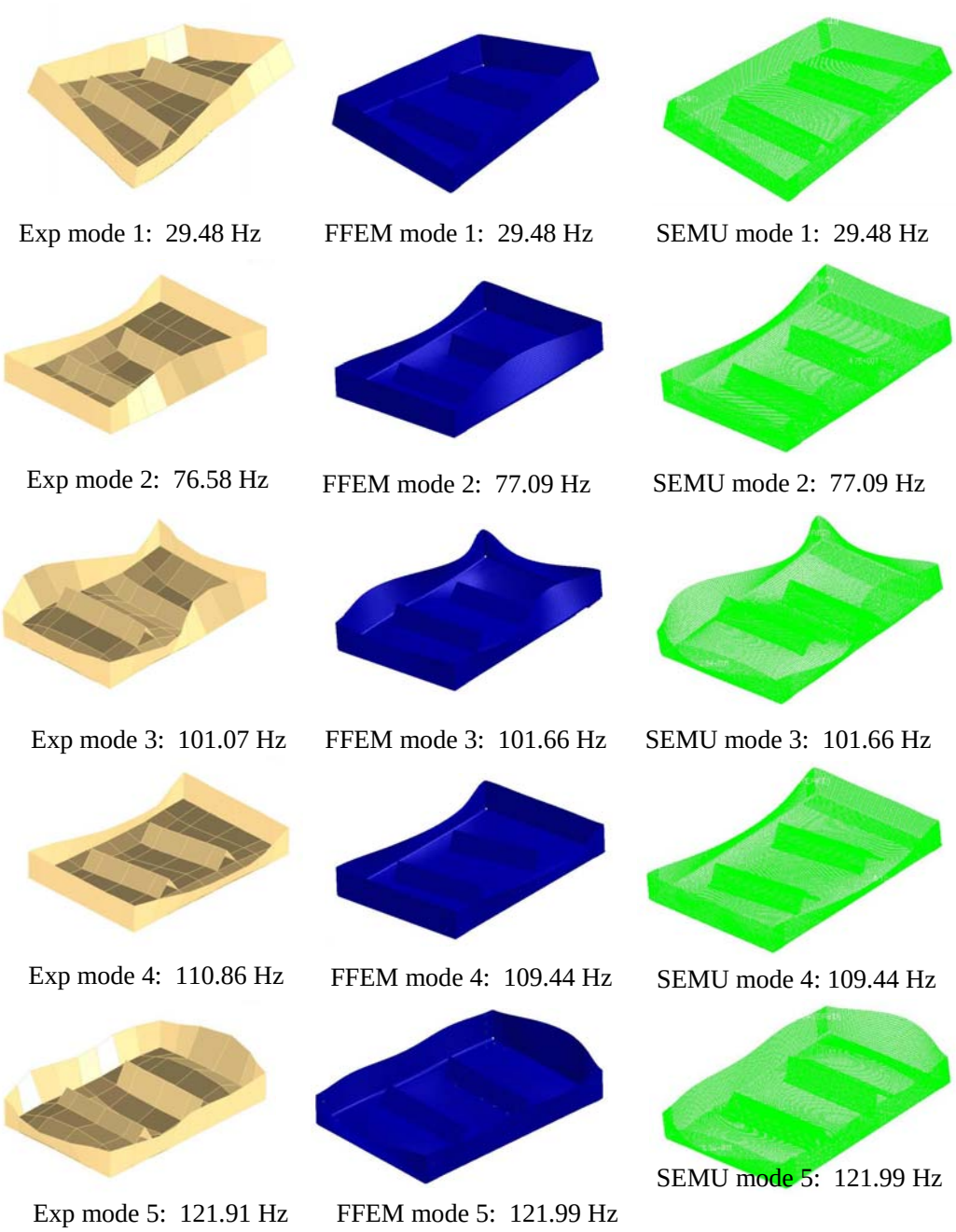

Figure 6.10: 1st, 2nd, 3rd, 4th and 5th triplets of mode shapes of welded structure calculated from experiment (Exp), full FE model (FFEM) and SEMU

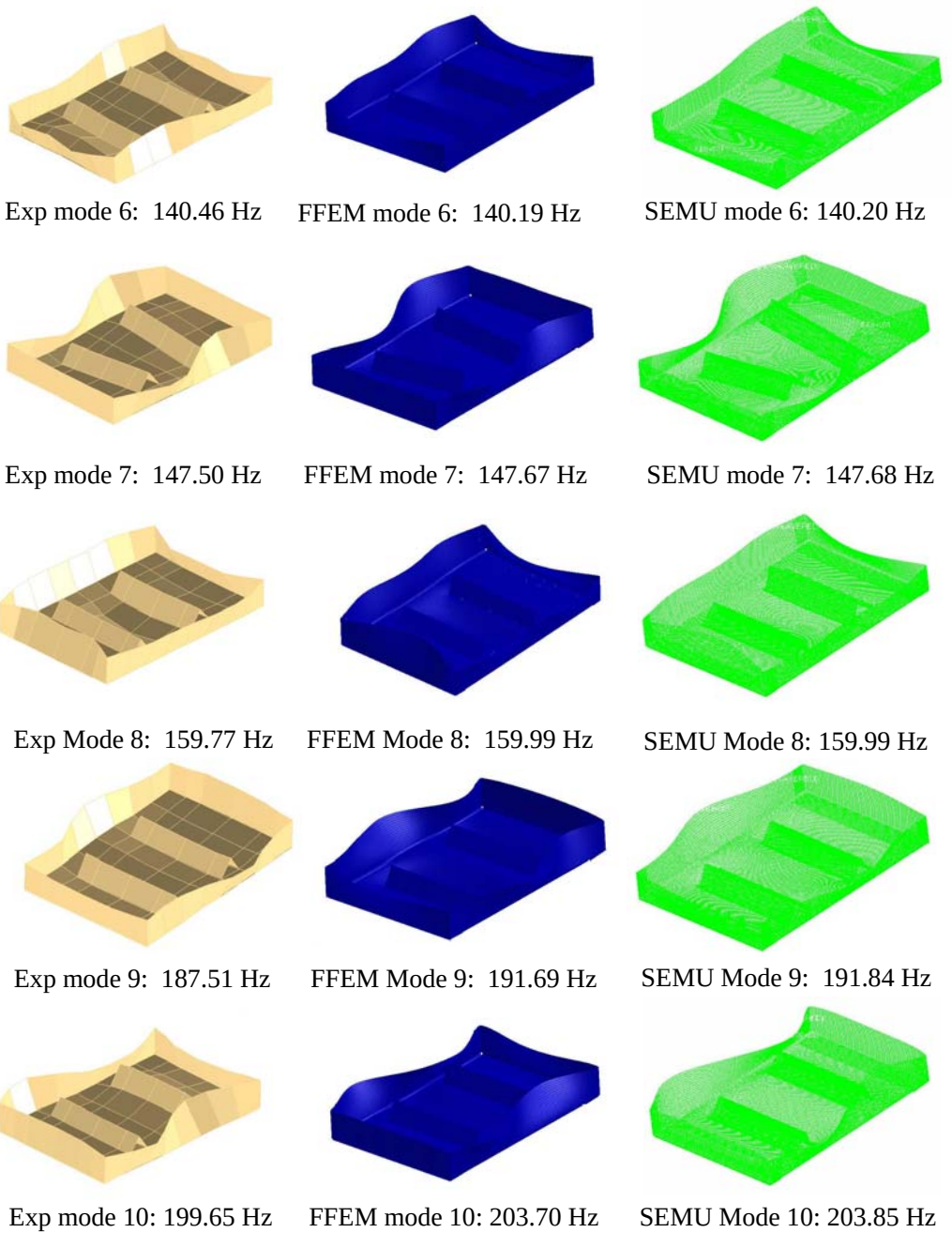

Figure 6.11: 6^{th}, 7^{th}, 8^{th}, 9^{th} and 10^{th} triples of mode shapes of welded structure calculated from experiment (Exp), full FE model (FFEM) and SEMU

6.6 Conclusions

The proposed method which is the use of the nodes of CWELD elements in form of branch elements has been successfully constructed and used in superelement based model updating (SEMU). On top of that the efficient settings (the frequency range of component modes and the augmentation) have also been successfully formularised and used in SEMU.

SEMU has been successfully used for the reconciliation of the finite element model with the tested structure of the welded structure. The use of the proposed method, the efficient settings and the augmentation (residual vectors) in SEMU is of the essence of the success.

SEMU has proven capability of accurately minimizing the uncertainties in the finite element model in comparison with the full finite element model and also shown better efficiency in dealing with the analysis involving a large number of iterations. This has been achieved by using the efficient settings in which the frequency range of component modes should be calculated two times the frequency range of interest in the residual structure and also the residual vectors should be included in the analysis.

Chapter 7

Conclusions and Future Work

7.1 Introduction

The chief goal of this research has been primarily driven by the fact that little success has been found in updating finite element model of welded structures in terms of accuracy and efficiency. To be specific, this research has sought to investigate the inaccurate assumptions about the initial finite element models that have significantly influenced the predicted results of dynamic characteristics of the welded structure which consists of substructures made from thin steel sheets joined together by a number of spot welds. This research also has sought to systematically adjust the inaccurate assumptions efficiently and accurately. Therefore, an efficient method for the identification and reconciliation of the dynamic characteristics of finite element models of the welded structure has been presented and discussed in this research.

The main contributions, conclusions and also recommendation for future work will be presented in this chapter.

7.2 Main contributions of this thesis

The main original contributions of this thesis are as follows:

1. The success of investigating the inaccurate assumptions that are believed to be the consequence of the stiffness of suspension springs, thickness of radius, initial stress, initial curvature in the finite element model of the substructures and the welded structure in the reconciliation of the finite element models with the tested models. In this work, MSC NASTRAN SOL 200 and modal testing (impact hammer and roving accelerometers) are used extensively.

2. The success of using the Craig-Bampton CMS based model updating in the reconciliation of the finite element model of the welded structure to the experimentally derived data via the application of branch elements. In this work, branch elements which would be necessarily required if the CWELD elements in ELPAT format are considered to be the interface nodes between the substructure and the residual structure are used as the interface nodes. To the author's best knowledge no work has been reported on this particular area.

3. The success of using bending moment of inertia ratio ($12I / T^3$) for representing the initial curvatures and initial stress that may arise from the assembly, fabrication and welding process in updating the finite element model of the welded structure, especially in the Craig-Bampton model and the full FE model. To the author's best knowledge no work has been reported on this particular area.

4. The use of CWELD element ELPAT format and MSC NASTRAN SOL200 in representing spot welds on the welded structure with thin large surface structure. In this work, the results calculated from CWELD element ELPAT format have shown better representation of spot welds in comparison those calculated from CWELD element ALIGN format.

7.3 Experimental modal analysis

A structure with a thin large surface like the welded structure is highly susceptible to rattling and also is easily prone to snap-through deformation. In consequence, modal test on this particular type of structure is very difficult to perform. However, with systematic approaches demonstrated and discussed in chapter 3, both modal tests on the substructures and welded structure have been successfully performed. For ensuring the accuracy of the experimental results measured several chief factors such as the number of measuring points and accelerometers, the weight of accelerometers, method of support and method of excitation are considered in measuring the modal properties of both the substructures and the welded structure.

On top of that the mode shapes calculated from finite element models are used to aid in determining the number and location of measuring points of the tested substructures and welded structure. The measured modal properties of the substructures and the welded structure have been discussed and demonstrated in chapter 3 including a series of comparisons between the measured and predicted modal properties of both substructures and welded structure as well.

The result comparisons revealed that there are big discrepancies between the measured and predicted modal properties of the welded structure in particular. The inaccurate assumptions made in the initial finite element models are attributed to the large discrepancies and are insufficient to represent the real tested model.

It can be concluded that based on author's experience in the measurement of modal properties for a thin structure with a large surface area, the use of roving accelerometers is observed to be more practical in comparison with roving hammer in terms of the accuracy of results measured, in particular mode shapes. It is imperative to note that measuring modal properties of this type of structures, limits the selection of excitation points because this particular type of structures which have a high flexibility are easily susceptible to rattling when the impact hammer is used to excite the structure.

7.4 Substructure modelling and model updating

The finite element method has been the most predominant method and been widely used by the scientist and engineering communities for the study of dynamic characteristics of structures. However, the results calculated from the method are often found to be uncorrelated with the experimentally observed results. Therefore, an adjustment process of reconciling the finite element models with the tested models namely model updating is highly required before the models are used for subsequent analyses.

Finite element modelling and model updating of five substructures namely side wall 1 & 2, stopper 1 & 2 and bent floor have been demonstrated and discussed in chapter 4. The model updating work on the substructures is one of the import steps required before the substructures are assembled together to form a welded structure. The significance of the work is to ensure that any uncertainties in the initial finite element model of the welded structure are solely due to the uncertainties of spot welds modelling and not because of the uncertainties of substructure modelling.

In this work, the discrepancies between the initial finite element models of the substructures and the tested models have been successfully reduced below 5 percent which is a successful achievement. This work also has revealed that identifying the main source of discrepancies is the most challenging aspect of the updating process. The differences can be caused by global effects such as geometry errors (thickness), exclusion of significant components from the model, local effects, mismatch in boundary conditions, incorrect material modelling and other factors. However, it is imperative to highlight that the inclusion of the CELAS element as one of the updating parameters could result in a dramatic reduction in the first frequencies of the substructure of bent floor. While the consideration of the thickness reduction in the backbone leading to more representative models of the substructures of stopper 1 & 2 for model updating process. The details of this work have been presented and discussed in chapter 4.

7.5 Welded structure modelling and model updating

The predicted results of dynamic behaviour of assembled complete structure achieved are often far from the experimental observation in comparison with those of substructures. The inaccuracy of prediction is believed to be largely due to the inaccurate assumptions about the initial finite element models of assembled complete structures, particularly those on joints, boundary conditions and also loads. Therefore, model updating methods are usually used to improve the initial finite element models by using the experimentally observed results.

The findings of this work which have been presented and discussed in chapter 5, thus lend credence to the aforementioned hypotheses. A large discrepancy between the initial finite element model of the welded structure and the tested model has been found. However, the results of this work have revealed that the large discrepancy is not merely due to the uncertainties of spot weld modelling but it is because the neglect of including the effects of initial stress and initial curvatures which are believed to arise as a result of the fabrication, assembly and welding process of the welded structure.

In chapter 5, finite element modelling and model updating work on the welded structure have been systematically presented and elaborated. The large discrepancies in the first ten modes between measured and predicted as shown in Table 5.12 (page 157) have been successfully reduced from 26.44 to 7.30 percent which is a significant achievement shown in this work. The success has been largely achieved through the close scrutiny of the sources of the uncertainties in the finite element model in which the inputs of the technical observation and engineering judgment coupled with the sensitivity analysis are systematically ustilised.

In this work, the sensitivity analysis has proved to be a powerful tool for localizing the sources of the inaccurate assumptions that happened to be the boundary conditions, initial stress and initial curvature. However the sensitivity analysis alone definitely would not have been able to achieve the satisfactory reduction in the discrepancies without the inputs of the technical observation and engineering

judgment. Therefore the efficiency and accuracy of the sensitivity analysis to be used in model updating process, especially for localizing the sources of errors in finite element model of a large complex structure in particular would be much better if the inputs from technical observation and engineering judgment are taken into account together.

7.6 The Craig-Bampton CMS based model updating

The implementation of conventional iterative model updating methods which use full finite element models is perceived by the scientist and engineering communities to be impractical and inefficient approach especially involving large, complex structures with a very large number of degrees of freedom. This application becomes impractical and computationally expensive due to the repeated solution of the eigensolution problem and repeated calculation of the sensitivity matrix. As such, substructuring schemes based model updating, particularly the Craig-Bampton component mode synthesis (CMS) or the Craig-Bampton fixed interface method has been the preferable technique and widely used by the communities for reconciling the finite element model of large complex structure with the tested model.

In this work, the Craig-Bampton CMS and iterative model updating are two techniques that are coupled together and used for reconciling the modal properties of the welded structure with the experimentally observed results. The development of the two coupled techniques for updating work on the welded structure is carefully carried out by taking account of several chief factors such as the uncertainties in spot weld modelling and the problems associated with initial stress, initial curvature and also boundary conditions which have a large influence on the accuracy of the predicted results. Since those important factors are largely believed to arise as a result of the effects of local parameters rather than the global ones such as the Young's modulus and density, therefore, the proposed method provides an efficient approach for adjusting the representation of the parameters and also obviates the need for re-analysing the unaffected substructures.

In this work, the Craig-Bampton fixed interface based model updating has been successfully used for the prediction and the reconciliation of the dynamic characteristics of the finite element model of the welded structure. The efficiency of the proposed method is gauged based on its capability of reducing the large error in the finite element model and of decreasing the expenditure of CPU time. The detailed discussions of the capability of the proposed method with the comparisons of the results calculated are available in chapter 6.

The proposed method has been successfully used in reducing the large error in the finite element model of the welded structure. The success of the proposed method is shown in Table 6.6 (page 202) in which the large errors in the first ten modes have been reduced from 26.44 to 7.37 percent with only 0.07 percent less than the reduction in errors in the conventional model updating methods (see Table 5.12). However in terms of the expenditure of CPU time involving a large number of iterations as shown in Table 6.5 (page 200), the proposed method is much better than the conventional model updating with 4448 seconds and 8607 seconds respectively. In addition, with the use of the proposed method the degrees of freedom of the full finite element model of the welded structure have been reduced from 177114 to 90670 degrees of freedom.

In conclusion, the essence of the success of the application of the proposed method in the prediction and reconciliation of the dynamic characteristics of the welded structure definitely lies in the use of branch elements as the interface elements of the substructures. In other words, the use of branch elements is undoubtedly necessary for the success of the construction and application of the Craig-Bampton CMS based model updating for the welded structure. On top of that, the proposed method has proven capability of accurately minimizing the uncertainties in the finite element model in comparison with the conventional model updating methods and also shown better efficiency in dealing with the analysis involving a large number of iterations. To achieve all this, the maximum frequency of component modes must be set as twice the maximum frequency of interest calculated in the residual structure. In addition, the residual vectors should be included in the

analysis. The proposed method may offer larger savings in terms of CPU time with increase in the number of degrees of freedom in the substructures.

7.7 Suggestions for future work

Finite element modelling and model updating of the substructures and the welded structure have been presented and discussed in this thesis. For model updating work, two types of methods namely the conventional model updating and the Craig-Bampton CMS based model updating have been successfully tested on the welded structure which consists of five substructures made from thin steel sheets joined together by spot welds. The results from the tests show that the proposed method has shown better capability in comparison with the conventional method in this research. However, some further investigations and improvements may be necessary or interesting in future work. They are highlighted below.

1. In this work, the use of the proposed method is only to a simplified welded structure due to the constraints of time available. The proposed method should be applied to more complicated structures with a larger number of degrees of freedom and the best example is a body-in-white which consists of many substructures with different types of local issues.

2. The substructures and the welded structure in this work are described as linear models. However, in many structural problems, nonlinearity, if any, is found in only a few local regions whereas the rest of the structure remains entirely linear elastic. For example, in automotive structural dynamic analysis, frame, cabin can be described by linear models but the engine-suspension may behave nonlinearly. In such locally nonlinear cases where the structure can be divided into linear and nonlinear substructures, it is interesting to study how these issues can be solved efficiently.

3. The prediction and reconciliation of dynamic behaviour of the welded structure have been performed using the Craig-Bampton CMS which is based on fixed-interface methods, however, these methods are generally not

suitable for handling data obtained from experiments. Therefore, other alternatives such as mass-loading method should be used for the investigation of the dynamic characteristics of the welded structure. This is very important for the real application in engineering industry in which some substructures are very difficult to be numerically modelled due to a lot of uncertainties. In this case, it would be better if the experimental results of the substructures can be directly coupled with the numerical models through the substructuring schemes.

4. CWELD element ELPAT format has been successfully used for spot weld modelling in this work. However, for the sake of research it is interesting to see the effects on the usefulness of branch elements proposed in this work when other predominant spot weld models such as ACM2 is used in substructuring schemes. This is important in case that ACM2 model is more suitable for representing spot welds in those investigations in which substructuring schemes are required.

Appendix 1

```
$ GENERATE REDUCED MATRICES THAT WILL BE ATTACHED TO THE
$ RESIDUAL STRUCTURE and THIS IS CALLED SUPERELEMENT 1(THE
$  SAME PROCEDURE IS USED FOR OTHER SUPERELEMENTS: 2, 3 and 4)
ASSIGN OUTPUT2='se100.op2',UNIT=41,DELETE
$
SOL 103
CEND
ECHO = NONE
METHOD = 1
DISP(PLOT)=ALL
EXTSEOUT(ASMBULK,EXTBULK,EXTID=100,DMIGOP2=41)
BEGIN BULK
EIGRL, 1, , 500.0, ,,, MASS
$
$ GENERATE  BRANCH ELEMENT AT BOUNDARY NODES
ASET1,123456,25614 THRU 25718,
SPOINT,1110001,thru,1110120
QSET1,0,1110001,thru,1110120
$
Model Data Section
$
Model Property Section
$
ENDDATA
```

Appendix 2

```
$ Assembly of External Superelements (1,2,3 and 4)
$
ASSIGN INPUTT2='se100.op2',UNIT=41
ASSIGN INPUTT2='se200.op2',UNIT=42
ASSIGN INPUTT2='se400.op2',UNIT=44
ASSIGN INPUTT2='se500.op2',UNIT=45
$
SOL 200
TIME 600
$ Direct Text Input for Executive Control
CEND
TITLE = Minimising the Error in FE Model
ECHO = NONE
MAXLINES = 999999999
DESOBJ(MIN) = 60
DSAPRT (START=1,END=LAST)=ALL
ANALYSIS = MODES
$ Case Control Data
SUBCASE 1
  METHOD = 1
  SPC = 1
  VECTOR(SORT1,REAL)=ALL
  SPCFORCES(SORT1,REAL)=ALL
$
BEGIN BULK
PARAM    POST    -1
PARAM   PRTMAXIM YES
EIGRL, 1, 0. , 250.,16 ,,, MASS
$
Model Data Section
$
Model Property Section
$
$STRUCTURAL RESPONSE IDENTIFICATION
DRESP1,1      ,FREQ_7 ,FREQ   ,       ,       ,7
DRESP1,2      ,FREQ_8 ,FREQ   ,       ,       ,8
DRESP1,3      ,FREQ_9 ,FREQ   ,       ,       ,9
DRESP1,4      ,FREQ_10,FREQ   ,       ,       ,10
DRESP1,5      ,FREQ_11,FREQ   ,       ,       ,11
DRESP1,6      ,FREQ_12,FREQ   ,       ,       ,12
DRESP1,7      ,FREQ_13,FREQ   ,       ,       ,13
DRESP1,8      ,FREQ_14,FREQ   ,       ,       ,14
DRESP2,60     ,SUU    ,70
DRESP1        1         2         3         4         5

                  6         7         8
```

```
DEQATN  70   SUU(F1,F2,F3,F4,F5,F6,F7,F8)=
                  (F1/29.48-1.)**2+(F2/76.58-1.)**2+
                  (F3/101.07-1.)**2+(F4/110.86-1.)**2+
                   (F5/121.91-1.)**2+(F6/140.46-1.)**2+
                   (F7/147.50-1.)**2+(F8/159.77-1.)**2

$ OPTIMIZATION CONTROL
        DOPTPRM  DESMAX  100    FSDMAX  0      P1     0      P2     1
         METHOD  1      OPTCOD  MSCADS  CONV1  .001    CONV2  1.-20
        CONVDV .001    CONVPR .01     DELP   .2      DELX   .5
        DPMIN  .01     DXMIN  .05     CT     -.03    GMAX   .005
         CTMIN  .003
$
$ INCLUSION OF SUPERELEMENTS (1, 2, 3 and 4)
INCLUDE 'se1.asm'
INCLUDE 'se2.asm'
INCLUDE 'se4.asm'
INCLUDE 'se5.asm'
INCLUDE 'se1.pch'
INCLUDE 'se2.pch'
INCLUDE 'se4.pch'
INCLUDE 'se5.pch'
$
ENDDATA
```

Bibliography

ABDUL RANI, M. N. A., STANCIOIU, D., YUNUS, M. A., OUYANG, H., DENG, H. & JAMES, S. 2011. Model Updating for a Welded Structure Made from Thin Steel Sheets. *Applied Mechanics and Materials,* vol. 70, pg. 117-122.

ABU HUSAIN, N., KHODAPARAST, H. H. & OUYANG, H. 2010a. FE model updating of welded structures for identification of defects. *International Journal of Vehicle Noise and Vibration,* vol. 6, no. 2-4, pg. 163-175.

ABU HUSAIN, N., KHODAPARAST, H. H., SNAYLAM, A., JAMES, S., DEARDEN, G. & OUYANG, H. 2010b. Finite-element modelling and updating of laser spot weld joints in a top-hat structure for dynamic analysis. *Proceedings of the Institution of Mechanical Engineers, Part C: Journal of Mechanical Engineering Science,* vol. 224, no. 4, pg. 851-861.

AHMADIAN, H., MOTTERSHEAD, J. E. & FRISWELL, M. I. 2001. Boundary condition identification by solving characteristic equations. *Journal of Sound and Vibration,* vol. 247, no. 5, pg. 755-763.

ALLEMANG, R. J. 2003. The modal assurance criterion - Twenty years of use and abuse. *Sound and Vibration,* vol. 37, no. 8, pg. 14-21.

ALLEMANG, R. J. & VISSER, W. J. 1991. A review of model updating techniques. *The Shock and Vibration Digest,* vol. 23, no. 1, pg. 9-20.

ARRUDA, J. R. F. & SANTOS, J. M. C. 1993. Mechanical joint parameter estimation using frequency response functions and component mode synthesis. *Mechanical Systems and Signal Processing,* vol. 7, no. 6, pg. 493-508.

BAKIRA, P. G., REYNDERS, E. & ROECK, G. D. 2007. Sensitivity-based finite element model updating using constrained optimization with a trust region algorithm. *Journal of Sound and Vibration,* vol. 305, no. 1-2, pg. 211-225.

BARUCH, M. 1978. Optimization procedures to correct stiffness and flexibility matrices using vibration tests. *AIAA Journal,* vol. 16, no. 11, pg. 1208-1210.

BENNUR, M. 2009. Superelement, component mode synthesis, and automated multilevel substructuring for rapid vehicle development. *SAE International Journal of Passenger Cars - Electronic and Electrical Systems,* vol. 1, no. 1, pg. 268-279.

BERMAN, A. & FLANNELLY, W. G. 1971. Theory of incomplete models of dynamic structures. *AIAA Journal,* vol. 9, no. 8, pg. 1481-1487.

BERMAN, A. & NAGY, E. J. 1983. Improvement of a large analytical model using test data. *AIAA Journal,* vol. 21, no. 8, pg. 1168-1173.

BIONDI, B. & MUSCOLINO, G. 2003. Component-mode synthesis method for coupled continuous and FE discretized substructures. *Engineering Structures,* vol. 25, no. 4, pg. 419-433.

BISPLINGHOFF, R. L., ASHLEY, H., & HALFMAN, R.L 1955. *Aeroelasticity*, Addison-Wiley Publishing Company, Inc., Cambridge, MA.

BLOT, B. 1996. Amélioration des résultats de calcul de caisse: *Third International SIA Congress,* Paris.

BURNETT, M. A. & YOUNG, W. G. 2008. Modal correlation and updating of a vehicle body-in-white: Proceedings of ISMA, , September 15 - 17, Leuven, Belgium, pg. 1823-1837.

CAESAR, B. 1986. Update and identification of dynamic mathematical models: Proceedings of the 4th IMAC, pg. 394-401.

CAESAR, B. 1987. Updating system matrices using modal test data: Proceedings of the 5th IMAC, pg. 453-459.

CARNE, T. G. & DOHRMANN, C. R. 1998. Support conditions, their effect on measured modal parameters. *Imac - Proceedings of the 16th International Modal Analysis Conference, Vols 1 and 2,* vol. 3243, pg. 477-483.

CARNE, T. G., GRIFFITH, D. T. & CASIAS, M. E. 2007. Support conditions for experimental modal analysis. *Sound and Vibration,* vol. 41, no. 6, pg. 10-16.

CERULLI, C., KEULEN, F. V. & RIXEN, D. J. 2007. Dynamic reanalysis and component mode synthesis to improve aircraft modeling for loads calculation. 48th AIAA/ASME/ASCE/AHS/ASC Structures, Structural Dynamics, and Materials Conference and Exhibit, AIAA Paper 2007- 2363.

CHANDLER, K. & TINKER, M. 1997. A general mass additive method for component mode synthesis. 38th AIAA/ASME/ASCE/AHS/ASC Structures, Structural Dynamics and Materials Conference and Exhibit, AIAA Paper 1997-1381.

CHANG, B., SHI, Y. & DONG, S. 1999. Comparative studies on stresses in weld-bonded, spot-welded and adhesive-bonded joints. *Journal of Materials Processing Technology*, vol. 87, no. 1-3, pg. 230-236.

CHANG, B., SHI, Y. & DONG, S. 2000. Studies on a computational model and the stress weld characteristics of weld bonded joints for a car body steel sheet. *Journal of Materials Processing Technology,* vol. 100, no. 1-3, pg. 171-178.

CHANG, D. C. 1974. Effect of flexible connections on body structural response. *SAE Transactions*, vol. 83, pg. 233-244.

CHEN, J. C. & GARBA, J. A. 1980. Analytical model improvement using modal test results. *AIAA Journal,* vol. 18, no. 6, pg. 684-690.

CLOUGH, R. W. 1960. The finite element in plane stress analysis: Proceedings of the 2nd ASCE conference on electronic computation Pittsburgh, USA, pg. 345-378.

COLLINS, J. D., HART, G. C., HASSELMAN, T. K. & KENNEDY, B. 1974. Statistical identification of structure. *AIAA Journal,* vol. 12, no. 2, pg. 185-190.

COOK, R. D. 1989. *Concepts and applications of finite element analysis,* New York, John Wiley and Sons, Inc.

CRAIG JR, R. R. 2000. Brief tutorial on substructure analysis and testing. *Proceedings of the International Modal Analysis Conference - IMAC,* vol. 1, no. 899-908.

CRAIG, J. R. R. & HALE, A. 1988. Block krylor component synthesis method for structural model reduction. *Journal of Guidance, Control and Dynamics,* vol. 11, no. 6, pg. 562-570.

CRAIG, R. R. 1981. *Structural dynamics: an introduction to computer methods,* New York, Wiley.

CRAIG, R. R. 1995. Substructure methods in vibration. *Journal of Vibration and Accoustics,* vol. 117, no. B, pg. 207-213.

CRAIG, R. R. 2000. Coupling of substructures for dynamic analyses: An overview. *Collection of the 41st AIAA/ASME/ASCE/AHS/ASC Structures, Structural Dynamics and Materials Conference and Exhibit* vol. 5, pg. 3-14.

CRAIG, R. R. & BAMPTON, M. C. C. 1968. Coupling of substructures for dynamic analyses. *AIAA Journal,* vol. 6, no. 7, pg. 1313-1319.

CRAIG, R. R. & CHANG, C. 1977. Substructure coupling for dynamic analysis and testing, NASA, TR CR-2781 pg. 1-94

CRAIG, R. R. & CHANG, C. J. 1976. Free interface methods of substructure coupling for dynamic analysis. *AIAA Journal,* vol. 14, no. 11, pg. 1633-1635.

CRAIG, R. R. & KURDILA, A. J. 2006. *Fundamentals of structural dynamics / Roy R. Craig, Jr., Andrew J. Kurdila,* Hoboken, N.J. : John Wiley, 2006. 2nd ed.

DASCOTTE, E. 1990. Practical applications of finite element tuning using experimental modal data: Proceedings of the 8th IMAC, January 29 - February 1, Kissimmee, Florida, pg. 1032-1037.

DASCOTTE, E. 2007. Model updating for structural dynamics: past, present and future: Proceedings of the International Conference on Engineering Dynamics (ICED), April 16-18, Carvoeiro, Algarve, Portugal, pg. 151-164.

DASCOTTE, E. & VANHONACKER, P. 1989. Development of an automatic mathematical model updating program: Proceedings of the 7th IMAC, Los Vegas, pg. 596-602.

DAVID-WEST, O. S., WANG, J. & COOPER, R. 2010. Finite element model updating of a thin wall enclosure under impact excitation. *Applied Mechanics and Materials*, vol. 24-25, pg. 337-342.

DE ALBA, R. O., FERGUSON, N. S. & MACE, B. R. 2009. A multipoint constraint model for the vibration of spot welded structures. ISVR Technical Memorandum 982.

DE FARIA, A. R. & DE ALMEIDA, S. F. M. 2006. The maximization of fundamental frequency of structures under arbitrary initial stress states. *International Journal for Numerical Methods in Engineering,* vol. 65, no. 4, pg. 445-460.

DE KLERK, D., RIXEN, D. J. & VOORMEEREN, S. N. 2008. General framework for dynamic substructuring: History, review, and classification of techniques. *AIAA Journal,* vol. 46, no. 5, pg. 1169-1181.

DENG, X., CHEN, W. & SHI, G. 2000. Three dimensional finite element analysis of the mechanical behaviour of spot welds. *Finite Elements in Analysis and Design*, vol. 35, pg. 17-39.

DICKENS, J. M. & STROEVE, A. 2000. Modal truncation vectors for reduced dynamic substructures. 41st AIAA/ASME/ASCE/AHS/ASC Structures, Structural Dynamics and Materials Conference and Exhibit, AIAA Paper 2000-1578.

DONDERS, S., BRUGHMANS, M., HERMANS, L., LIEFOOGHE, C., VAN DER AUWERAER, H. & DESMET, W. 2006. The robustness of dynamic vehicle performance to spot weld failures. *Finite Elements in Analysis and Design,* vol. 42, no. 8-9, pg. 670-682.

DONDERS, S., BRUGHMANS, M., HERMANS, L. & TZANNETAKIS, N. 2005. The effect of spot weld failure on dynamic vehicle performance. *Sound and Vibration,* vol. 39, no. 4, pg. 16-25.

EWINS, D. J. 2000. *Modal testing : Theory, Practice, and Application,* Baldock Research Studies Press. 2nd Edition.

EWINS, D. J. & IMREGUN, M. 1986. State-of-the-art assessment of structural dynamic response analysis models (DYNAS). *Shock and Vibration Bulletin*, vol. 56, no. 1, pg. 59-90.

EWINS, D. J., SILVA, J. M. & MALECI, G. 1980. Vibration analysis of a helicopter with an externally-attached structure. *Shock and Vibration Bulletin,* vol. 50, no. 2, pg. 155-170.

FANG, J., HOFF, C., HOLMAN, B., MUELLER, F. & WALLERSTEIN, D. 2000. Weld modelling with MSC.NASTRAN. Proceedings of Second MSC Worldwide Automotive User Conference, Dearborn, MI, USA.

FONG, K. L. J. 2003. *A Study of Curvature Effects on Guided Elastic Wave.* PhD, Imperial College London, University of London.

FRISWELL, M. I. & MOTTERSHEAD, J. E. 1995. *Finite Element Model Updating in Structural Dynamics*, Kluwer Academic Publisher.

FRISWELL, M. I., PENNY, J. E. T. & GARVEY, S. D. 1997. Parameter subset selection in damage location: Inverse Problems in Engineering, pg. 189-215.

FRITZEN, C. P., JENNEWEIN, D. & KIEFER, T. 1998. Damage detection based on model updating methods. *Mechanical Systems and Signal Processing*, vol. 12, pg. 163-186.

GAUL, L. & NITSCHE, R. 2001. The role of friction in mechanical joints. *Applied Mechanics Review*, vol. 125, pg. 93-106.

GLADWELL, G. 1964. Branch mode analysis of vibrating analysis systems. *Journal of Sound and Vibration,* vol. 1, no. 1, pg. 41-59.

GOLDMAN, R. L. 1969. Vibration analysis by dynamic partitioning *AIAA Journal*, vol. 7, no. 6, pg. 1152-1154.

GOOD, M. R. & MARIOCE, D. J. 1984. Using experimental modal analysis to characterize automobile body joints and improve finite element analysis: Proceedings of the 2nd IMAC, Orlando, Florida, pg. 106-110.

HEISERER, D., SIELAFF, J. & CHARGIN, M. 1999. High performance, process oriented, weld spot approach. 1st MSC Worldwide Automotive User Conference.

HEYLEN, W., LAMMENS, S. & SAS, P. 1998. *Modal Analysis Theory and Testing*, KULeuven Publisher. 2nd Edition.

HINKE, L., MACE, B. R. & FERGUSON, N. S. 2007. Uncertainty quantification and CMS: free and fixed-interface methodologies: Proceedings of the 25th IMAC, February Orlando, Florida, pg. 306-318.

HINTZ, R. M. 1975. Analytical methods in component modal synthesis. *AIAA Journal,* vol. 13, no. 8, pg. 1007-1016.

HORTON, B., GURGENCI, H., VEIDT, M. & FRISWELL, M. I. 1999. Finite element model updating of the welded joints in a tubular H-frame. *Imac - Proceedings of the 17th International Modal Analysis Conference, Vols I and Ii*, vol. 3727, pg. 1556-1562.

HOU, S. N. 1969. Review of modal synthesis techniques and new approach. *Shock and Vibration Bulletin,* vol. 40, no. 4, pg. 25-39.

HURTY, W. C. 1960. Vibrations of structural systems by component mode sysnthesis. *Journal of the Engineering Mechanics Division,* vol. 86, no. EM 4, pg. 51-70.

HURTY, W. C. 1965. Dynamic analysis of structural system using component modes. *AIAA Journal,* vol. 3, no. 4, pg. 678-685.

IBRAHIM, R. A. & PETTIT, C. L. 2005. Uncertainties and dynamic problems of bolted joints and other fasteners. *Journal of Sound and Vibration,* vol. 279, no. 3-5, pg. 857-936.

IDIADA 2005. *Automotive NVH Training for Proton Signal Processing,* IDIADA NVH Department.

IMREGUN, M. 1992. Correlation and updating of fnite element models using vibration test data. *Noise and Vibration Worldwide,* vol. 23, no. 9, pg. 16-24.

IMREGUN, M. & VISSER, W. J. 1991. A review of model updating techniques. *The shock and Vibration Digest,* vol. 23, no. 1, pg. 9-20.

JOURMAT, P. & ROBERTS, J. E. 1955. Assessment of spot weld quality by torsion test. *British Welding Journal,* vol. 2, no. 5, pg. 225-233.

KAMAL, M. M., A., J. & JR, W. 1985. *Modern Automotive Structural Analysis,* CRC Press Second Edition.

KENIGSBUCH, R. & HALEVI, Y. 1998. Model updating in structural dynamics: A generalised reference basis approach. *Mechanical Systems and Signal Processing,* vol. 12, no. 1, pg. 75-90.

KIM, B. G., LEE, J. I. & CHUNG, T. J. 2007. A structural analysis of vehicle body-in-white using a substructuring technique. *Journal of Materials: Design and Applications,* vol. 221, no. 3, pg. 157-164.

KIM, T. R., WU, S. M. & EMAN, K. F. 1989. Identification of joint parameters for a taper joint. *Journal of engineering for industry,* vol. 111, no. 3, pg. 282-287.

LARDEUR, P., LACOUTURE, E. & BLAIN, E. 2000. Spot weld modelling techniques and performances of finite element models for the vibrational behaviour of automotive structures, pg. 409-416.

LEISSA, A. W. & KADI, A. S. 1971. Curvature Effects on Shallow Shell Vibrations. *Journal of Sound and Vibration,* vol. 16, no. 2, pg. 173-187.

LI, W. L. 2002. A new method for structural model updating and joint stiffness identification. *Mechanical Systems and Signal Processing*, vol. 16, no. 1, pg. 155-167.

LIM, S. H., NIISAWA, J., TOMIOKA, N. & KOISO, A. 1990. On stress distribution of spot-welded box beams with a longitudinal partition subjected to torsion. *International Journal of Materials and Product Technology*, vol. 5, no. 1, pg. 95-108.

LINK, M. 1990. Identification and correction of errors in analytical models using test data-theoretical and practical bounds: Proceedings of the 8th IMAC, January 29 - February 1, Kissimmee, Florida, pg. 570-578.

LINK, M. 1997. Updating local physical and global generalized parameters of coupled substructure: Proceedings of the 15th IMAC, February 3-6, Orlando, Florida, pg. 579-586.

LINK, M. 1998. Updating analytical models by using local and global parameters and relaxed optimisation requirements. *Mechanical Systems and Signal Processing,* vol. 12, no. 1, pg. 7-22.

LIU, Y., DUAN, Z. & LI, H. 2008. An updating method suitable for finite element model updating of large-scakled structures. *Materials Forum*, vol. 33, pg. 79-86.

MACNEAL, R. H. 1971. A hybrid method of component mode synthesis. *Computers & Structures,* vol. 1, no. 4, pg. 581-601.

MAGUIRE, J. 1995. A Correlation Benchmark for Dynamic Analysis: Proceeding, second international conference structural Dynamics Modelling test, analysis and correlation, pg. 1-12.

MAIA, N. M. M. & SILVA, J. M. M. 1997. *Theoretical and Experimental Modal Analysis*, Baldock Research Studies Press.

MALONEY, J. G., SHELTON, M., T. & UNDERHILL, D. A. 1970. Structural dynamic properties of tactical missile joints. Phase I, CR-6-348-945-001, pg. 1-135

MARES, C., MOTTERSHEAD, J. E. & FRISWELL, M. I. 2002. An updated model of the garteur SM-AG19 test structure and its validation: Proceedings of the Third International Conference, Swansea, UK, pg. 130-141.

MARES, C., MOTTERSHEAD, J. E. & FRISWELL, M. I. 2005. Stochastic model updating of a spot welded structure. *Proceedings of ISMA 2004: International Conference on Noise and Vibration Engineering*, vol. 1-8, pg. 1885-1898.

MASSON, G., AIT BRIK, B., COGAN, S. & BOUHADDI, N. 2006. Component mode synthesis (CMS) based on an enriched ritz approach for efficient structural optimization. *Journal of Sound and Vibration,* vol. 296, no. 4-5, pg. 845-860.

MOON, Y. M., JEE, T. H. & PARK, Y. P. 1999. Development of an automotive joint model using an analytically based formulation. *Journal of Sound and Vibration,* vol. 220, no. 4, pg. 625-640.

MOTTERSHEAD, J. E. & FRISWELL, M. I. 1993. Model Updating in Structural Dynamics - a Survey. *Journal of Sound and Vibration,* vol. 167, no. 2, pg. 347-375.

MOTTERSHEAD, J. E., LINK, M. & FRISWELL, M. I. 2010. The sensitivity method in finite element model updating: A tutorial. *Mechanical Systems and Signal Processing,* vol. 25, no. 7, pg. 2275-2296.

MOTTERSHEAD, J. E., MARES, C., FRISWELL, M. I. & JAMES, S. 2000. Selection and updating of parameters for an aluminium space-frame model. *Mechanical Systems and Signal Processing,* vol. 14, no. 6, pg. 923-944.

MOTTERSHEAD, J. E., MARES, C., JAMES, S. & FRISWELL, M. I. 2006. Stochastic model updating: Part 2--application to a set of physical structures. *Mechanical Systems and Signal Processing,* vol. 20, no. 8, pg. 2171-2185.

MSC.2. 2010. *MD/MSC Nastran 2010 Quick Reference Guide,* MSC. Software.

MSC.4. 2001. *MSC.Nastran 2001 Superelement User's Guide,* MSC. Software.

MSC.5. 2004. *MSC.Nastran 2004 Reference Manual,* MSC. Software.

MSC.6. 2011. *'Superelements and Large Problems '.* MSC. Nastran Discussion Community. Available from: http://forums.mscsoftware.com [Accessed 7th September 2011].

MUIRA, H. 1988. *MSC/NASTRAN Handbook for Structural Optimization,* The MacNeal-Schwendler Corporation

NATKE, H. G. 1998. Updating computational models in the frequency domain based on measured data: a survey. *Probabilistic Engineering Mechanics,* vol. 3, no. 1, pg. 28-35.

NATKE, H. G., LALLEMENT, G., COTTIN, N. & PRELLS, U. 1995. Properties of various residuals within updating of mathematical models. *Inverse Problems in Engineering,* vol. 1, no. 4, pg. 329-348.

NIED, H. A. 1984. Finite element modelling of the resistance spot welding process. *Welding Journal (Miami, Fla),* vol. 63, no. 4, pg. 123-132.

O'CALLAHAN, J. 2000. Reduced model concepts: Proceeding of IMAC-XVIII: A Conference on Structural Dynamics, pg. 1528-1536.

OLDFIELD, M., OUYANG, H. & MOTTERSHEAD, J. E. 2005. Simplified models of bolted joints under harmonic loading. *Computer and Structures,* vol. 84, pg. 25-33.

ORTS, D. H. 1981. Fatigue strength of spot welded joints in a HSLA steel: International Congress and Exposition (SAE paper 810355), February 23-27, Detroit, MI, pg. 81-95.

OUYANG, H., OLDFIELD, M. & MOTTERSHEAD, J. E. 2006. Experimental and theoretical studies of a bolted joint excited by a torsional dynamic load. *International Journal of Mechanical Sciences,* vol. 48, pg. 1447-1455.

PAL, K. & CRONIN, D. L. 1995. Static and dynamic characteristics of spot welded sheet metal beams. *Journal of engineering for industry,* vol. 117, no. 3, pg. 316-322.

PAL, T. K. & CHATTOPADHYAY, K. 2011. Resistance spot weldability and high cycle fatigue behaviour of martensitic (M190) steel sheet. *Fatigue & Fracture of Engineering Materials & Structures,* vol. 34, no. 1, pg. 46-52.

PALMONELLA, M., FRISWELL, M. I., MARES, C. & MOTTERSHEAD, J. E. 2003. Improving spot weld models in structural dynamics. *ASME Design Engineering Technical Conferences and Computer and Information in Engineering Conference,* vol. 1 A, pg. 379-388.

PALMONELLA, M., FRISWELL, M. I., MOTTERSHEAD, J. E. & LEES, A. W. 2004. Guidelines for the implementation of the CWELD and ACM2 spot weld models in structural dynamics. *Finite Elements in Analysis and Design,* vol. 41, no. 2, pg. 193-210.

PALMONELLA, M., FRISWELL, M. I., MOTTERSHEAD, J. E. & LEES, A. W. 2005. Finite element models of spot welds in structural dynamics: Review and updating. *Computers and Structures,* vol. 83, no. 8-9, pg. 648-661.

PAPADIOTI, D. C. & PAPADIMITRIOU, C. 2011. Finite element model validation and predictions using dynamic reduction techniques: 3rd International Conference on Computational Methods in Structural Dynamics and Earthquake Engineering May 26-28, Corfu, Greece, pg. 110-121.

PERERA, R. & RUIZ, A. 2008. A multistage FE updating procedure for damage identification in large-scale structures based on multiobjective evolutionary optimization. *Mechanical Systems and Signal Processing,* vol. 22, no. 4, pg. 970-991.

QU, Z.-Q. 2004. *Model order reduction techniques : with applications in finite element analysis / Zu-Qing Qu,* London : Springer, 2004.

RADAJ, D. 1989. Stress singularity, notch stress and structural stress at spot-welded joints. *Engineering Fracture Mechanics,* vol. 34, no. 2, pg. 495-506.

RADAJ, D. & ZHANG, S. 1995. Geometrically nonlinear behaviour of spot welded joints in tensile and comprehensive shear loading. *Engineering Fracture Mechanics,* vol. 51, pg. 281-294.

RAO, M. K., ZEBROWSKI, M. P. & CRABB, H. C. 1983. Automotive body joint analysis for improved vehicle response. *Proceedings of International Symposium on Automotive Technology and Automation,* vol. 2, pg. 953-973.

RIXEN, D. 2002a. High order static correction modes for component mode synthesis: *Fifth World Congress on Computational Mechanics*, Vienna, Austria.

RIXEN, D. J. 2001. Generalized mode acceleration methods and modal truncation augmentation. 42nd AIAA/ASME/ASCE/AHS/ASC Structures, Structural Dynamics and Materials Conference and Exhibit, AIAA Paper 2001-1300.

RIXEN, D. J. 2002b. A Lanczos procedure for efficient mode superposition in dynamic analysis. 43th AIAA/ASME/ ASCE/AHS/ASC Structures, Structural Dynamics, and Materials Conference, AIAA 2002-1393.

ROBERTO, D. I. 2008. Multi-disciplinary optimization of a vehicle spot weld layout under durability and NVH constraints: Conference on Noise and Vibration Engineering, 23th ISMA, September 15- 17, Leuven, Belgium, pg. 4111-4125.

RODDEN, W. P. 1967. A method for deriving influence coefficients from ground vibration test. *AIAA Journal,* vol. 5, no. 5, pg. 991-1000.

ROSE, T. 1991. Using residual vectors in MSC/NASTRAN dynamic analysis to improve accuracy. MSC World Users' conference.

ROSSETTO, E. 1987. The fatigue limit of spot welded lap joints: *The International Congress and Exposition (SAE paper 870640)*, Detroit, MI, February 23-27.

RUBIN, S. 1975. Improved component mode representation for structural dynamic analysis. *AIAA Journal,* vol. 13, no. 8, pg. 995-1006.

SCHEDLINSKI, C., WAGNER, F., BOHNERT, K., FRAPPIER, J., IRRGANG, A., LEHMANN, R. & MULLER, A. 2004. Experimental modal analysis and computational model updating of a car body in white: Proceedings of ISMA, Leuven, Belgium, pg. 1925 -1938.

SHYU, W. H., GU, J., HULBERT, G. M. & MA, Z. D. 2000. On the use of multi quasi static mode compensation sets for component mode synthesis of complex structures. *Finite Elements in Analysis and Design,* vol. 35, no. 2, pg. 119-140.

SHYU, W. H., MA, Z. D. & HULBERT, G. M. 1997. A new component mode synthesis method: Quasi-static mode compensation. *Finite Elements in Analysis and Design,* vol. 24, no. 4, pg. 271-281.

SMITH, M. J. 1993. *An evaluation of component mode synthesis for modal analysis of finite element models.* PhD Thesis, Engineering Physics, University of British Columbia.

TORSTEN, E. & ROLF, S. 2007. *Modelling of spot welds for NVH simulations in view of refined panel meshes.* Master's Thesis, Department of Civil and Environmental Engineering, Chalmers University of Technology.

VOPEL, H. G. & HILLMANN, J. 1996. Berücksichtigung der schweipunkte bei der FEM-modellierung von karosserien. *VDI-Berichte,* vol. 1283, pg. 171-181.

VORST, V. D., F.L. 1991. Component mode synthesis. TNO Report Bouw, BI-91-146.

WALZ, J. E., FULTON, R. F. & CYROS, N. J. 1969. Accuracy and Convergence of Finite Element Approximations: Proceedings of the Second Coference on Matrix Methods in Structural Mechanics, Wright Patterson Air Force Base, Ohio, pg. 995.

WEI, F. S. 1980. Stiffness matrix Correction from incomplete test data. *AIAA Journal,* vol. 18, no. 10, pg. 1274-1275.

WENG, S., XIA, Y., XU, Y. L. & ZHU, H. P. 2011. Substructure based approach to finite element model updating. *Computers and Structures,* vol. 89, no. 9-10, pg. 772-782.

WIJKER, J. 2004. *Mechanical vibrations in spacecraft design,* Germany, Springer.

WOLF JR, J. A. 1984. The influence of mounting stiffness on frequencies measured in a vibration test SAE Paper 840480, Society of Automotive, Inc.

XU, S. & DENG, X. 2004. An evaluation of simplified finite element models for spot-welded joints. *Finite Elements in Analysis and Design,* vol. 40, no. 9-10, pg. 1175-1194.

YU, Q. L., MOSTAGHEL, N. & FU, K. C. 1994. Effect of Initial Curvature on Natural Frequency of Thin-Plate on Hinge Supports. *Journal of Engineering Mechanics-Asce,* vol. 120, no. 4, pg. 796-813.

YUEH, C. K., WEN, W. L. & SHUFANG, X. 2009. A New Model Updating Method for Quadratic Eigenvalue Problems. *World Congress on Engineering 2009*, vol. 2, pg. 1109-1114.

YUNUS, M. A., RANI, M. N. A., OUYANG, H., DENG, H. & JAMES, S. 2011. Identification of damaged spot welds in a complicated joined structure. *Journal of Physics: Conference Series,* vol. 305, no. 1, pg. 1-10.

ZABEL, V. & BREHM, M. 2009. Model updating methods – a comparative study: Proceedings of the IMAC-XXVII, Society for Experimental Mechanics Inc, February 9-12, Orlando Florida USA, pg. 134-144.

ZANG, G. & RICHTER, B. 2000. A new approach to the numerical fatigue life prediction of spot welded structure. *Fatigue Fract Engng Mater Struct,* vol. 23, pg. 499-508.

ZHANG, J. H. & NATKE, H. G. 1991. *Mechanical Systems and Signal Processing* vol. 5, no. 6, pg. 501-514.